Performance of Epoxy-Coated Reinforcing Steel in Saline Media

by

Hengching Chen, B.S., M.S.

Dissertation

Presented to the Faculty of the Graduate School of

The University of Texas at Austin

in Partial Fulfillment

of the Requirements

for the Degree of

Doctor of Philosophy

The University of Texas at Austin

May 1996

Acknowledgments

Performance of Epoxy-Coated Reinforcing Steel in Saline Media

Publication No. _____

Hengching Chen, Ph.D.

The University of Texas at Austin, 1996

Supervisor: Harovel G. Wheat

The effectiveness of epoxy coatings in providing long-term corrosion resistance for reinforcing steel in concrete has given rise to much controversy recently. However, inadequate coating quality is usually believed to be the most probable factor causing failure. In this study, the crucial causes of unsatisfactory performance of epoxy-coated reinforcement (ECR) were identified.

ECRs with nine kinds of coater/powder/steel/size combinations were characterized with respect to coating thickness, integrity, and pre-exposure adhesion. Their performance was evaluated based on 200 days of continuous immersion in 3.5% NaCl solution and exposure in concrete blocks with wet-dry

ponding cycles. Both straight and bent ECR specimens were tested. During the exposure periods, their corrosion resistance was assessed based on measurements of corrosion potential, polarization resistance as well as electrochemical impedance spectroscopy (EIS) and macrocell corrosion current between bars in the concrete blocks. At the conclusion of exposure, the bars were further characterized by their outer appearance and post-exposure adhesion. In addition to ECRs, some polished reinforcing steel disks and uncoated reinforcing steel bars were also tested for comparison and to provide a more comprehensive investigation of the corrosion behavior of reinforcing steel.

The results obtained through various methods generally show consistent trends. Among them, EIS is especially useful since it can detect coating deterioration at very early stages, and it can provide both quantitative and mechanistic information about ECR degradation. The ECR performance varied significantly between different coater/powder/steel/size combinations. ECR free of defects should provide adequate protection against corrosion; however, it is difficult to keep ECR intact in real construction practices, and doubts are raised about its effectiveness as the probability of defects increases.

Table of Contents

Chapter 1

Introduction

1.1 Background: Evolution of the Problem

The practice of embedding steel bars within concrete to provide the required strength for load bearing applications was introduced during the second half of the nineteenth century [1]. Due to its very good composite properties and generally long-term durability, the reinforced concrete has been extensively used in a great variety of buildings and civil engineering works since the turn of the present century. Although it is a very versatile construction material capable of being exposed to many different types of environments, several deleterious processes may lead to the loss of serviceability. For reinforced concrete structures, the most common cause of deterioration is corrosion of reinforcing steel [2]. Moreover, the damage caused by corrosion of reinforcing steel is especially prominent in highways and bridge decks.

In the early 1960's, after the Federal Highway Administration (FHWA) instituted the "bare road" policy, millions of tons of chemical deicing salts were used every year to keep all roads throughout the United States open all year round [3]. Several years later, in the early 1970's, many bridge decks in the snow belt areas of the country started to show signs of deterioration only 2 to 3 years after construction and frequently required extensive repair after only 5 to 10 years [4]. The problem was quickly traced to corrosion of reinforcing steel caused by

1

chloride ions present in deicing salts. One factor which seems to implicate deicing salts is that surface spalls were quite rare in California until the late 1960's when the use of deicing salts was instituted in that state [5]. Similar deterioration was also found on structures exposed to sea water and marine environments [6] where chloride salts are also present.

Even though the adverse effects of chloride salts on reinforced concrete structures have been well recognized for a long time, the use of deicing salts has increased tremendously [7] in order to keep the roads clean. This has made corrosion of reinforcing steel in concrete a major problem in the United States for the past three decades. The significance of this problem is not just that it may occasionally cause catastrophic structural failures resulting in the loss of some lives and/or the damage to some properties, but it also results in enormous economic consequences to the society. When placed in service, highway bridges are expected to provide maintenance-free service for 30 years or more. But it turns out that many of them require major repair after only 5 to 10 years in operation and even have to be replaced after only 10 to 15 years of service [4] [8] [9]. The problem becomes very serious when we consider the large number of bridges all over this country. It is reported that approximately half of the 575,000 bridges in the U.S. highway system are in need of repair [10], and it is estimated that billions of dollars are spent every year in the United States to repair and replace those bridges prematurely damaged due to corrosion [11].

Faced with huge repair bills, a variety of measures have been proposed to prevent the problem from occurring in new structures. After a series of investigations and the successful application of epoxy coatings on underground

transmission pipes, the U.S. Federal Highway Commission concluded that fusion bonded epoxy-coated reinforcement (ECR) could provide many years of protection against corrosion (Report FHWA RD-74-18) [8]. Later, research by NIST [12] and FHWA [13] based on laboratory accelerated testing further indicated that ECR performed well in salt contaminated concrete. Since then, ECR has been extensively used in the U.S., Canada, the Middle East, and elsewhere during the past twenty years. Even more, its use has even been nearly mandatory in Federal-funded bridge and viaduct constructions [14].

Thus far, the performance of ECR in highway bridge decks has been reported to be successful [15]. There has been relatively little corrosion-induced concrete deterioration found on the great majority of ECR bridge deck structures. However, in the late 1980's, instances of premature corrosion of ECR and concrete deterioration have been recorded in the substructures of four major bridges in the Florida Keys after about 6 to 10 years in service [16]. Other cases of unsatisfactory performance of ECR have also been reported [17]. These findings have again raised a lot of concern nationwide about the effectiveness of epoxy coatings in preventing corrosion of reinforcing steel in highly corrosive environments. The Texas Department of Transportation (TxDOT) used a total of 34,300,000 lbs of ECR in bridge construction in fiscal years 1993 and 1994 [18] and so the effectiveness of ECR is a local concern as well. In order to evaluate the overall performance of ECR as a means of effectively protecting highway concrete structures from early deterioration due to corrosion, a research program (Project 1265) sponsored by the TxDOT and FHWA is being conducted at The University of Texas at Austin and this work was part of that project.

1.2 Corrosion Behavior of Reinforcement in Concrete: An Overview

Experience has shown that, in the absence of certain deleterious factors and agents, reinforced concrete structures can perform well without corrosion problems. On the contrary, in environments where water and aggressive elements, e.g. chloride ions, are abundant, reinforced concrete structures are prone to premature damage through corrosion-induced deterioration, which is often seen first as potholing or spalling. Although causes for these phenomena are still not fully understood, we will briefly review currently available information on mechanisms of corrosion of reinforcing steel in concrete.

1.2.1 Mechanism of Corrosion Protection in Concrete

Concrete is a mixture of Portland cement, graded aggregates, and water. From the view point of corrosion, the nature of the steel-in-concrete system is most dominated by the concrete pore structure and the chemical composition of the solution phase within the pores. These two factors, in turn, are affected most by the hydraulic binder, Portland cement. Portland cement in its unhydrated form consists mainly of four minerals of the following approximate compositions: $3CaO \cdot SiO_2$, $2CaO \cdot SiO_2$, $3CaO \cdot Al_2O_3$, and $4CaO \cdot Al_2O_3 \cdot Fe_2O_3$. When Portland cement is mixed with water, these constituent minerals undergo a complex sequence of hydration reactions which gradually transform the paste into a hardened matrix of hydrated products [19]. The most significant feature of cement hydration that relates to the electrochemical behavior of steel in concrete, is that

the aqueous phase rapidly acquires a high pH value. It is recorded that the pH values will be well in excess of 13 after a few weeks of hydration [20] [21]. According to the Pourbaix diagram for iron [22], as shown in Fig. 1.1, steel may remain passive over a wide range of potentials in such an alkaline environment. Moreover, a very small supply of oxygen is sufficient to provide the necessary degree of anodic polarization to maintain conditions within this range [23].

The passivation of metals has been generally attributed to the formation of a protective film which shields the surface from further corrosion. Extensive work has been carried out over the past hundred years to elucidate the mechanisms of the growth and breakdown of the passive film, but until now there is still relatively little known about this film, even its composition and structure [11]. Many researchers [24] [25] believe the passivity is provided by the iron oxide film which may possibly be a single layer of $Fe(OH)_2$, or be made up of two layers of oxides: an inner layer of Fe_3O_4 and an outer layer of γ-Fe_2O_3. For the case of steel in concrete, some researchers [26] [27] [28] otherwise point out that the film should also incorporate elements derived from the cement, e.g. Ca, since the interfacial zone between concrete and steel is mainly composed of $Ca(OH)_2$.

1.2.2 Breakdown of Passivity by Chloride Ions

The exact mechanism of the breakdown of the passive film on steel due to chloride ions is still unknown. Some researchers [29] [30] proposed that the chloride ions can get preferentially adsorbed onto the steel surface in competition with dissolved oxygen and hydroxyl ions. The chloride ions then react at a faster rate with iron to form soluble complexes. This process suppresses the reaction
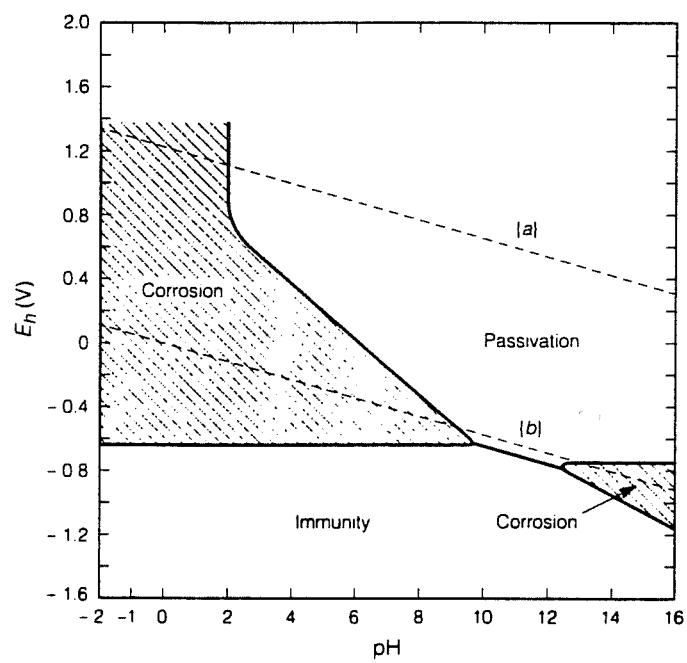
Fig. 1.1. Pourbaix diagram for iron with dissolved species
at activities of 10^{-6} g-equiv/L [22].

between iron and the passivating species, OH⁻, the formation of the passive film ceases (or chloride ions dissolve the film), and this leads to an increase in corrosion rate. Other researchers [28] [31] show that the chloride ions attack the film/substrate bond, but do not chemically dissolve the film. After the initial film/substrate bond is broken, pressure within the film forces the disbondment of the chemically unaltered film. The process expands the size of the depassivation site and accelerates the corrosion.

One important point that needs to be stressed is that the depassivation of steel in concrete by chloride ions is not necessarily due to the reduction of alkalinity, such as that caused by carbon dioxide. It is reported that chloride ions are able to cause depassivation even in high pH environments [29].

1.2.3 Corrosion-Induced Concrete Deterioration

When water, oxygen, and aggressive elements are able to enter the concrete by diffusion or through hairline cracks, they react to destroy the passivation of steel and severe corrosion takes place. The corrosion products of steel which occupy about 2.2 times the volume of the steel from which it formed will generate tremendous tensile stresses in the surrounding concrete and concrete often cracks. (The tensile strength of concrete is much lower than the compressive strength.) Once the concrete has cracked, the impact of vehicular traffic, the freezing of water within the cracks during cold weather, and the increased free access for deleterious chemicals accelerate the deterioration of the concrete [32].

1.2.4 Attempts to Solve the Problem

As we mentioned earlier, ECR has been a popular choice to deal with the corrosion problem of reinforcing steel in concrete, and its performance is the main concern of this research. However, other measures which have had some success in minimizing the problem have been proposed [33]. A concise list of some ideas is shown below for reference:

Means to prevent ingress of water and aggressive ions:

- using waterproof membranes topped with asphaltic concrete wearing courses;

- using latex-modified Portland cement mortar overlays;

- impregnating concrete with polymeric materials; and

- developing an internally sealed concrete using wax particles.

Means to protect the reinforcing steel:

- using corrosion inhibitors;

- galvanizing the reinforcing steel;

- performing cathodic protection; and

- neutralizing or removing the chloride ions from contaminated concrete.

1.3 The Epoxy Coating: Some General Information

1.3.1 Material

Epoxy materials have long been known for their excellent characteristics. Some of the most desirable features as a coating material are [34]:

- resistance to solvents and chemicals;

- low oxygen and chloride ion permeability;

- high electrical insulation;

- good mechanical strength;

- good heat resistance;

- ease of cure; and

- low shrinkage upon polymerization.

Epoxy, which refers to an epoxy system, generally consists of two main components, an epoxy resin and a curing compound. Besides, fillers, pigments, and flow control agents are usually added in various quantities to the epoxy.

Epoxy resins are fundamentally polyethers, but retain their name on the basis of their starting material and the presence of epoxide groups in the polymer before crosslinking. They are classified as thermosetting materials which will change irreversibly under the influence of heat from a fusible and soluble state into one that is infusible and insoluble through the formation of a covalently crosslinked, thermally stable network [35]. Upon full curing, they can retain their shape up to their decomposition temperatures. Moderate changes of service temperature will not readily cause a change in their physical properties [36].

The epoxy used for steel reinforcement coating is usually a bisphenol-amine formulation available in powder form [37].

1.3.2 Coating Process

A good quality coating material does not guarantee a good coating. Two major causes have been reported for failure in a coating system [32]: poor or inadequate surface preparation; and application of the coating under unsuitable atmospheric conditions or by inappropriate methods. These indicate that a proper

coating process is also crucial to the performance of a coating in resisting corrosion. A coating process consists of several major steps. A schematic for the whole process is shown in Fig. 1.2 [10] and the important aspects of each step are reviewed below.

Surface Preparation

The reinforcement surface must be carefully prepared to be extremely clean (near white) and with an optimum surface profile to ensure strong bonding between steel and epoxy. Usually, a rougher surface is preferred because it has larger surface area available for molecular bonding to the epoxy. However, if the surface is too rough, micro-peaks will be poorly covered by the coating and premature penetration of the film will occur, as illustrated in Fig. 1.3 [32]. Current specifications require the maximum roughness depth readings of the profile to be in the range of 1.5 to 4.0 mils (0.04 to 0.1 mm) for a suitable anchor pattern [38].

Grit blasting is the commonly used method to remove grease, dirt, corrosion product and scale from reinforcements. It can also be combined with a high pressure water spray or air jet to wash away all the debris, dust, and contaminants which would reduce the coating adhesion [32] [39]. A graded abrasive with certain shape, size, and hardness [36] must be selected for blasting to produce the desired surface profile.

After the surface is cleaned, the bare steel reinforcement is very susceptible to atmospheric corrosion. Therefore, those freshly cleaned reinforcements are usually preheated to a sufficiently high temperature, near 232°C, to remove moisture [40], and the application of epoxy should be
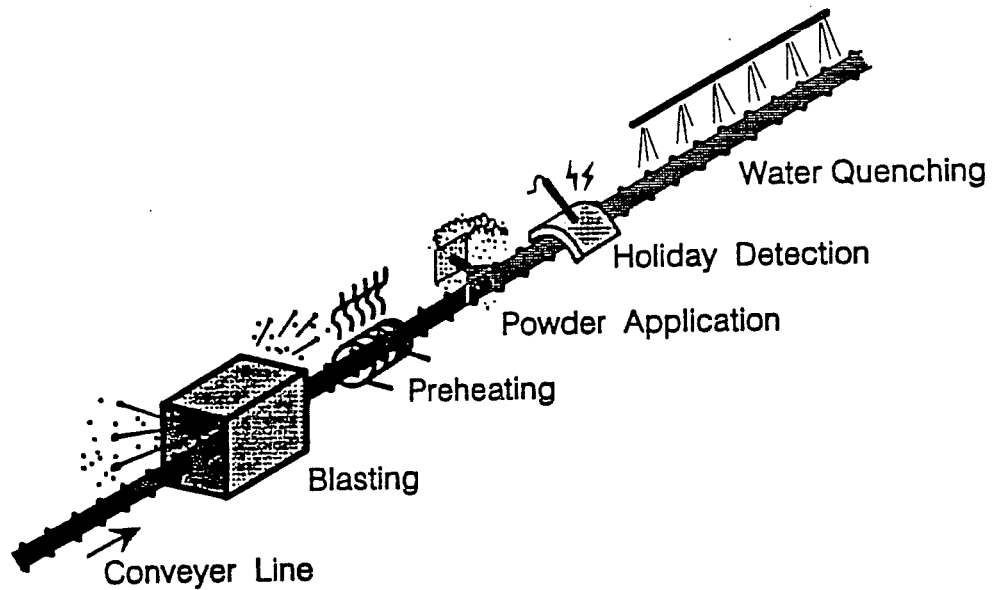
Fig. 1.2. Schematic of fusion-bonded epoxy coating process [10].
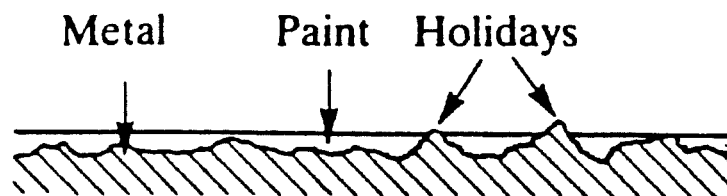
Fig. 1.3. Schematic showing the effect of substrate surface roughness
on paint thickness [32].

performed as soon as possible. ASTM specifications [38] permit delaying coating application up to 4 hours after cleaning.

Preheating

Properly preheating the steel reinforcement is important because the thermosetting process, a cross-linking reaction triggered by heating of epoxy, is temperature-dependent. The adhesion, flexibility, and performance of the cured epoxy coating is affected by the temperature of the steel substrate during the coating process [12] [36]. Underheating usually results in incomplete cross-linked networks and subsequently poor coating performance, while overheating will cause severe damage to the coating process, such as burning and blistering [10]. The optimum temperature for steel reinforcement at the entrance of coating station depends on the type of epoxy and generally lies between 232°C and 246°C [41].

Ovens or electrical induction coils are usually used for heating, and the temperature is monitored through an infra-red heat sensor or contact thermocouple [36]. To control the heat for a constant even temperature, the speed at which the reinforcement travels and the heat generated by the source need to be varied according to the mass of the reinforcement being heated. Small size reinforcements requiring less heat can travel at a higher speed, while large size ones requiring more heat need to travel at a lower speed [10].

Powder Application

Electrostatic spraying is one of the most common methods used to apply epoxy powder onto the steel reinforcement. In this practice, the epoxy powder is

charged and injected through an array of specially designed nozzles which connect with an electrode that provides a constant static charge of approximate 20,000 volts. The charged epoxy powder can then easily adhere onto the surfaces of the grounded reinforcements [36].

When the epoxy particles come in contact with the heated reinforcement, they melt instantly and flow over the steel surface. The liquid epoxy takes about 5 to 7 seconds to gel and further solidifies within 15 to 25 seconds [41]. The coating is gradually built up to the desired thickness with time being allowed between coats for the epoxy to cure. The pattern of spraying for each coat should be varied to ensure the entire surface is covered and any holidays (small holes in the coating) are sealed by subsequent coats [32].

After the coating solidifies, the coated reinforcements are conveyed on wetted, non-metallic rollers to the second curing phase [40]. Coating discontinuity should be checked through holiday detection at this point to make sure it is maintained within the specification allowable limits.

Water Quenching

After coating, water quenching is normally used to cool the reinforcements and provide the necessary thermal treatment for a fully cured finished coating [36].

At the beginning of the water quench area, the reinforcements are moved on the wetted, non-metallic rollers for about 30 seconds to allow slow curing. Cooling too fast may result in incomplete cure of epoxy [40]. There is no direct water spill at this stage because it may damage the semi-set epoxy coating [41]. In

the second cooling period, the reinforcements are brought under direct water spray to cool to the required handling temperature, typically around 95°C [36].

1.3.3 Requirements for Epoxy Coated Reinforcements

The primary function of epoxy coating is as a barrier-type isolator to prevent the steel from contact with oxygen, moisture, and chloride ions [32]. It offers corrosion protection to steel reinforcements in concrete by two main mechanisms: increasing the electrical resistance along the corrosion cell path; and retarding the cathodic reduction process [42]. The protection provided by a barrier coating can be remarkable based on adequate coating thickness, continuity, and adhesion, as well as the intrinsic properties of the coating material. ASTM specifications [38] set some requirements for ECRs to meet at the manufacturers plant prior to shipment. The key points are restated as follows:

(a.) Thickness of coating: At least 90% of all recorded thickness measurements of the coating after curing shall be 7 to 12 mils (175 to 300 μm). Thickness measurements below 5 mils (125 μm) shall be considered cause for rejection.

(b.) Continuity of coating: After curing, the coating shall be free of holes, voids, cracks, and deficient areas discernible to the unaided eye. With a $67\frac{1}{2}$ volts d-c holiday detector, there shall not be more than an average of two holidays per linear foot of the coated reinforcement.

(c.) Adhesion of coating: By bending production coated reinforcements at a uniform rate around a mandrel of specified size within a maximum specified time period, no cracking or disbonding of the coating shall be visible to the unaided eye on the outside radius of the bent reinforcement.

1.4 Outline of This Dissertation

Chapter 2 reviews some previous studies, both in the laboratory and in the field, regarding the performance of ECR. The exposure conditions, the methods of evaluating ECR performance, and the test results are briefly summarized. The goals of this research are then pointed out at the end of the chapter.

Chapter 3 narrates the methodology and procedure of this experiment. The specifications of materials evaluated, the configurations of specimens and cells, the exposure conditions, and the measuring periods are described in detail.

Chapter 4 introduces the techniques and the instruments applied in this study. The theories of various electrochemical methods and the practices for coating characterizations are summarized. In the final section, a detailed review of the application of electrochemical impedance spectroscopy (EIS) to evaluate ECR performance is given.

Chapter 5 presents the experimental results. Firstly, the representative electrochemical behavior determined from the overall test results is discussed in detail. Also, the correlation between results obtained through different electrochemical methods is explored. Secondly, the performances of various types of ECRs are ranked through EIS. These ECRs' performances are then correlated to their corresponding coating characteristics in order to find out the crucial factors affecting the overall ECR performance. Additionally, some photographs and micrographs are presented to help interpret the test results more clearly.

Finally, Chapter 6 draws conclusions from this work, and makes some recommendations for the ECR industry and for future studies.

Chapter 2

Literature Review on Studies of ECR Performance and Research Goals

The extensive use of epoxy coating on steel reinforcement began in the middle 1970's. Most of today's knowledge on ECR performance in corrosion protection was accumulated over the past 20 years. In this chapter we will first review some previous studies, including both field and laboratory ones, to get an idea about the trends and the needs for current research. The sequence of review is arranged according to the year of publication to provide an overview of the historical evolution of research in this field. The goals of this research will be pointed out at the end of this chapter.

2.1 Literature Review on Studies of ECR Performance

2.1.1 National Bureau of Standards (NBS); 1974 [12] [43]

Researchers at NBS performed an exploratory study for the FHWA to identify suitable organic coatings for corrosion protection of steel reinforcement in concrete. Altogether, 47 different commercially available coatings were evaluated. Items of evaluation included chemical resistance, chloride permeability, film integrity, coating adhesion, bond strength in concrete, abrasion resistance, electrical potential and resistance. It was concluded that fusion-bonded

epoxy coatings could provide the most satisfactory defense against corrosion. In addition, four types of epoxy resins were identified to be suitable for use in reinforced concrete construction. This study is a landmark in the ECR history and widespread use of ECR commenced afterward. Specifications and procedures for current quality control and inspection largely emerged from this work and are still greatly affected by it.

2.1.2 Oklahoma Department of Transportation; 1981 [40]

The Oklahoma DOT established a field monitoring system to study the durability of ECR under corrosive influence. The test site was on a rehabilitated bridge on I-35 in Noble county, Oklahoma. The performance of epoxy coating was monitored by electrical resistance measurement. A drop of resistance was considered as a signal of the onset of deterioration. The resistance data collected during the first nine months showed that the ECR was in stable condition within the concrete. This was an encouraging experience in the early stage of using ECR.

2.1.3 Federal Highway Administration; 1983 [13] [42]

The FHWA performed outdoor exposure experiments to evaluate the performance of two corrosion protection systems: the epoxy coating and the calcium nitrite admixture (a corrosion inhibitor). Uncoated reinforcement in plain concrete was also tested for comparison. All reinforced concrete slabs were fabricated to have the macrocell configuration which has a chloride-free bottom portion and chloride-contaminated top portion with the reinforcements in the two portions connected externally to allow electrical measurements. The corrosion

rate and corrosion activity of reinforcement were traced through measurements of corrosion current, half-cell potential, and electrical resistance for about two years. It was found that both ECR and calcium nitrite reduced the corrosion rate at least an order of magnitude relative to that of uncoated reinforcement in plain concrete. The difference in performance between ECRs with and without visible damage (although both had holidays) was not significant. The ECR was many times more resistant to corrosion than the uncoated reinforcement even if the coating did not meet the specifications.

2.1.4 Pennsylvania State University; 1987 [44]

Researchers at The Pennsylvania State University conducted a field study to evaluate the performance of ECR in concrete bridge decks in Pennsylvania after 10 years in service. Twenty two bridge decks, half of them constructed with ECR and the other half with uncoated reinforcement, were selected for evaluation. Visual inspection was the main approach and four bridge decks were thoroughly examined. Visual inspection found that none of the decks using ECR showed any sign of corrosion-induced deterioration while 40% of the decks using uncoated reinforcement were at the initial stage of deterioration. Moreover, detailed examination found that no corrosion occurred on ECR while extensive corrosion was seen on uncoated reinforcement. The results indicated that epoxy coating did provide very satisfactory corrosion resistance.

2.1.5 Pennsylvania Department of Transportation; 1988 [45]

The Pennsylvania DOT carried out a field study to compare several bridge deck corrosion protection systems which included coatings, concrete overlays, and waterproofing membranes. Totally 169 bridge decks were evaluated. Evaluation was based on visual inspection and measurement of half-cell potentials and electrical resistance in the field. In addition, 125 cores from 23 bridge decks were submitted for laboratory testing to determine the chloride content in concrete and concrete permeability. It was found that coatings, both fusion-bonded epoxy coating and hot dip galvanized coatings, provided the most effective corrosion protection. They performed well despite the high chloride contents in the concrete.

2.1.6 Florida Department of Transportation, 1988 [46] [47]

After the Long Bridge in the Florida Keys was reported to show signs of severe ECR corrosion in its substructure in 1986 after only 6 years in service, the Florida DOT conducted an investigation on the other bridges in that area. In 1988, the report revealed that significant corrosion of ECR occurred in four of the five major bridge substructures in the Keys. It was found that corrosion was limited to the splash zone, about 0.6 to 2.4 m above the mean water level. The corrosion was in an advanced stage and caused spalling only 7 to 11 years after construction. The chloride concentration was found to be unusually high at the reinforcement level, ranging from 3 to 11 $\frac{Kg}{m^3}$ with a typical value of 9 $\frac{Kg}{m^3}$. This was attributed to the high salinity of the seawater in the Florida Keys, which is 70% more saline than the normal ocean seawater, and the early concrete cracking found on those

substructures. Complete coating debonding was observed on ECR samples extracted from regions above the deteriorating splash zone. Visual examination indicated that corrosion may have initiated in the fabricated bars at bends and progressed to the straight portion. This result raised a lot of concerns about the effectiveness of epoxy coating and initiated a series of research investigations to reveal the causes of the unexpected ECR corrosion.

2.1.7 University of South Florida; 1989 [36] [48]

The University of South Florida conducted experiments to investigate the effect of fabrication on the performance of ECR in concrete prisms exposed to salt solution. The bent-after-coating and coated-after-bending ECRs were tested for comparison; straight ECR and uncoated reinforcement were also included in the study. Open circuit potentials were measured during the test and autopsies of the samples were done at the end of the tests. It was found that fabrication of the coated reinforcements led to reduction of coating adhesion, formation of cracks and holidays on the outer bend surfaces, and loss of corrosion resistance. Corrosion was more severe for ECRs fabricated after coating than for those coated after fabrication or for the unfabricated straight ones. However, even though coating defects tended to shorten the time for corrosion initiation, the corrosion on bent-after-coating ECR was still much less severe than that on uncoated reinforcement. Detailed examination of the coating indicated that defective sites could allow corrosion to initiate and advance beneath the coating.

2.1.8 University of South Florida; 1991 [49]

After four major bridges in the Florida Keys were reported to show severe deterioration in their substructures due to corrosion of ECR after 6 to 10 years of service, a study was conducted at the University of South Florida in 1988 to determine the key aspects of the mechanism of ECR corrosion in reinforced concrete used in marine substructures. Factors addressed included the causes of coating disbondment and the mechanism of corrosion progression. The causes of disbondment were investigated through immersion tests. Open circuit potentials were monitored throughout the exposure period and a peeling-off practice was performed after removal of the bars from the solution. The mechanism of corrosion progression was studied by placing ECR reinforced concrete columns in contact with sodium chloride solution to establish a macrocell; then measuring the macrocell current, half-cell potential, and concrete resistivity as a function of exposure time.

The results of immersion tests indicated that degradation of the coating due to weathering before placement in concrete may occur. The amount of debonding varied considerably from one product to another. Generally, the disbondment was proportional to the exposure time. After placement in simulated concrete pore solution which contained NaOH and $Ca(OH)_2$, the amount of debonding was found to be comparable for cases with and without the presence of NaCl. However, there was no corrosion product formation when NaCl was absent. This finding suggested that disbondment could occur under both cathodic and anodic conditions. After ECR was placed in concrete, cathodic disbondment was dominant before the arrival of chloride, however the amount of disbondment in

this period was not affected significantly by prior placement degradation. As chloride arrived at the ECR surface, the disbondment occurred under anodic conditions and the debonding could be significantly affected by prior placement degradation, such as damage and early corrosion encountered in the seaside construction yard. In macrocell experiments, it was found that corrosion currents took place in reinforced concrete columns built with ECR containing about 2% surface defects. It was inferred that prior degradation tended to facilitate cathodic reactions at the cathodic portion of the macrocell during early exposure because more surface under the debonded coating was available for oxygen reduction. However, the cathodic efficiency of ECR without prior degradation might increase later in the exposure period, approaching that of the pre-degraded ECR. Increases in cathodic efficiency set the stage for enhanced corrosion damage.

2.1.9 University of South Florida; 1994 [50] [51]

With their compelling laboratory finding that coating debonding might occur prematurely in concrete under both anodic and cathodic conditions, i.e. with and without chloride ions, concerns were raised about the ECR's susceptibility to similar deterioration in more than 300 bridges in Florida. The University of South Florida carried out a field investigation to determine the extent of this problem statewide. Over thirty bridges were subjected to detailed examination. The field activities included visual inspection as well as measurements of electrical continuity between reinforcement segments, half-cell potential, macrocell corrosion current, concrete resistivity, and polarization resistance. Laboratory tests of field specimens included evaluation of coating characteristics (thickness

and coating breaks), determination of the extent of coating disbondment and chloride penetration profiles.

The results indicated that there was severe corrosion of ECR in the substructures of bridges in the Florida Keys, while structures outside the Keys were generally corrosion-free. Extensive metal-coating disbondment was observed in virtually all structures whether or not significant chloride contamination existed at the reinforcement level. The structures showing corrosion tended to exhibit much higher chloride diffusivity and lower concrete resistivity than those constructed with modern concrete formulations. The important questions of the effect of coating disbondment and chloride concentration threshold on corrosion initiation were not resolved. A conclusion was drawn that the corrosion-related durability of those structures was primarily dominated by the concrete quality and cover thickness, and not necessarily due to the use of ECR.

2.1.10 University of Texas at Austin, 1994 [10]

Researchers at The University of Texas conducted a laboratory study to investigate the structural integrity of ECR in terms of coating damage on bent bars. Defects introduced prior to, during and after the bending operation were thoroughly identified and suggestions to prevent such damage were provided. The performance of ECRs damaged to various levels was evaluated through a three-part experimental program which included salt water immersion testing, macrocell study, and beam exposure study. The evaluation was done by visual characterization, measurement of corrosion currents and half-cell potentials, and

forensic examination. It was found that ECR in highly corrosive environments was susceptible to chloride-induced corrosion governed by the level of coating damage, the extent of coating disbondment, the degree of concrete consolidation around ECR, the concrete cracking, and the formation of macrocells. The larger the damage and coating disbondment, the higher the rate of corrosion. Patching the damage could reduce the incidence and severity of corrosion but could not prevent corrosion. Variations in concrete consolidation around ECR encouraged corrosion initiation and progression on surfaces facing voids in the concrete. Concrete cracking facilitated the ingress of chloride ions and oxygen and accelerated the corrosion process. Performance of ECR deteriorated progressively during macrocell development; electrical continuity between reinforcements exposed to different chloride environments promoted macrocell current development and corrosion. However, the use of epoxy coating did improve the performance of steel reinforcements in concrete exposed to aggressive chloride environments. It could delay the initiation of corrosion and the extent of concrete deterioration could be diminished.

2.1.11 Florida Atlantic University; 1995 [52] [53]

Aiming to understand better the influence of coating defects on ECR performance in aqueous environments and predict the long-term ECR service performance based on short-term (accelerated) laboratory tests, investigators at Florida Atlantic University performed a series of tests including short-term immersion in 80°C distilled water and 3.5% NaCl solution, and long-term outdoor exposure in concrete slabs with different wet-dry ponding cycles. ECRs from ten

different sources were evaluated. Coating performance was assessed during the course of exposure by electrochemical impedance spectroscopy (EIS) and defect characterization; and at the conclusion of exposure by adhesion testing.

It was found that the impedance decreased with exposure duration in essentially all experiments suggesting an increase in the corrosion rate. The magnitude of this impedance change was larger and the distinction between different specimens was more apparent in 3.5% NaCl solution compared to distilled water. In some cases the impedance reduction was associated with the development of defects; while in other cases the reduced coating pore resistance alone was considered responsible. The coating adhesion after hot water immersion and one day drying was less than the pre-exposure adhesion; and the adhesion loss was greater after immersion in hot distilled water compared to 3.5% NaCl solution. There was no correlation found between the adhesion and EIS results, indicating that separate mechanism(s) might control degradation in the two types of testings. Generally speaking, ECR without holidays and bare areas and with good wet adhesion could provide corrosion protection; however quantitative criteria for assuring such performance has not been adequately defined. A 24-hour hot water immersion test with qualification based upon achieving certain impedance values at an appropriate single frequency might have potential for being an in-plant ECR quality control practice.

2.1.12 Summary of Previous Studies

Early research generally addressed bridge deck construction. Both laboratory accelerated corrosion tests and field examinations indicated that the

performance of ECR was satisfactory. Since the corrosion observed was found to be very slight and of no concern, little damage morphology was given in terms of the coating characteristics, namely the adhesion, integrity, and thickness of coating. However, the absence of deterioration on the outer surface of the coating should not be considered as an indication that the epoxy film and the steel substrate were completely unaffected.

After the premature corrosion of ECR in the substructures of four major bridges in the Florida Keys was reported, debate was raised on how well epoxy coatings could function in severe corrosive environments and a better understanding of the mechanism of ECR corrosion was demanded. Current studies of ECR performance usually focus on the effect of coating damage, loss of adhesion, and underfilm corrosion. Electrochemical methods, especially EIS, which can monitor the corrosion behavior nondestructively during continuous exposure, are becoming more and more popular in these kinds of studies.

2.2 Research Goals

The first goal of this research is to make a comprehensive investigation of the corrosion behavior of reinforcing steel. Various types of specimens including polished reinforcing steel disks, uncoated reinforcing steel, and ECR will be tested. The tests will include continuous immersion in 3.5% NaCl solution, and exposure in concrete blocks with wet-dry ponding cycles.

The second goal is to survey the various methods commonly used in evaluating ECR performance. Measurements of corrosion potential, polarization resistance, EIS, and macrocell corrosion current will be performed in this work.

The meanings of results obtained through various methods, especially EIS, will be discussed in detail, and the correlation between them will be explored.

The final goal is to evaluate the performance of various types of ECRs. The effectiveness of ECR in preventing corrosion and the effects of various coating characteristics on ECR performance will be discussed. These results are expected to provide some suggestions on how to improve the ECR performance.

Chapter 3

Experimental Methodology and Procedure

3.1 Methodology

The main purpose of this study was to experimentally determine the crucial coating characteristic(s) affecting the ECR performance in preventing corrosion in saline corrosive environments. The exposure conditions in these laboratory tests were designed to be much more aggressive than those actually encountered in the field in order to accelerate the ECR deterioration and obtain information in a shorter time frame. Therefore, the test results do not necessarily signify that those failed ECRs are inadequate for service. Two types of exposures of ECR were used: the continuous salt solution immersion, and exposure in concrete blocks (macrocell specimens) which were subjected to periodic ponding with salt solution. Continuous immersion tests are the main focus of this work; while corrosion macrocell tests provide some supplementary information regarding the performance of embedded ECR in actual concrete. Experimental variables in the immersion test include the coating thickness, adhesion, integrity, and the fabrication (bending) on ECR. The details of these two tests will be described later.

The other important concern of this study was to find out the feasible and appropriate methods for quality control and for in-service performance evaluation of ECR. To attain this purpose, various techniques were applied, and efforts were

made to correlate the results obtained through different methods. The techniques and instruments applied in this work will be introduced in Chapter 4.

In addition to ECR specimens, some polished reinforcing steel disks and uncoated reinforcing steel were also subjected to immersion tests. The intention was first to provide a baseline for comparison of ECR performance, and also to make a comprehensive investigation of the corrosion behavior of reinforcing steel.

3.2 Materials Description

ECRs of varying sizes, obtained from three different coaters, using steel from four different steel mills, and coated with two types of epoxy powders were acquired for tests. The coaters were identified as A, B, and C; the steel mills were identified as a, b, and c; the epoxy powders were identified as # and *; and the bar sizes were either 4, 5, 9 or 10. These materials were identified by a designation composed of four indexing symbols. The first symbol represents the coater, the second one stands for the powder, the third one is assigned for the mill, and the fourth one is the size of the bar. Thus, as an example, A#a4 means an ECR of size no. 4, using steel from the mill designated a, and coated by coater A with the powder designated #. Nine types of combinations of ECR were tested in addition to black reinforcements b4, d4, and d10 and one with size no. 5 from another source which served as control materials. A list of these materials is shown in Table 3.1.

Reinforcement code	Quantity of straight specimens	Quantity of bent specimens (patched)
ECR A#a10	4 patched 2 not patched	
ECR A#a4	4 patched 2 not patched	2
ECR A#b10	2 patched 2 not patched	2
ECR A#b4	4 patched 2 not patched	2
ECR B*c9	4 patched 2 not patched	2
ECR B*c5	4 patched 2 not patched	2
ECR B*c4	4 patched 2 not patched	2
ECR C#d10	4 patched 2 not patched	2
ECR C#d4	4 patched 2 not patched	2
Uncoated reinforcement c4	2	
Uncoated reinforcement d10	2	
Uncoated reinforcement d4	2	

Table 3.1. List of test materials and bar specimens for immersion tests.

3.3 Specimen Preparation

In order to obtain preliminary information about the control materials, disks were cut from a size no. 5, grade 60 reinforcement meeting the ASTM specification A615 and machined (5/8" diameter and 1/8" thickness) to fit the commercial sample holder of a five-mouthed corrosion flask. The surface to be exposed was polished using abrasive papers of 240, 320, 400, and up to 600 grit. The samples were then ultrasonically cleaned in methanol, air dried, and immediately mounted for testing. Four disk samples were tested.

For the continuous immersion test. The as-received reinforcements, both uncoated and epoxy-coated ones, were cut into pieces of bar specimens with lengths around 12 cm using an abrasive saw. Both straight and bent specimens were prepared for ECRs. Caution was taken to avoid physical damage on the coating of ECR during the cutting process. At one end of the specimens, a hole was drilled and tapped in order to screw in an electric wire for electrochemical measurements; the other end of the specimens were sealed with a plastic cap filled with epoxy cold mount resin. The finished specimens were then cleaned with methanol. Some of the ECR specimens were further patched with 3M Scotchkote 213/215 Patch Compound over the defective and damaged sites, while the others remained in their as-received conditions. The quantity of specimens for each type of material is shown in Table 3.1, too. In all, there were seventy four bar specimens tested.

The test reinforcements for the macrocell corrosion study were ECR A#a4 and its uncoated form, a4. Reinforcing bars 50 cm long were bent 180° to represent the worst condition of fabrication on ECR. A hole was drilled and

tapped at one end of each bar for electrical connection during electrochemical measurements. The ECR specimens were not patched at the defective sites before being placed in concrete in order to allow fast development of corrosion. Six coated and four uncoated specimens were tested.

3.4 Pre-Exposure Coating Characterization

ECR specimens were visually examined for their coating defects, and were measured to determine the coating thicknesses before exposure. Two specimens from each type of ECR were subjected to adhesion testing to get their pre-exposure adhesion ranking, based on the peeling off exercise. Details of these coating characterization practices will be introduced in Chapter 4.

3.5 Electrochemical Testing during Exposure Period

3.5.1 Corrosion Cell Configuration

Cell for Immersion Tests

The polished reinforcement disks were mounted in an EG&G sample holder, which exposed an area of 1 cm², and immersed in a standard five-mouthed corrosion flask of 1000 ml capacity. A saturated calomel reference electrode and two graphite-rod counter electrodes were employed. The electrolyte used was 3.5% NaCl solution made of reagent grade sodium chloride crystals and distilled water. The flask and the sample holder accessories are shown in Fig. 3.1.

Thermometer

Gas outlet

Salt bridge
connection

Gas inlet

Auxiliary electrode
holder

Luggin-Haber probe

Working electrode

(a)

KIOS FLAT SPECIMEN HOLDER

O RING

TEST SPECIMEN

WASHER

SAMPLE
HOLDER
PLUG

O RING

SAMPLE HOLDER CAP

SAMPLE HOLDER BODY

(b)
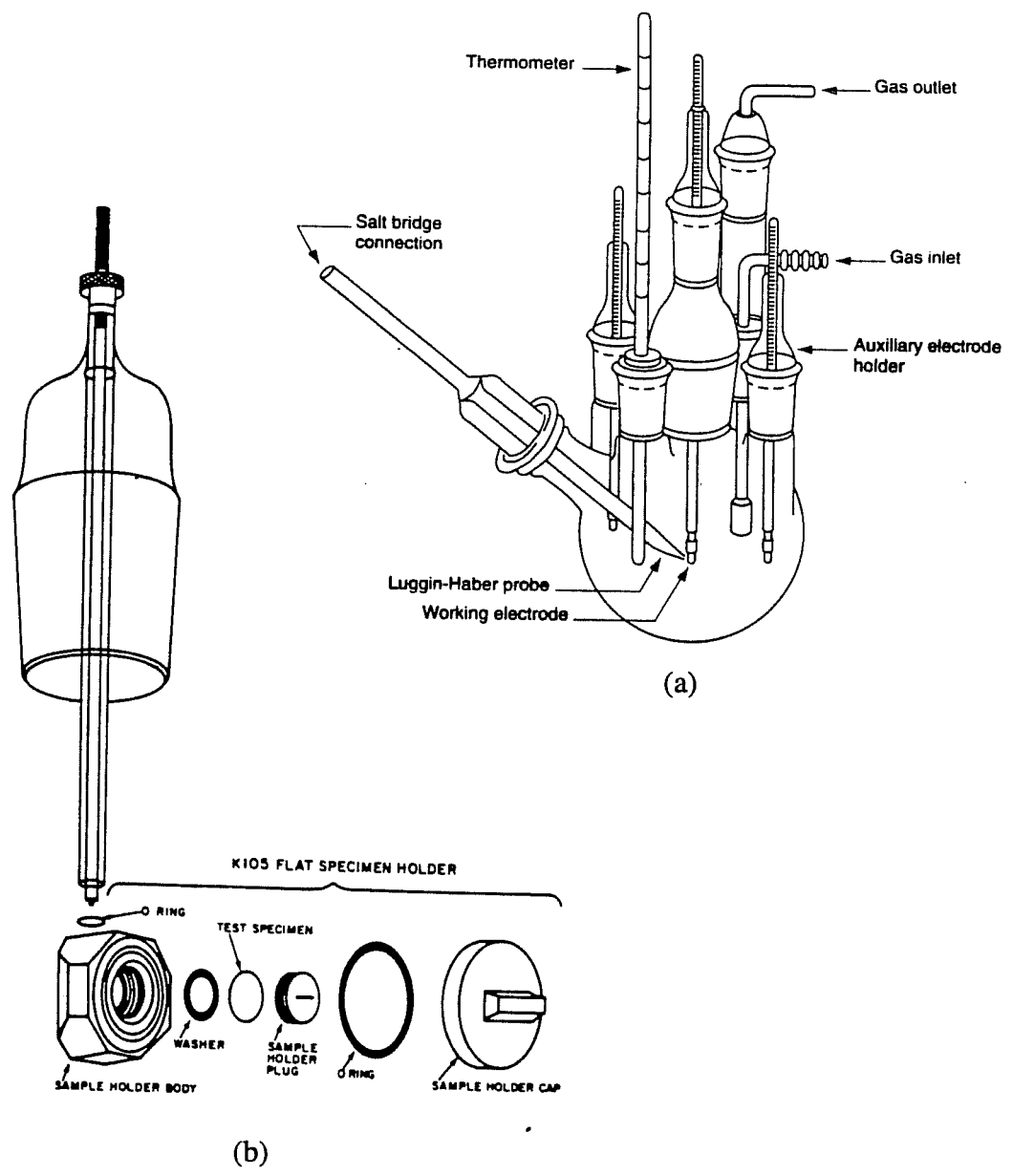
Fig. 3.1. (a) Standard corrosion flask used in testing polished rebar disks,
and (b) the exploded view of the specimen holder.

The bar specimens were immersed individually in one liter plastic containers with the electrolyte filled to cover 8 cm. The graphite counter electrodes and the calomel reference electrode with Luggin probe were placed around the specimens in a similar manner as in the standard cell used for coupon specimens, with the aid of a specially made apparatus stand. The electrolyte was also 3.5% NaCl solution. The configuration of this kind of cell is shown in Fig. 3.2.

Corrosion Macrocells

The bent test specimens were placed at the upper portion of the concrete prism. At the lower portion, two no. 6 uncoated reinforcement bars were placed to serve as the cathode. The composition of the concrete, on a 5 yd.^{3} basis, was 1350 lbs. of cement, 400 lbs. of fly ash, 7461 lbs. of sand, 9422 lbs. of 3/4" rock, 459 lbs. of water, and 53 ozs. of Pozz-R. The permeability of this concrete is considerably high and the chloride ions can diffuse fast through it. Also, a thin concrete cover, 1" thick, above the test reinforcement layer was used to reduce the time for chloride penetration. On the top of the concrete prism, an acrylic dam was built for ponding the 3.5% NaCl solution. A 100-ohm resistor was introduced externally between the two layers of reinforcement to provide a direct electrical link for the corrosion cell to operate and for the measurement of macrocell corrosion current. When performing electrochemical measurements, the resistor was removed temporarily, and the graphite counter electrodes and calomel reference electrode were placed inside the dam. The cathode reinforcement at the

Top view of the electrode holder

Counter electrode

Working electrode
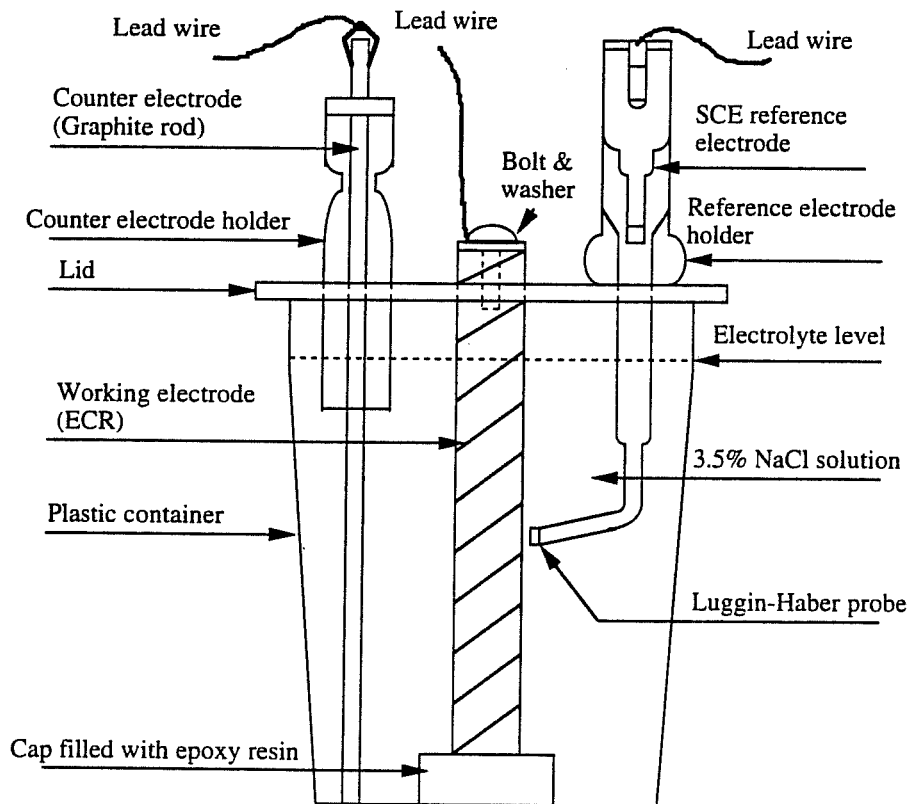
Reference electrode
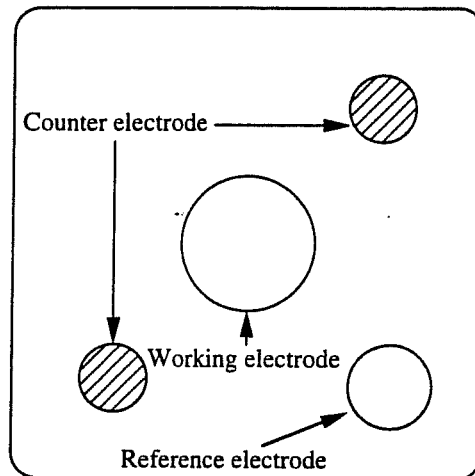
Side view of the corrosion cell

Lead wire   Lead wire   Lead wire

Counter electrode
(Graphite rod)   SCE reference
                                                 electrode
                              Bolt &
                              washer   Reference electrode
Counter electrode holder   holder

Lid

                                                 Electrolyte level

Working electrode
(ECR)
                                                 3.5% NaCl solution

Plastic container

                                                 Luggin-Haber probe

Cap filled with epoxy resin

Fig. 3.2. Configuration of corrosion cell used in testing bar specimens.
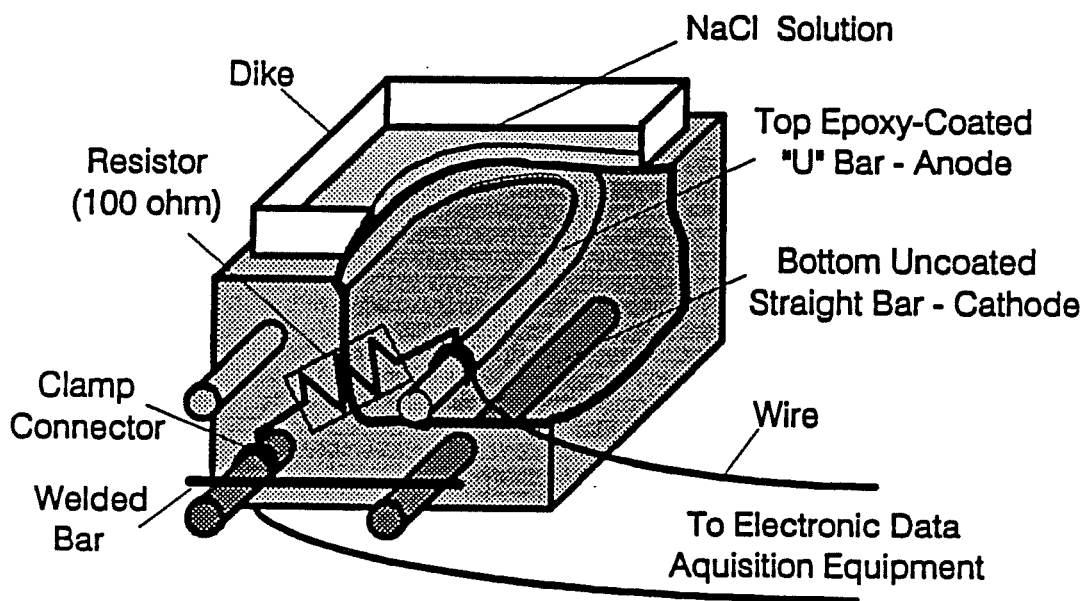
Fig. 3.3. Configuration of concrete block macrocell specimen [10].

lower portion did not function at this time. The configuration of a macrocell specimen is shown in Fig. 3.3.

3.5.2 Exposure Period and Measurement Interval

The disk samples were immersed for 10 days; and the measurements were carried out at 2, 12 hours, 1 day, and daily thereafter. The uncoated reinforcement specimens were immersed for 105 days with measurements performed at 4, 8, 16 hours, 1 day, 2, 4, 7, 10, 14, 18, 23, 28, 35, 42, 49, 63, 77, 91, and 105 days after immersion. The ECR specimens were immersed for 200 days and measurements were taken at 4, 8, 16 hours, 1 day, 2, 3, 5, 7, 11, 15, 20, 25, 30, 37, 44, 51, 58, 65, 72, 86, 100, 114, 128, 149, 170, 190, and 200 days after immersion. Very frequent measurements were carried out in the first week in order to monitor the possibly fast-changing coating pore resistance and the initiation of corrosion. The corrosion macrocells were subjected to two-week wet and two-week dry cycles. Measurements were performed, once every four weeks, at the beginning of the second week of ponding. These tests have continued for 10 months so far and are still ongoing.

3.5.3 Measuring Procedure

Corrosion potential, polarization resistance, and impedance measurements were performed on each sample at its scheduled time. The $E_{corr.}$ value was measured first, followed by the polarization resistance measurement, and then the impedance measurement. A fifteen minute delay period was allowed after the polarization resistance measurement was finished (before starting the impedance

measurement) in order that the specimen could return from the polarized condition back to its rest state.

The polarization resistance measurement was run between ± 20 mV with respect to the $E_{corr.}$ using a scan rate of 0.1 mV/sec. This experiment took about seven minutes. An impedance measurement actually consists of three independent measurements to cover a wide frequency range. One measurement applied with the Lock-in Amplifier (single-sine wave) technique was set to cover the range from 10 hertz to 100 kilo-hertz, with 8 data points obtained per decade of frequency. The other two measurements are based on Fast Fourier Transform (multi-sine wave) technique; one was run using a base frequency 0.1 hertz to cover the range from 0.1 hertz to 10 hertz, and the other was run using a base frequency 0.001 hertz to cover the range from 0.001 hertz to 0.1 hertz. Two data acquisition cycles were used for both measurements. All three measurements used sinusoidal voltage excitations with amplitudes of 15 mV, and were run at the specimen's open circuit potential. The data obtained from three measurements were merged into one curve for analysis. One complete measurement required about one hour and forty minutes. Frequencies lower than 0.001 hertz were not used because of the long times to complete the testing and the instability problems that might occur during data acquisition could become very serious.

For the corrosion macrocells, an additional measurement of the potential difference between the two layers of reinforcements was carried out before the electrochemical measurements.

3.5.4 Routine Maintenance on Corrosion Cell

Immersion cells were checked every three days for their electrolyte levels and replenished with distilled water to keep the solution at a fixed height. The screws securing the electric wires were checked for signs of corrosion due to the moisture; any suspected one was replaced by a new one immediately. For the corrosion macrocells, loose fitting covers were used to minimize evaporation during the ponding period and distilled water was added if necessary. After the wet period, solution was vacuumed out of the dam, and the dam was rinsed twice with distilled water to clean the residual NaCl. The portions of the reinforcements, both anode and cathode, that protrude out of the concrete prism were greased every two weeks to prevent undesired corrosion.

3.6 Post-Exposure Analysis

At the conclusion of immersion tests, specimens were removed from solution and air dried. The ends of the bar specimens were examined for signs of corrosion. The electrochemical measurements for bar specimens with corrosion found at their ends are considered suspicious and were discarded. The specimens were then stored in a vacuumized desiccator awaiting further analyses. Later on, the corrosion products on specimens were removed with a soft paintbrush and collected for x-ray analysis. The ECR specimens were then visually examined for their coating deterioration. Photographs were taken for every specimen, particularly the corroded sites. Adhesion tests were performed on every ECR specimen to get the post-exposure adhesion ranking using the practice that will be described later. Finally, microscopic examination was done to examine the corroded region, the coating surfaces, and the cross-sections of bar specimens.

Chapter 4

Testing Methods and Instrumentation

In this chapter, the techniques and equipment used in this study are introduced. They are functionally classified into three categories:

- coating characterization;

- electrochemical measurements; and

- corrosion morphology analysis.

We will review the principles and instrumentation of each method first. In the last section of this chapter, a detailed review regarding the application of electrochemical impedance spectroscopy (EIS) to the study of coating performance is given.

4.1 Coating Characterization

4.1.1 Thickness Measurements

The test method for nondestructive measurement of film thickness of pipeline coatings on steel described in ASTM G12 is applied here [38]. A calibrated "Mikrotest" magnetic gage is used to measure the coating thickness. Its accuracy is within $\pm$ 10% of the true thickness of the coating. A number of readings are taken on one site and then averaged for better accuracy. The thickness of the coating is measured on the body of a straight portion of ECR

between the deformations or ribs. Every single recorded thickness is the average of three individual readings obtained between three consecutive deformations. In some cases where the magnetic gage may not yield reliable results, such as when the surface is too rough, a microscope can be used to observe the ECR cross-section to determine the coating thickness. Thickness measurements were performed on the as-received specimens prior to immersion.

4.1.2 Integrity Examination

Coating integrity was characterized mainly by visual examination. The types and number of defects on as-received ECR were recorded. Photographs for every sample prior to exposure were taken as a record. In some cases, an optical microscope was used to observe the micro defects on coatings. A Nikon 8008 camera with a 60 mm micro lens was used to take pictures, and a Nikon optical microscope mounted with a polaroid camera was used to obtain optical micrographs.

4.1.3 Adhesion Test

The method to evaluate coating adhesion on ECR is the "peeling off test". This test is not a part of the current standard specifications for ECR but has been used with coated pipes. It requires cutting an "X" through the coating between deformations with a sharp knife, as shown in Fig. 4.1. The coating is then peeled off by exerting a fixed force on the knife blade tip against the sheared coating and performing a levering action. An "X-ACTO" No.2 knife with #23 double edge blade is used for this practice. For each specimen, three tests are conducted to get
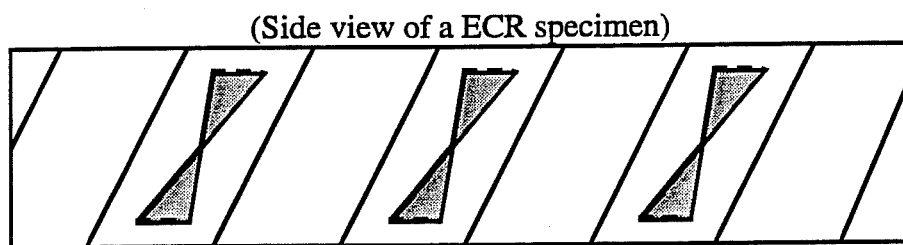
Fig. 4.1. Locations for adhesion testing.
(Levering action is performed on the six shadowed regions)

the average state of adhesion. Coating adhesion rating is evaluated by assigning a numerical value according to the following test conditions:

- Rank 1: Unable to insert blade tip under the coating;

- Rank 2: Blade tip can be inserted under the coating; levering action only removes small chips of coating around the center of the "X" cut;

- Rank 3: Blade tip can be inserted under the coating; levering action removes about half section of coating between the lines cut into the coating;

- Rank 4: Blade tip can be inserted under the coating; levering action removes the whole section of coating between the lines cut into the coating;

- Rank 5: Blade tip slides easily under the coating; coating is peeled back outside the lines cut into the coating without any resistance.

Adhesion test was performed on both as-received and post-exposure specimens to determine the influence of exposure on coating adhesion.

4.2 Electrochemical Measurements

4.2.1 Corrosion Potential (E_{corr}) Measurement

The corrosion potential, or the rest potential, of the working electrode (i.e. the specimen) is always measured relative to a reference electrode. In this study, a saturated calomel electrode (SCE) is used. The measured potential has long been used as an indication to the corrosion activity of steel reinforcement in concrete. Even though many criteria have been proposed to interpret this potential, a strict interpretation is difficult. Two versions of the criteria are given in Table 4.1 [54] and Table 4.2 [55]. Recent studies, however, have raised some doubts using these

$E_{corr.}$(V vs Cu/CuSO$_4$)	Probability of Corrosion
> -0.20	< 5%
-0.20 to -0.35	~ 50%
< -0.35	> 95%

Table 4.1. Interpretation of corrosion potential measurements [54].

$E_{corr.}$(V vs SCE)	Condition of Steel
> -0.22	Passive
-0.22 to -0.27	Active or Passive
< -0.27	Active

Table 4.2. Interpretation of corrosion potential measurements [55].

criteria. One case [56] showed that specimens cracked when $E_{Corr.}$ was only -230 mV vs. SCE; while in the other case [57] reinforcement was in good condition with an $E_{Corr.}$ value about -600 mV vs. SCE. The use of $E_{Corr.}$ along with other test results is thus preferred.

4.2.2 Polarization Resistance Measurement

This method originated from experimental observations [58] [59] that the degree of polarization (ε) at a given applied current ($i_{app.}$) was greater for a lower corrosion rate, and that there was a linearity at the origin of the polarization curve for overvoltages up to a few milli-volts. The slope of this linear curve is thus inversely proportional to the corrosion rate. The measurement based on the above concept is performed by applying a controlled potential scan over a small range, typically $\pm$ 20 mV with respect to $E_{corr.}$. The necessary current applied at each scanning potential is recorded. The data are then correlated to the polarization resistance and corrosion current by the derived equation [60]:

$$\left[\frac{d\varepsilon}{di_{app.}}\right]_{\varepsilon \to 0} = \frac{\Delta\varepsilon}{\Delta i_{app.}} = R_p = \frac{\beta_a \beta_c}{2.3 i_{corr.}(\beta_a + \beta_c)}$$

where β_a and β_c are the anodic and cathodic Tafel slopes respectively. The Tafel slopes can be accurately determined by conducting polarization tests on two separate specimens. However, approximate values of $\beta_a = \beta_c = 0.1$ volt are usually used because the constant error in calculating the corrosion rate based on them is only a factor of two maximum [61] and this is often within experimental

scatter in corrosion measurements [62]. A typical polarization resistance plot is shown in Fig. 4.2.

The equipment used for this measurement is an EG&G Model 273 Potentiostat/Galvanostat connected to an IBM PC-XT. The measurement, calculation, and plotting are executed through EG&G's Model 342c controlling software.

4.2.3 Electrochemical Impedance Spectroscopy (EIS)

With the development of modern electrochemical theory of aqueous corrosion, a corrosion cell can be represented by a purely electronic model. For example, the interface of a corroding electrode during a corrosion process is analogous to an electronic circuit consisting of an array of resistors and capacitors. This allows the researcher to apply well established circuit theory to characterize the corrosion system in terms of its "equivalent circuit". Of particular significance is the well-developed branch of alternating current (AC) theory concerned with the response of a given circuit to an alternating current or voltage as a function of frequency [63].

This technique includes applying small amplitude sinusoidal voltages to the working electrode over a wide frequency range and analyzing its response by impedance spectroscopy. Two measurement techniques are used to cover the wide frequency range: the Lock-In Amplifier (LIA) technique is used at frequencies above 1 hertz to provide the highest accuracy while the Fast Fourier Transform (FFT) technique is used for frequencies from 0.1 milli-hertz to 10 hertz to solve the long measurement time problem at low frequencies. The time-dependent
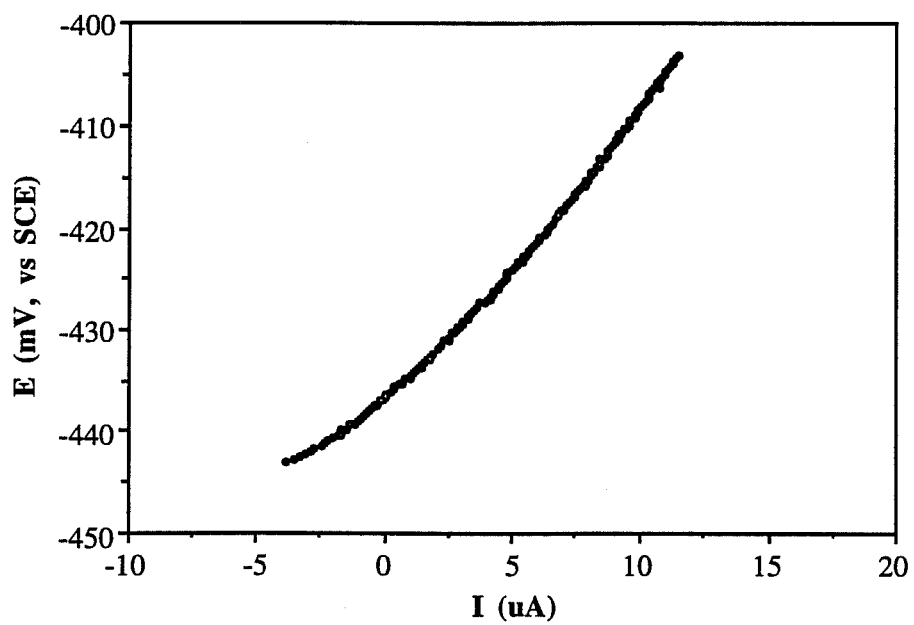
Fig. 4.2. A typical polarization resistance plot.

current response I(t) of an electrode surface to a sinusoidal alternating potential signal V(t) has been expressed as an angular frequency (ω) dependent impedance $Z(\omega)$ [64]:

$$Z(\omega) = \frac{V(t)}{I(t)} \quad \text{while} \quad V(t) = V_0 \sin \omega t \quad \text{and} \quad I(t) = I_0 \sin (\omega t + \theta)$$

where t is time and θ is the phase angle between V(t) and I(t). The above waveform expressions for Z, V, and I can also be expressed in terms of complex numbers through vector analysis and the impedance at each specific frequency is then expressed as:

$$Z = \frac{V' + V''j}{I' + I''j} = Z' + Z''j \quad \text{or}$$

$$|Z| = \sqrt{(Z')^2 + (Z'')^2} \quad \text{with} \quad \tan \theta = \frac{Z''}{Z'}$$

Once an experiment is complete, the raw data at each measured frequency consist of V', V", I', and I". From this data it is possible to compute Z', Z", |Z|, and θ for every applied frequency. A variety of formats can be used to plot these impedance results and each format provides specific advantages for revealing certain characteristics of a given system. The two most used plots for corrosion study [63] are the Nyquist plot and the Bode plot. The Nyquist plot is also known as a Cole-Cole plot or a complex impedance plane diagram with the imaginary component of impedance, Z", plotted versus the real component of impedance, Z', for each excitation frequency. The Bode plot actually consists of two plots with

the logarithmic value of absolute impedance, $\log |Z|$, and the phase angle of the resultant waveform, Θ, each plotted versus the logarithm of their corresponding excitation frequency separately. Examples of these two types of plots are shown in Fig. 4.3 and Fig. 4.4. The interpretations of these plots will be discussed later in this chapter.

The impedance measurement system used includes an IBM PC-XT, EG&G's Model 273 Potentiostat/Galvanostat, and Model 5301A Lock-In Amplifier (with a Model 5315 Two Channel Preamplifier). The measurement, data manipulation and display, file management are all executed through the EG&G Model 378 controlling software.

4.2.4 Macrocell Current Measurement

This measurement originated from the ASTM standard G 109-92 for determining the effects of chemical admixtures on the corrosion of metals in concrete [65]. It is known that in an electrochemical corrosion process, the availability of a cathodic area drives corrosion at anodic sites when there is electrical continuity between anode and cathode. A macrocell is established based on this concept by placing reinforcements in two different portions of the same concrete, one layer in a chloride rich zone as the corroding anode and the other in low chloride zone as the cathode. A direct measure of the macrocell current (the electrons released by the corrosion process) is obtained by measuring the voltage drop across a known resistance bridged between the two reinforcement layers. The higher the voltage measured, the higher the corrosion current at the constant circuit resistance. The measured current is considered as an indicator of the
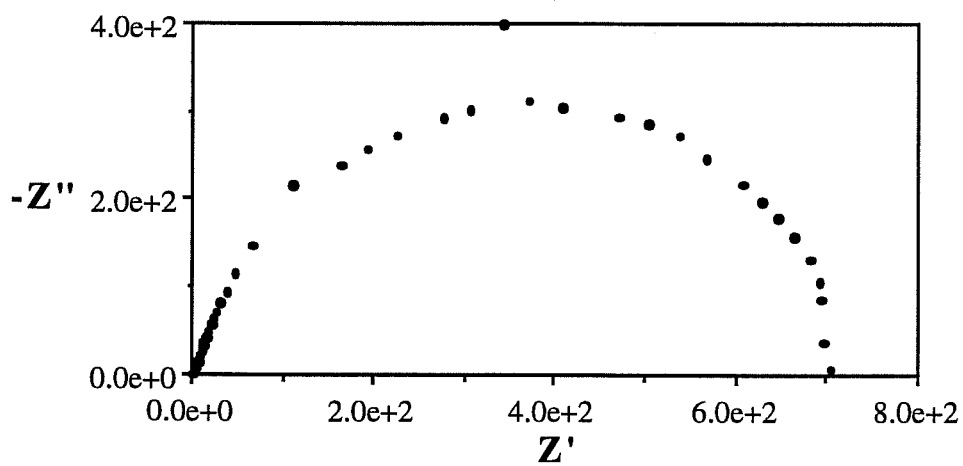
Fig. 4.3. A typical EIS Nyquist plot.
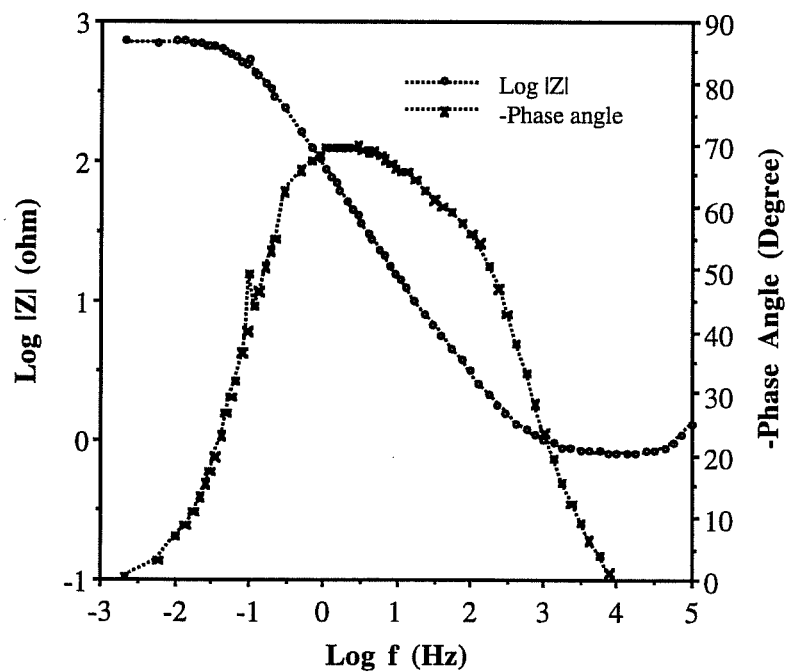
Fig. 4.4. A typical EIS Bode plot.

metallic iron lost during the corrosion process [66]. However, the accuracy of the results should be questioned if the corrosion rate is very low, and if both connected metals are corroding [67].

The equipment used for this measurement was a high impedance voltmeter (at least one Mohm) capable of measuring to 0.01 mV; specifically a Model DM-8700 Digital Multimeter from A.W. Sperry Instruments Inc.

4.3 Corrosion Morphology Analysis

4.3.1 Visual Examination

Visual examination was made to observe the outer appearance change of specimens at the end of exposure. Photographs for every sample and close-up views of the deteriorated sites on the coatings were taken as a record. A Nikon 8008 camera with a 60 mm micro lens and an extension tube were used to take pictures.

4.3.2 X-Ray Powder Diffraction

The corrosion product, if any, was analyzed by x-ray powder diffraction to determine the constituents. Finely ground corrosion products were exposed to monochromatic Cu K_a radiation; the intensities of diffracted beams at various diffraction angles were detected with a counter mounted on a rotating stage which moved at constant angular velocity. The diffraction pattern, a plot of diffracted intensity versus diffraction angle, was used to identify the constituent elements

and/or compounds through indexing the Powder Diffraction File. A Model 1729 Diffractometer from Philips Electronic Instruments Inc. was used.

4.3.3 Microscopic Observation

The corroded regions and cross-sections of the ECR specimens were examined by means of a scanning electron microscope (SEM). Microscopic observation was performed to observe the morphology changes of the coating and the steel substrate due to exposure and corrosion. Information from this may help us interpret more clearly the data from previous tests. A JOEL JSM-35C Scanning Electron Microscope system was used to get secondary electrons and/or back scattered electron images of the corroded sites and the cross-sections.

4.4 Review of Previous EIS Studies on Corrosion

EIS, when applied to the study of electrochemical systems, can provide a wealth of kinetic and mechanistic information [63]. This advantage comes from the use of an equivalent circuit to represent the electrochemical system. With a proper physical model and its corresponding electrical circuit, one can analyze the system being tested into its component elements and calculate the value of each element in the circuit. For this reason, EIS is becoming a very popular technique for both qualitative and quantitative studies of corrosion. However, EIS is also a very sophisticated technique and its interpretation is often very complicated since a system may be represented by a number of equivalent circuits. In the following, we will review the two most popular equivalent circuit models related to this study, along with approaches for obtaining circuit component values from the

corresponding impedance plots. Some important findings from previous works, numerical and experimental, regarding the use of EIS are also included.

4.4.1 Modeling of Corroding Systems

Corrosion of Uncoated Metal

The corrosion process at a metal surface is basically a charge transfer reaction. The anodic reaction releases electrons while the cathodic reaction consumes them. The corrosion rate is thus controlled by the ability to exchange electrons. Besides, during the above process, while the metal is in contact with the aqueous solution, an interfacial structure of separated charge forms, and this is commonly referred to as the electrical double layer, as shown in Fig. 4.5 [62]. This metal/solution interfacial structure behaves experimentally like a charged capacitor that will prevent easy charge transfer, thereby limiting the corrosion reaction at the metal surface. In sum, the corrosion reaction at the metal surface is controlled by the parallel effects of the charge transfer process and the double layer structure.

With knowledge of the above physical phenomena, the equivalent circuit of the uncoated metal/solution interface can be drawn as in Fig. 4.6. R_Ω is the uncompensated resistance between the working electrode and the reference electrode; R_{ct} is called charge transfer resistance which represents the corrosion resistance of the metal; and C_{dl} represents the double layer capacitance at the interface. The corresponding Nyquist and Bode plots of this circuit are shown in
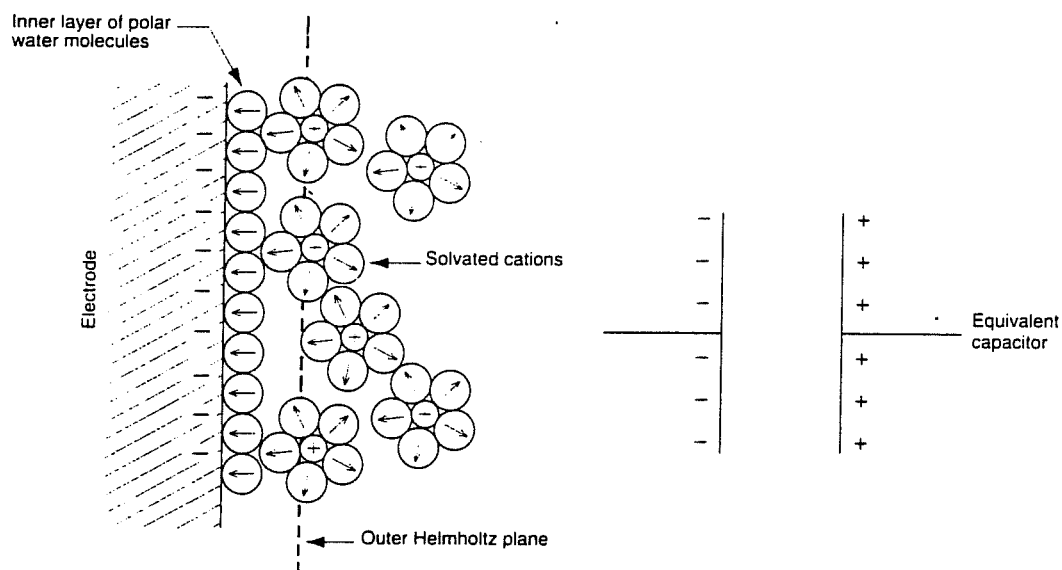
Fig. 4.5. Schematic electrode surface structure and its equivalent electric capacitor (i.e. electrical double layer) [62].
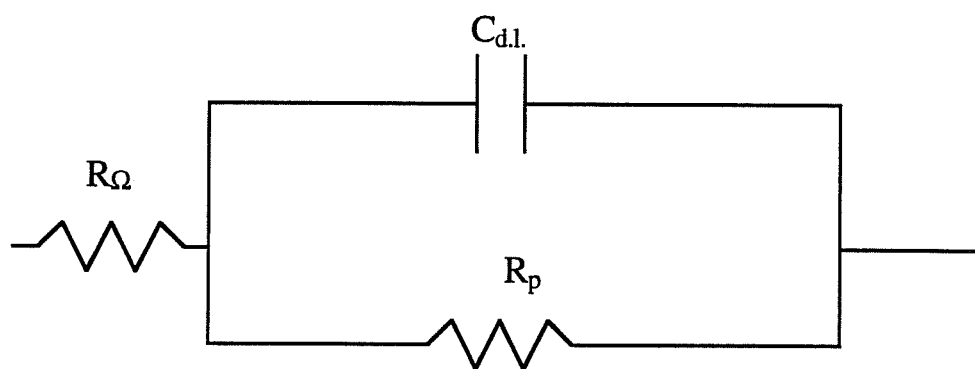
Fig. 4.6. Equivalent circuit model for a simple corroding system. (R_Ω electrolyte resistance; R_p polarization resistance or charge transfer resistance; $C_{d.l.}$ double layer capacitance)

Fig. 4.7 and Fig. 4.8, with the approaches to extract the circuit component values marked on them for direct reference [68].

Corrosion of Coated Metal

For a coated metal, the model of the interface requires incorporation of the coating parameters into the uncoated metal case mentioned above. Several models are described in the literature [37] [68] [69]. The one proposed by Epelboin et al. [69], slightly modified by the inclusion of a diffusion impedance term, is most observed and is chosen to interpret the impedance plots in this study. A sketch of the metal/coating/solution interface together with its equivalent circuit are shown in Fig. 4.9 [70]. R_Ω, R_{ct}, and C_{dl} were defined in the preceding paragraph. In addition, R_{cp} is the pore resistance which represents the resistance of areas on the coating where more rapid solution uptake occurs. Possible regions are holes and porous areas which may pre-exist or develop with immersion as corrosion proceeds. Corrosion of the substrate metal is assumed to take place via these areas by the same mechanisms that occur on uncoated metal. C_c is the capacitance of areas where the coating remains intact (no solution uptake) during immersion. Z_w is called the Warburg impedance which accounts for diffusion processes within the coating film. The corresponding Nyquist and Bode plots of this circuit, with Z_w ignored, are shown in Fig. 4.10 and Fig. 4.11 [68]. The effect of Z_w on the plot shape will be discussed in the next paragraph.
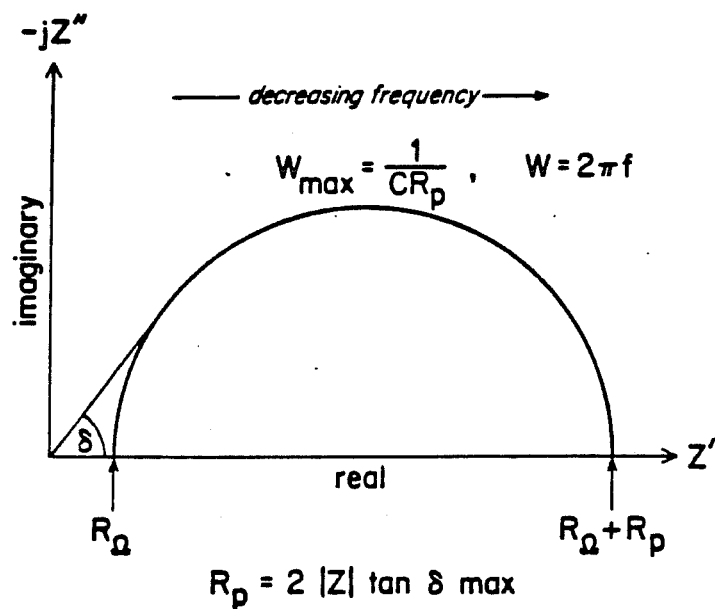
Fig. 4.7. The corresponding EIS Nyquist format of Fig. 4.6 [68].
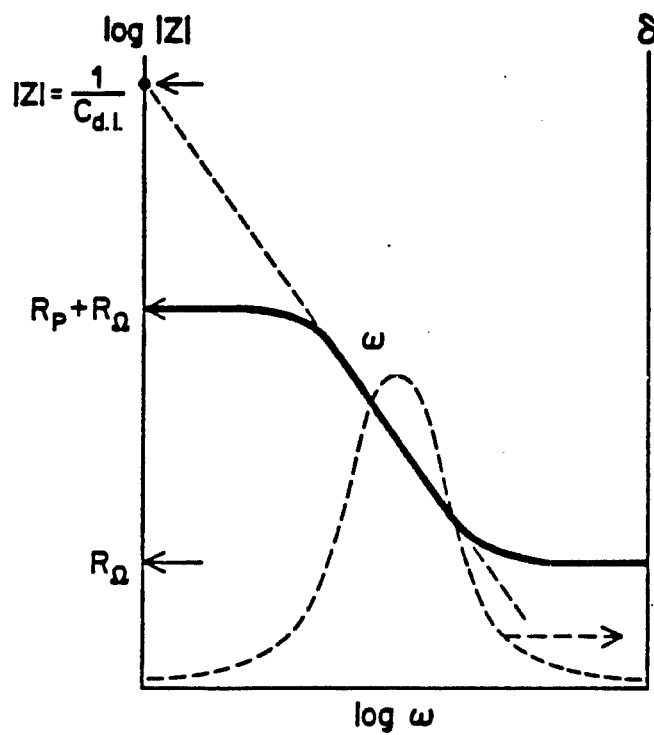
Fig. 4.8. The corresponding EIS Bode format of Fig. 4.6 [68].

(a)

(b)
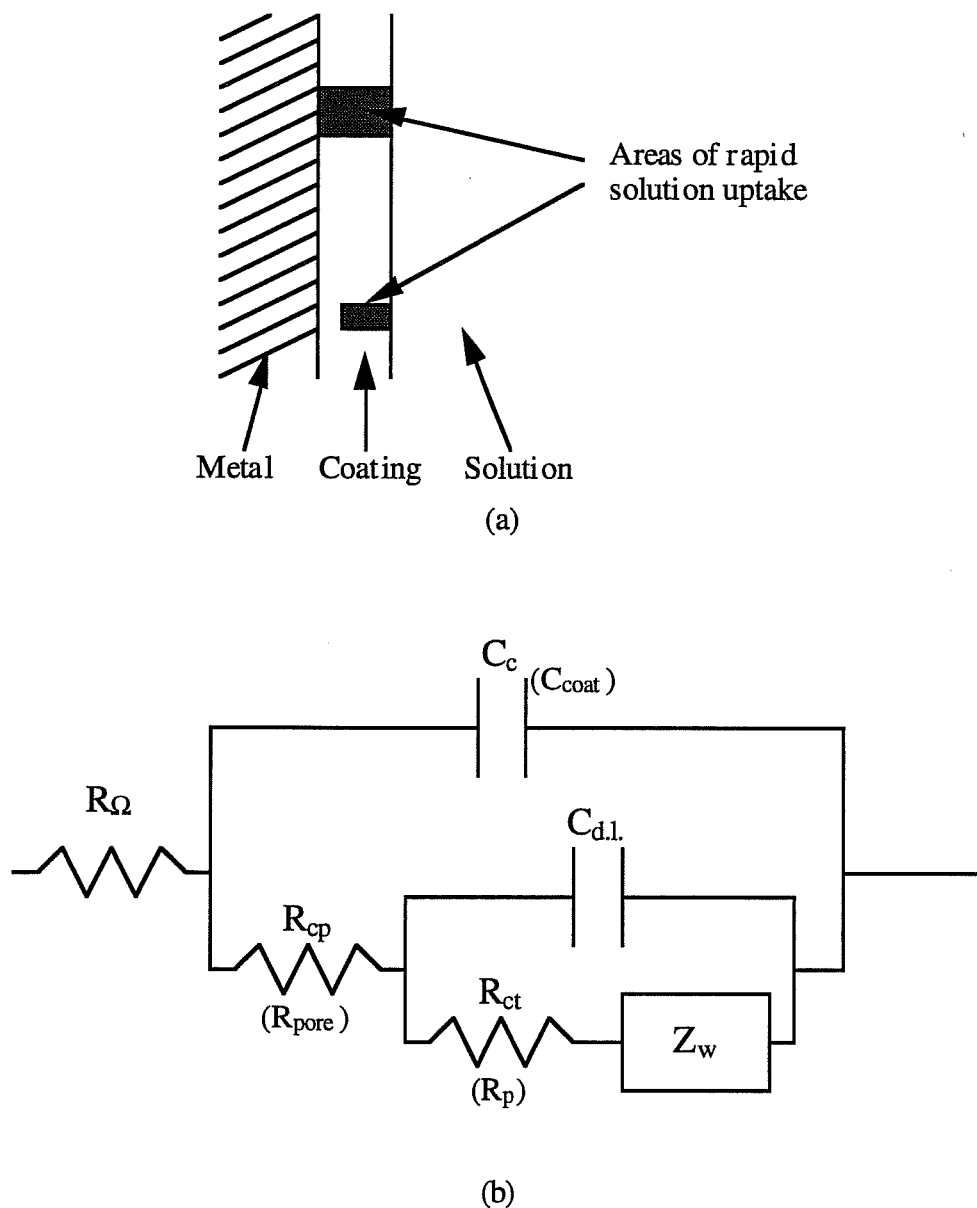
Fig. 4.9. (a) Physical model of the coated metal / solution interface, and
(b) its corresponding equivalent circuit model [70].
(R_Ω, $C_{d.l.}$, R_{ct} or R_p as defined in Fig. 4.6; R_{cp} coating pore resistance;
C_c coating capacitance; and Z_w Warburg diffusion impedance)
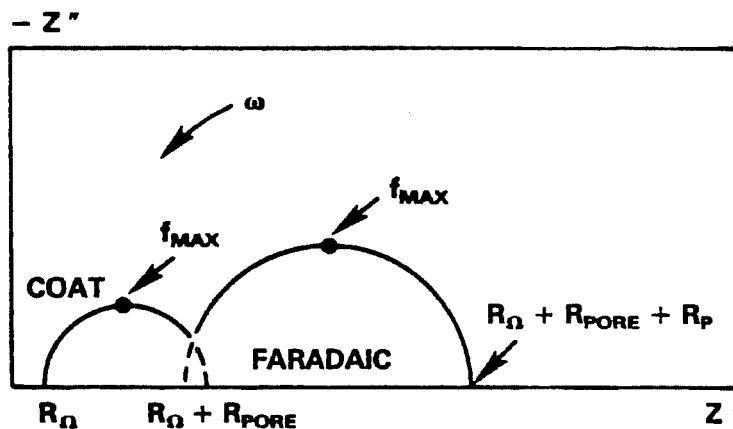
Fig. 4.10. The corresponding EIS Nyquist format of Fig. 4.9
in the absence of diffusion [68].
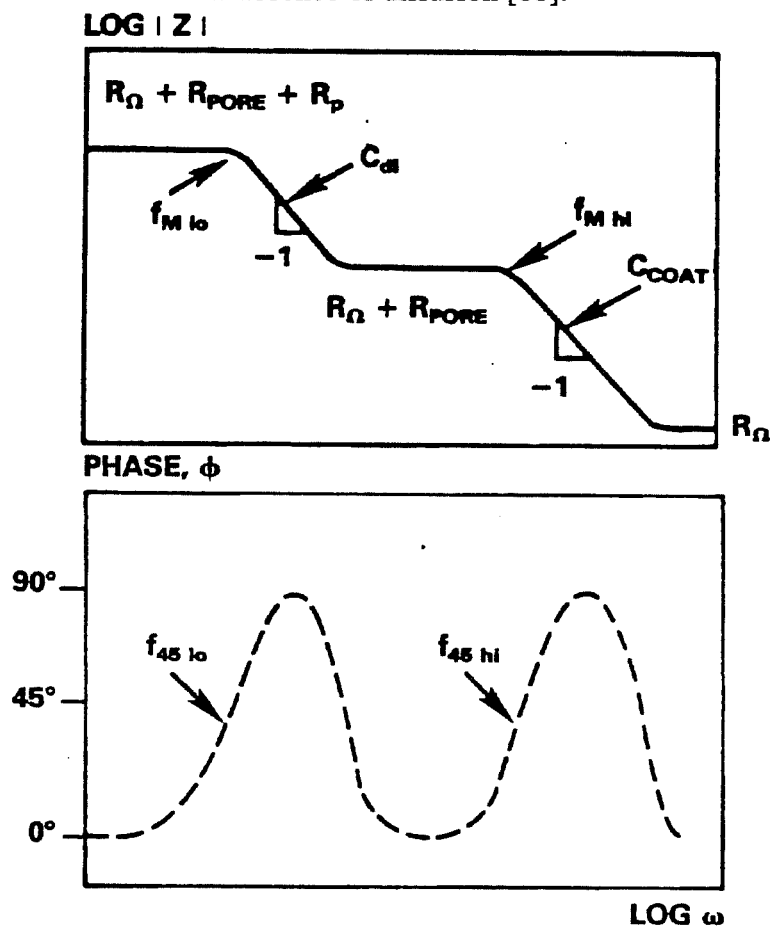
Fig. 4.11. The corresponding EIS Bode format of Fig. 4.9
in the absence of diffusion [68].

4.4.2 Numerical Simulation

Some researchers [68] [70] [71] [72] have tried to simulate the above theoretical impedance responses by computation methods. Different values of the equivalent circuit components for dummy corrosion cells were input into the computer program in order to investigate their effect on impedance plots. The results indicated that the responses for uncoated metal systems, which have only one time constant, fit the theoretical plots very well; however ambiguities were introduced for the coated metal systems which have more than one time constant. First, it was found that the two semicircles in the Nyquist plot can be distinguished only if their diameters are not too different, with a criterion $0.2 \le (\frac{R_{ct}}{R_{cp}}) \le 5$, and their time constants are not too close, with criteria $\frac{\tau_{ct}}{\tau_{cp}} \ge 20$ or $\frac{\tau_{ct}}{\tau_{cp}} \le 0.05$ where $\tau_{ct} = R_{ct}C_d$ and $\tau_{cp} = R_{cp}C_c$. The examples for these situations are shown in Fig. 4.12 [68]. Secondly, with the presence of the Warburg diffusion impedance, Z_w, the curve shape at the low frequency end of the Nyquist plot will deviate from the original charge transfer semicircle. It then depends on the two competitive controlling mechanisms of corrosion rate, i.e. charge transfer control and diffusion control. A demonstration for some possible curve shapes is shown in Fig. 4.13 [70]. It was noted that these are not the only shapes that have been obtained experimentally, but rather a reasonable cross-section representing the plot shapes where some success in analysis has been achieved. From these, we know the real impedance response of a coated metal system might be much more complicated than the theoretical case introduced in the preceding section, and extreme care is necessary in interpreting the impedance
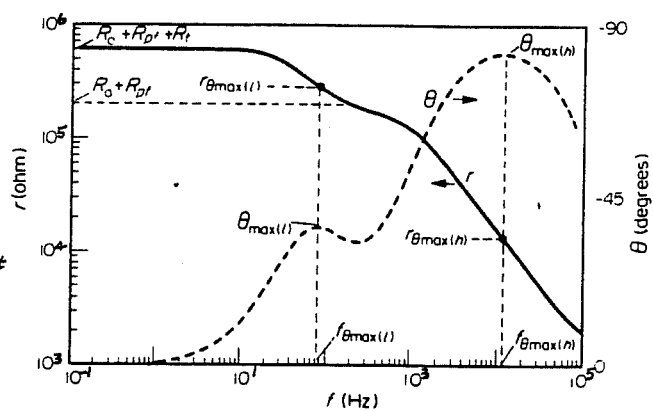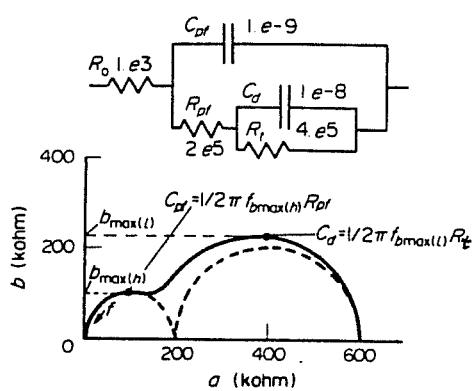
(a)
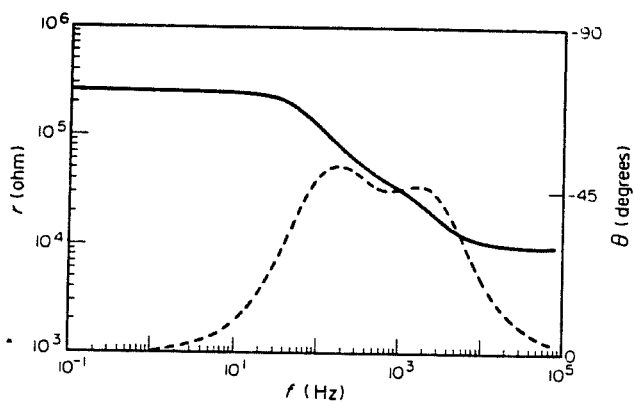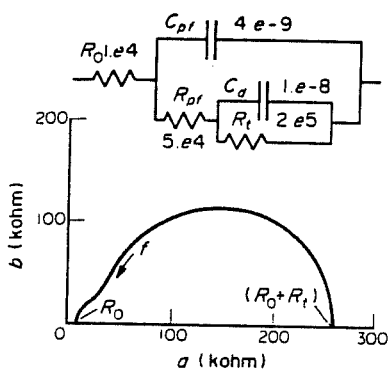
(b)

Fig. 4.12. Examples of EIS responses for the coated metal / solution interface in the absence of diffusion showing (a) clear separation and (b) indistinct separation of coating and metal components [68].
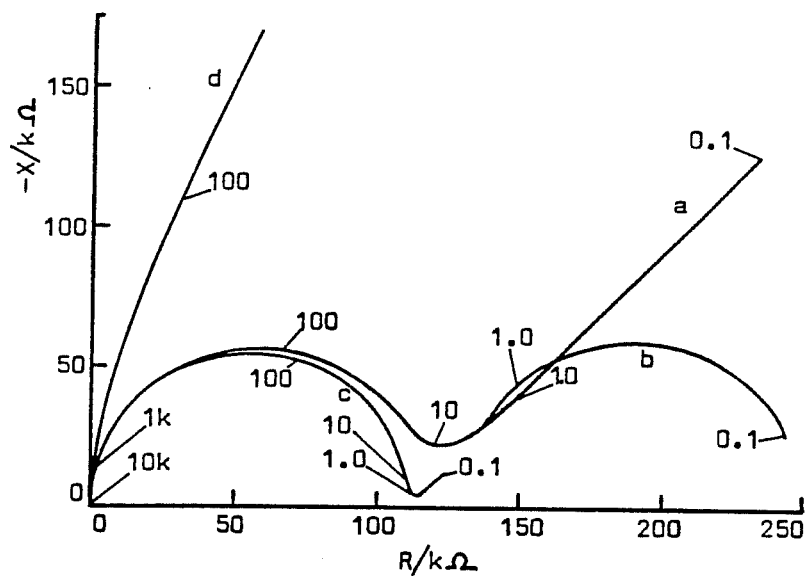
Fig. 4.13. Nyquist plot for the equivalent circuit in Fig. 4.9 showing the influence of diffusion on charge-transfer semi-circle: (a) and (b) combined charge-transfer and diffusion rate control; (c) charge-transfer rate control; and (d) diffusion rate control [70]. (Numbers on the curves indicate frequencies in Hz; $R_{cp} = 1e4$ ohm and $R_{ct} = 1e5$ ohm)

plots to avoid omitting some important factors. Both Bode and Nyquist plots shall be referred to for the best assurance.

4.4.3 Limitations and Uses of EIS for Real Corrosion Systems

Even though EIS is generally proven to be useful and has certain advantages over the traditional DC techniques in corrosion studies, its use is not without limitations. Theoretically, analysis of impedance data can only lead to corrosion resistance but not corrosion rates in coated metal system [73]. Moreover, for the evaluation of corrosion performance of coated metals, it is possible that an appropriate model cannot be found to fit the impedance data during the whole immersion period, especially if degradation of the coated metal causes the chosen model to become inappropriate [68]. Technically, the frequency ranges, the time taken for measurement, and the accuracy are defined by currently available measuring techniques and equipment [68]. This may lead to situations where even when the equivalent circuit model is known, circuit component values cannot be resolved at all, or can only be calculated approximately.

So far, some works using EIS to study the corrosion of uncoated metals have been reported to be successful [72] [74] [75], the values of R_{ct} and C_d can generally be determined from the impedance plots without difficulty. For coated metals, however, even though some researchers have tried to determine the values of R_{ct}, C_d, R_{cp}, and C_c from the impedance plots [76] [77] [78] [79] [80], the values of R_{ct}, C_d, and sometimes C_c obtained in these cases were generally considered to be unreliable. This is because the impedance plots were incomplete and/or with diffusion tails as discussed earlier. Currently, R_{cp} is the parameter

more often used as an quantitative indicator to evaluate the coating quality [53] [81] [82]. Even though it is often impossible to obtain values for all of the parameters, EIS can provide valuable qualitative information of corrosion processes if one compares the plot shape changes during the exposure period [52] [53] [74] [81] [82] [83]. Moreover, a simplified criteria using the absolute impedance value at a single frequency, for example 5 milli-hertz, to correlate the corrosion rate has been proposed for field use [84]. This still needs to be examined in more detail. To sum up, it is apparent that considerable future work, both on measuring technique and data analysis, is still needed to make the maximum use of this method.

Chapter 5

Results and Discussion

This chapter is basically comprised of two parts. Part one summarizes the representative electrochemical test results for each type of specimen used in this research. Discussion focuses on the interpretation of various types of electrochemical test results, especially the EIS, as they relate to predicting corrosion behavior; and the correlation between results obtained through different electrochemical methods. Some photographs, optical and scanning electron micrographs, and X-ray powder diffraction spectra are presented to provide better insight into the steel corrosion. Part two comprises the performance ranking of various types of ECRs evaluated through EIS in the immersion tests, together with some test results with regard to the coating characteristics of ECRs. Photographs and SEM micrographs are also presented to explain the coating deterioration more clearly. The intention is to provide information concerning the controversy regarding the effectiveness of ECR, and indicate the crucial needs in improving ECR performance.

5.1 Summary of Electrochemical Test Results

A tremendous amount of data was collected due to the large number of samples used. Fortunately, consistent similarities among the test results are observed in every particular type of specimen. In the following, some

representative samples are chosen for illustration of the types of corrosion behavior observed.

5.1.1 Electrochemical Impedance Spectroscopy

Polished Reinforcing Steel Disk

The typical Nyquist and Bode plots for a polished reinforcing steel disk are shown in Fig. 5.1 and Fig. 5.2. It is apparent from those plots that only one time constant appears throughout the 10-day immersion period. The perfect semi-circle in the Nyquist plot forms under the combined effects of charge transfer resistance and double layer capacitance at the steel/solution interface, and it indicates that the corrosion process at the disk surface is dominated by a charge transfer reaction, i.e. charge transfer rate control. The diameter of the semi-circle represents the magnitude of the charge transfer resistance, which is inversely proportional to the corrosion rate for a simple (single time constant) corrosion system. From the Bode magnitude plot, it is observed that the charge transfer resistance decreases rapidly in the first few days and then fluctuates around certain values. This finding indicates that the corrosion rate increases intensely right after the disk is immersed, and changes slowly later on.

Uncoated Reinforcing Steel

The typical Nyquist and Bode plots for an uncoated reinforcing steel specimen are shown in Fig. 5.3 and Fig. 5.4. The first day's Nyquist plot in this case seems to have a similar semi-circle as that of a polished disk, except a
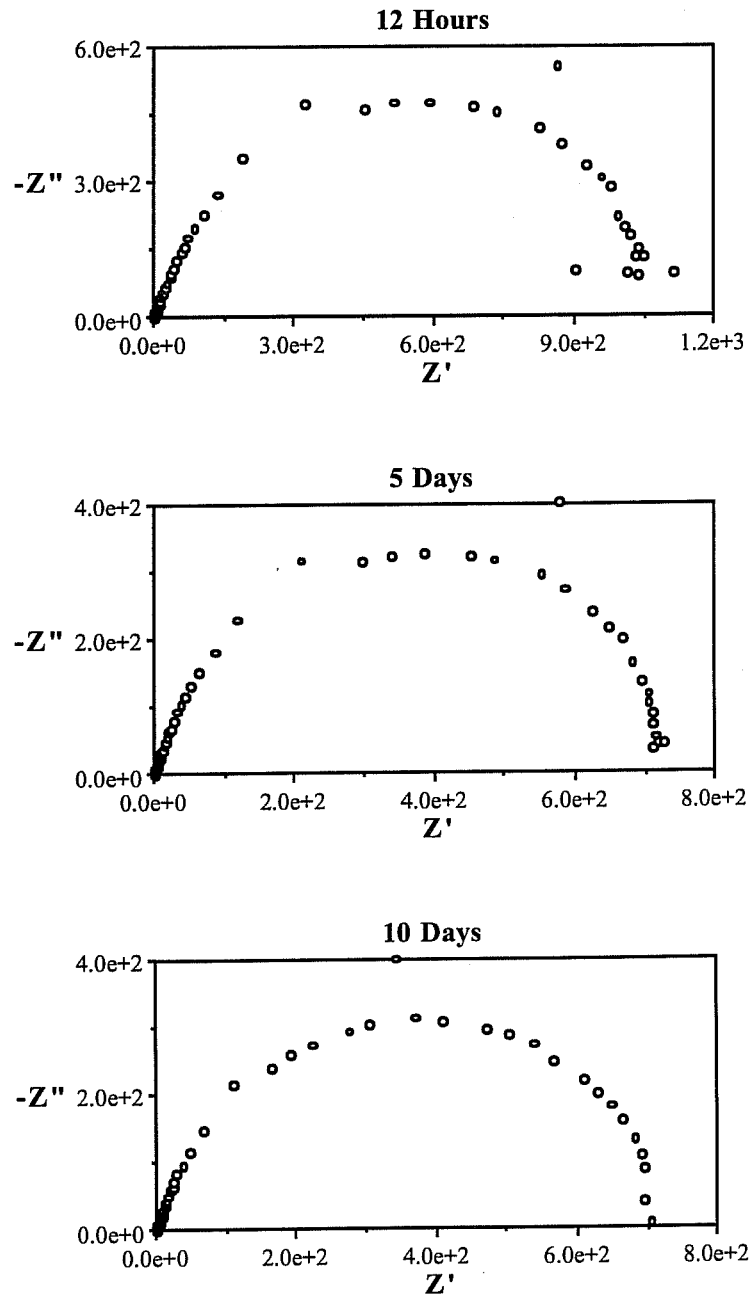
Fig. 5.1.   Nyquist plots for the representative polished reinforcing steel disk during 10-day immersion in 3.5% NaCl solution.
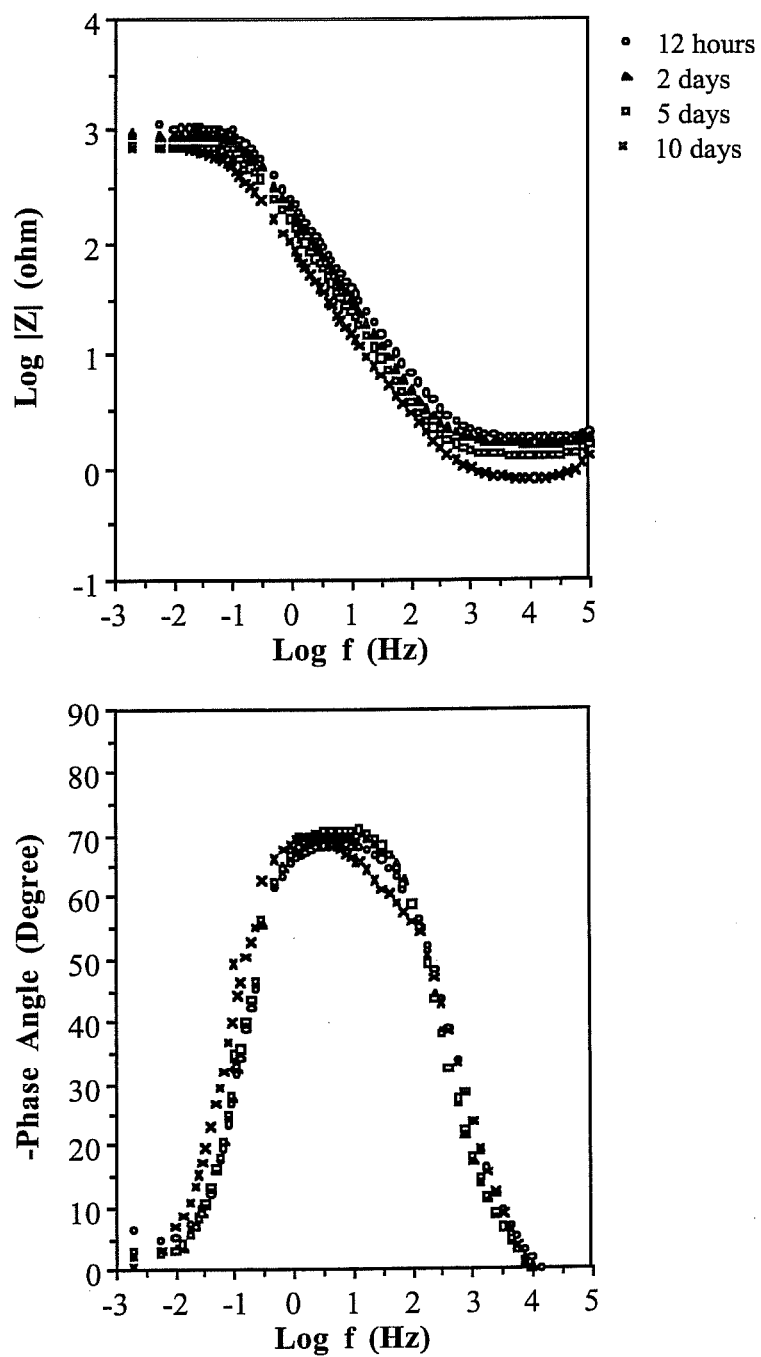
Fig. 5.2. The corresponding Bode plots of Fig. 5.1.
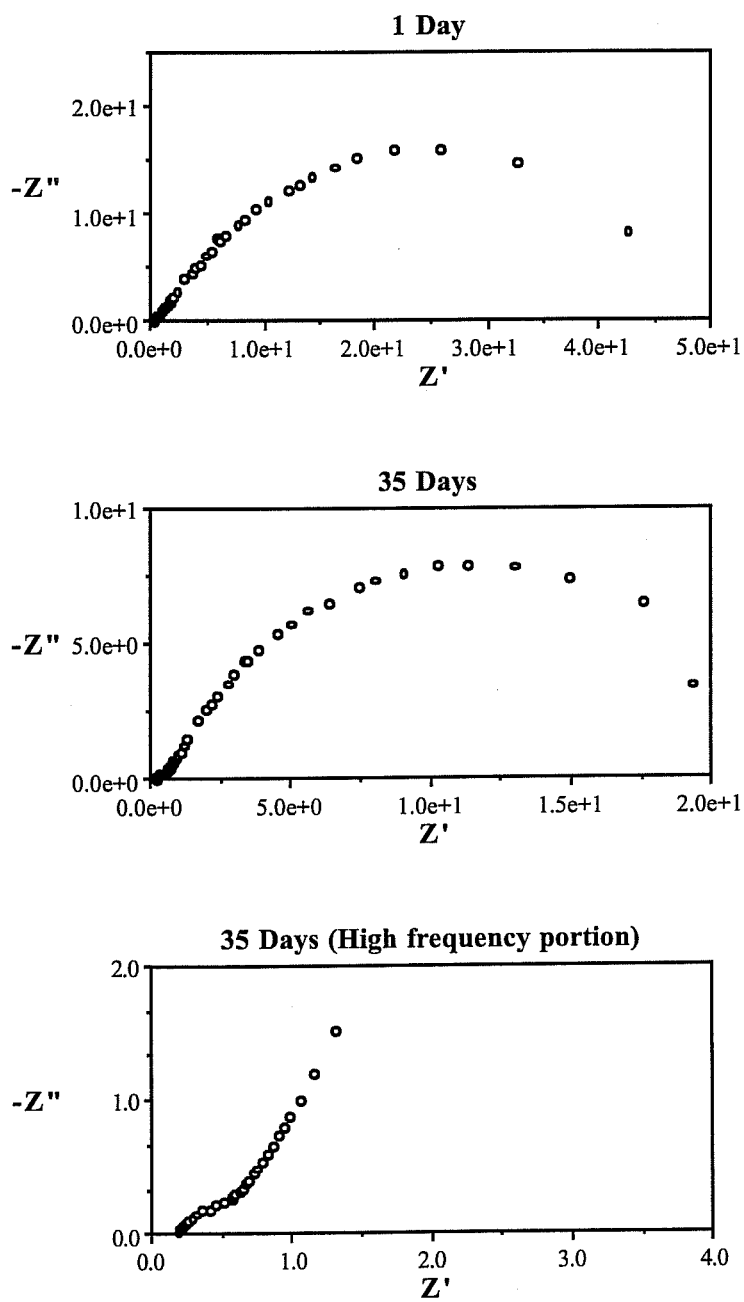
Fig. 5.3.   Nyquist plots for the representative uncoated reinforcing steel bar specimen during 105-day immersion in 3.5% NaCl solution.
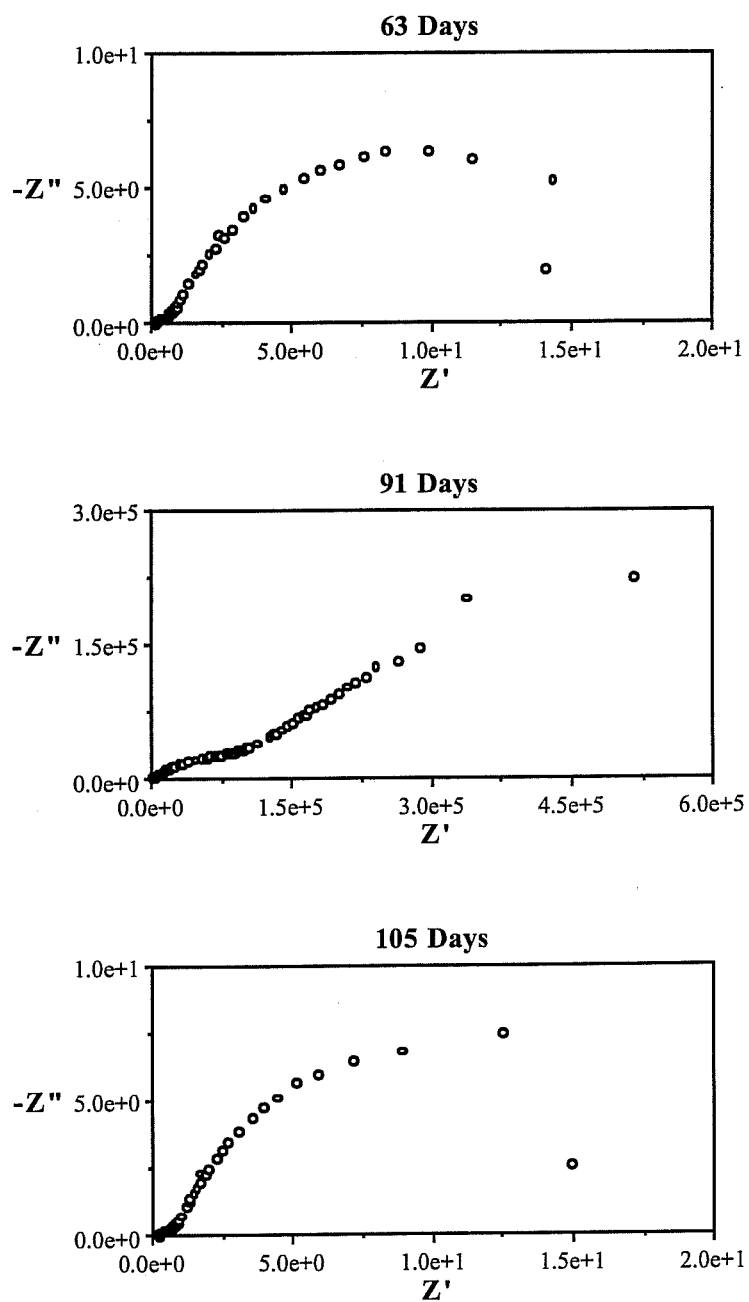
Fig. 5.3. (continued) Nyquist plots for the representative uncoated reinforcing steel bar specimen during 105-day immersion in 3.5% NaCl solution.
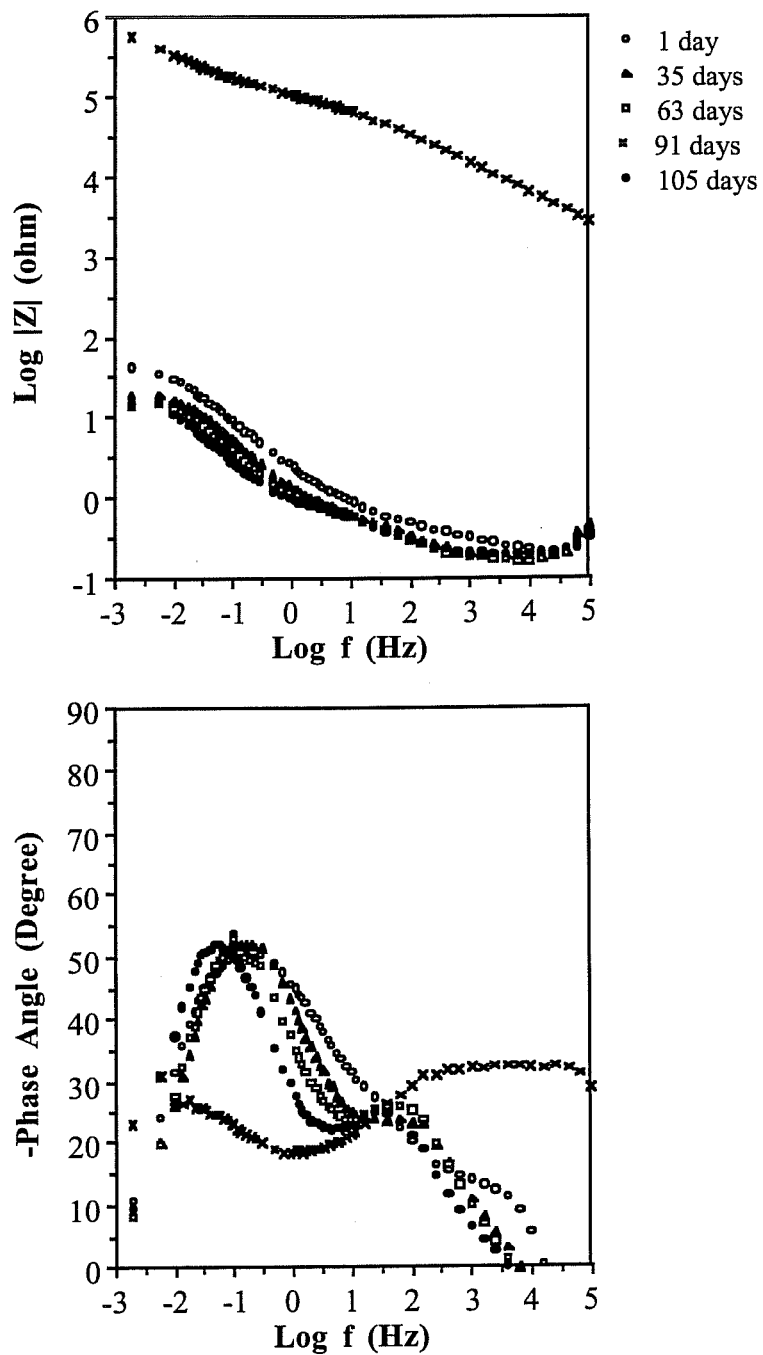
Fig. 5.4. The corresponding Bode plots of Fig. 5.3.

slightly depressed high frequency portion and an incomplete low frequency end. The depression of the curve at the high frequencies becomes more and more evident with time, and a distinct second semi-circle is observed on the 35th day after immersion. This second semi-circle is much smaller than the first one and is easily overlooked if one does not look into the extended high frequency portion or refer to the Bode plots. The appearance of this high frequency semi-circle is believed to be due to the formation and accumulation of certain corrosion product(s) which may act like a protective film on the steel surface. But, for most of the time, this film does not reduce the corrosion rate since the charge transfer resistance is found to drop continuously. This may be because the protective corrosion product layer(s) does not fully (or effectively) cover the active areas of the steel substrate. Generally, the corrosion process in this case is still under charge transfer rate control as that of a polished disk. However, a situation of passivation of steel is observed on the 91st day in which the charge transfer resistance becomes five orders larger than usual, and the diffusion process also plays a role in determining the corrosion rate. At that time, the semi-circle that is related to the film resistance (the value of which is not supposed to change too much since it is an intrinsic property of the film) is not seen because of the insufficient frequency range covered in this experiment due to the limits of the instrumentation. This kind of passivation behavior was found on two of the eight uncoated reinforcing steel specimens and on a couple of ECR specimens. It occurred occasionally on those specimens and usually did not last long each time. Finally, from the Bode plots, two time constants are observed at all times, even though it is not quite clear on the first day. This shows that there are some

differences between the steel/solution interface of this type of specimen and those of the polished disks.

Epoxy-Coated Reinforcing Steel

The impedance responses of all ECR specimens are generalized and classified into three categories, which are labeled as ECR with "good", "intermediate", and "poor" coating quality, respectively. Representative cases for the three categories are described below:

ECR with good coating quality

The typical Nyquist and Bode plots for an ECR specimen with good coating quality are shown in Fig. 5.5 and Fig. 5.6. It is observed that, even after 200 days of immersion, there is still only a vertical line seen in the Nyquist plot; while, in the Bode plots, there is a straight line with slope -1 in the magnitude plot and an angle shift of 90 degrees in the phase angle plot. All these curves represent purely capacitive behavior which is indicative of a high quality coating with no defects.

ECR with intermediate coating quality

ECR specimens whose impedance responses deviate from the capacitive behavior but which still have coating pore resistance values greater than 10^5 ohms after 200 days of immersion are put in this category. The responses of two specimens are described below:

The Nyquist and Bode plots of the first specimen are shown in Fig. 5.7 and Fig. 5.8. It was found that this specimen remained intact and with capacitive behavior up to the 51st day of immersion. On the 58th day, an incomplete semi-

1 Day
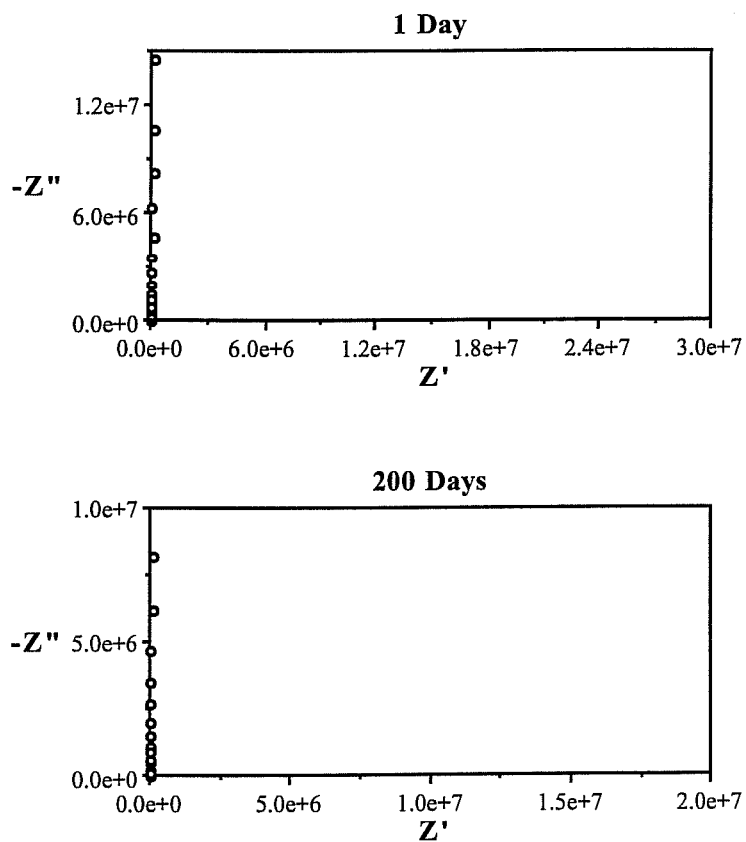
200 Days

Fig. 5.5.   Nyquist plots for the representative ECR bar specimen exhibiting good
coating performance during 200-day immersion in 3.5% NaCl solution.
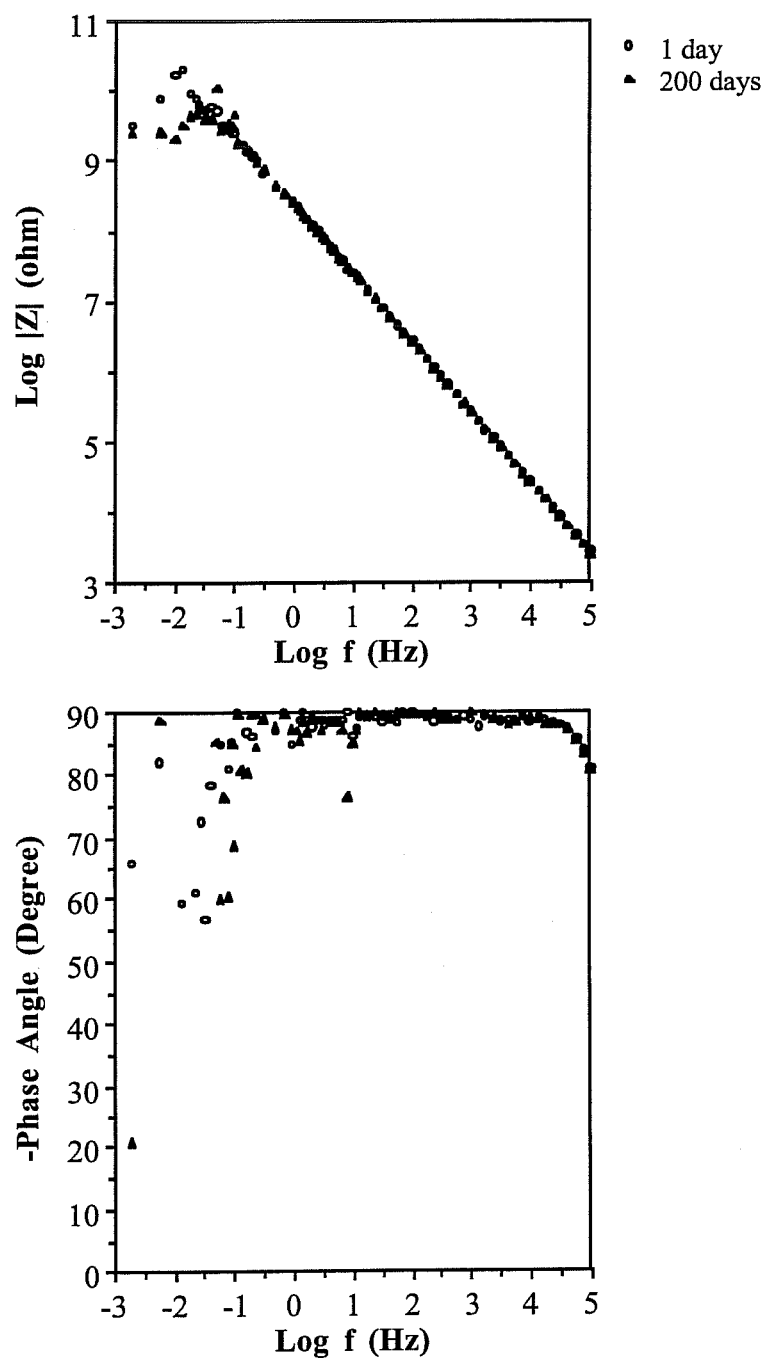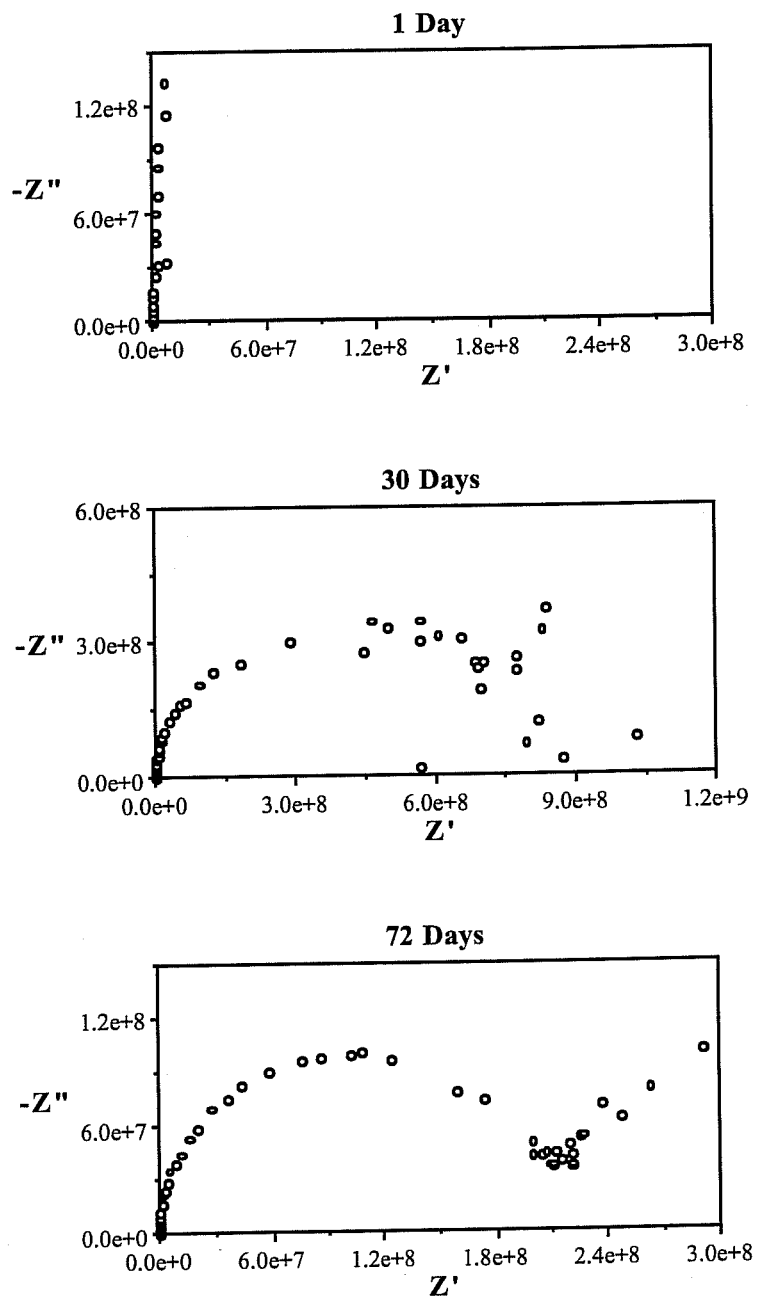
Fig. 5.6. The corresponding Bode plots of Fig. 5.5.
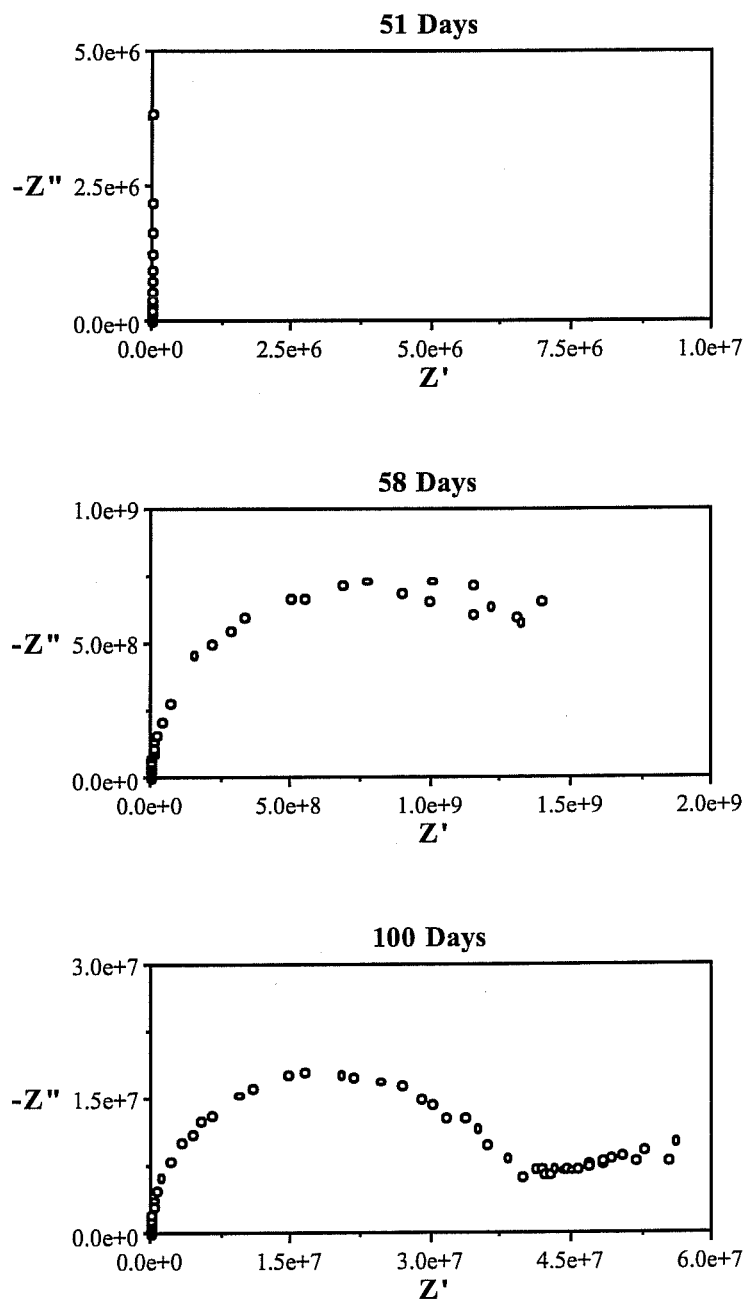
Fig. 5.7.   Nyquist plots for the first representative ECR bar specimen exhibiting intermediate coating performance during 200-day immersion in 3.5% NaCl solution.
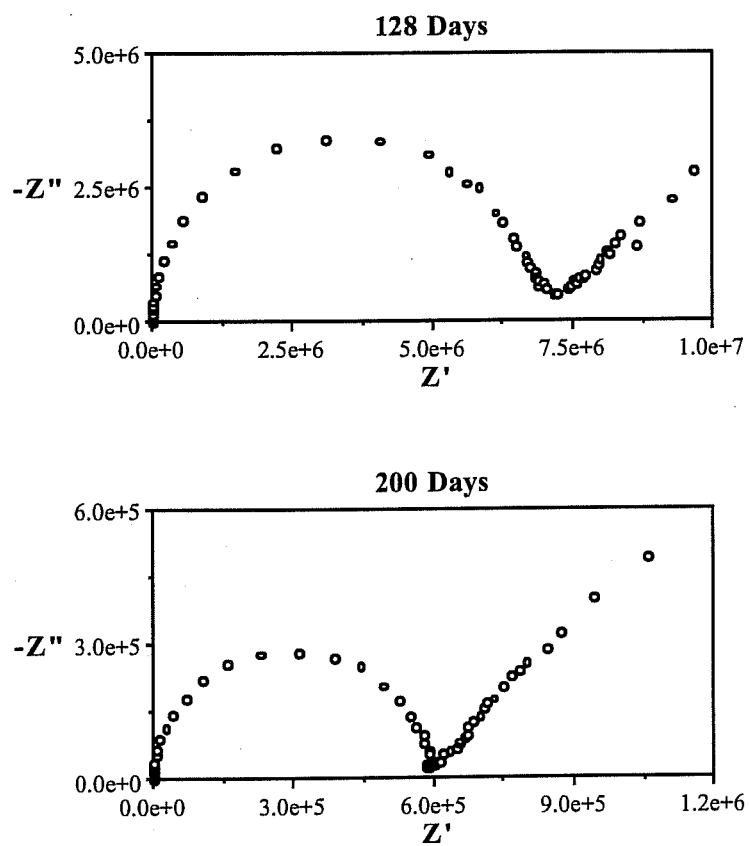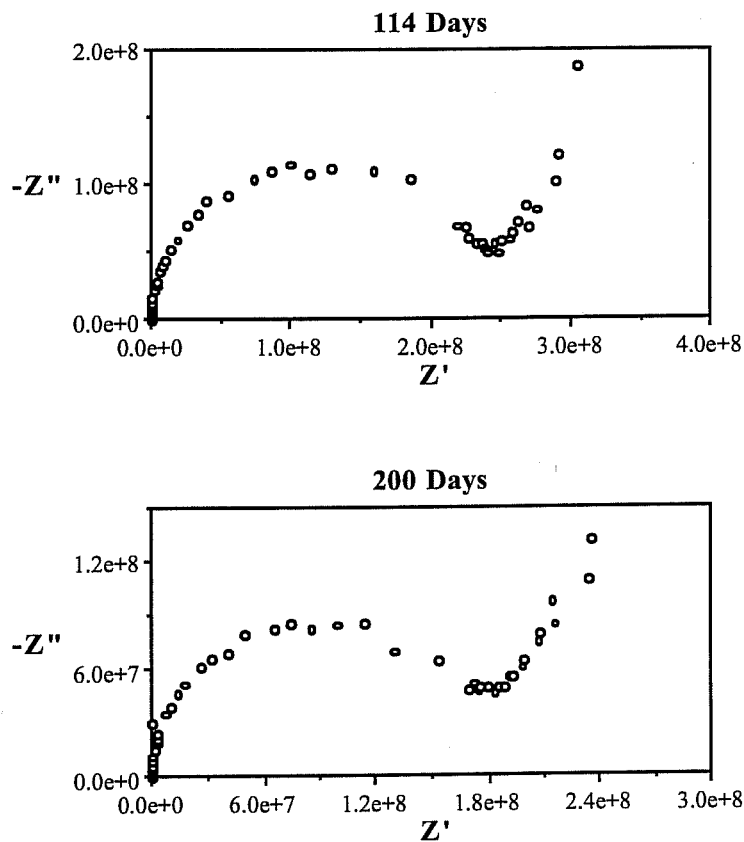
Fig. 5.7. (continued) Nyquist plots for the first representative ECR bar specimen exhibiting intermediate coating performance during 200-day immersion in 3.5% NaCl solution.
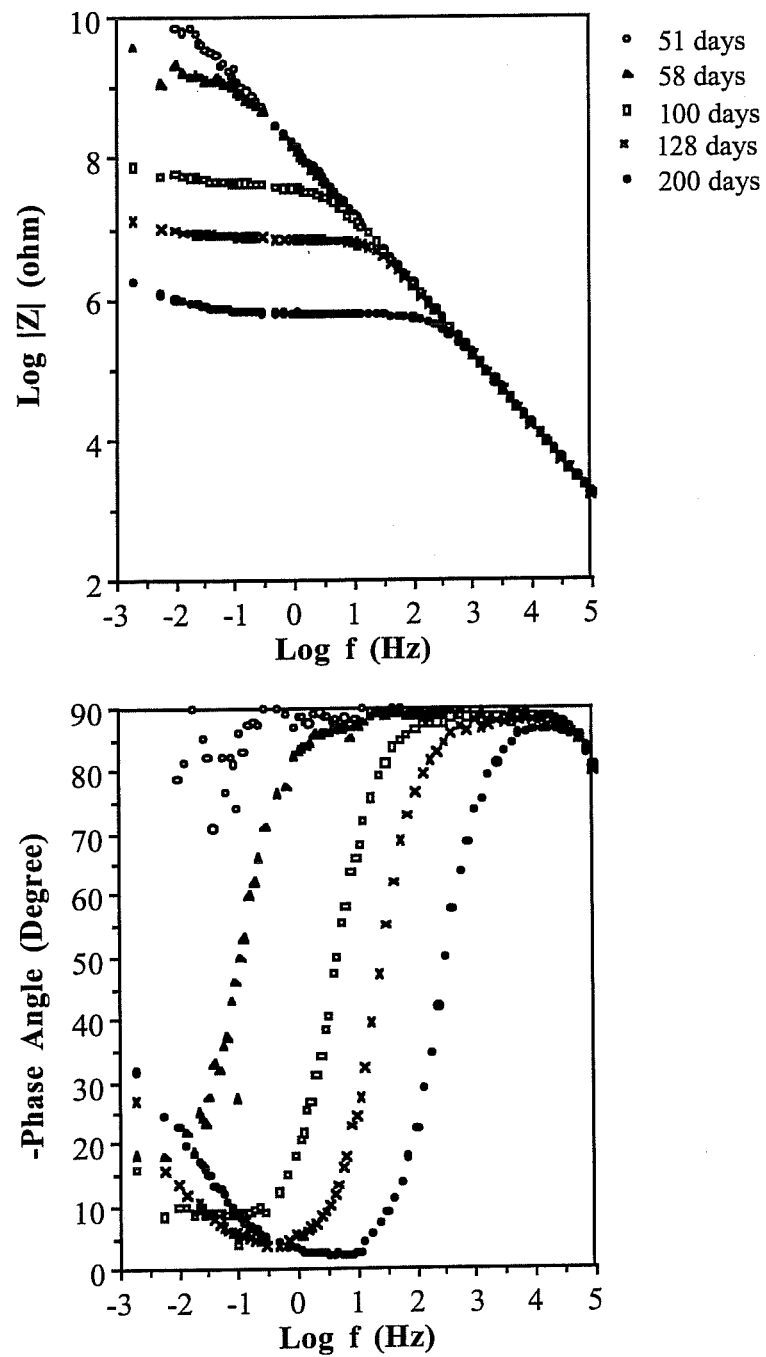
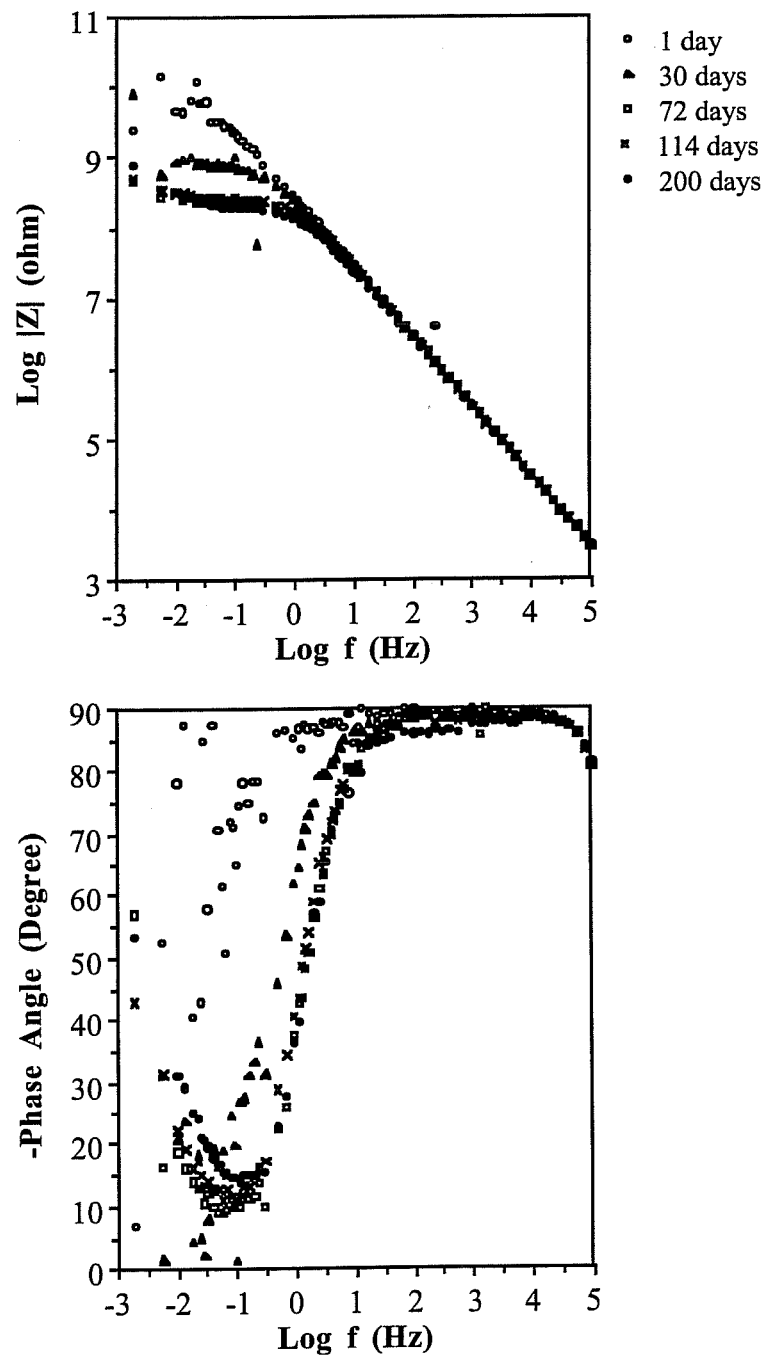Fig. 5.8. The corresponding Bode plots of Fig. 5.7.

circle formed in the Nyquist plot, and this is considered as an indication that conductive pathways have developed through the coating. It shall be noted that the establishment of conductive pore(s) does not necessarily result in corrosion of the steel substrate or poor service performance of ECR, even though it may be a precursor for them. On the 100th day, a more well defined semi-circle with an unclear diffusion tail was observed. Later on, the semi-circle became smaller and smaller and the diffusion tail became more apparent. As the high frequency semi-circle is believed to relate to the formation of pore(s) penetrating the coating, its diameter shall represent the magnitude of the coating pore resistance. This parameter is very important since it is an intrinsic property of coating and can serve as a useful indication of the coating quality. Therefore, in this case, the situation is that the coating pore resistance decreases with time as the coating degrades by an increasing number of conductive pores forming on it. Another semi-circle which is related to the charge transfer reaction can not be observed in the plot, and there is only a diffusion tail seen at the low frequency portion. This is believed to be due to the occurrence of a charge transfer reaction with its resistance value being much smaller and of no significance when compared to the diffusion impedance. In this situation, the corrosion process is controlled by the diffusion of corrosive ions and oxygen to the steel surface, i.e. diffusion rate control. From the Bode plots, we can clearly observe the deterioration of the coating with time, and the rise of the second time constant which is attributed to the diffusion process at the low frequencies.

For the second specimen, its Nyquist and Bode plots have similar curve shapes to those of the first specimen. They are shown in Fig. 5.9 and Fig. 5.10.

1 Day

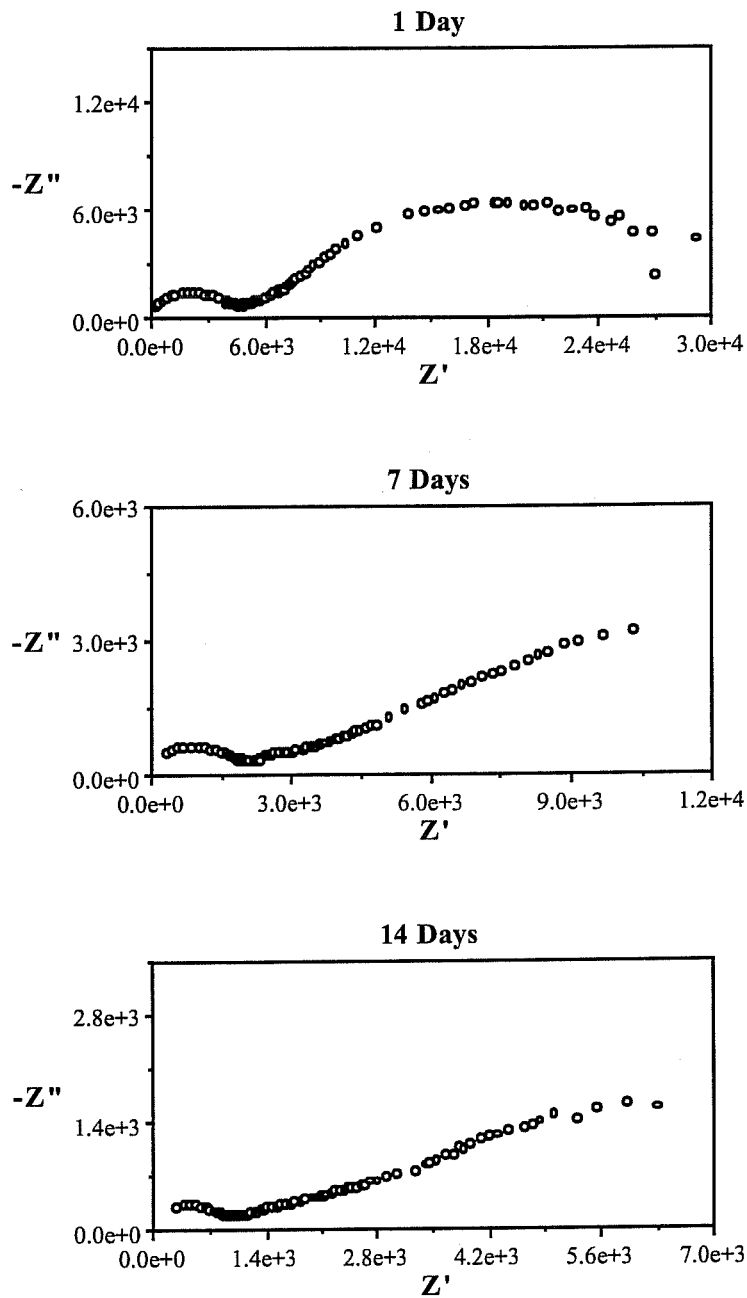**30 Days**

72 Days

Fig. 5.9.   Nyquist plots for the second representative ECR bar specimen exhibiting intermediate coating performance during 200-day immersion in 3.5% NaCl solution.
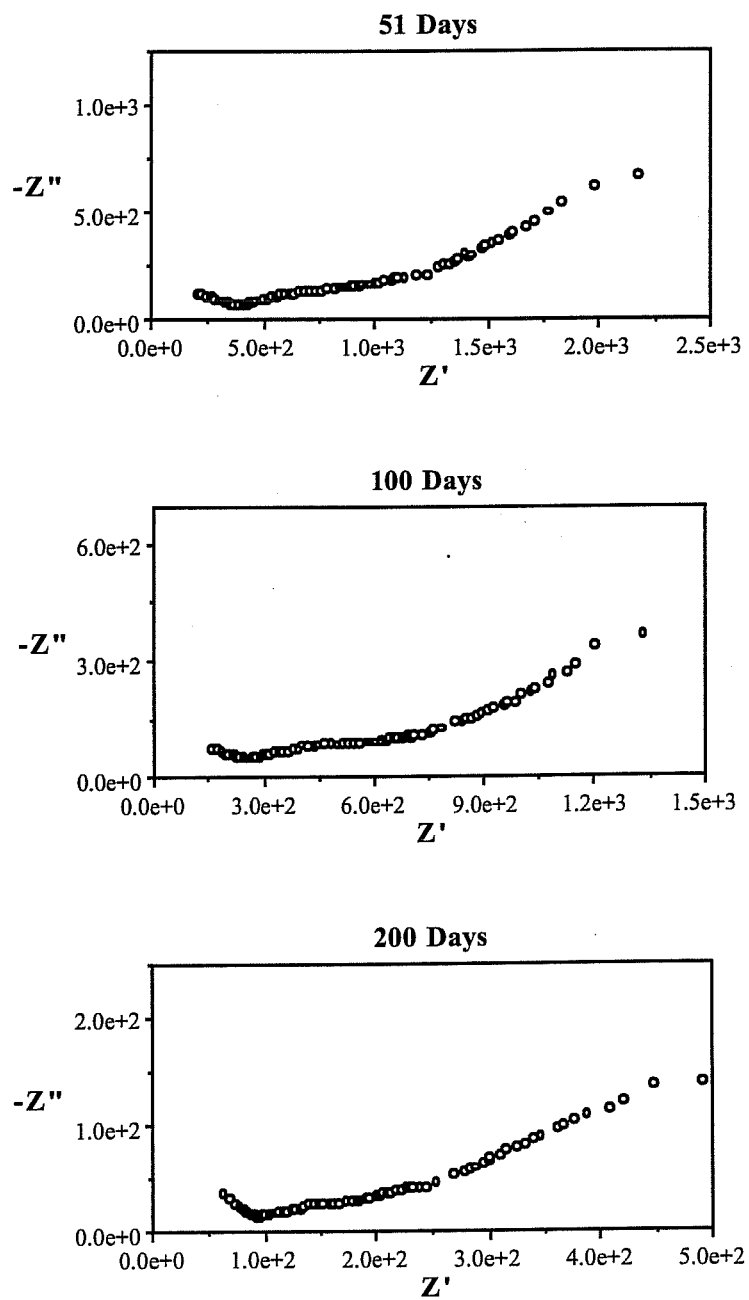
Fig. 5.9. (continued) Nyquist plots for the second representative ECR bar specimen exhibiting intermediate coating performance during 200-day immersion in 3.5% NaCl solution.
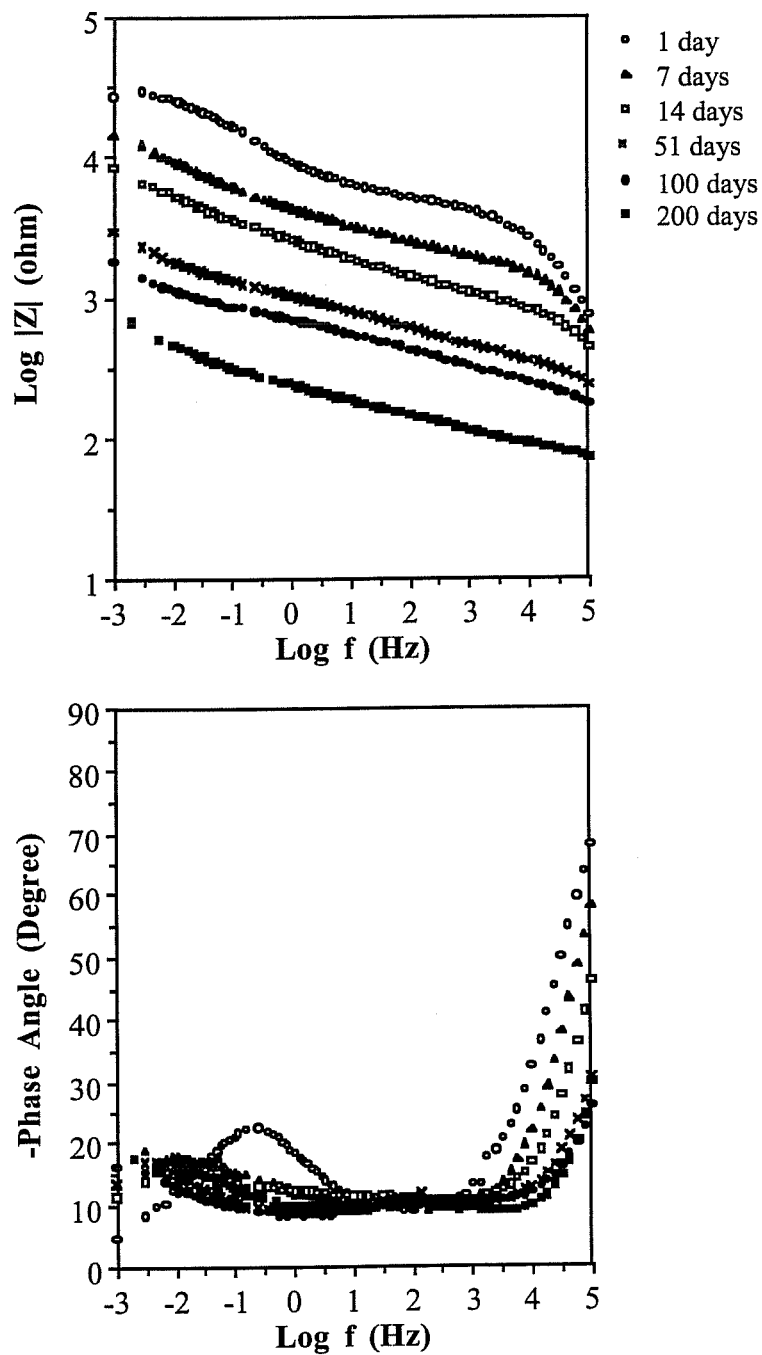
Fig. 5.10. The corresponding Bode plots of Fig. 5.9.

This specimen is observed to show signals of coating deterioration earlier than the first one does; however, it degrades at a much slower rate. The coating pore resistance value for this specimen is about two orders larger than that of the first one after 200 days of immersion.

<u>ECR with poor coating quality</u>

ECR specimens with coating pore resistance values less than 10^5 ohms after 200 days of immersion are considered to be in this category. Again, the responses of two specimens are described:

The Nyquist and Bode plots of the first specimen are shown in Fig. 5.11 and Fig. 5.12. Two semi-circles are observed in the Nyquist plot on the first day. The high frequency semi-circle in the Nyquist plot is attributed to the coating pore resistance; while the skewed one at the low frequencies is believed to be due to the combined effects of charge transfer reaction and diffusion processes. The actual charge transfer reaction semi-circle in this case is smaller than the skewed one observed in the plot, and may still be masked when interacting with the impedance tail. The fact that the charge transfer reaction also plays a role in controlling the corrosion rate is actually an indication that this coating does not retard the ingress of corrosive elements as effectively as those coatings with good and intermediate qualities do. By the 7th and 14th day, the low frequency curve is gradually changing from the skewed semi-circle shape to a depressed tail. This depressed tail is also believed to be due to the combined effects of charge transfer reaction and diffusion processes. On the 51st day and later on, it is observed that an intermediate frequency semi-circle and a low frequency tail gradually become more and more distinguishable (even though they still interact with each other).

1 Day

7 Days

14 Days

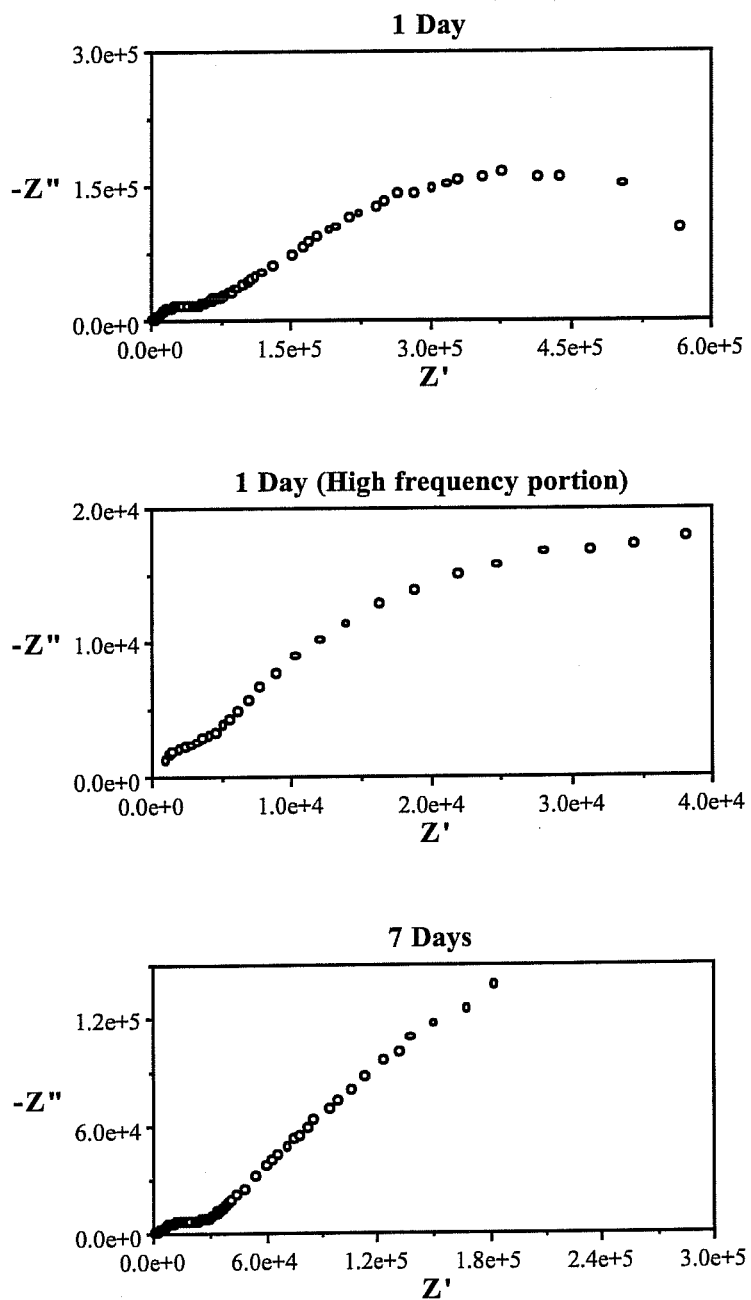

Fig. 5.11. Nyquist plots for the first representative ECR bar specimen exhibiting poor coating performance during 200-day immersion in 3.5% NaCl solution.
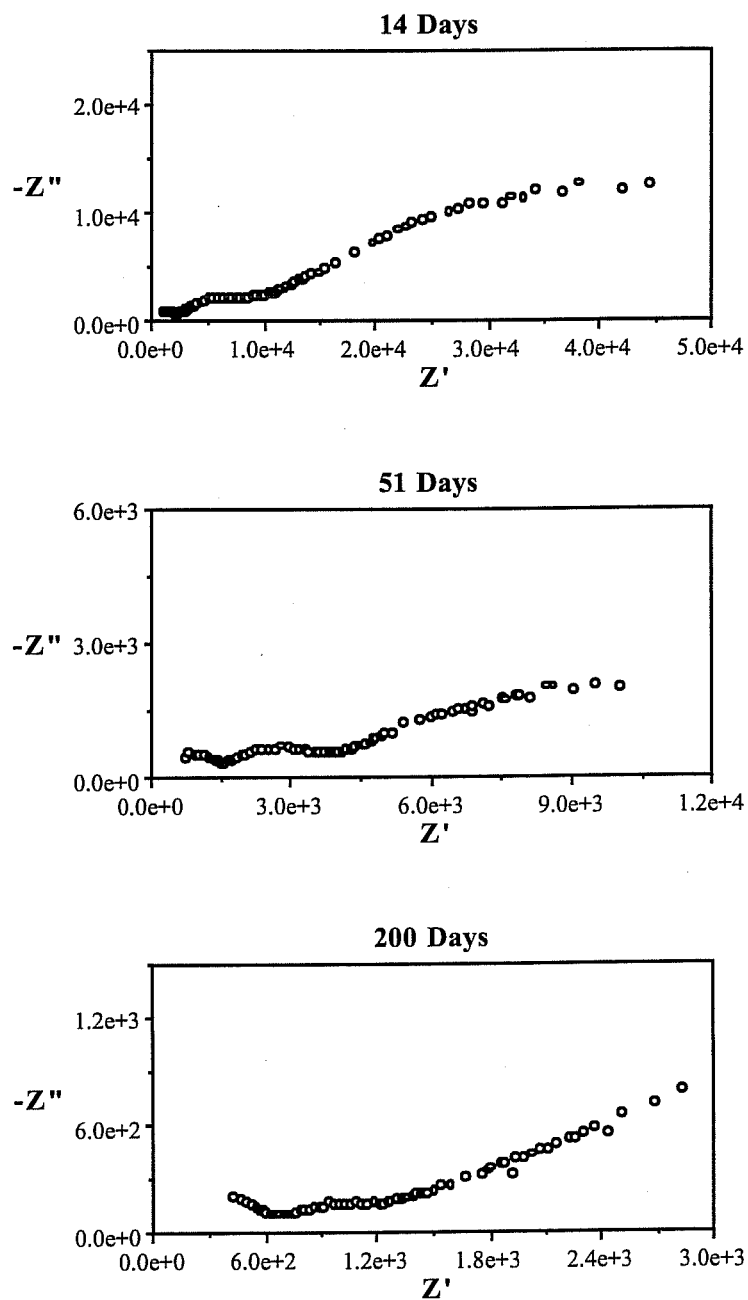
51 Days

100 Days

200 Days

Fig. 5.11. (continued) Nyquist plots for the first representative ECR bar specimen exhibiting poor coating performance during 200-day immersion in 3.5% NaCl solution.
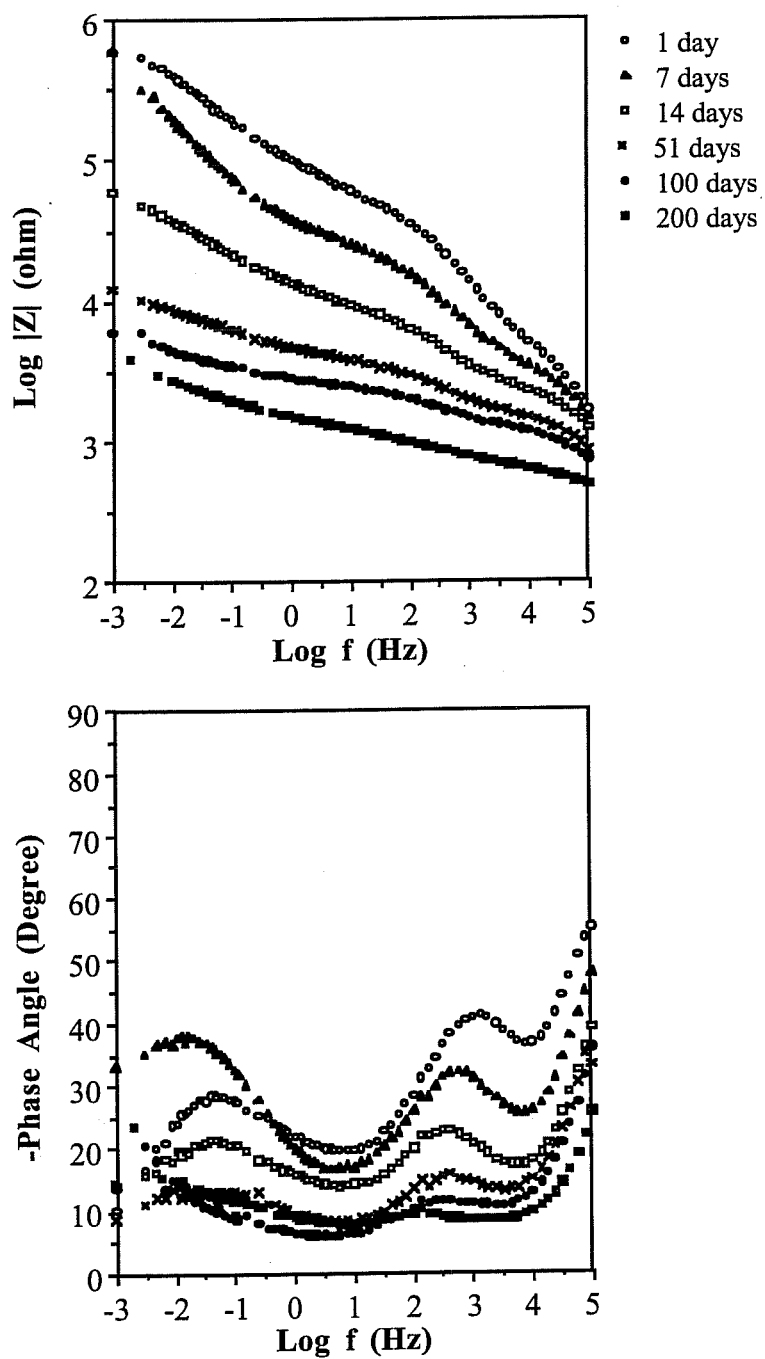
Fig. 5.12. The corresponding Bode plots of Fig. 5.11.

This finding confirms the possibility of combined effects of two mechanisms on controlling the corrosion process at the early stages as just mentioned above. The charger transfer reaction semi-circle is actually masked at the early stages due to its relatively small scale and becomes distinguishable when the total impedance (i.e. the impedance value at the lowest measuring frequency, 0.001 mV in this case) drops below a certain value. From the Bode plots, we can easily observe the coating deterioration, the decrease of total impedance with immersion time, and the change of impedance behavior at the intermediate frequencies which is attributed to the charge transfer reaction.

The Nyquist and Bode plots of the second specimen are shown in Fig. 5.13 and Fig. 5.14. For this case, at first glance, it seems that there are two semi-circles in the Nyquist plot on the first day, with the high frequency one presumably related to the coating quality as discussed in the case of the first specimen. However, another semi-circle which actually represents the coating quality is observed on an extended plot of the highest frequency portion. Therefore, the intermediate and low frequency semi-circles are actually attributed to the combined effects of charge transfer reaction and diffusion processes. The very important point is that for the Nyquist plots during the early immersion period, the high frequency semi-circle which is related to the coating quality may be masked due to its relatively small scale; and this may lead to misinterpretation of the results if one does not look into the extended highest frequency portion or refer to the Bode plots. On the 14th day and later on, two semi-circles and a diffusion tail become distinguishable on a single plot (even thought they are always incomplete and skewed). Thus, the corrosion process is known to be under

1 Day

1 Day (High frequency portion)

7 Days

Fig. 5.13. Nyquist plots for the second representative ECR bar specimen exhibiting poor coating performance during 200-day immersion in 3.5% NaCl solution.

14 Days

51 Days

200 Days

Fig. 5.13. (continued) Nyquist plots for the second representative ECR bar specimen exhibiting poor coating performance during 200-day immersion in 3.5% NaCl solution.

Fig. 5.14. The corresponding Bode plots of Fig. 5.13.

the combined effects of charge transfer reaction and diffusion processes throughout the immersion period. This situation is further confirmed by the Bode phase angle plot in which three time constants are distinguishable from the very beginning. Also, from the Bode magnitude plot, both the coating pore resistance and the total impedance are observed to decrease continuously with immersion time.

Concrete Block Corrosion Macrocell

Two types of EIS responses were observed on the concrete block corrosion macrocells. They are associated with uncoated reinforcing steel embedded in concrete and ECR embedded in concrete, respectively. Representative examples of the two types of behavior are described below:

Uncoated reinforcing steel embedded in concrete

The typical Nyquist and Bode plots for uncoated reinforcing steel embedded in concrete are shown in Fig. 5.15 and Fig. 5.16. A small fraction of a semi-circle and a highly reactive diffusion tail are observed at the extremely high and low frequencies respectively in the Nyquist plot of the first exposure cycle. The high frequency semi-circle is believed to be due to the accumulation of corrosion product layer(s) on the steel surface, such as that described in the case of immersion tests of uncoated reinforcing steel specimens. However, the resistance value associated with the film is observed to increase more dramatically with time in this case. This is considered to be because the corrosion products are more compact for this type of specimen due to the wet and dry cycles applied and the confinement by the surrounding concrete. Since the
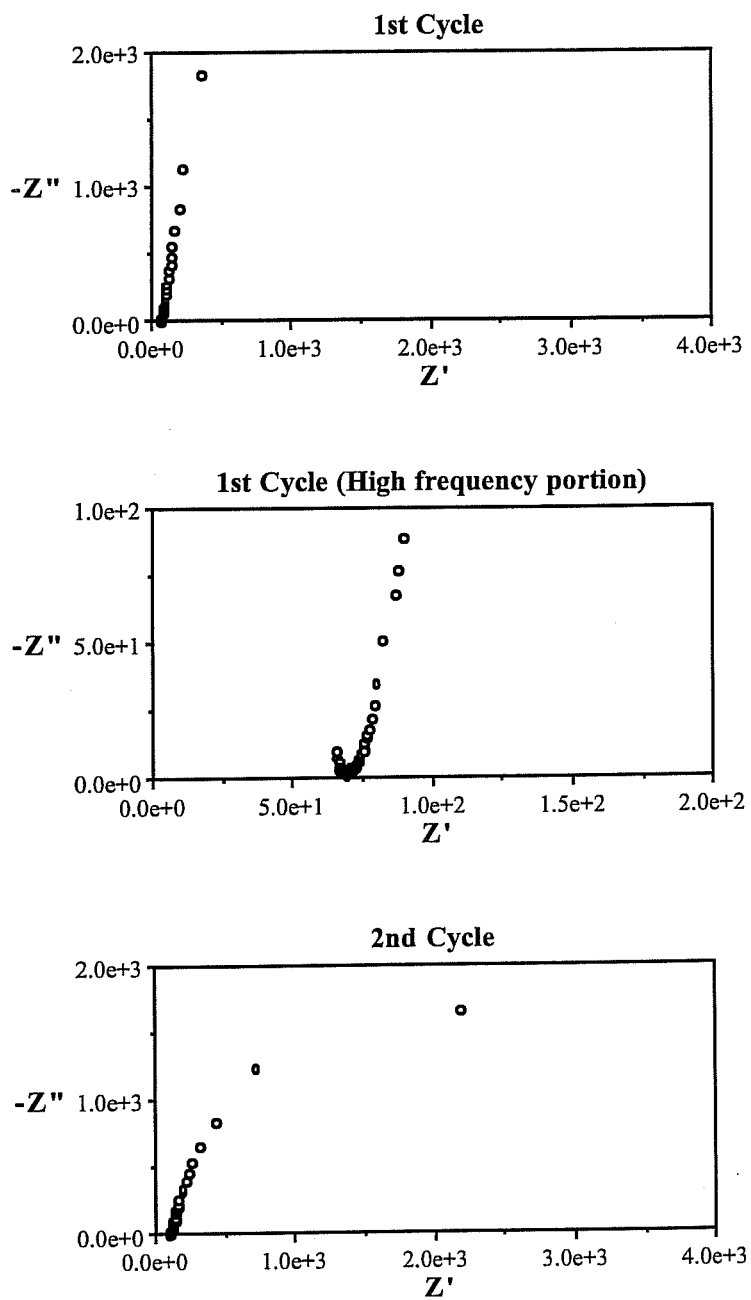
Fig. 5.15. Nyquist plots for the representative uncoated reinforcing steel bar embedded in a concrete block and subjected to periodic wet-dry ponding with 3.5% NaCl solution.
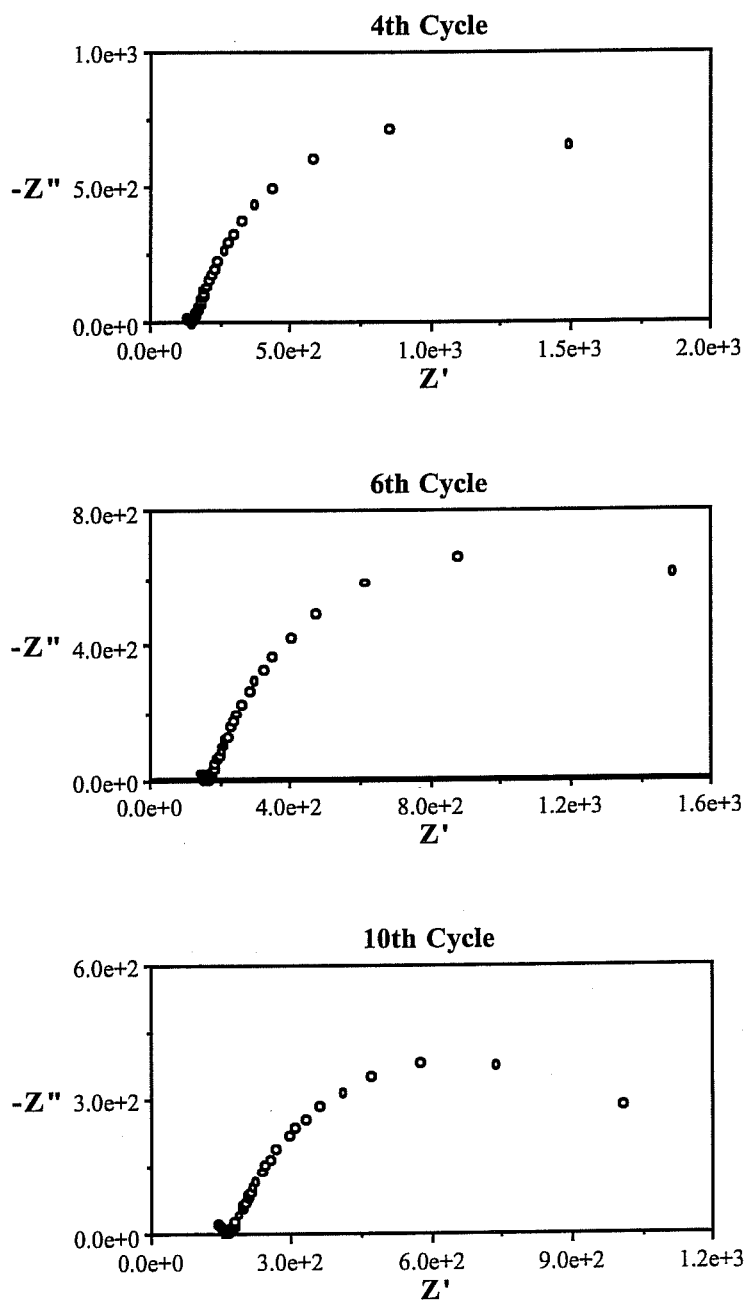
Fig. 5.15. (continued) Nyquist plots for the representative uncoated reinforcing steel bar embedded in a concrete block and subjected to periodic wet-dry ponding with 3.5% NaCl solution.
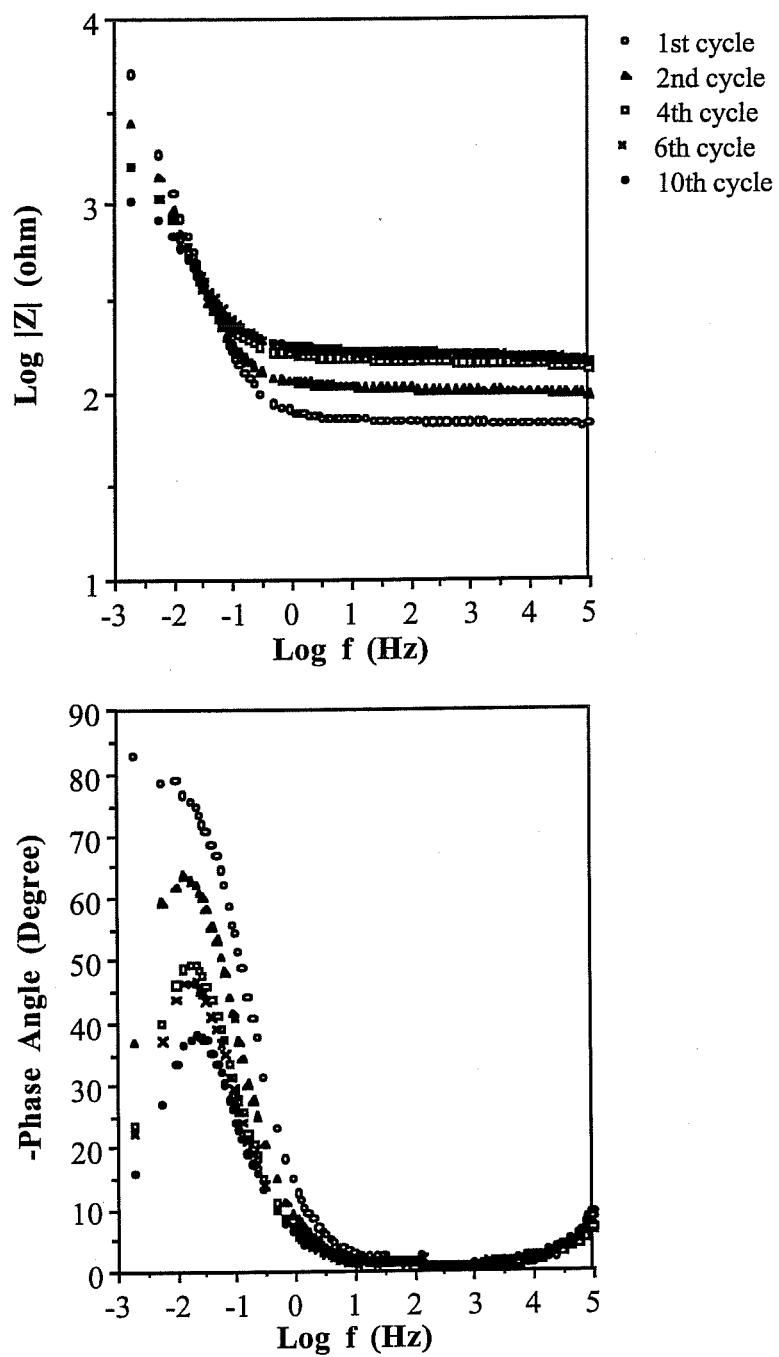
Fig. 5.16. The corresponding Bode plots of Fig. 5.15.

conductive pathways are supposed to be fewer on a more compact film, the film resistance increases. The highly reactive diffusion tail at the low frequencies indicates that the corrosion rate is controlled by the diffusion process. Later on, the diffusion tail tends to curve down more and more at the very low frequencies, and a semi-circle shape becomes clearer and clearer. This is due to the growing effect of the charge transfer reaction on controlling the corrosion process. However, it is believed that, even on the 10th cycle, diffusion processes still have a dominant effect on the low frequency curve shape; and the actual charge transfer reaction semi-circle is smaller than the incomplete, skewed one observed in the plot and may still be masked by the diffusion tail. From the Bode plots, it is observed that the effect of diffusion impedance at the low frequencies is decreasing with time, but the charge transfer resistance is still too small to be observed at the 10th cycle. This finding confirms the explanation above. Also, it is observed that while the film resistance increases with time, the total impedance decreases with time.

ECR embedded in concrete

Typical Nyquist and Bode plots of ECR embedded in concrete are shown in Fig. 5.17 and Fig. 5.18. Two semi-circles and a tail are observed in all the Nyquist plots throughout the exposure period, even though the high frequency semi-circle is not always complete and the intermediate frequency semi-circle always interacts with the low frequency tail. As described previously, the high and intermediate frequency semi-circles are related to the coating quality and charge transfer reaction respectively, while the low frequency tail represents the diffusion process. This type of Nyquist plot curve indicates that the corrosion

1st Cycle

2nd Cycle

4th Cycle
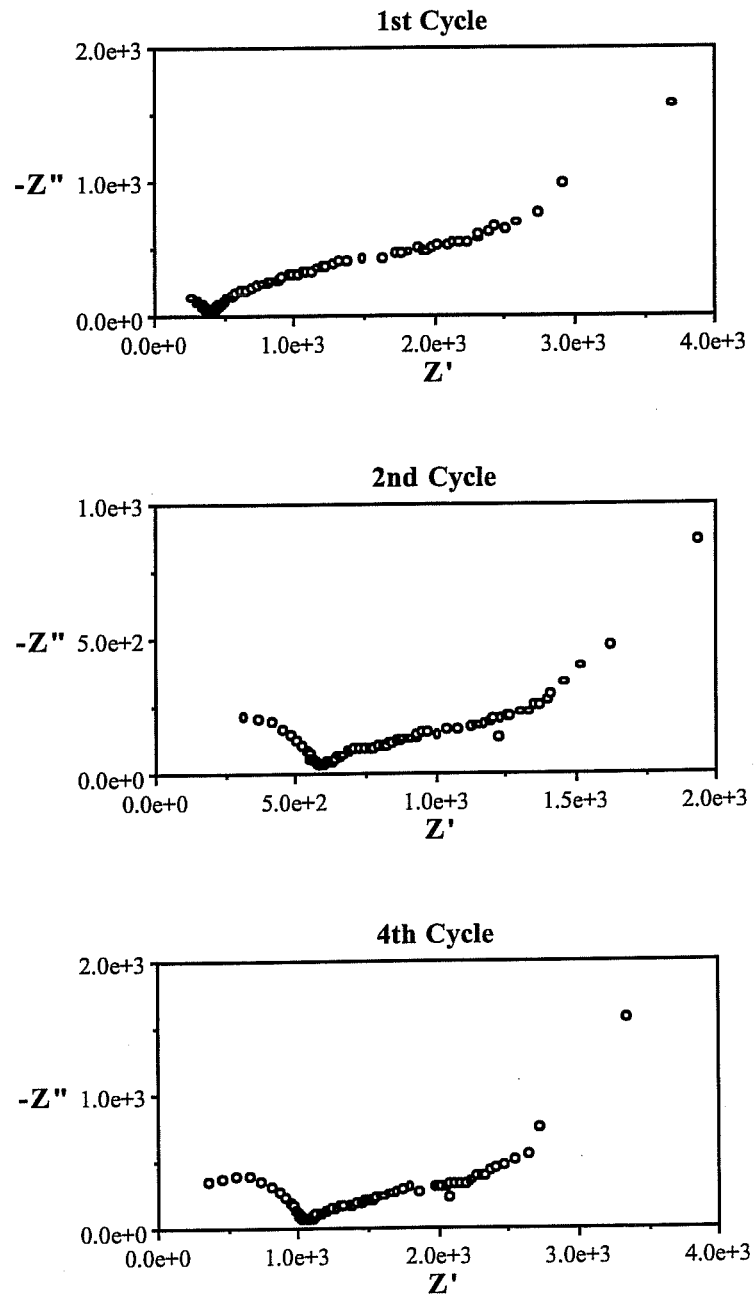
Fig. 5.17. Nyquist plots for the first representative ECR bar embedded in a concrete block and subjected to periodic wet-dry ponding with 3.5% NaCl solution.
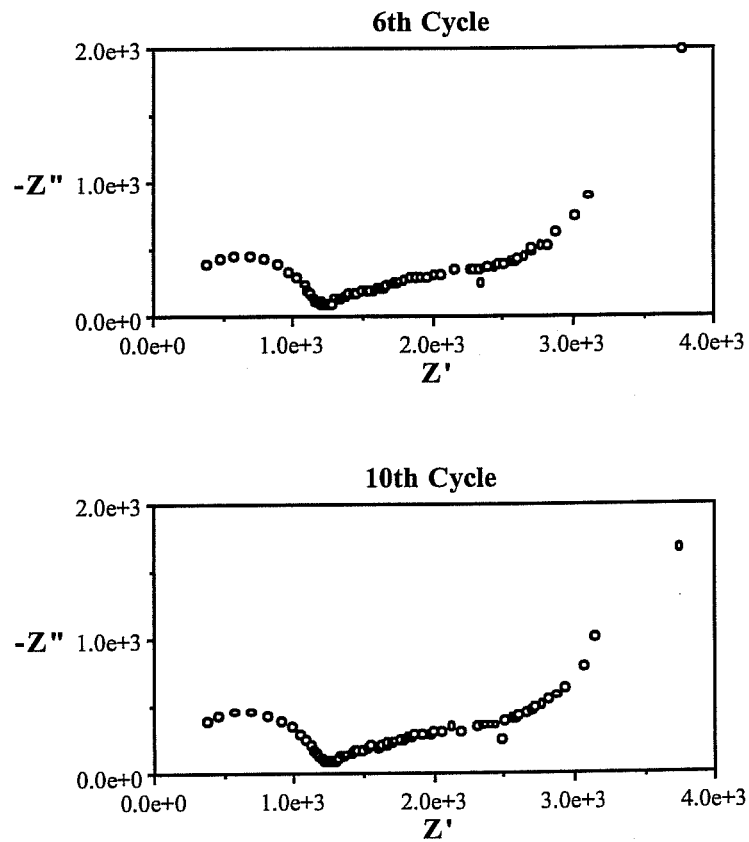
Fig. 5.17. (continued) Nyquist plots for the first representative ECR bar embedded in a concrete block and subjected to periodic wet-dry ponding with 3.5% NaCl solution.
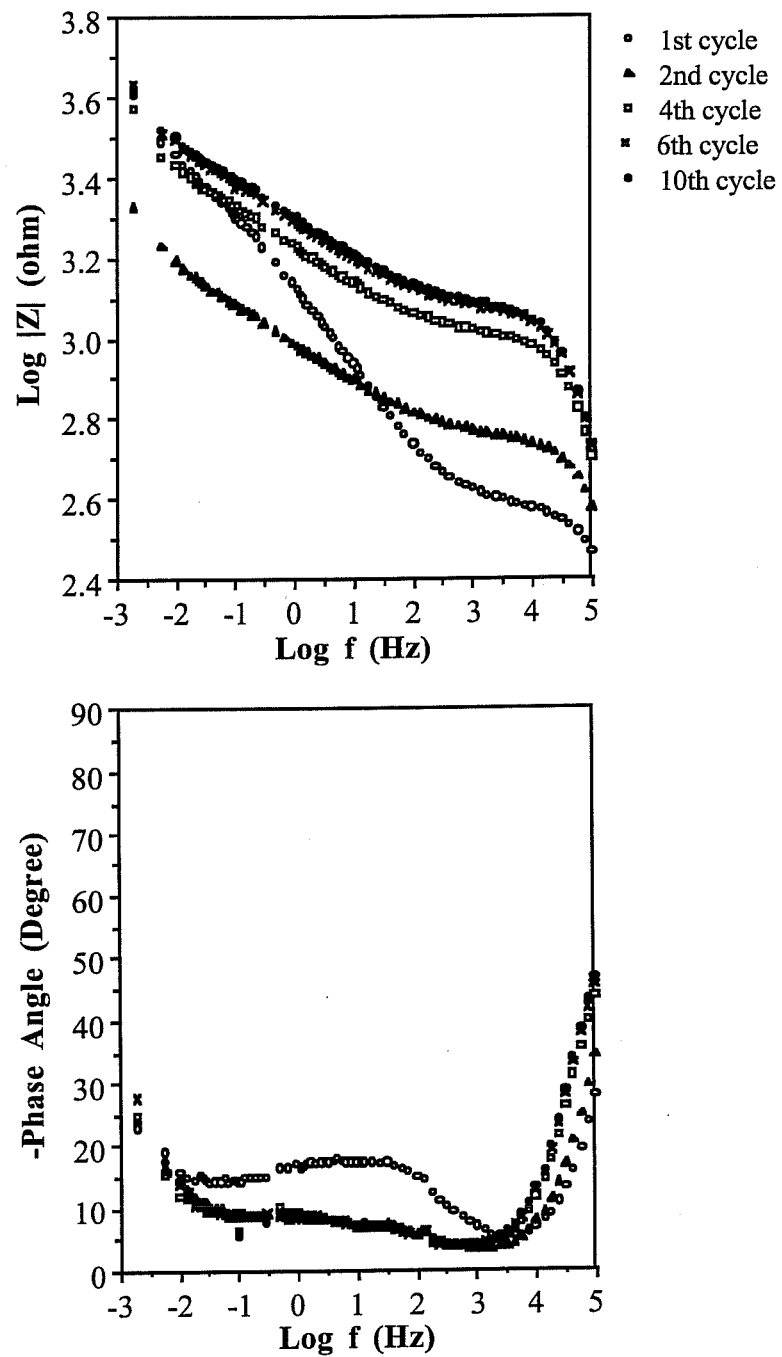
Fig. 5.18. The corresponding Bode plots of Fig. 5.17.

process on the exposed steel surface is controlled by combined effects of charge transfer reaction and diffusion processes. From the Bode magnitude plot, it is observed that the coating pore resistance increases with time continuously; and, the total impedance generally also increases with time, although a decrease is observed during the second cycle. It is interesting to take a look at the Bode plots of another specimen as shown in Fig. 5.19. In this case, it is observed that the coating pore resistance also increases with time continuously; however, the total impedance generally decreases with time. There is an increase during the second cycle, however.

It is summarized from the observations of the impedance responses of all the corrosion macrocells exposed to ten wet/dry cycles that: both the film resistance of uncoated reinforcing steel and the coating pore resistance of ECR always increase with time and reach certain stable values; while the total impedance may increase, decrease, or fluctuate. No specific correlation between the two parameters was observed.

5.1.2 Corrosion Potential Monitoring and Polarization Resistance Measurement

The records of corrosion potential variation and the results of polarization resistance measurements for those representative specimens during their exposure periods are plotted in Fig. 5.20 through Fig. 5.26. It is noted that no stable values could be obtained for ECRs with intermediate to good coating qualities, as classified in the previous section. The meanings of the two types of results and their correlation are described below:
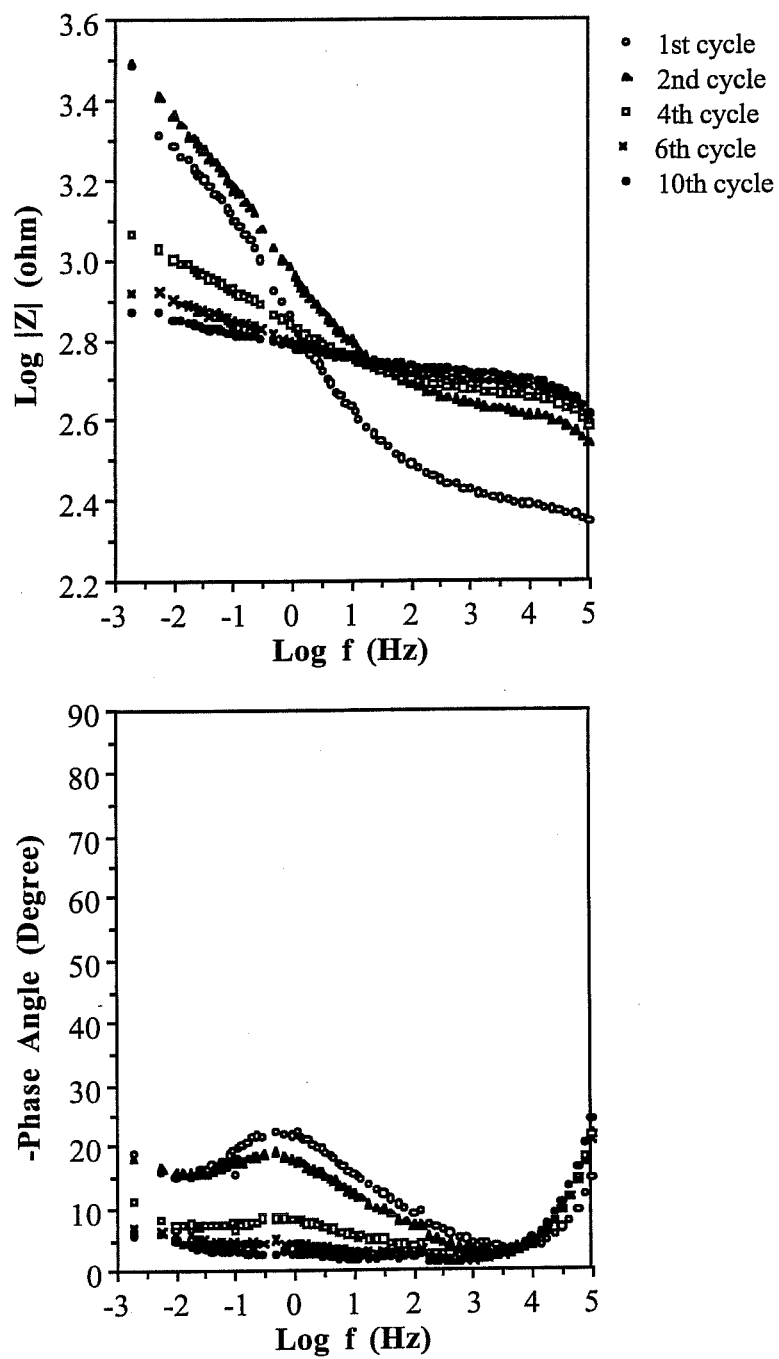
Fig. 5.19. Bode plots for the second representative ECR bar embedded in a concrete block and subjected to periodic wet-dry ponding with 3.5% NaCl solution.

First, the corrosion potential distributions observed on various types of specimens are generally summarized (from all test samples) as follows:

ECR with medium or good coating quality: Unstable around ± 200 mV SCE.

Concrete block corrosion macrocells: -100 to -550 mV SCE.

ECR with poor coating quality: -450 to -650 mV SCE.

Uncoated reinforcing steel: -600 to -700 mV SCE.

Polished reinforcing steel disks: -700 to -750 mV SCE.

These corrosion potential distributions are reasonable and expected since it is known from experimental observations that with an increase in the exposure to corrosive anions, i.e. chloride ions, the corrosion potential of steel will be shifted to more active (negative) values [85]. Thus, a polished reinforcing steel disk which has a completely charge transfer controlled corrosion process, as indicated from its EIS response, is supposed to have the fastest and most abundant supply of corrosive anions to its uncovered surface. This may result in the most active corrosion reaction and the most negative corrosion potential. The uncoated reinforcing steel, when compared to the polished disk, has a similar charge transfer controlled corrosion process but with an additional, slight effect from a deficient film in blocking the supply of corrosive anions on its surface. The effect is believed to lower the corrosion activity somewhat, and shift the corrosion potential to slightly more noble (positive) values. For ECR with poor coating quality and the concrete block corrosion macrocells, the coating and the concrete can block the corrosive anions even more effectively, and the diffusion processes take part in controlling the corrosion rate. In these cases, the corrosion potential is further shifted to more and more noble values. For ECRs with intermediate to

good coating qualities, there may be no immediate penetration through the coating, or the diffusion process may highly restrain the supply of corrosive anions to the steel surface. There is thus no corrosion activity strong enough to be detected, and no stable corrosion potential can be measured. The above reasoning gives a general trend of the distribution of corrosion potentials for different types of steel/solution interfaces; however, some other factors, such as the properties (i.e. composition and/or structure) of the steel substrates, may also affect the corrosion activity. Therefore, some overlap of corrosion potentials between different types of interfaces are observed in the above situations.

In Fig. 5.20 through Fig. 5.23, it is observed that the corrosion potential values for specimens in continuous immersion tests all have a general trend to decrease with time and become stable within relatively narrow ranges, although increases are also observed sometimes. For corrosion macrocells, however, various trends are observed. The corrosion potential values may reach stable values, either active or noble, or may still fluctuate irregularly after long exposure times, as shown in Fig. 5.24 through Fig. 5.26. This indicates that the concrete may still protect the steel against corrosion to a certain extent even under corrosive exposure conditions.

Polarization resistance measurement is probably the most straightforward electrochemical method of determining the corrosion rate. The polarization resistance value is inversely proportional to the corrosion current, and $\frac{1}{R_p}$ can be used directly for comparison of the instantaneous corrosion rate in corrosion study. Again, referring to Fig. 5.20 through Fig. 5.26 in which the polarization resistance and the corrosion potential are plotted together, it is observed that the
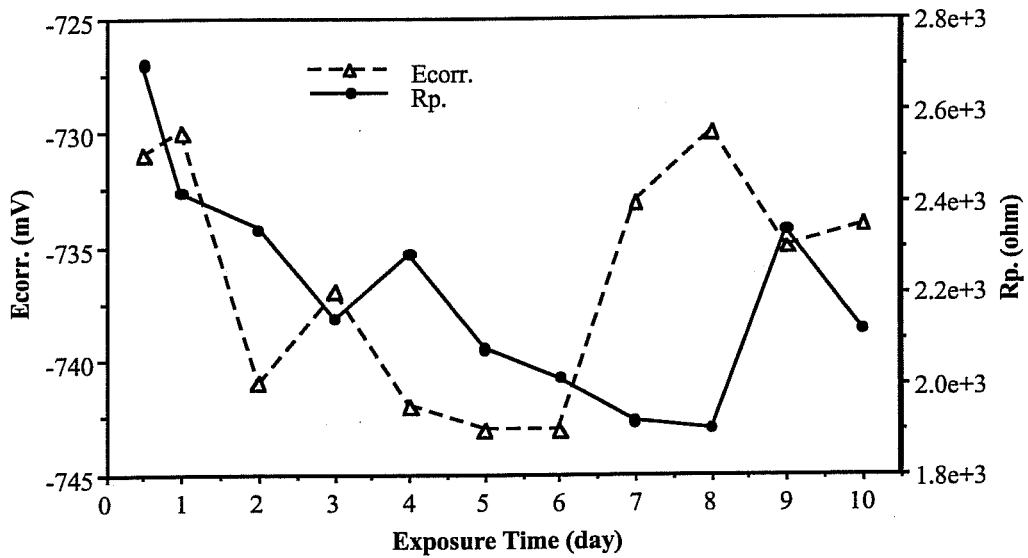
Fig. 5.20. Variation of $E_{corr.}$ and R_p with time for the representative polished reinforcing steel disk.
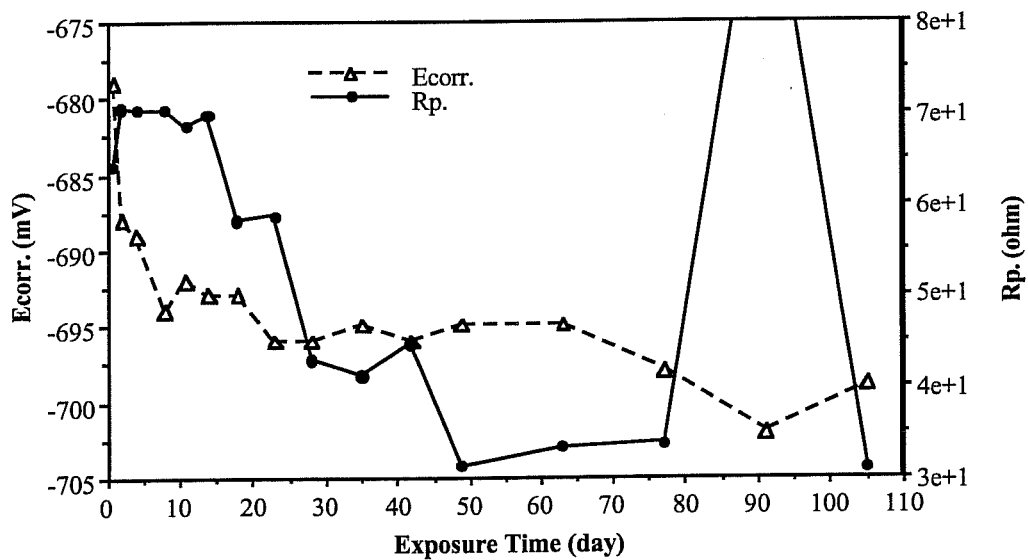
Fig. 5.21. Variation of $E_{corr.}$ and R_p with time for the representative uncoated reinforcing steel bar specimen.
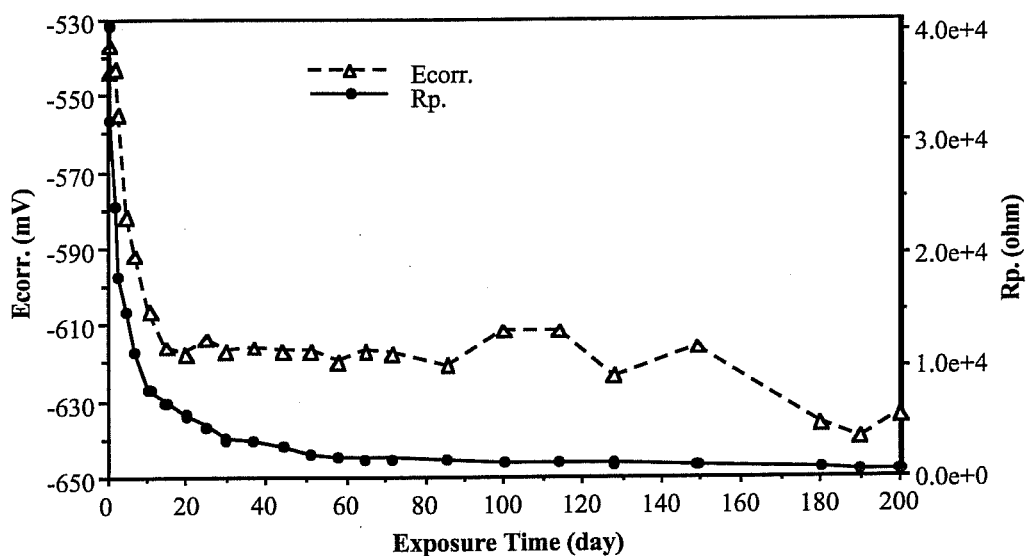
Fig. 5.22. Variation of $E_{corr.}$ and R_p with time for the first representative ECR bar specimen exhibiting poor coating performance.
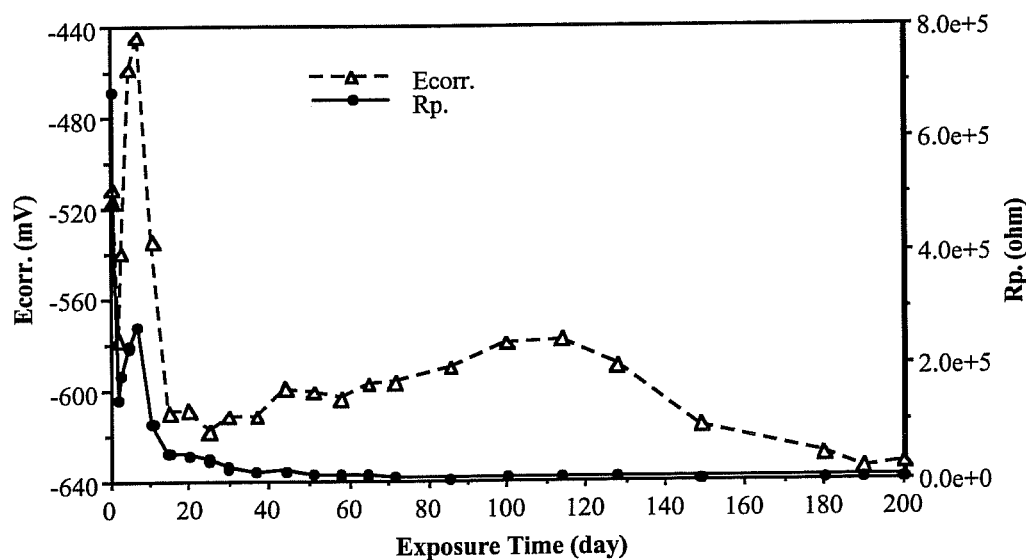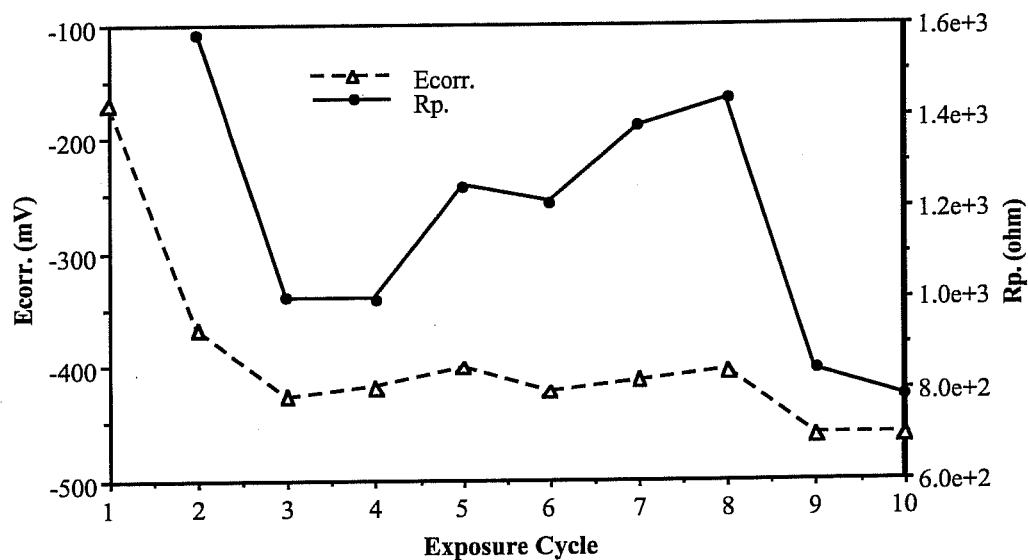

Fig. 5.23. Variation of $E_{corr.}$ and R_p with time for the second representative ECR bar specimen exhibiting poor coating performance.

Fig. 5.24. Variation of $E_{corr.}$ and R_p with time for the representative uncoated reinforcing steel bar embedded in a concrete block.
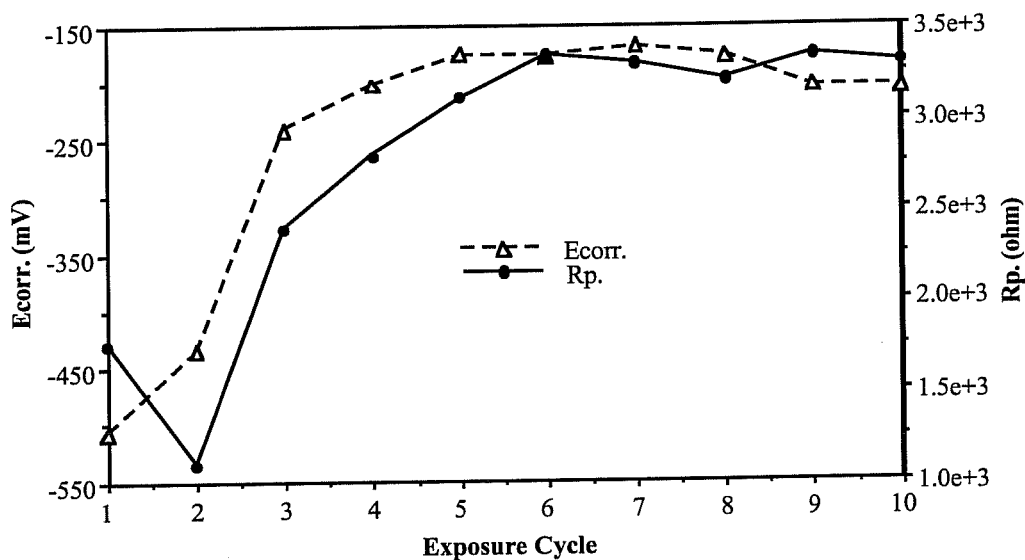
Fig. 5.25. Variation of $E_{corr.}$ and R_p with time for the first representative ECR bar embedded in a concrete block.
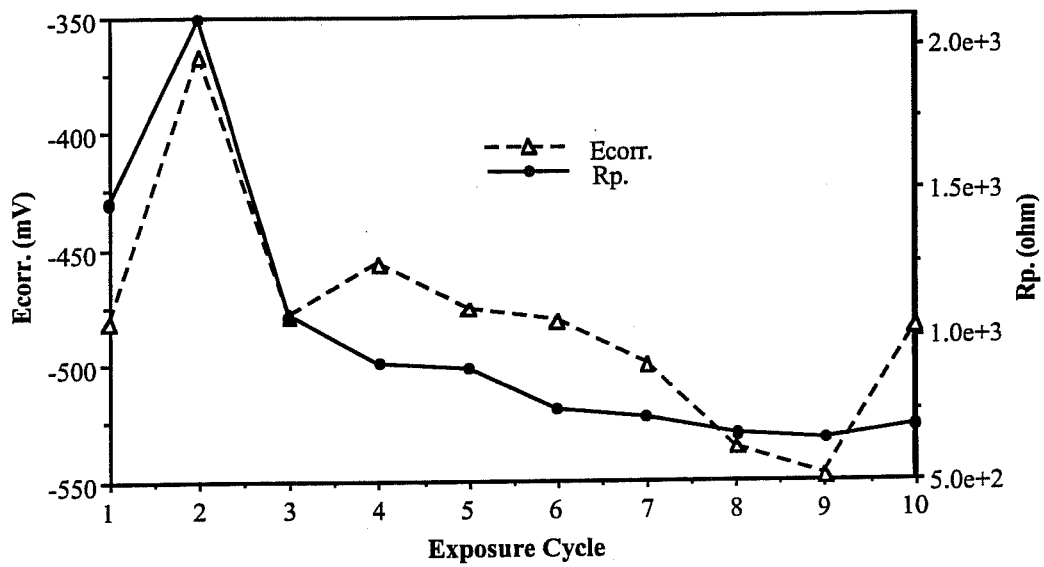
Fig. 5.26. Variation of $E_{corr.}$ and R_p with time for the second representative ECR bar embedded in a concrete block.

variation of polarization resistance generally follows the trend of corrosion potential change in cases where the overall change of corrosion potential is more than about 100 mV, i.e. change from a certain level of corrosion activity to another. Fig. 5.22 through Fig. 5.26 may represent the above situation. However, it is also important to note that the variations of the two curves do not always coincide with each other. These observations show that the corrosion potential can qualitatively indicate the level of corrosion activity, but it can not quantitatively relate to the corrosion rate. Fig. 5.20 and Fig. 5.21 represent cases in which the corrosion potentials are always very active and yet there is apparently no correlation between R_p and corrosion potential.

One surprising result was the passivation behavior observed in Fig. 5.21, in which the polarization resistance becomes four orders larger than usual, while the corrosion potential still remains in the very active range. This may be because the passivation behavior is due to the masking of a large portion of the active surface area by the protective film(s); which results in an increase in charge transfer resistance due to the area factor (i.e. resistance is inversely proportional to the area of a conductive path) and an additional effect from the diffusion impedance. The above may occur although corrosion is still thermodynamically favored on the surface. The components of the polarization resistance are actually different between the passive and the active conditions. The meaning of polarization resistance will be discussed more in the next section.

Finally, one important point to emphasize is that the polarization resistance values shown on the above figures do not take the area into account. Thus, they represent the overall corrosion resistance of various specimens

separately. One can change from Ω to $\Omega \cdot cm^2$ by multiplying the polarization resistance values by the reacting surface areas of various specimens before making comparisons. However, it is usually difficult, or even realistically impossible, to determine the actual reacting area, since the corrosion in this experiment is really not uniform in nature. This point will be proved later when we characterize the corroded surface.

5.1.3 Correlation between Results of Impedance Spectroscopy and Polarization Resistance Measurement

As the theory for the polarization resistance method was developed for corrosion cells completely under charge transfer rate control, the result of polarization resistance measurements is considered equivalent to the charge transfer resistance only in that type of simple corrosion cell. For more complex systems, such as a coated metal, where other factors also contribute to the corrosion resistance, the measured polarization resistance values are comprised of the contributions from all the factors present. The correlation between the results of impedance spectroscopy and polarization resistance measurement for those representative specimens are described under three main categories according to their corrosion controlling mechanisms as below.

Corrosion under Complete Charge Transfer Rate Control

Strictly speaking, only the polished reinforcing steel disk belongs to this category. The uncoated reinforcing steel, which also corrodes under charge transfer rate control, actually has an extra effect from a film resistance (as

determined from EIS), even though that contribution is relatively minor. Therefore, it is still proper to be discussed in this category. The Nyquist plots for the above two specimens all have well defined semi-circles in which the diameters represent the magnitude of the charge transfer resistance.

The values of the polarization resistance (or charge transfer resistance in this case) obtained from the two methods are shown in Fig. 5.27 and Fig. 5.28 for the polished disk and the uncoated reinforcing steel, respectively. It is observed that the two results usually show similar trends even though the result extracted from the impedance plot is always smaller than the result determined from the polarization resistance measurement. This observation shows that these two methods can provide consistent quantitative information on the corrosion rate.

There is one more observation that the difference between the two results, in terms of their ratio (since $\log A - \log B = \log \frac{A}{B}$), is generally bigger in the case of the polished disk than in the case of uncoated reinforcing steel. This may be explained by the slight discontinuity observed between curves at the high and the low frequencies in the case of the polished disk, which makes the semi-circle shrink at the low frequency portion as shown in Fig. 5.1. The discontinuity may be due to the relatively long measuring time required at the low frequencies for the EIS technique, and the very unstable reacting interface (as observed in Fig. 5.20) of the polished disk. The discontinuity is less apparent in the case of uncoated reinforcing steel which has a more stable reacting interface (as observed in Fig. 5.21).
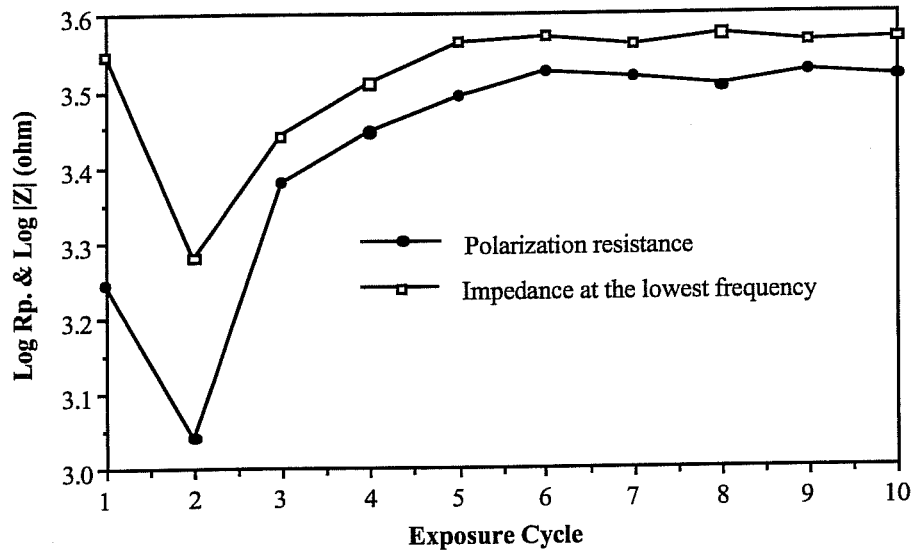
Fig. 5.32. Comparison of the corrosion resistance values obtained from polarization measurement and impedance spectroscopy for the first representative ECR bar embedded in a concrete block
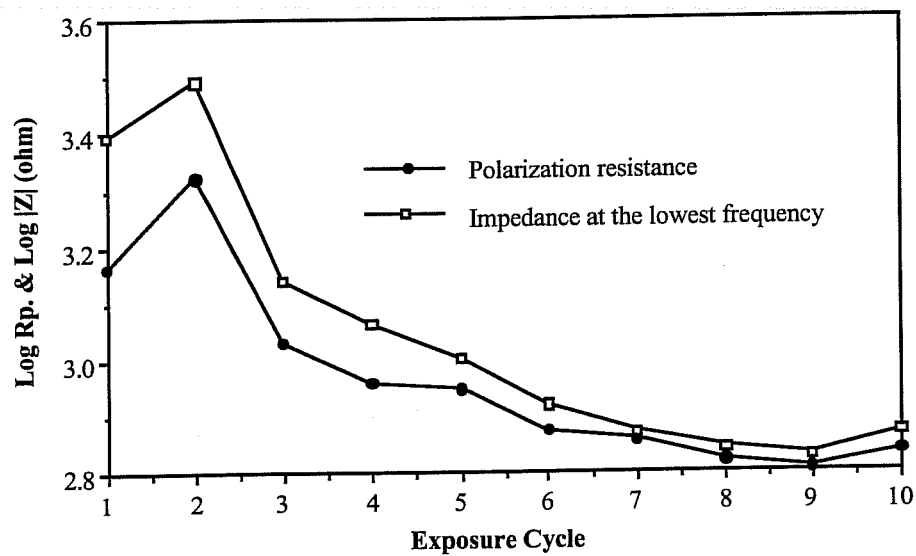
Fig. 5.33. Comparison of the corrosion resistance values obtained from polarization measurement and impedance spectroscopy for the second representative ECR bar embedded in a concrete block

exposure times due to the build up of the corrosive concentration around the reinforcing steel. If the total impedance value is used to correlate with the corrosion rate; certain safety factors must be taken into account since it may underestimate the actual corrosion rate.

Corrosion under Complete Diffusion Rate Control

For ECRs with intermediate and good coating qualities, there is usually no polarization resistance value that can be obtained due to the instrumental limitation. It is generally observed from the experimental results that the resistance can be measured only when its value is below about 10^6 ohms. The only data available here are for the first specimen in the category of ECR with intermediate coating quality; the data were taken on the 200th day. The corresponding Nyquist plot is shown in the Fig. 5.7. The total impedance value ($\log |Z| = 6.154$) is also a little larger than the polarization resistance value ($\log R_p = 5.992$), as in the preceding case.

5.1.4 Macrocell Corrosion Current

The measured macrocell corrosion current values together with the corrosion potential values for the three representative concrete block specimens are shown in Fig. 5.34 through Fig. 5.36. It is observed that the variation of the macrocell corrosion current follows the variation in corrosion potential even more consistently than the polarization resistance, as shown in Fig. 5.24 through Fig. 5.26. The corrosion current always decreases as the corrosion potential shifts to a more positive (noble) value and vice versa.
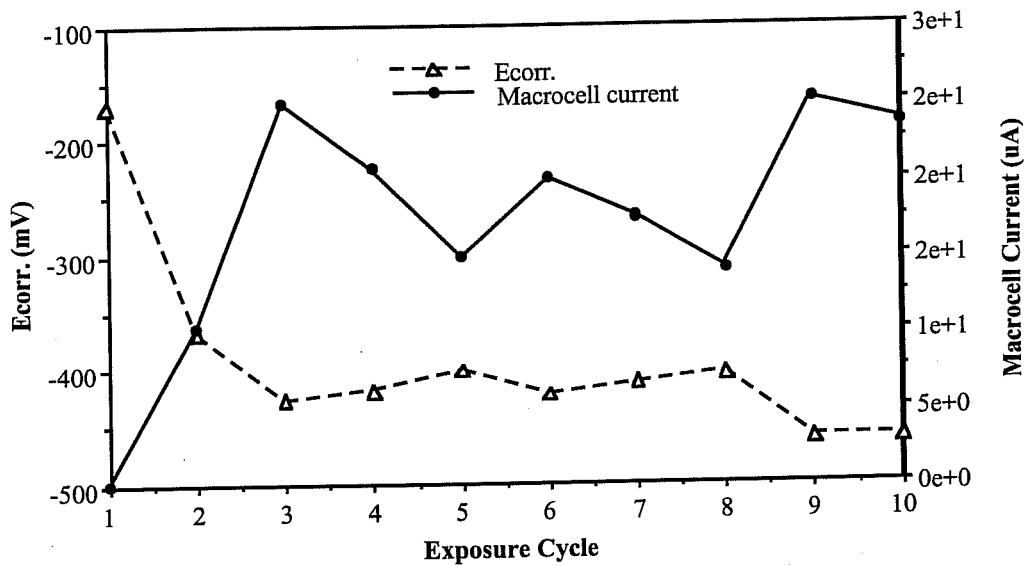
Fig. 5.34. Variation of E_{corr} and macrocell corrosion current with time for the representative uncoated reinforcing steel bar embedded in a concrete block.
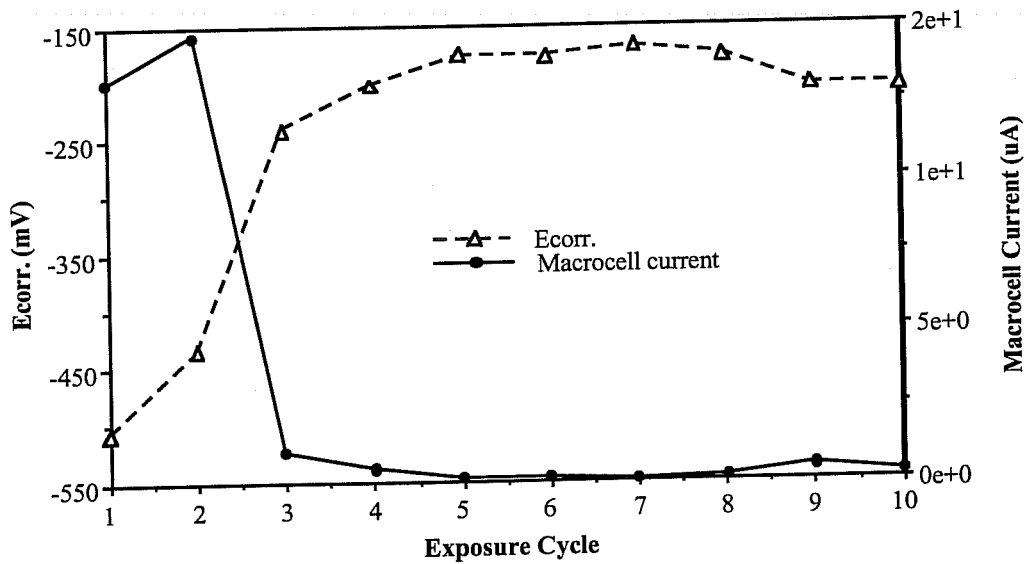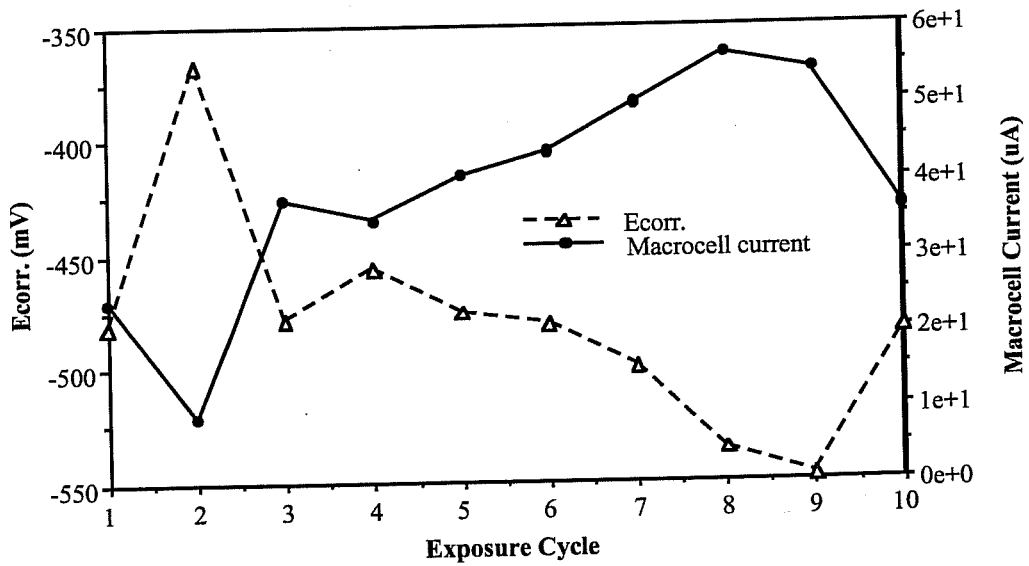

Fig. 5.35. Variation of E_{corr} and macrocell corrosion current with time for the first representative ECR bar embedded in a concrete block.

An attempt to find out a general relationship between corrosion current and corrosion potential for reinforcing steel embedded in concrete block is made by arranging all the results of the ten macrocells in a current versus potential plot, as shown in Fig. 5.37. Both the macrocell current and the current calculated from the polarization resistance are included. It is observed that macrocell corrosion current apparently has a more well defined distribution curve and a better correlation with the corrosion potential.

Finally, it must be noted that the corrosion current discussed above is the overall corrosion current measured on each specific specimen. It may relate to the total metallic loss of a specimen. For the actual corrosion rate or the corrosion severity, one should divide the corrosion current value presented above by the actual reacting surface area. However, this is considered unrealistic as discussed previously in section 1.2.

5.1.5 Supplemental Information on Corrosion Morphology

In this section, photographs as well as optical and scanning electron micrographs, and results of X-ray powder diffraction for the polished reinforcing steel disk and the uncoated reinforcing steel are presented. The information about the microstructural changes on the steel surface due to corrosion may help us understand the previous electrochemical test results. The photographs and micrographs for ECR specimens will be presented later in part two.

Fig. 5.36. Variation of $E_{corr.}$ and macrocell corrosion current with time for the second representative ECR bar embedded in a concrete block.
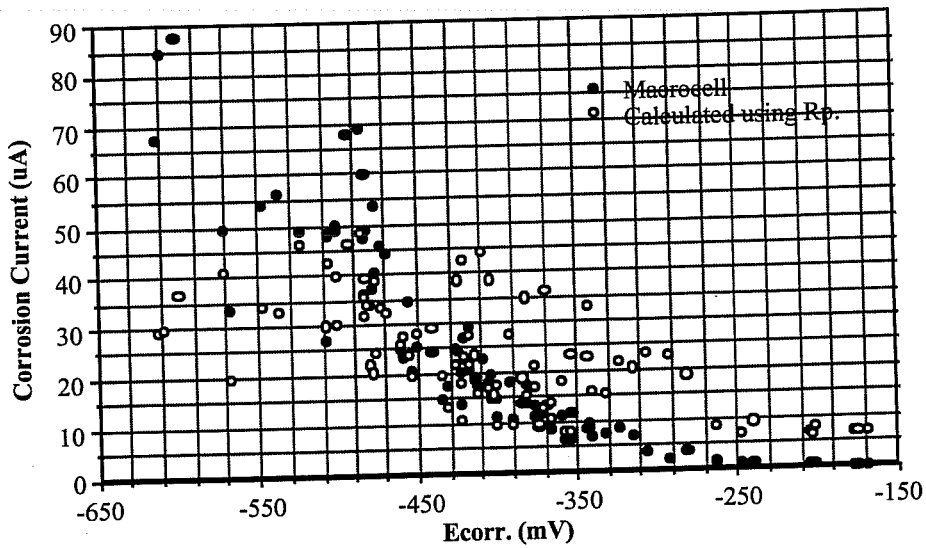
Fig. 5.37. Corrosion currents versus $E_{corr.}$ for all the reinforcing steel bars embedded in concrete blocks.

Polished Reinforcing Steel Disk

Photo 5.1 shows the surface of a polished reinforcing steel disk right before exposure to solution. The uniformly distributed grooves are the traces of polishing cloth (600 grit), while the dark spots may be the impurities or contamination which results from the polishing process. An optical microscope is used in this case, since the contrast is too low on this surface and SEM cannot provide a clear image. Photo 5.2 through Photo 5.7 are SEM micrographs of the same polished disk surface, right after ten days of immersion in 3.5% salt solution for electrochemical testing. Photo 5.2 shows the boundary between the uncorroded and the slightly corroded regions. Photo 5.3 through Photo 5.5 show the slightly corroded region at various magnifications. While the corrosion of steel immersed in salt solution has been considered to be of uniform type, it is evident from these photos that the appearance is similar to intergranular corrosion; while a few scattered signs of pitting corrosion are also observed. Photo 5.6 and Photo 5.7 are taken at the severely corroded region. In Photo 5.6, extensive surface pitting is observed in addition to the intergranular-like corrosion; also, different degrees of corrosion in this region are distinguishable. Photo 5.7 shows an isolated, uncorroded area among the severely corroded regions.

The above observations show us two significant points. First, the existence of regions which are corroded to various extents (or even uncorroded) indicates the formation of local-action corrosion cells on the steel surface. Some areas of the surface may act as the anode while others act as the cathode. The anode and the cathode areas may interchange and shift from place to place as the
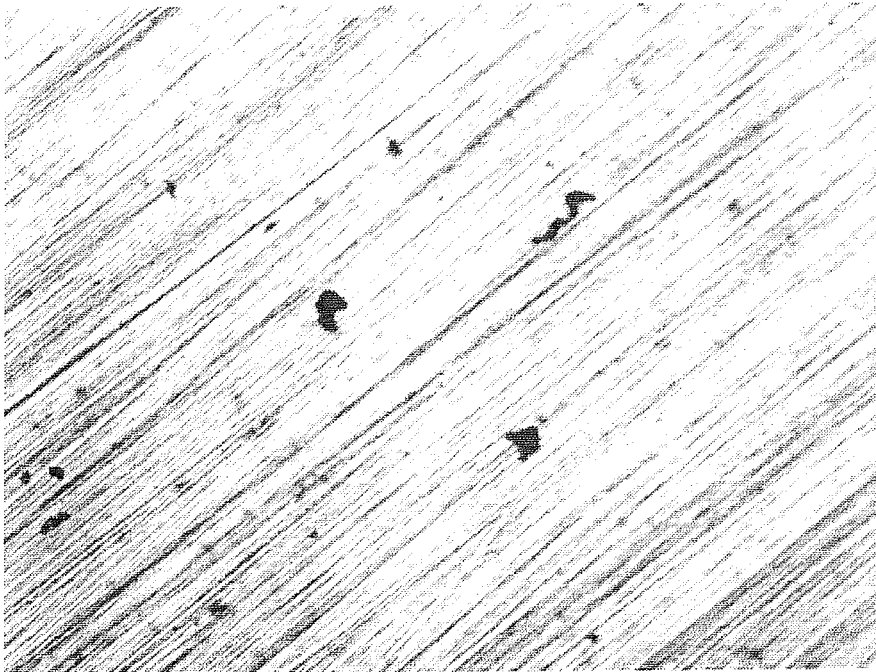
Photo 5.1. Optical micrograph of a polished reinforcing steel disk before exposure to solution. (x80)
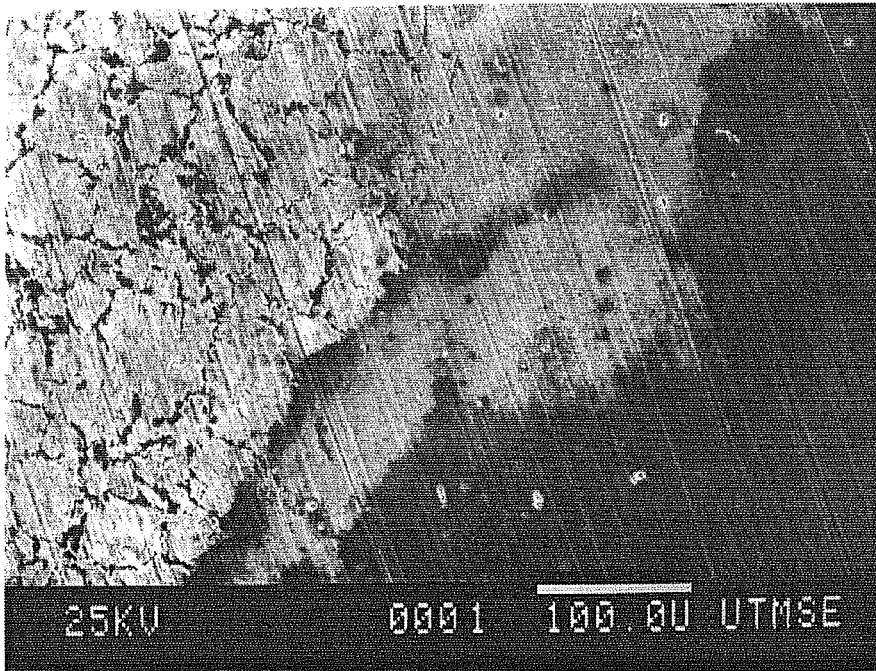

Photo 5.2. SEM micrograph of a polished reinforcing steel disk after 10-day immersion in 3.5% NaCl solution, showing the boundary between slightly corroded and uncorroded regions. (x200)
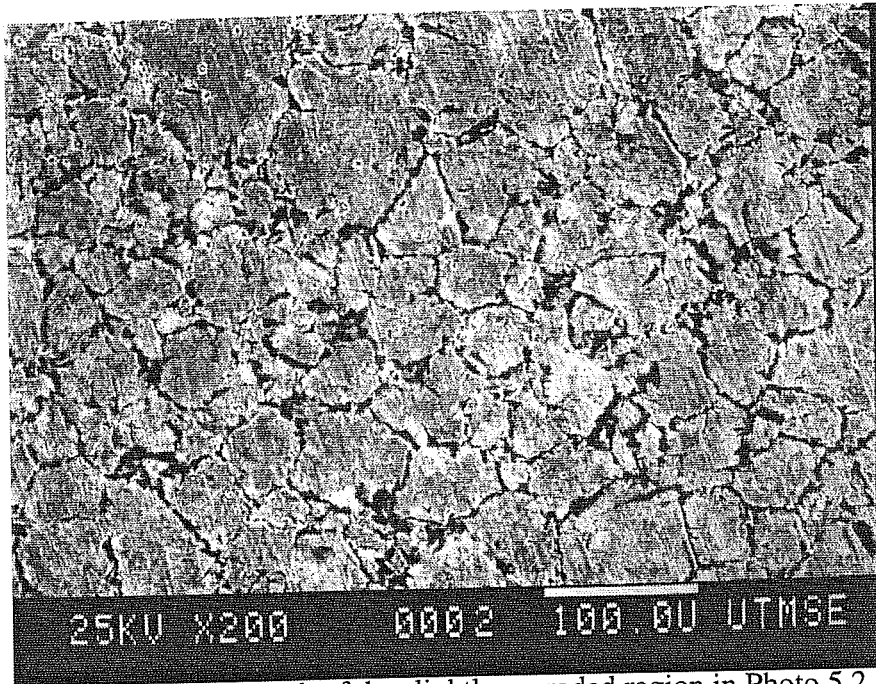
Photo 5.3.　SEM micrograph of the slightly corroded region in Photo 5.2 showing intergranular-like corrosion.
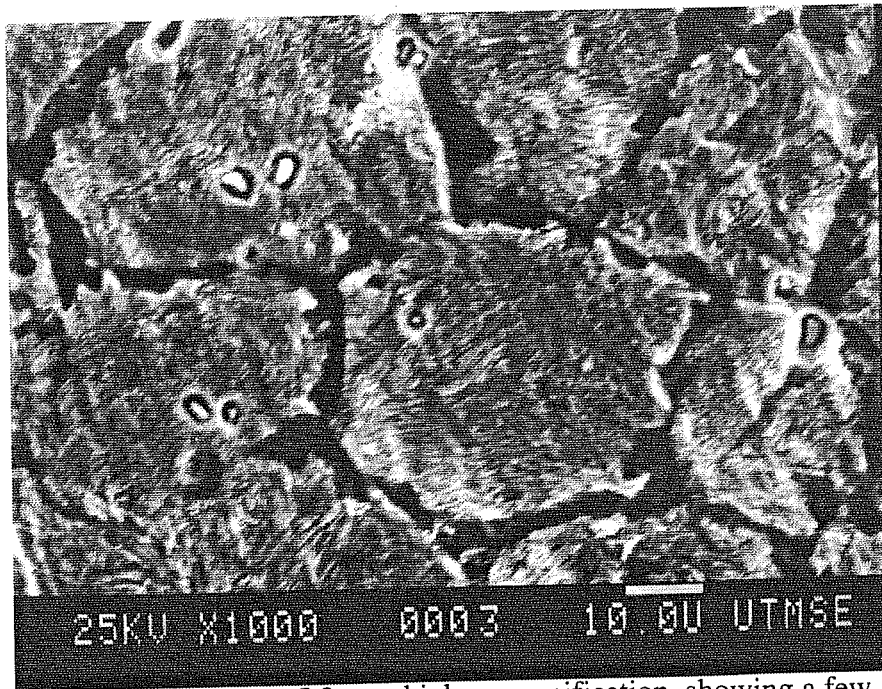

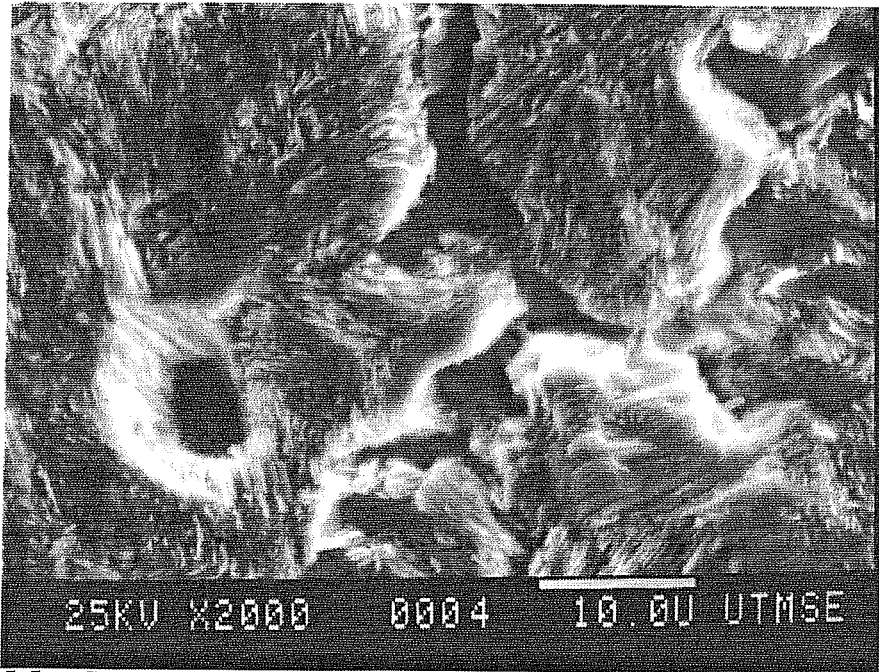Photo 5.4.　Same as Photo 5.3, at a higher magnification, showing a few scattered signs of pitting corrosion.

Photo 5.5.   Same as Photo 5.4, at an even higher magnification, showing a pit.
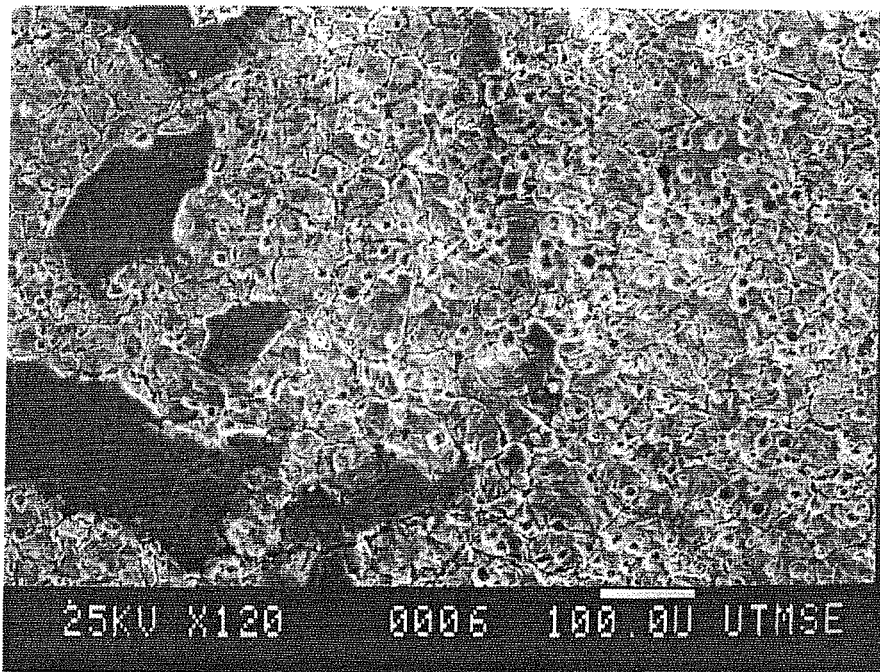
Photo 5.6.   SEM micrograph of the severely corroded region on the same disk in
Photo 5.2 through Photo 5.5 showing extensive surface pitting in
addition to the intergranular-like corrosion.

corrosion reaction proceeds. Secondly, the corrosion observed on this evenly polished steel surface generally has a localized form. While the intergranular-like corrosion is dominant when the surface just starts to corrode, pitting corrosion occurs afterwards. As a conclusion here, it is sometimes impossible to get the actual reactive surface areas of the specimens under these exposure conditions; and thus attempts to obtain actual corrosion rates (or corrosion current densities) for a specimen may lead to erroneous results.

Uncoated Reinforcing Steel

Before exposure to solution

The typical appearance of the as-received uncoated reinforcing steel specimens before exposure to solution is shown in Photo 5.8. The surface is black due to the formation of mill scale, which is believed to be mostly Fe_3O_4 (magnetite). Fe_3O_4 is an oxidation state between FeO and Fe_2O_3 (i.e. some Fe in magnetite is in the FeO and the rest in the Fe_2O_3 oxidation state). Photo 5.9 is an SEM micrograph of the black surface, which shows a shell-like outer layer and a portion of exposed area underneath. Micrographs with higher magnifications of the two regions are further shown in Photo 5.10 (outer shell) and Photo 5.11 (underneath area), respectively. It is observed that both surfaces show continuous and uniform films, only with difference in the coarseness. They are both believed to be mill scales formed at high temperature, but with a little difference in the degree of oxidation. From experience in handling the uncoated reinforcing steel, it is also observed that some of the outermost layer of mill scale may fall off sometimes, and the uncovered surface still looks similar in appearance to the
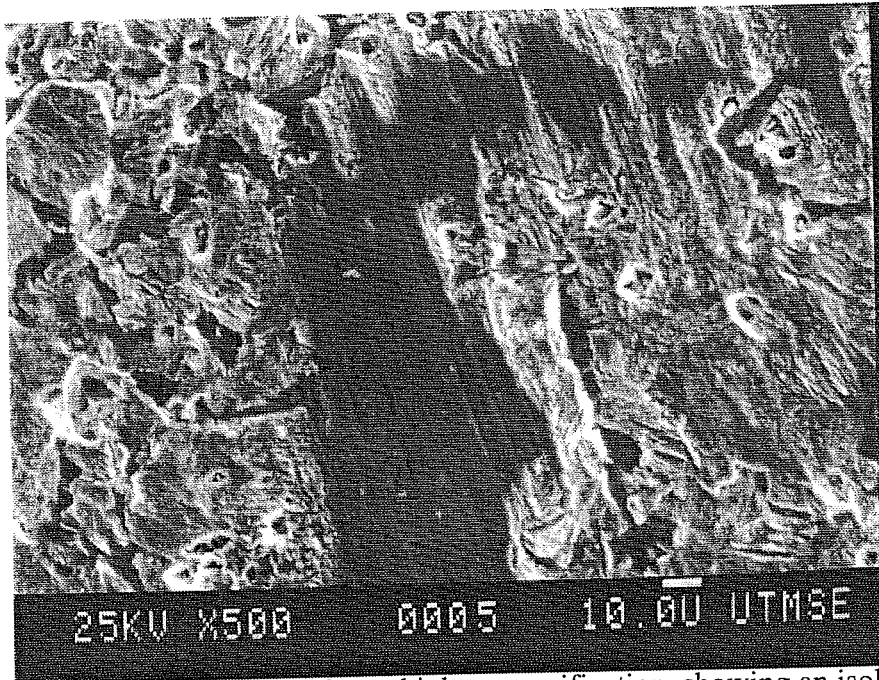
Photo 5.7. Same as Photo 5.6, at a higher magnification, showing an isolated, uncorroded area among the severely corroded region.
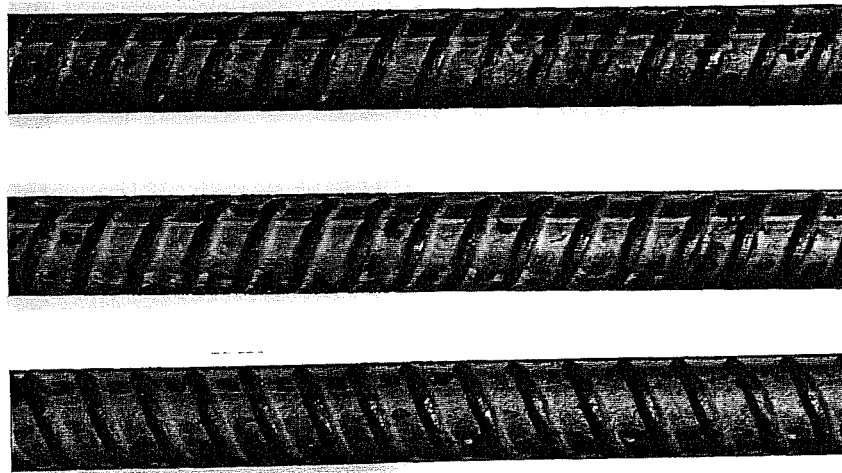

Photo 5.8. Photograph showing typical appearance of as-received uncoated reinforcing steel bars before exposure to solution.
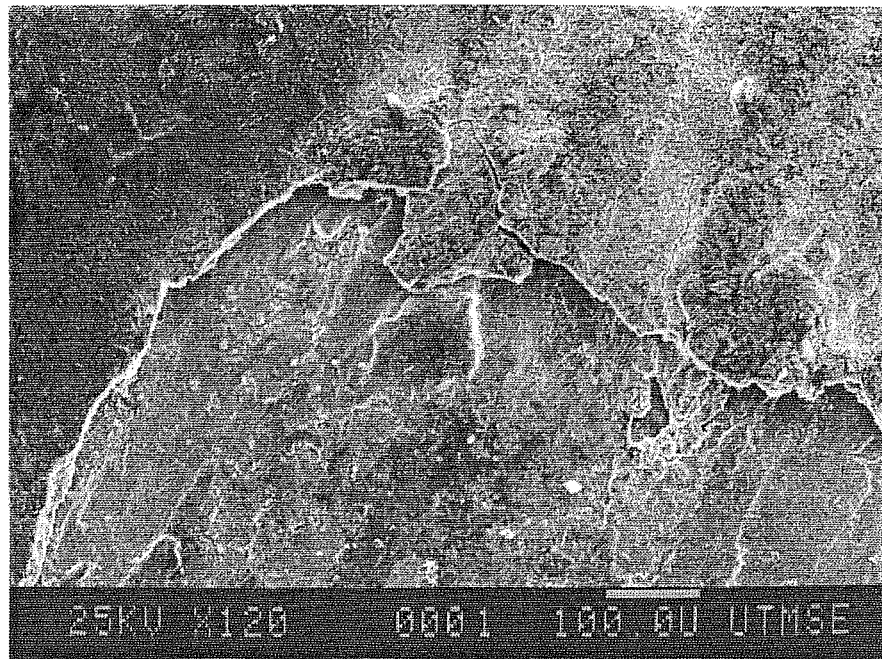
Photo 5.9. SEM micrograph of an uncoated rebar before exposure to solution showing a shell-like outer layer and a portion of exposed area underneath.
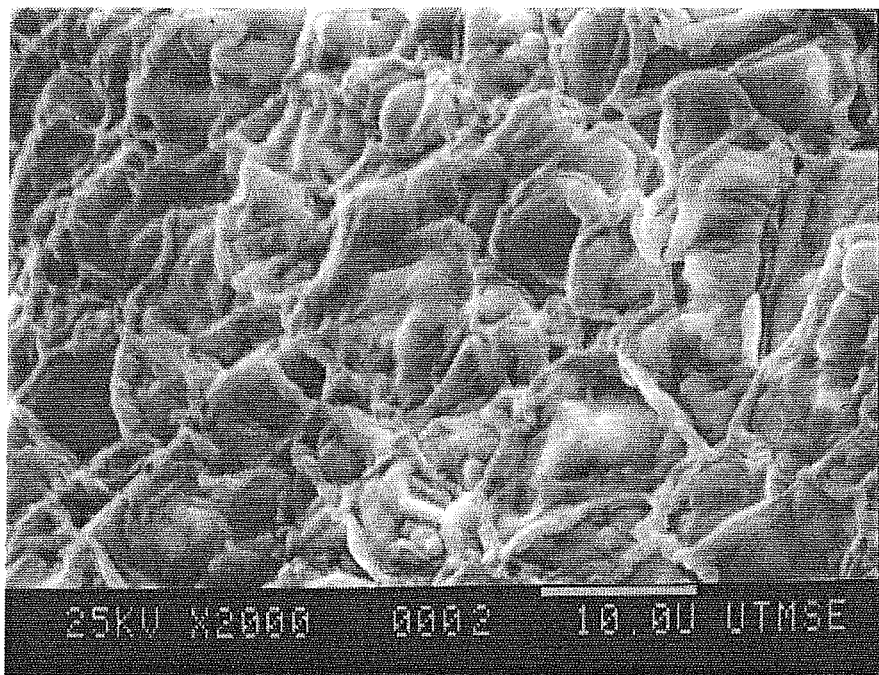

Photo 5.10. High magnification picture of the shell-like outer layer in Photo 5.9 showing continuous and uniform film.

intact portion. In some cases, orange-colored areas are observed on the surfaces of specimens that have not been immersed. The orange-colored rust is $Fe_2O_3 \cdot H_2O$ (hydrated ferric oxide) or $FeOOH$ ($Fe_2O_3 \cdot H_2O = 2FeOOH$); and a representative micrograph of those areas is shown in Photo 5.12, in which a layer of mottled, irregularly sized and shaped corrosion products is observed to form over the originally uniform surface of mill scale. This further oxidation from Fe_3O_4 to $Fe_2O_3 \cdot H_2O$ is due to the presence of moisture on the reinforcing steel surface after it is removed from the mill. It is generally believed that the magnetite mill scale can protect the steel substrate from corrosion to a certain extent; and it can remain protective even in the presence of uncontaminated water vapor since the pores in it will be further plugged by the newly formed, insoluble oxide corrosion products such as $Fe_2O_3 \cdot H_2O$ [62].

<u>After exposure to 3.5% NaCl solution</u>

During the immersion period, flocculent oxide corrosion products are observed to form on the surface of the reinforcing steel. They are very loose and may fall off from the surface sometimes. However, corrosion products that are orange to red brown in color always continue to form at the outermost rim, while the layer right beneath it is black in color. After removal from the solution, the orange-colored corrosion product becomes more compact and turns dull as it dries up. Typical appearance of the specimens after 105 days of immersion is shown in Photo 5.13. A close-up picture of the corroded surface is shown in Photo 5.14, in which various types of corrosion products are observed. The corrosion products are generally characterized by their colors as below:

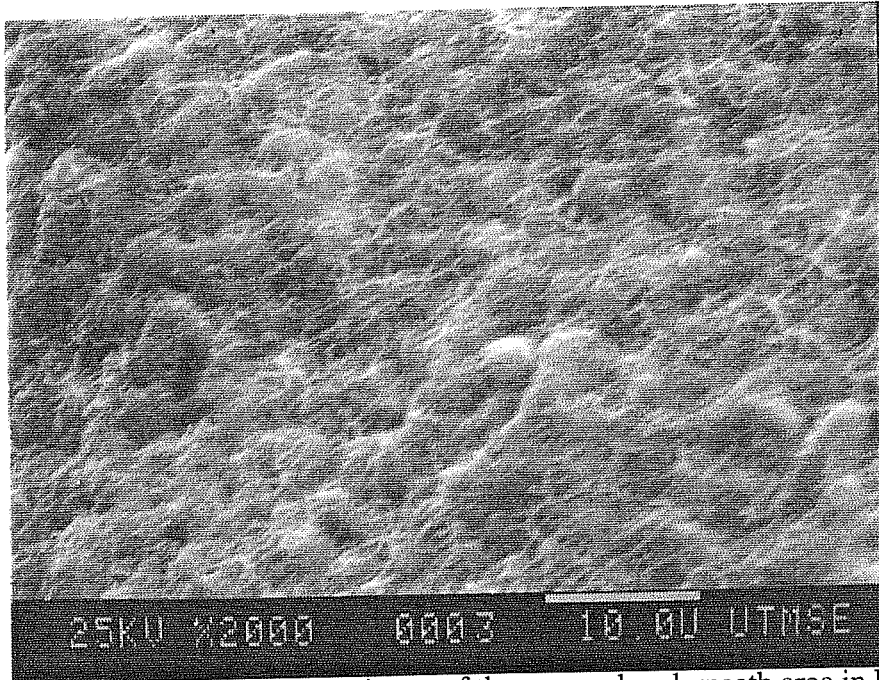<u>Outer layer</u>: $Fe_2O_3 \cdot H_2O$ (or $FeOOH$) which is orange to red brown in color;

Photo 5.11. High magnification picture of the exposed underneath area in Photo 5.9, also showing continuous and uniform film but with different coarseness compared to that in Photo 5.10.
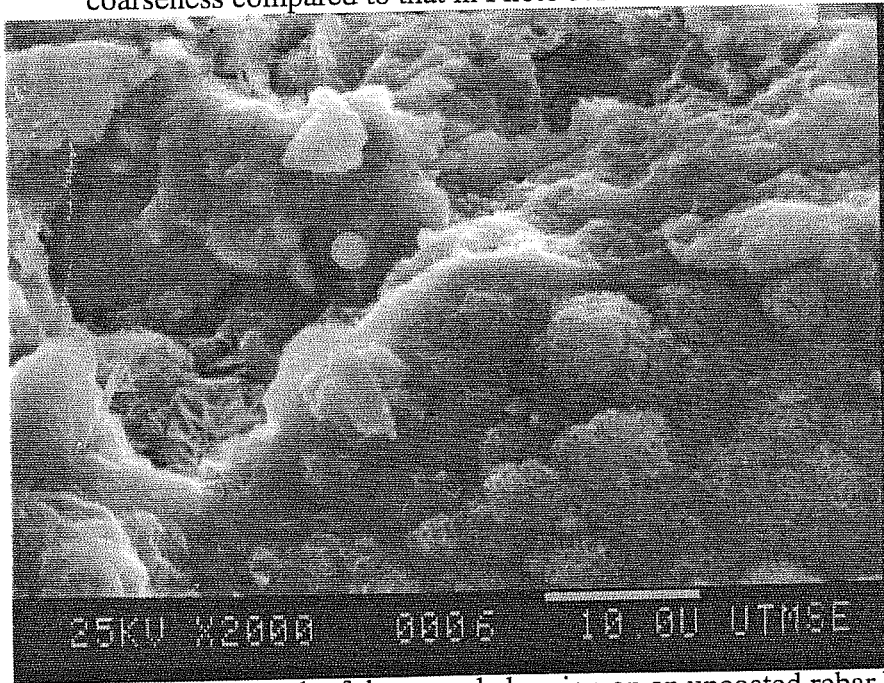

Photo 5.12. SEM micrograph of the corroded region on an uncoated rebar before exposure to solution showing irregularly sized and shaped corrosion products.

Photo 5.13. Photograph showing typical appearance of uncoated reinforcing steel bars after 105 days of immersion in 3.5% NaCl solution.

Photo 5.14. Close-up picture of a corroded surface showing various types of corrosion products.

Intermediate layer: Fe_3O_4 (or $FeO \cdot Fe_2O_3$) which is black in color;

Inner layer: $FeO \cdot H_2O$ (or $Fe(OH)_2$) which is brown to greenish black in color.

A series of SEM micrographs for the various layers of corrosion products and the corroded steel surfaces underneath them are shown in Photo 5.15 through Photo 5.24. Photo 5.15, which is taken from the surface of the orange-colored outer layer of corrosion product, shows that the corrosion particles here are arranged in a coralloid, jagged and porous, network. Photo 5.16, which is taken from the same area as in Photo 5.15 but at a higher magnification emphasizes the porous structure. Photo 5.17 is taken from the surface of the black-colored intermediate layer of corrosion product. In this photo, some residue of the outer layer is still seen; and this layer is generally observed to be structurally very uniform and solid, except there are some cracks in it. Photo 5.18 is the close-up view of a crack observed in this layer. The inner layer of corrosion product usually sticks on the steel surface and cannot be peeled off in pieces as in the cases of the above two layers. Thus, the micrographs for this corrosion product are taken from the residue that adheres to the inner side of the intermediate layer. They are shown in Photo 5.19 and Photo 5.20 for the low and high magnification views, respectively. Photo 5.19 shows that the corrosion product of this layer also has a jagged and porous structure, but with different shape and packing pattern when compared to that of the outer layer. Photo 5.20 further shows that the corrosion particles grow in an arrangement of platelet stacking. Finally, the corroded steel surface, after removal of the corrosion products by soft brush and cleaning with methanol, is examined. Photo 5.21 gives a general view of the surface. It is interesting to find that a shell-like layer, as described in the
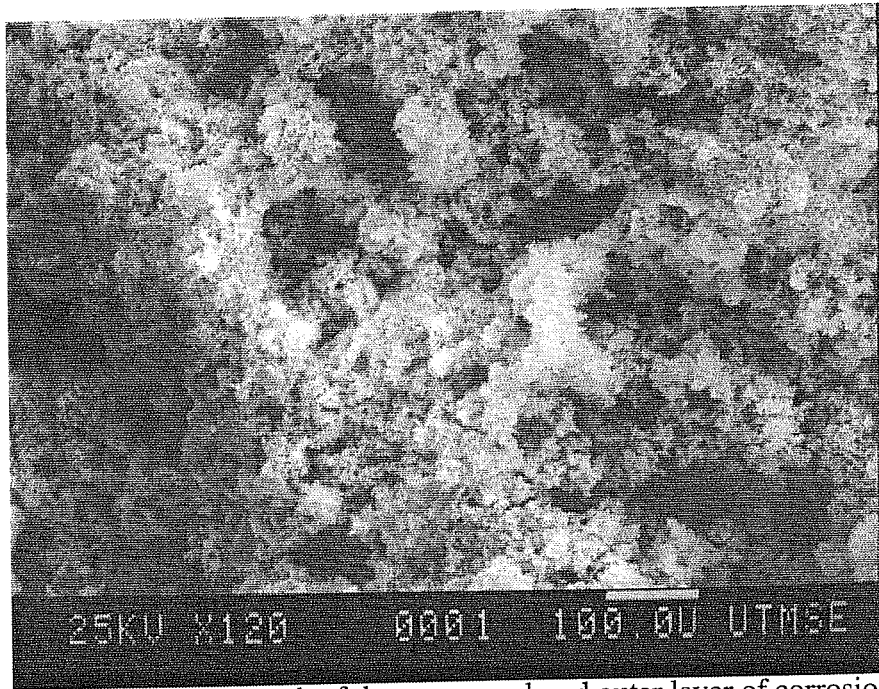
Photo 5.15. SEM micrograph of the orange-colored outer layer of corrosion product showing a coralloid, jagged and porous, network.
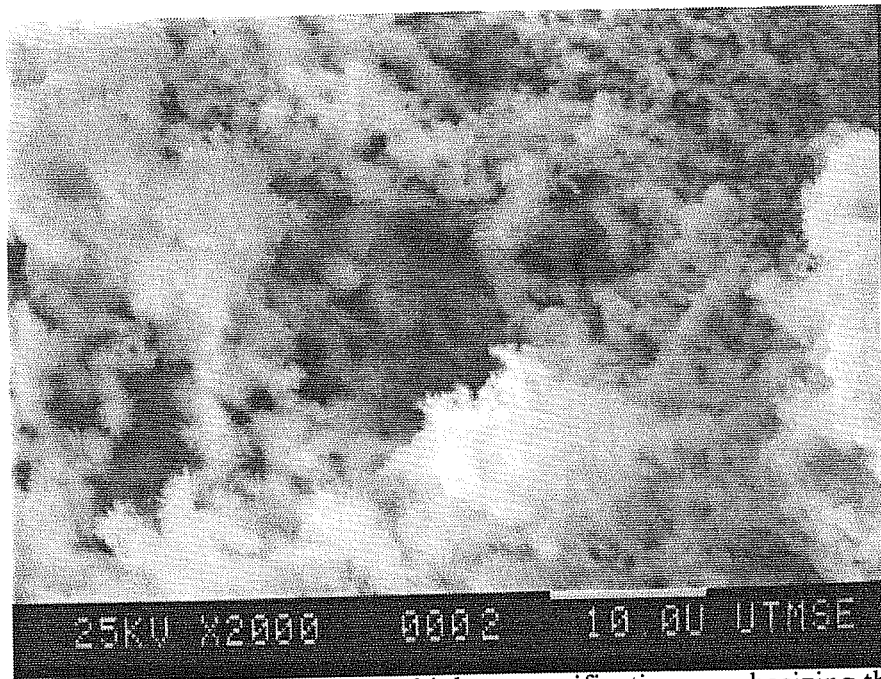

Photo 5.16. Same as Photo 5.15, at a higher magnification, emphasizing the porous structure.
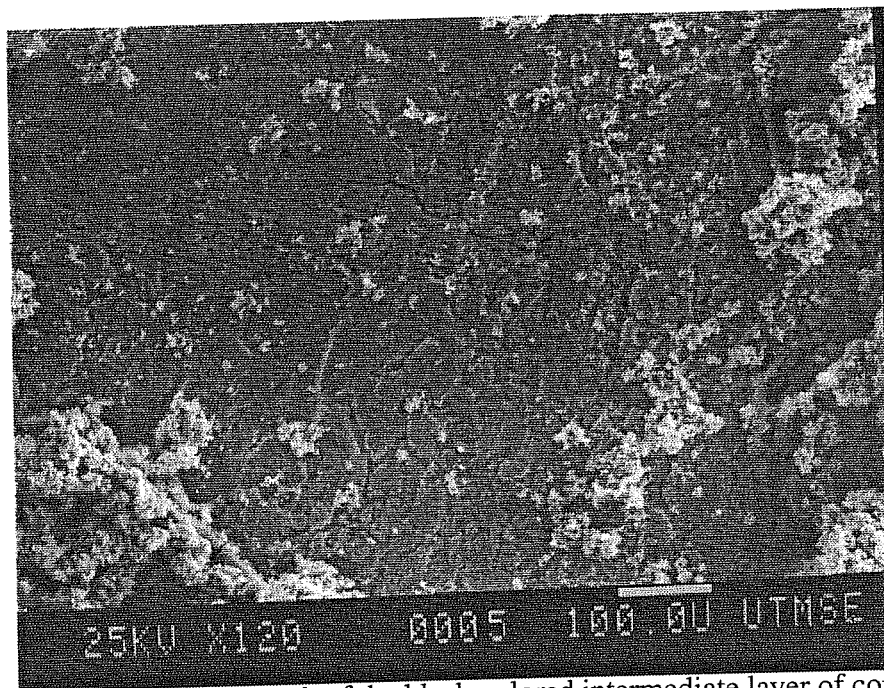
Photo 5.17. SEM micrograph of the black-colored intermediate layer of corrosion product showing a solid and uniform film.
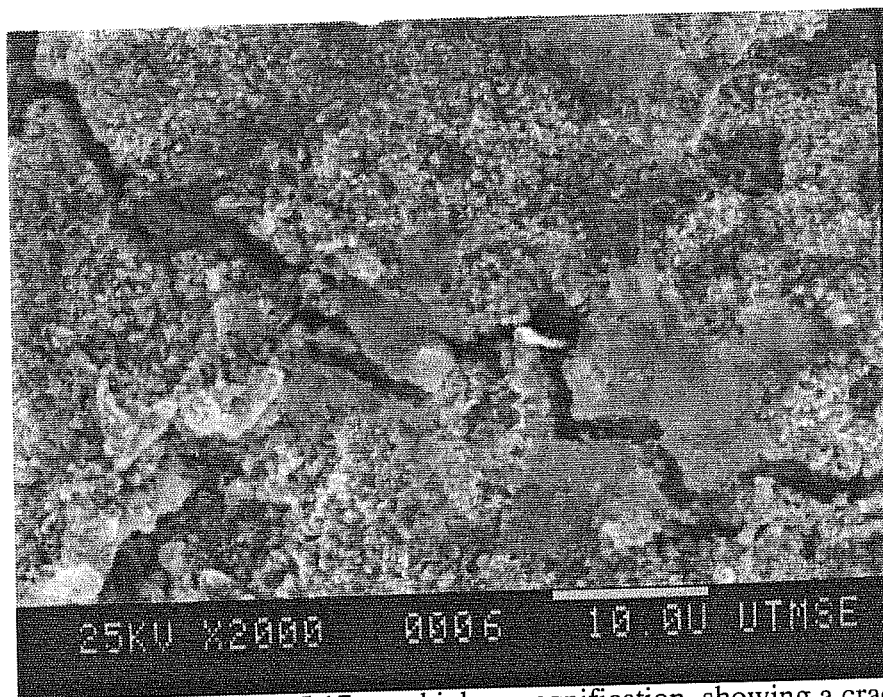

Photo 5.18. Same as Photo 5.17, at a higher magnification, showing a crack on the generally solid and uniform film.
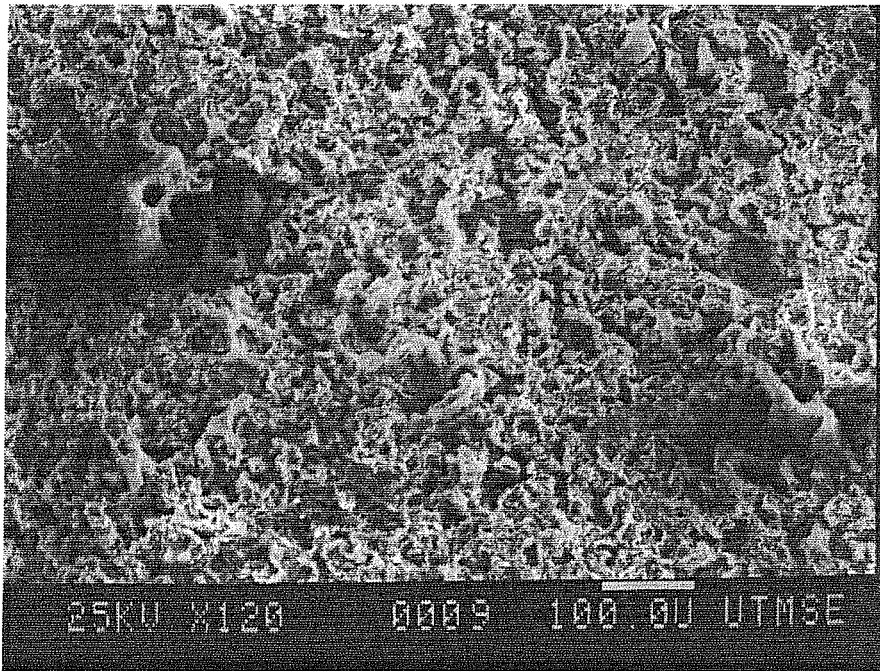
Photo 5.19. SEM micrograph of the inner layer of corrosion product, also showing a jagged and porous structure but with different shape and packing pattern compared to that of the outer layer in Photo 5.15.
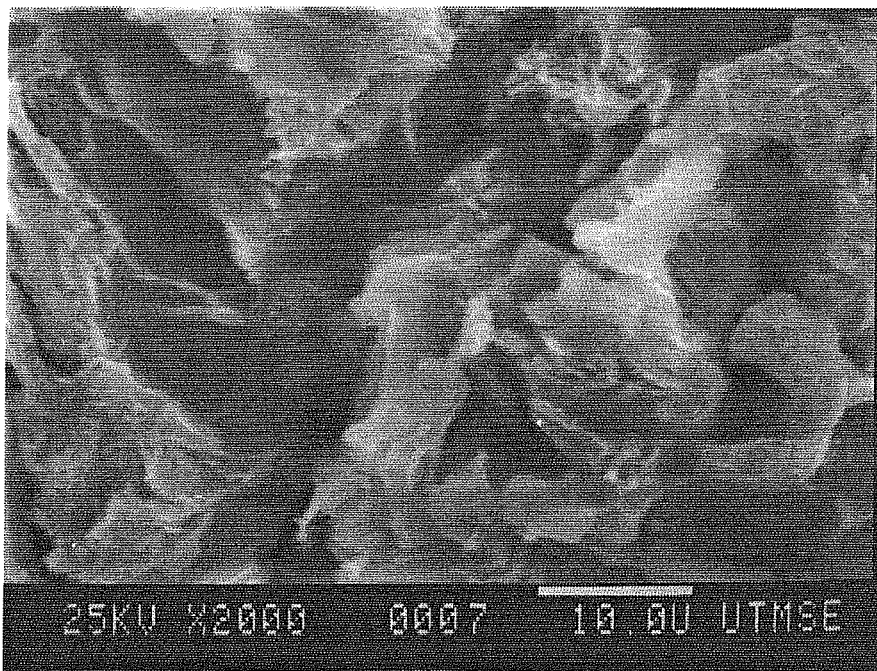

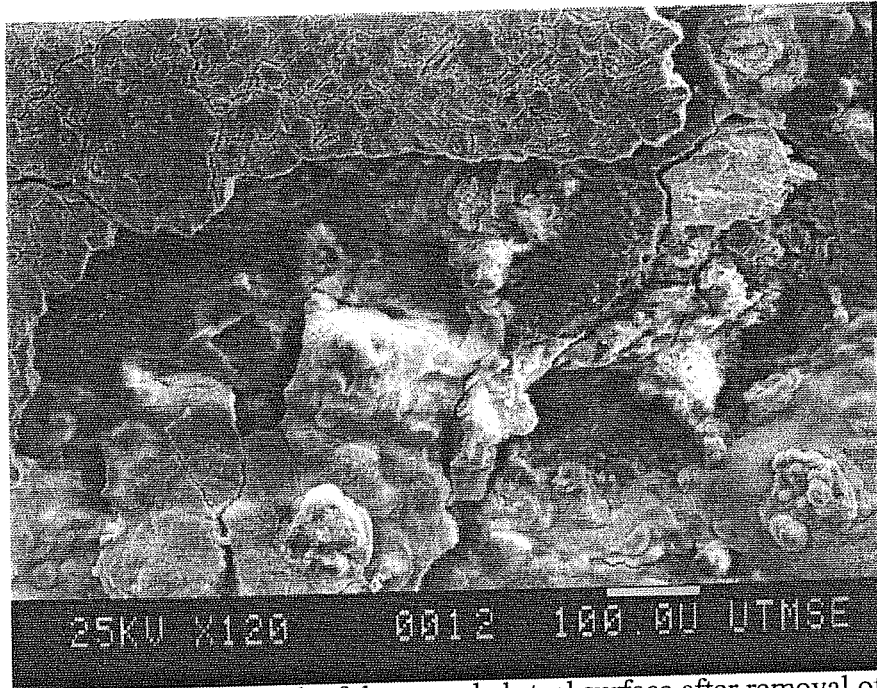Photo 5.20. Same as Photo 5.19, at a higher magnification, showing platelet stacking of corrosion particles.

Photo 5.21. SEM micrograph of the corroded steel surface after removal of the corrosion products showing a shell-like outer layer and a portion of exposed area underneath, as in Photo 5.9.
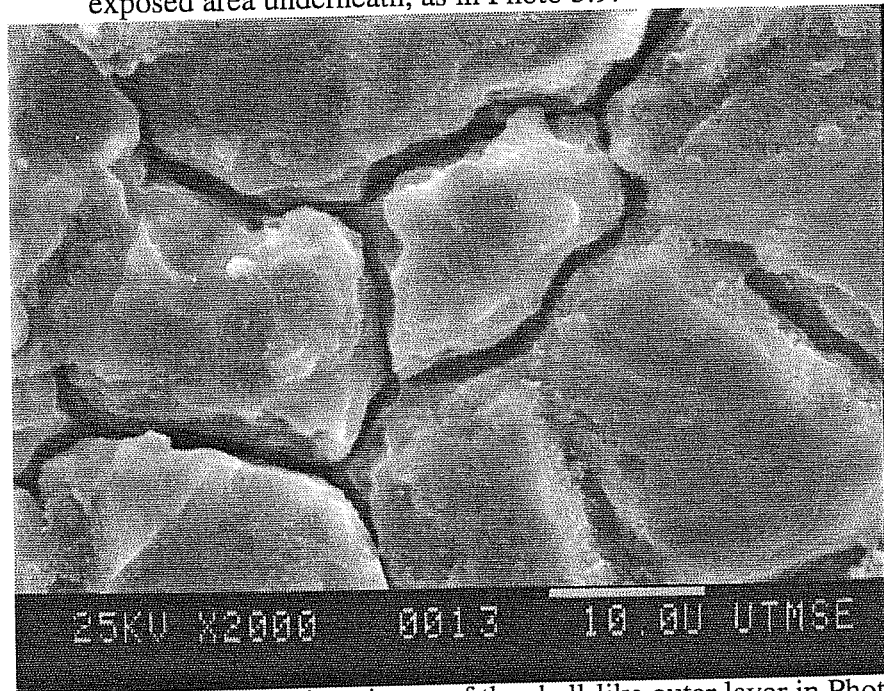

Photo 5.22. High magnification picture of the shell-like outer layer in Photo 5.21 showing intergranular-like corrosion.
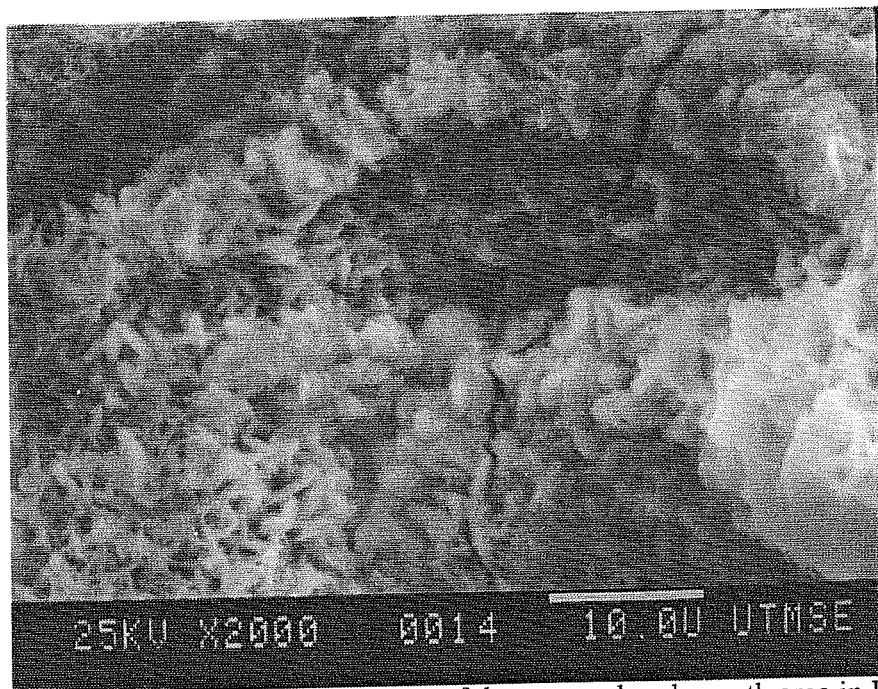
Photo 5.23. High magnification picture of the exposed underneath area in Photo 5.21 showing a gathering of irregularly sized and shaped particles that are believed to be some residual corrosion products.
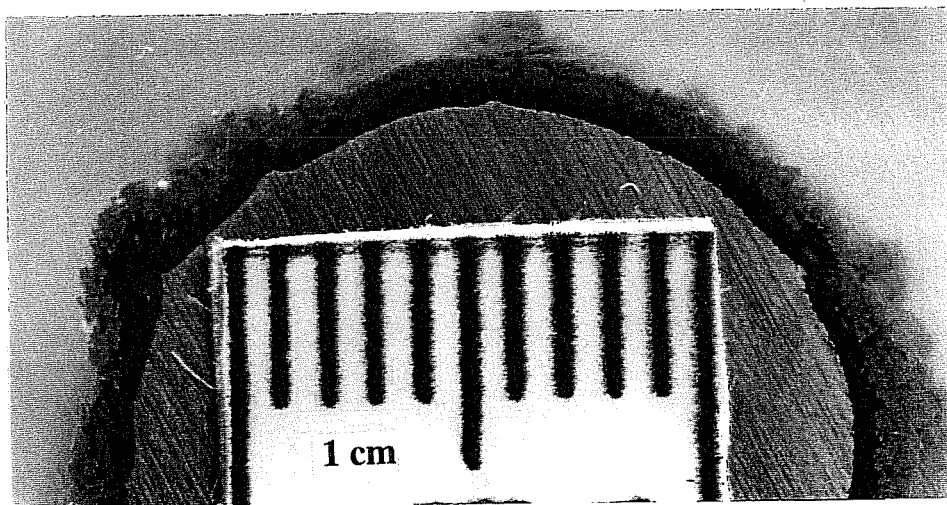

1 cm

Photo 5.24. Close-up picture of the cross-section of a corroded reinforcing steel bar, showing three layers of corrosion products.

preceding paragraph, is still observable in shape here; and it is observed that the corrosion is much more severe in its surrounding area. Photo 5.22 which shows a higher magnification view of the shell surface indicates that the intergranular-like corrosion is the dominant form on the shell during exposure. Photo 5.23 which is taken from the severely corroded surrounding area shows a gathering of irregularly sized and shaped particles that are believed to be some residual corrosion products. It is hard to tell what are the dominant corrosion forms here.

Another attempt to look into the layered structure of the corrosion products is made by cutting the corroded specimen transversely. The close-up picture of a cross-section is shown in Photo 5.24, in which the three different layers of corrosion products described above can be roughly distinguished by their colors. It is noted that the outermost layer of material in this picture is epoxy cold mount applied to fix those corrosion products in position. Photo 5.25 is an SEM micrograph of the three layers of corrosion products formed on the steel surface. It is observed that the outermost layer is generally much thicker than the inner two layers; while the intermediate layer has the most solid structure. The bright areas shown in the photo are caused by the charging effect on the nonconducting epoxy cold mount which flows into the voids among the corrosion products during curing. Furthermore, Photo 5.26, which shows a section of nicely formed intermediate layer, indicates that the intermediate layer can effectively block the flow of the epoxy cold mount if it is complete and thick enough; while in Photo 5.27, which shows a section of discontinuous intermediate layer, a flow path between the outer and the inner layers is clearly observed. Sometimes, no
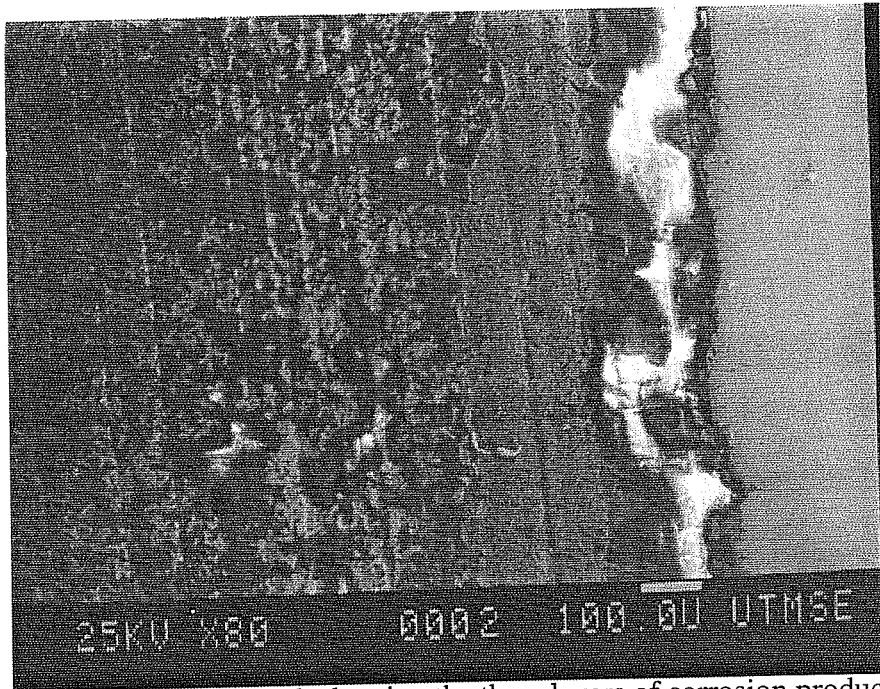
Photo 5.25. SEM micrograph showing the three layers of corrosion products formed on the steel surface. (The bright areas are caused by the charging effect on nonconducting epoxy cold mount.)
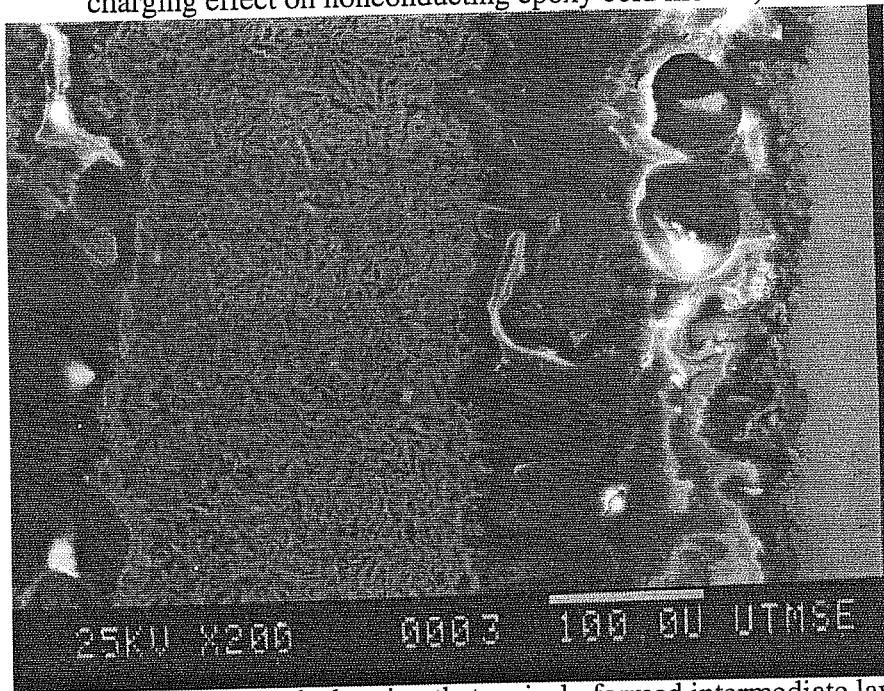

Photo 5.26. SEM micrograph showing that a nicely formed intermediate layer can effectively block the flow of epoxy cold mount.

clear intermediate layer is observed and the epoxy cold mount flows everywhere as shown in Photo 5.28.

The corrosion products were subjected to X-ray powder diffraction to identify the constitutive substances. They were roughly separated into two parts, the inner and the outer parts; however, some mixing did occur. The results were very consistent in all tests of the corrosion products. For the outer part, which is mostly composed of the orange-colored rust, the typical X-ray diffraction spectrum is shown in Fig. 5.38. It is apparent that FeOOH (Lepidocrocite) or $Fe_2O_3 \cdot H_2O$ is the main constituent here, while only an insignificant amount of Fe_3O_4 (Magnetite) is present. The typical spectrum for the inner part, which comprises mostly the intermediate and the inner layers of corrosion products, is shown in Fig. 5.39. It is observed that, contrary to preceding case, Fe_3O_4 is the dominant constituent here, with the FeOOH being relatively insignificant. In both cases, NaCl is observed to be present; while no distinguishable peaks for $FeO \cdot H_2O$ or $Fe(OH)_2$ can be observed at all. The meanings of all the above observations are discussed in the following.

First, even though it is generally known that the mill scale can protect the substrate steel in dry or uncontaminated humid air; severe corrosion is observed all over the steel surface when corrosive anions (Cl^-) are present. However, the corrosion observed on the outermost layer of mill scale (with intergranular-like form) is apparently less severe than that of the layer underneath it, as observed in Photo 5.9 and Photo 5.21. This may indicate that the outermost layer of mill scale is generally more resistant to the corrosive environments. Unfortunately, this layer is very fragile and usually falls off in practice. As corrosion takes place,
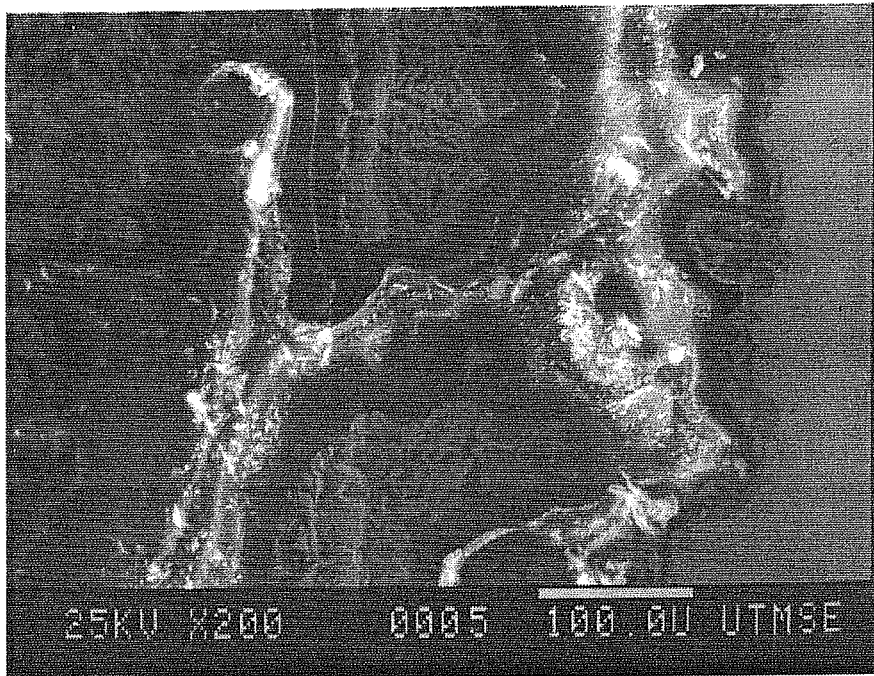
Photo 5.27. SEM micrograph showing a section of discontinuous intermediate layer and a flow path formed between the outer and the inner layers.
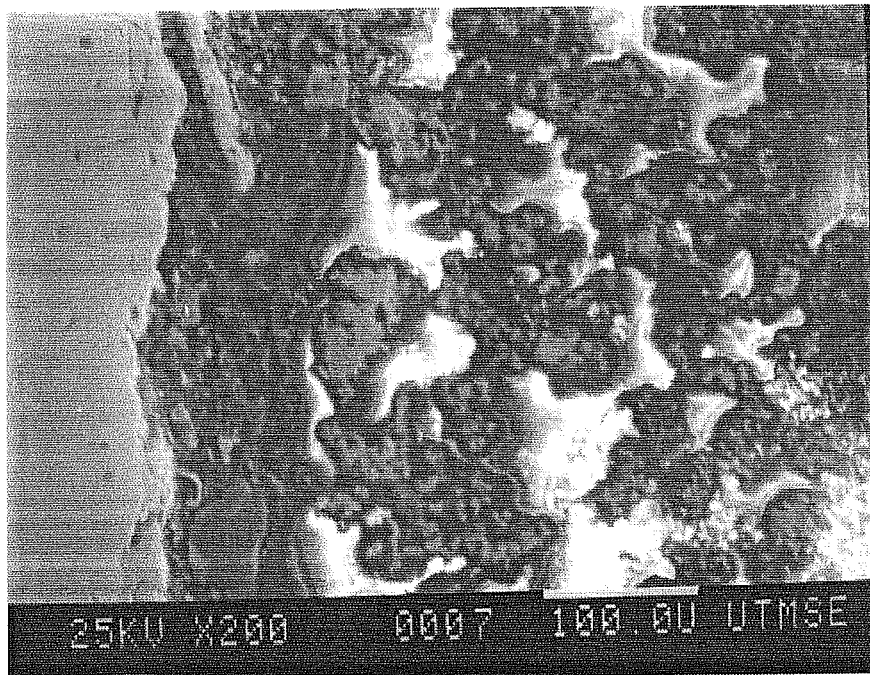

Photo 5.28. SEM micrograph showing an area where no clear intermediate layer formed and the epoxy cold mount flowed everywhere.
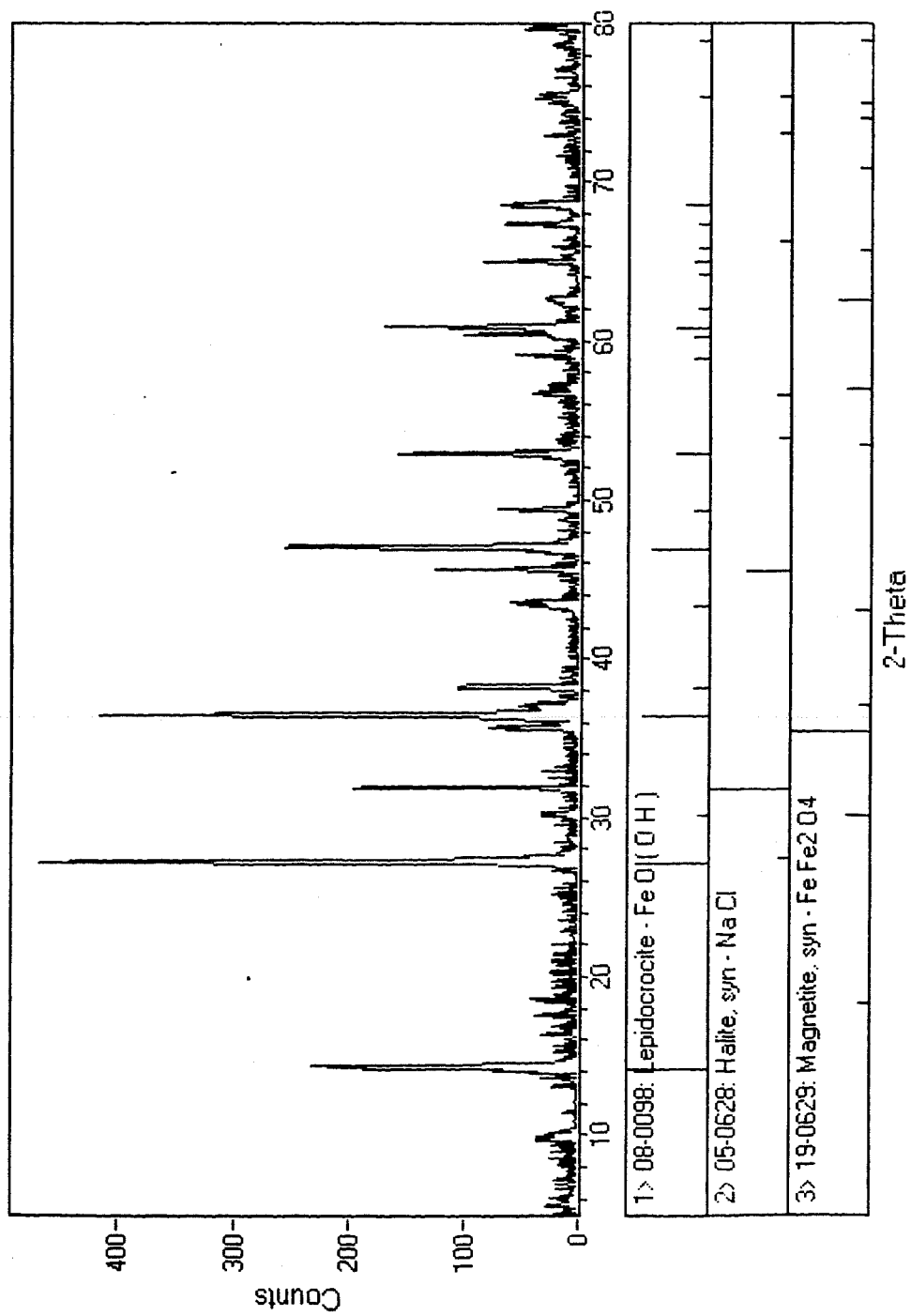
Fig. 5.38. X-ray diffraction spectrum of the corrosion products which comprise mostly the outer layer of orange-colored rust.
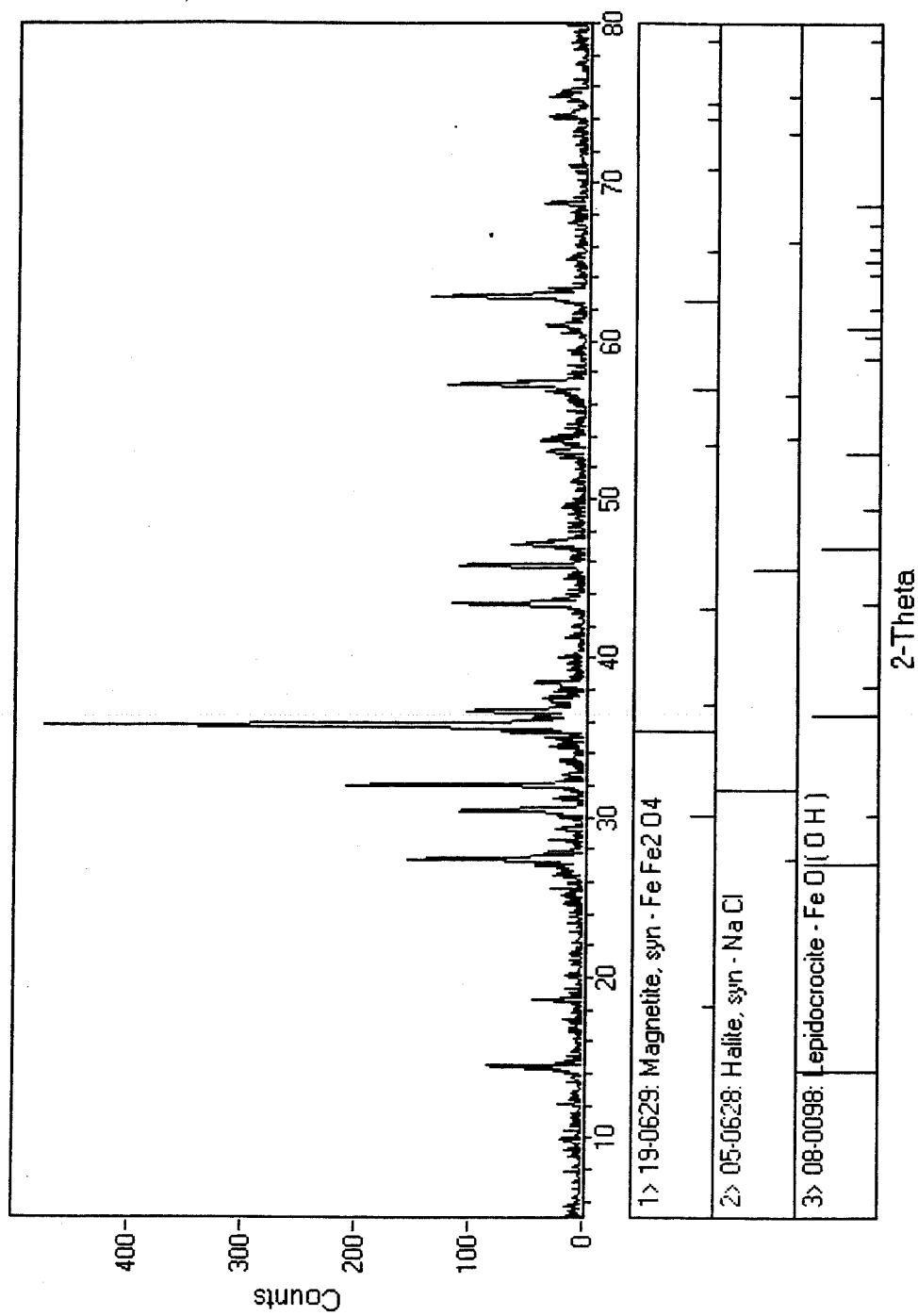
Fig. 5.39. X-ray diffraction spectrum of the corrosion products which comprise mostly the inner layers of dark-colored rust.

corrosion products begin to form. The exact manner in which corrosion products grow and the mechanisms of further oxidation are still not clear at this time; however, it is generally believed that the corrosive anions and the oxygen will diffuse in to the steel surface through the corrosion products for further iron oxidation, while the iron cations diffuse out to form more corrosion products. The corrosion product layers are thus considered to play a role in controlling the corrosion rate. The above observations regarding the constituents of the corrosion products, i.e. the X-ray diffraction spectrum and the color characterization, are basically very consistent. $FeO \cdot H_2O$ is not observed in the diffraction spectrum because it (white in color when is pure) is very unstable in nature and readily oxidized by air or even water to other states (brown or greenish black in color) [86] [87]. However, the relatively small amount of it is also a factor since no other apparent peaks can be observed at all. An important point, which comes from the observations of the layered structure of the corrosion products and the morphology of each layer, is that the intermediate layer of corrosion product, i.e. Fe_3O_4, should be the protective layer or the diffusion-barrier layer. This is, somehow, different from the statement made in the Uhlig's book [86] that $FeO \cdot nH_2O$ or $Fe(OH)_2$ composes the diffusion-barrier layer next to the iron surface through which O_2 must diffuse. Meanwhile, it is rare to have a perfect intermediate layer covering the entire steel surface; therefore, the corrosion reaction is usually very active in the case of uncoated steel.

5.2 Coating Characterization and Evaluation of ECR Performance in Immersion Test

The results regarding the coating characteristics shown in the following are the averaged values from the results of all specimens of every specific type of ECR. They thus may represent the overall coating properties of each particular type of ECR. The ECR performance is evaluated by comparing the Bode magnitude plots obtained on the 7th and 200th day after immersion. The EIS responses of all specimens with the same ECR code are arranged in one plot to provide a general idea of the overall performance for that particular type of ECR. In addition, pictures are presented to help us interpret more clearly the results of ECR performance.

5.2.1 Coating Thickness

The average coating thicknesses for every type of ECR before exposure to solution are listed in Table 5.1. The maximum and the minimum readings obtained as well as the percentage of the readings that are below the lower bound of ASTM standard (7 mil) are also reported. It is observed, in every type of ECR, that the coating thickness is actually not uniform. Generally, coating on one side of ECR is found to be thicker than on the other side. Also, it is apparent that A#a10 and A#a4 are far below the requirement for acceptance, while A#b10, B*c5, and B*c4 may be within the acceptable range, since ASTM specification requires 90 % of readings to be above 7 mil.

ECR code	Average (mil)	Maximum (mil)	Minimum (mil)	% of readings below 7 mil
A#a10	7.1	9.0	5.5	**57 %**
A#a4	6.7	9.0	5.0	**70 %**
A#b10	8.4	11.8	6.3	13 %
A#b4	9.6	12.7	7.3	0
B*c9	9.5	10.8	8.0	0
B*c5	8.3	11.5	6.2	14 %
B*c4	9.1	10.5	6.0	11 %
C#d10	11.3	14.8	8.3	0
C#d4	10.4	14.3	7.5	0

Table 5.1. Summary of coating thickness of various ECRs.

5.2.2 Coating Integrity

The ECR surfaces were examined for the as-received coating integrity. Examples of typical ECRs with good and poor coating integrity are shown in Photo 5.29 and Photo 5.30, respectively. The coating defects observed visually include cracks, pin-holes, and physical damage (bare areas and scratches). Cracks and pin-holes are more likely to be inherent flaws of the coating, which are related to the epoxy powder and the coating process; while bare areas and scratches are caused by external influences, such as the handling and shipping processes. Close-up pictures of some representative defects are shown in Photo 5.31 through Photo 5.36. A summary of surface conditions for various ECRs is listed in Table 5.2, in which the ECRs are roughly rated in each category of defect, according to the overall counts of each particular type of defect in all specimens (excluding the bent ones). The number of defects on the bent specimens was not recorded at that time; but it was noted that there is generally more damage on the bent specimens than on the straight ones, and this condition is more apparent for those ECRs with originally good coating integrity. The rating criteria are as follows: when overall counts were less than 3 → good; when overall counts were between 3 and 10 → medium; when overall counts were more than 10 → poor. It is observed that A#a10, A#a4, and A#b10 might all have inherently poor coating integrity at the manufacturers plant already, and subsequent handling resulted in even more damage; while the rest of ECRs generally have good coating integrity at the plant, but with some minor damage (scratches) introduced onto them afterwards. The defects on certain ECR specimens were repaired by patching before exposure to solution.
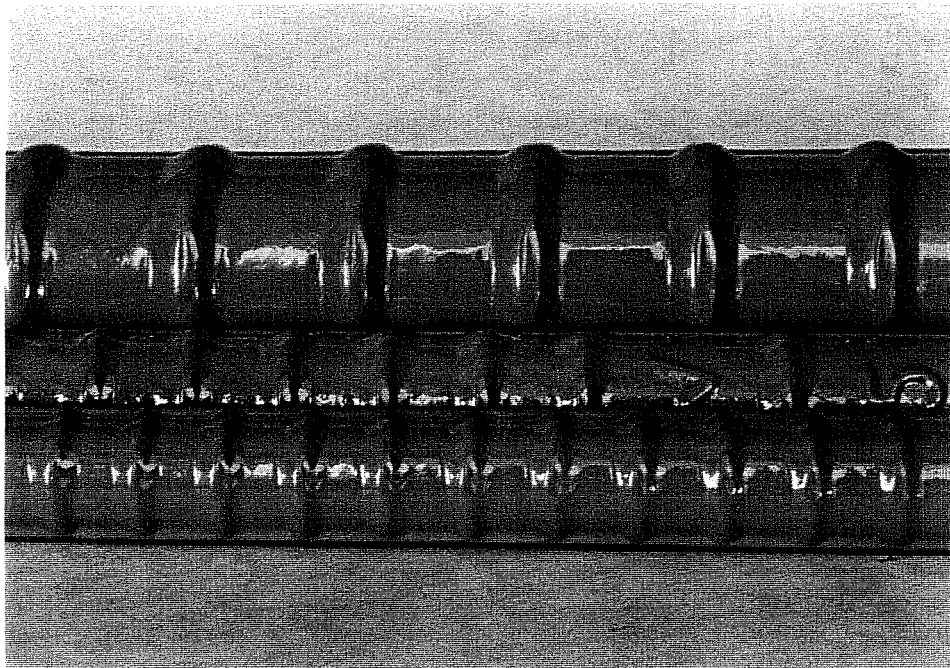
Photo 5.29. Photograph showing typical appearance of as-received ECRs with good coating integrity.
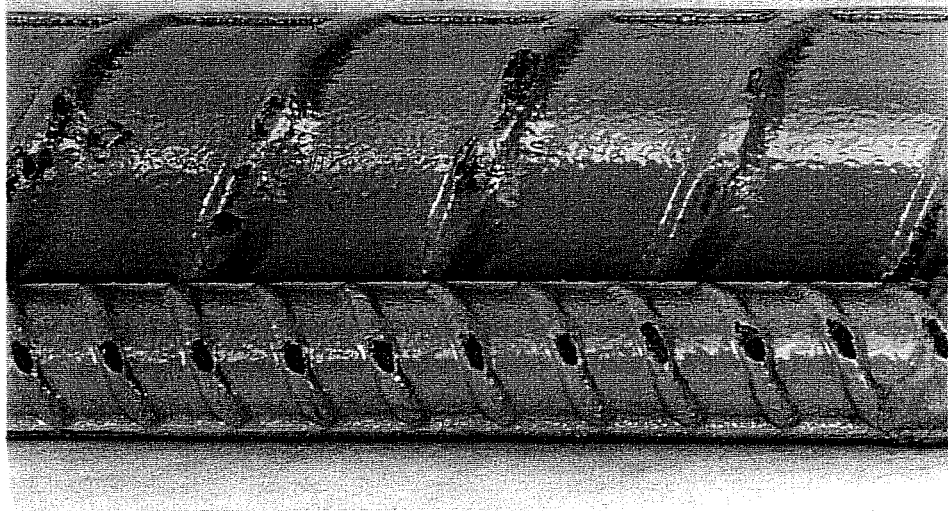

Photo 5.30. Photograph showing typical appearance of as-received ECRs with poor coating integrity.
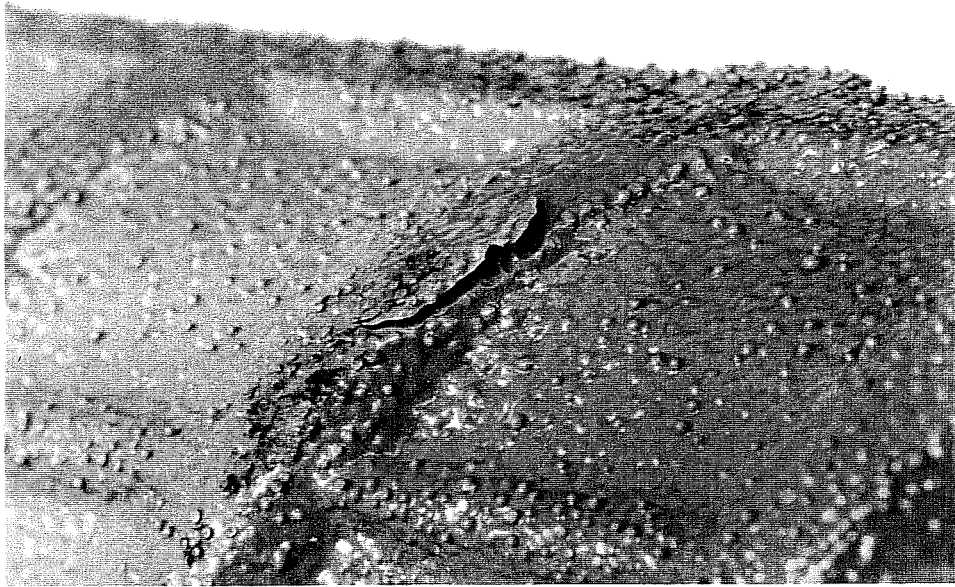
Photo 5.31. Close-up picture of a coating crack on an as-received ECR.
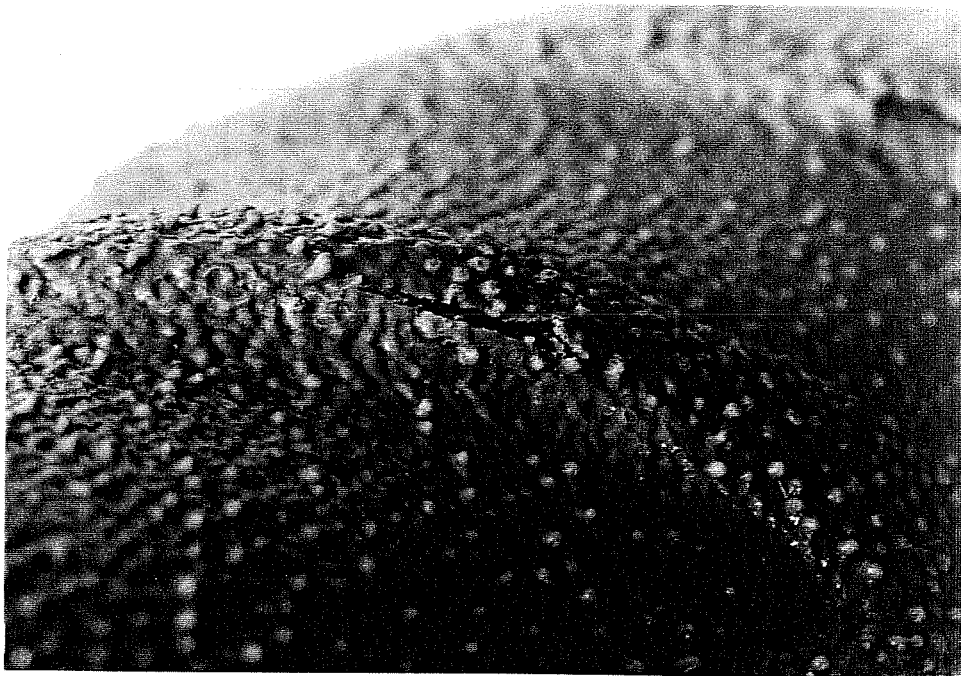
Photo 5.32. Close-up picture showing another coating crack on an as-received ECR and the abnormally rough surface.
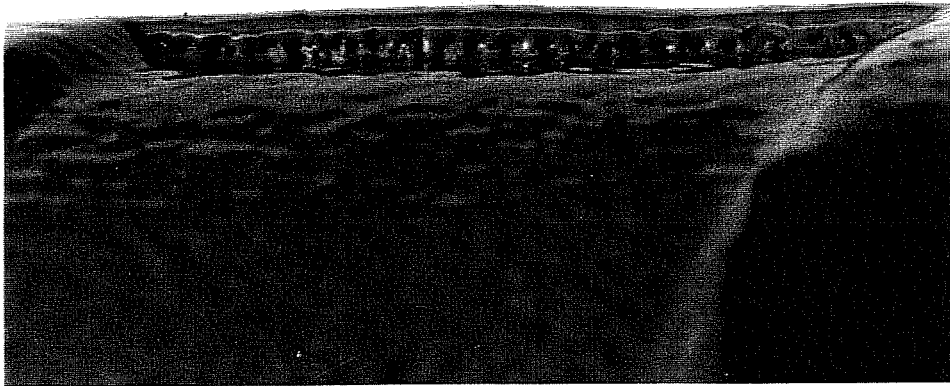
Photo 5.33. Close-up picture of pin-holes on the base of a rib for an as-received ECR.
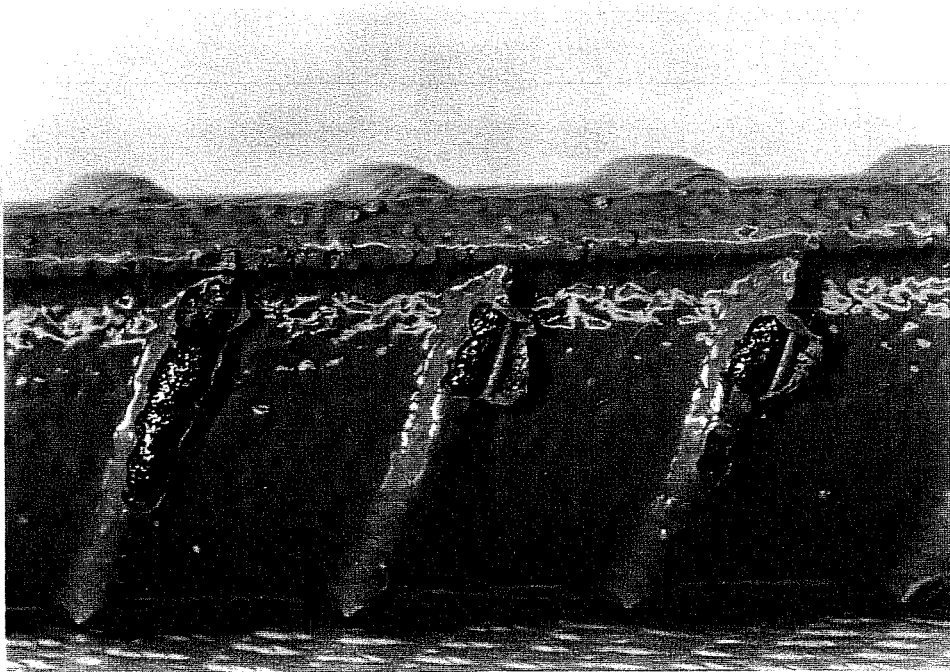
Photo 5.34. Photograph of bare areas on an as-received ECR showing premature corrosion.
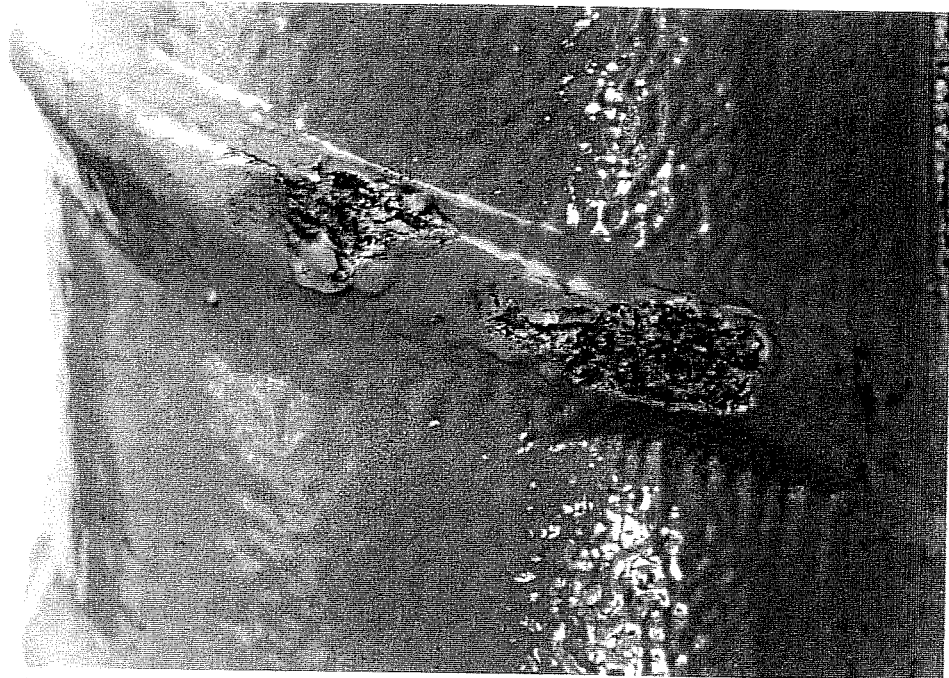
Photo 5.35. Close-up picture of two severe scratches on the rib of an as-received ECR.
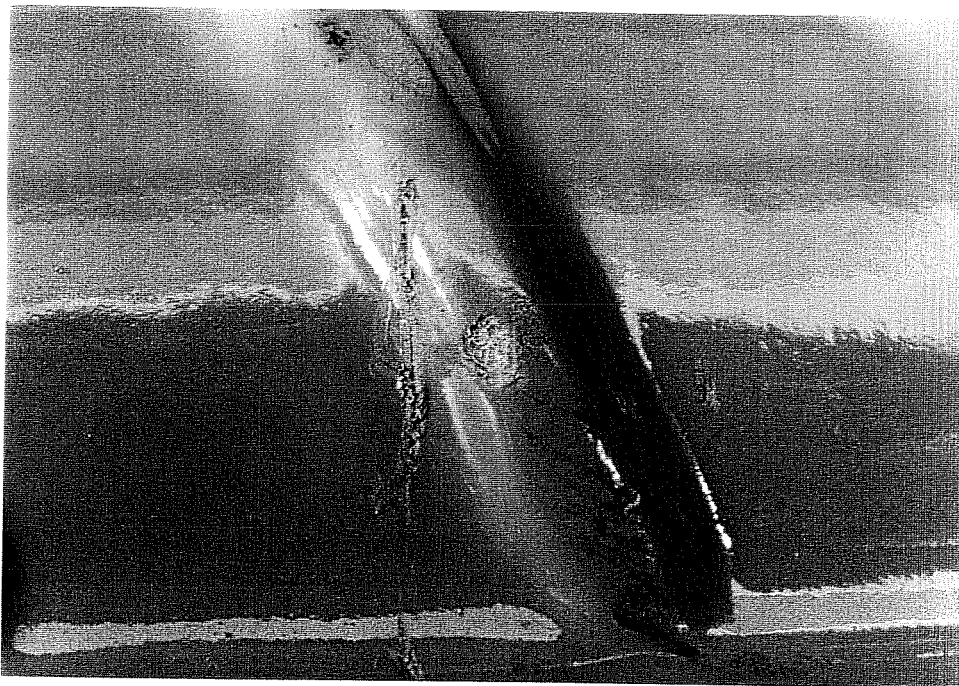
Photo 5.36. Close-up picture of some minor scratches on an as-received ECR.

ECR code	Crack	Pin-hole	Bare area	Scratch
A#a10	Good	**Poor**	**Poor**	**Poor**
A#a4	Medium	**Poor**	**Poor**	**Poor**
A#b10	**Poor**	**Poor**	Good	Medium
A#b4	Good	Good	Good	Medium
B*c9	Good	Good	Good	Medium
B*c5	Good	Good	Good	Good
B*c4	Good	Good	Good	Good
C#d10	Good	Good	Medium	**Poor**
C#d4	Good	Good	Good	Medium

Table 5.2. Summary of coating integrity of various ECRs.

5.2.3 Coating Adhesion

Coating adhesion was rated on both the as-received and the post-immersion specimens. The real view of the five-rank adhesion rating system is shown in Photo 5.37. Strictly speaking, this test is very subjective and sometimes ambiguities may rise between the adjacent rankings. However, the statistical general trend of adhesion change from this test can still provide valuable information. The overall test results are summarized in Table 5.3.

It is first observed that almost all the as-received straight ECR specimens have at least a rank of 3 (intermediate) in terms of coating adhesion, with only an exception of A#b10. After the immersion test, the statistical adhesion is observed to drop for almost every type of ECR (bent or straight specimens etc). A remarkable difference in the extent of adhesion loss does exist among them. For the straight specimens, complete loss of coating adhesion was observed on ECRs with A#a10, A#a4, and A#b10 combinations; while A#b4 has an intermediate degree of adhesion loss. The rest of the ECRs generally only have slight loss of their coating adhesion, and still have at least a rank of 2. For the bent specimens, it is observed that the adhesion loss becomes much more serious than that of the straight ones. Most specimens, except those of B*c5, have their coating adhesion drop to rank 4 and rank 5. Two inferences can be drawn from the above observations. First, immersion of ECR may lead to the coating adhesion loss, while the extent of adhesion loss is strongly dependent on the ECR (coating) type. Second, bending (deformation) practice will reduce the coating adhesion significantly on generally all types of ECRs.
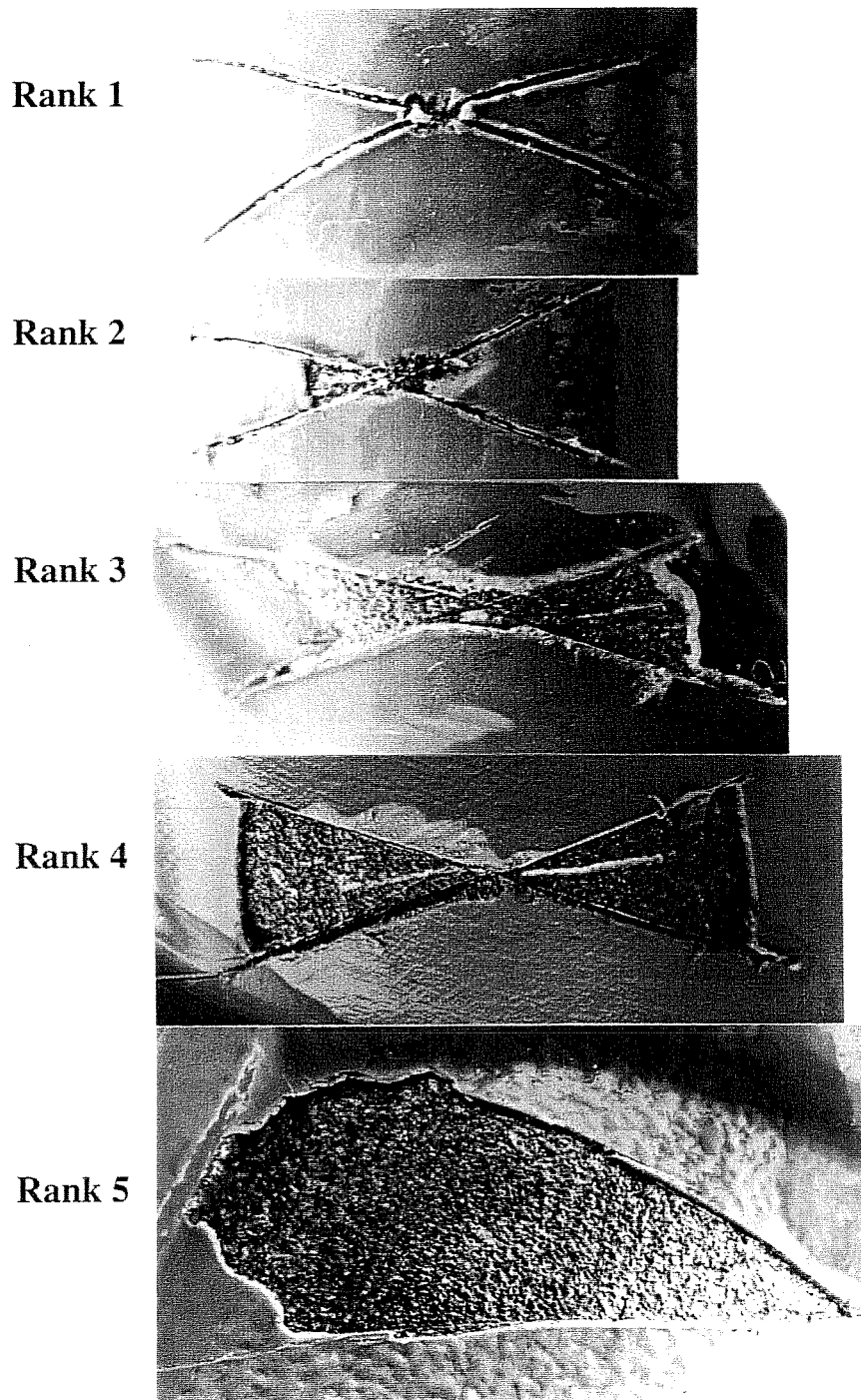
Rank 1

Rank 2

Rank 3

Rank 4

Rank 5

Photo 5.37. Photograph showing the real view of the five-rank adhesion rating system.

ECR code	As-received, straight specimen	Post-immersion, straight specimen	Post-immersion, bent specimen
A#a10	Rank 2 → 83 % Rank 3 → 17 %	Rank 5 → 100 %	
A#a4	Rank 2 → 100 %	Rank 5 → 100 %	Rank 5 → 100 %
A#b10	Rank 3 → 83 % Rank 4 → 17 %	Rank 5 → 100 %	Rank 5 → 100 %
A#b4	Rank 2 → 75 % Rank 3 → 25 %	Rank 3 → 83 % Rank 4 → 17 %	Rank 5 → 100 %
B*c9	Rank 2 → 100 %	Rank 1 → 17 % Rank 2 → 83 %	Rank 3 → 50 % Rank 4 → 50 %
B*c5	Rank 1 → 50 % Rank 2 → 50 %	Rank 1 → 25 % Rank 2 → 75 %	Rank 2 → 17 % Rank 3 → 83 %
B*c4	Rank 1 → 58 % Rank 2 → 42 %	Rank 1 → 25 % Rank 2 → 75 %	Rank 3 → 42 % Rank 4 → 58 %
C#d10	Rank 1 → 33 % Rank 2 → 67 %	Rank 1 → 11 % Rank 2 → 89 %	Rank 4 → 92 % Rank 5 → 8 %
C#d4	Rank 1 → 50 % Rank 2 → 50 %	Rank 1 → 50 % Rank 2 → 50 %	Rank 4 → 75 % Rank 5 → 25 %

Table 5.3. Summary of coating adhesion ranking of various ECRs.

5.2.4 ECR Performance in Immersion Test

The Bode magnitude plots obtained on the 7th and 200th day after immersion are shown in Fig. 5.40 through Fig. 5.48 for each type of ECR, respectively. Moreover, Table 5.4 and Table 5.5 summarize, from the above results, the rating of coating quality for every type of ECR on the 7th and 200th day, respectively. The rating criteria are as mentioned previously: with capacitive behavior → good; with a coating pore resistance value greater than 10^5 ohms → medium; with a coating pore resistance value less than 10^5 ohms → poor.

From Table 5.4 and Table 5.5, it is observed that all ECR specimens with A#a10, A#a4, and A#b10 combinations generally have poor performance at the very beginning, no matter whether they are straight or bent, patched or not patched; while there are some variations for ECR specimens with the rest of the combinations. For the straight ECR specimens, both the patched and unpatched ones, with combinations other than A#a10, A#a4, and A#b10, generally have good coating quality at early stages, although some of them deteriorate to have intermediate coating quality during the 200 days of exposure. The patched bent specimens, generally have inferior performance when compared to the straight ones. From the above observations, it is believed that most of the ECRs, except A#a10, A#a4, and A#b10, can possibly perform well under "ideal" conditions. Also, it is apparent that the bending process is prone to damage the coating, and the usefulness of the patching practice still needs further investigation. This conclusion is based on the Bode magnitude plots. In the cases of ECRs that are believed to perform well, there is no specific relationship between the patching practice and the performance observed, since most of these specimens have

Fig. 5.40. Bode magnitude plots for A#a10 specimens on the 7th day (top) and the 200th day (bottom) after being immersed in 3.5% NaCl solution.

Fig. 5.41. Bode magnitude plots for A#a4 specimens on the 7th day (top) and the 200th day (bottom) after being immersed in 3.5% NaCl solution.

Fig. 5.42. Bode magnitude plots for A#b10 specimens on the 7th day (top) and the 200th day (bottom) after being immersed in 3.5% NaCl solution.

Fig. 5.43. Bode magnitude plots for A#b4 specimens on the 7th day (top) and the 200th day (bottom) after being immersed in 3.5% NaCl solution.
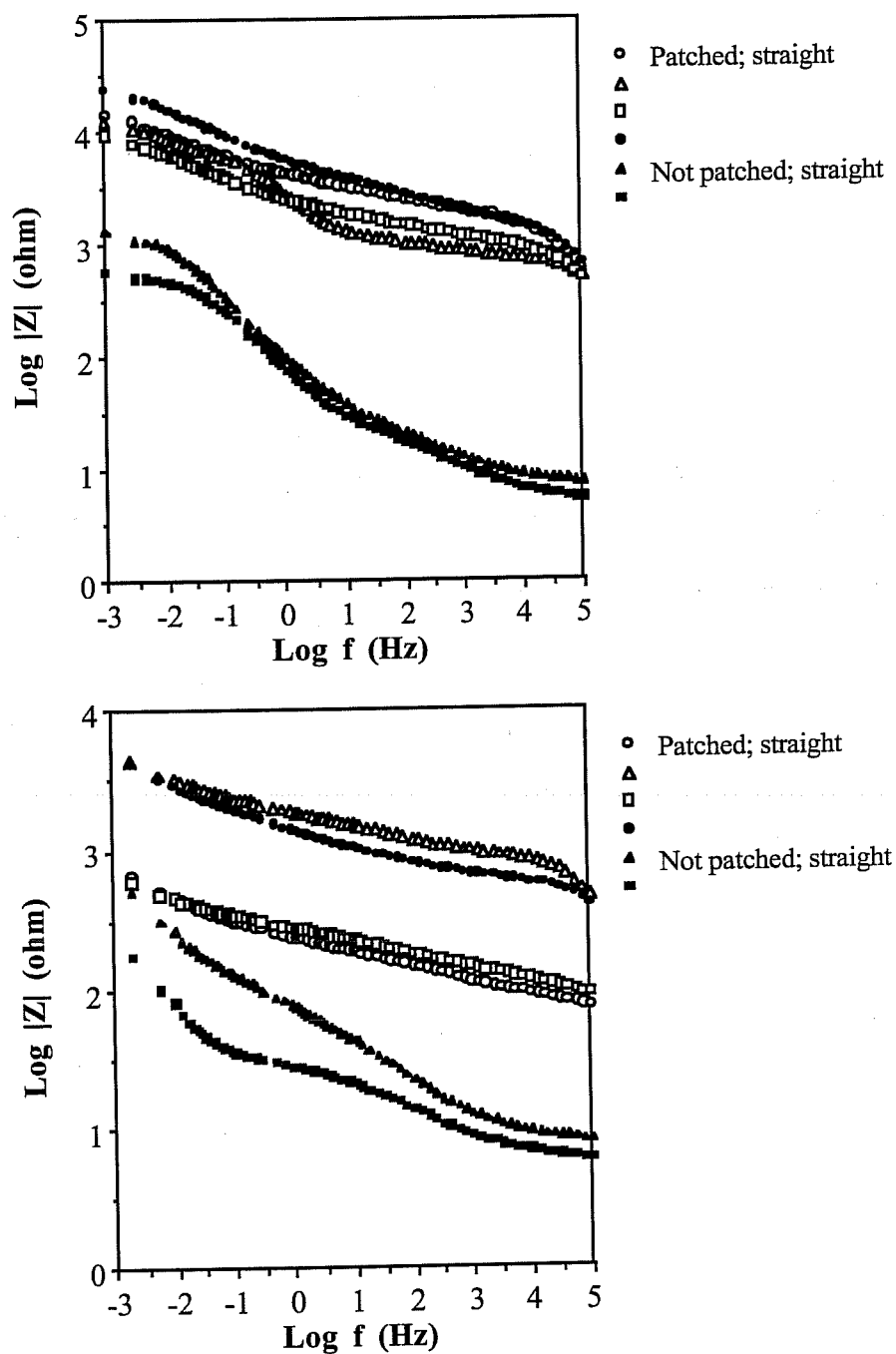
Fig. 5.44. Bode magnitude plots for B*c9 specimens on the 7th day (top) and the 200th day (bottom) after being immersed in 3.5% NaCl solution.

Fig. 5.45. Bode magnitude plots for B*c5 specimens on the 7th day (top) and the 200th day (bottom) after being immersed in 3.5% NaCl solution.
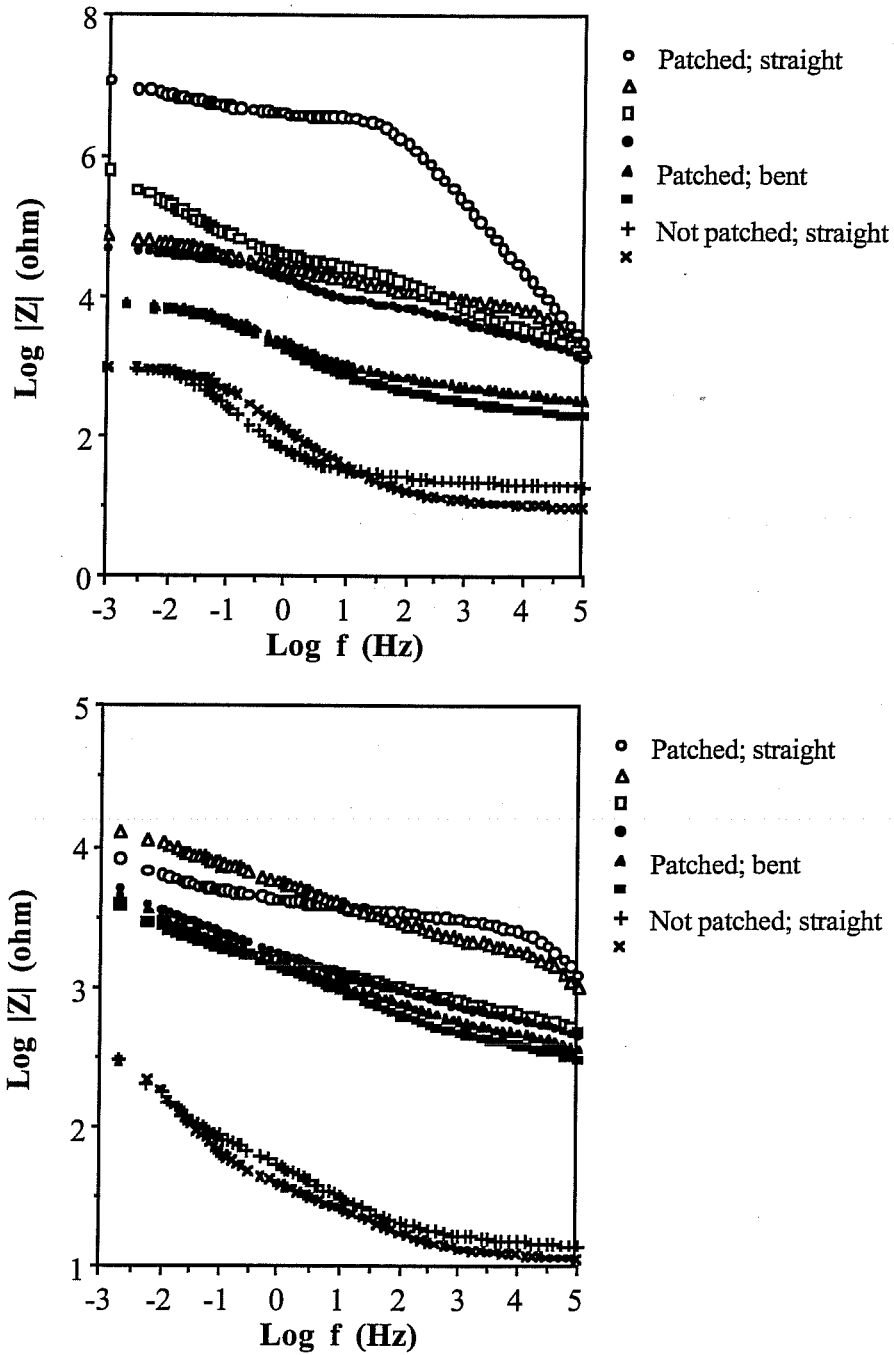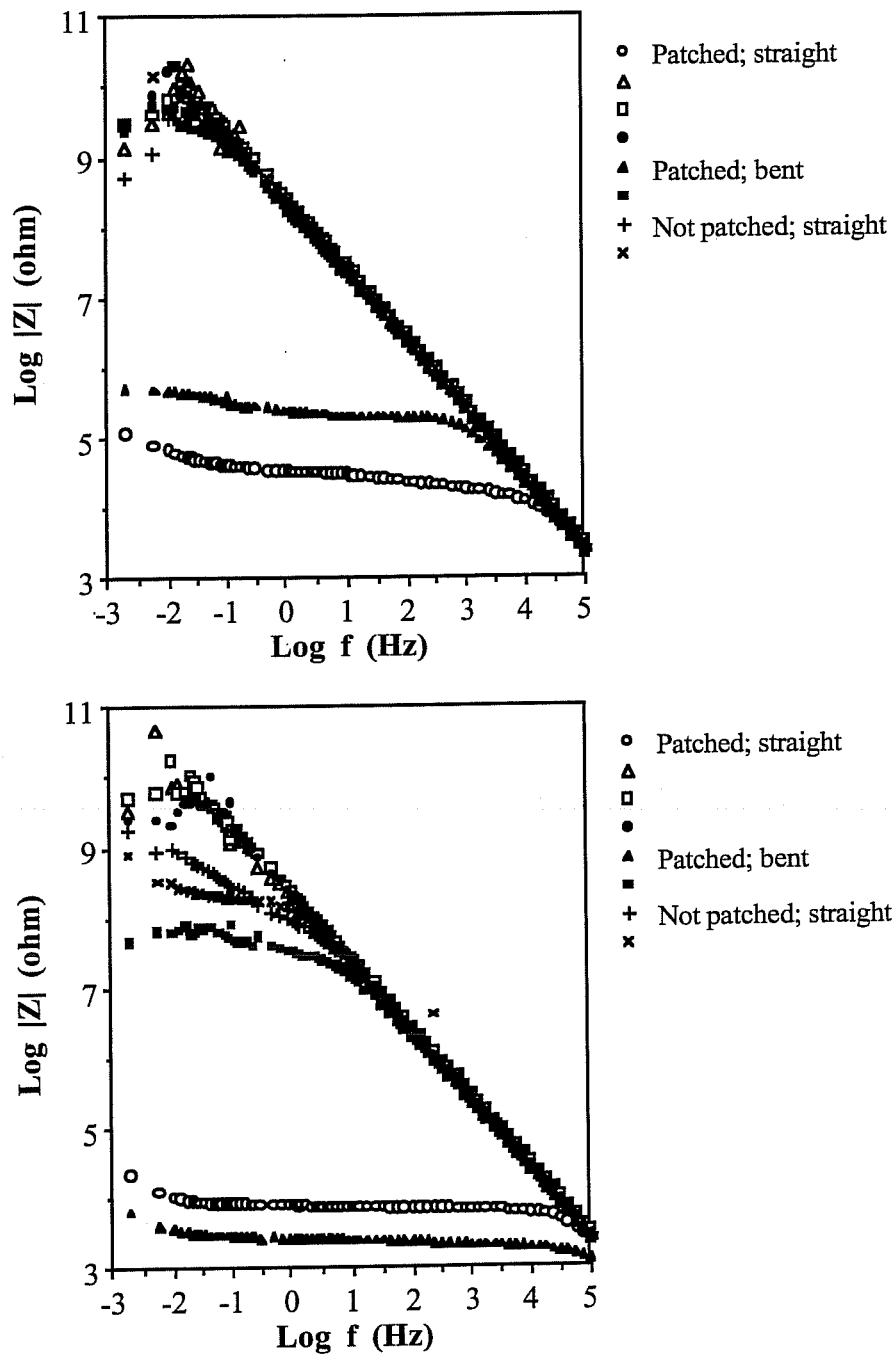
Fig. 5.46. Bode magnitude plots for B*c4 specimens on the 7th day (top) and the 200th day (bottom) after being immersed in 3.5% NaCl solution.
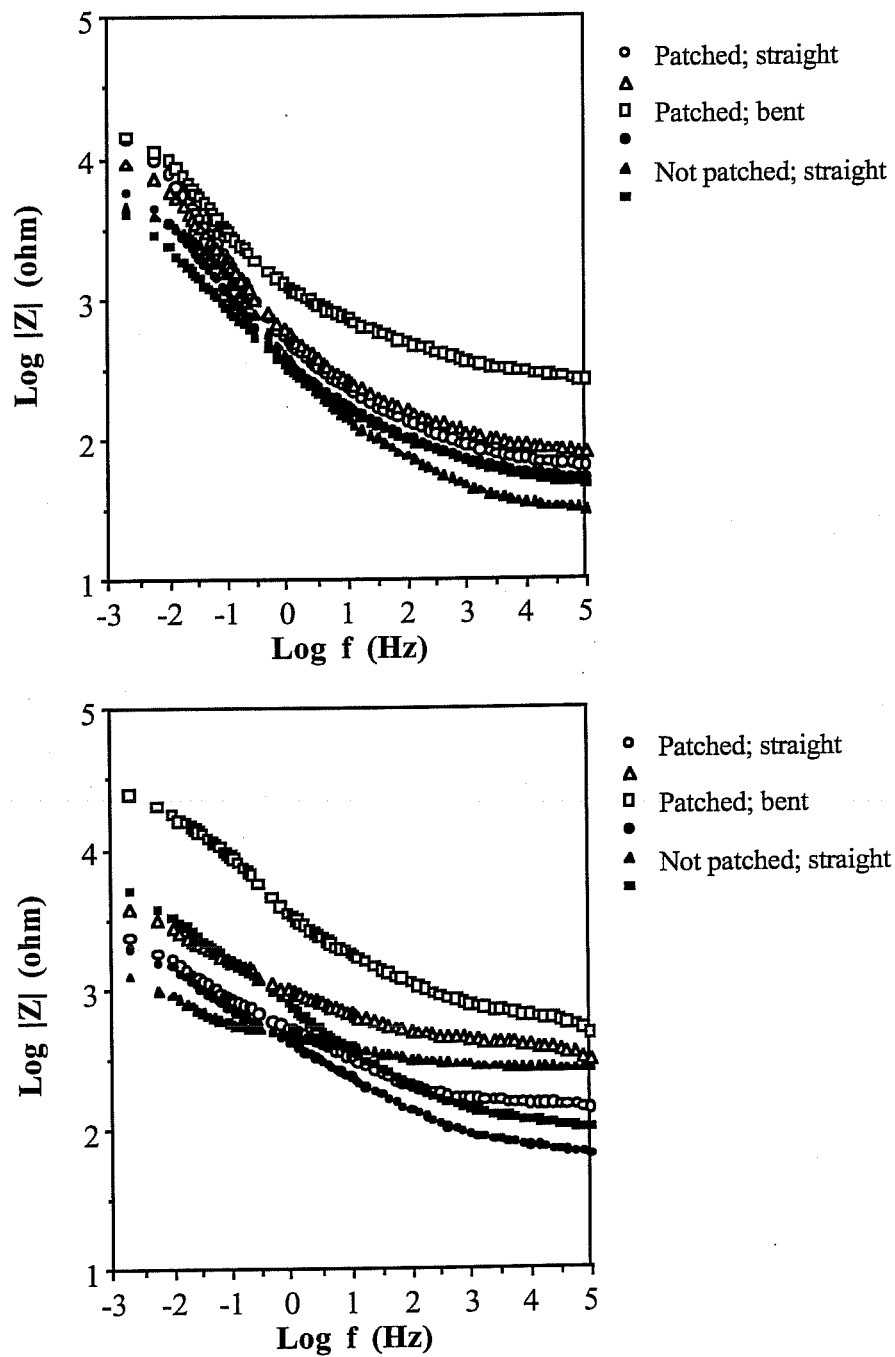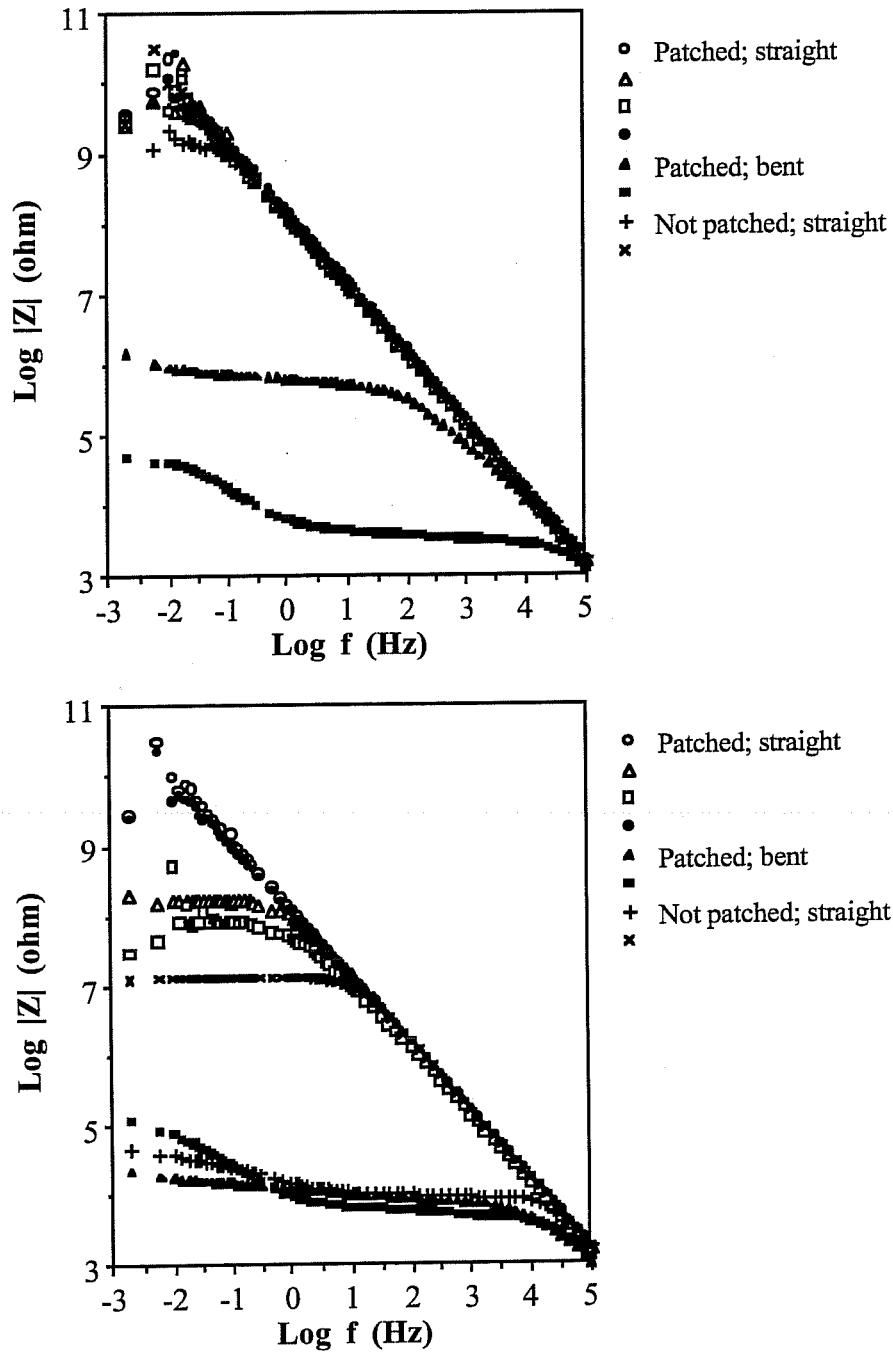
Fig. 5.47. Bode magnitude plots for C#d10 specimens on the 7th day (top) and the 200th day (bottom) after being immersed in 3.5% NaCl solution.
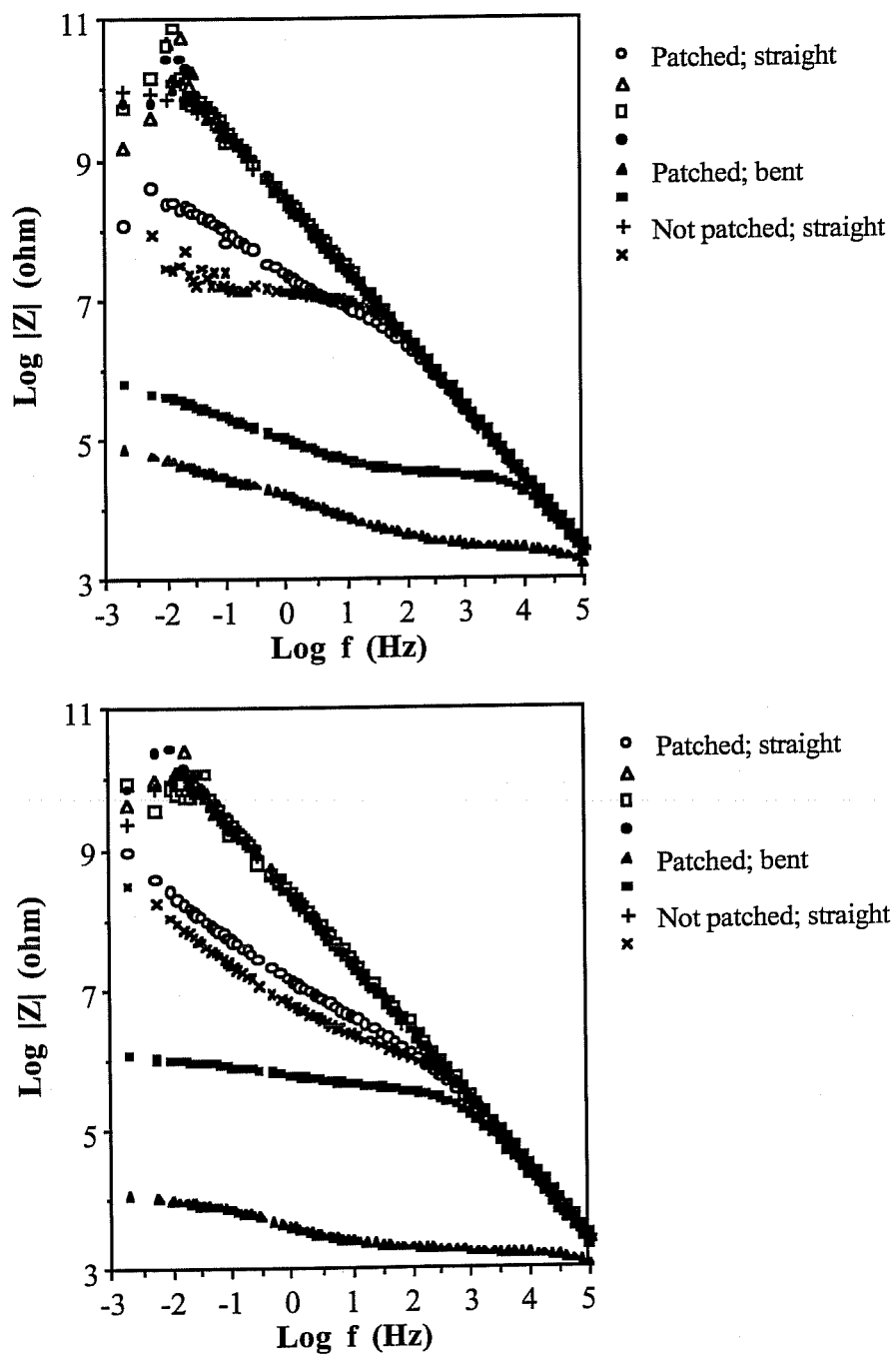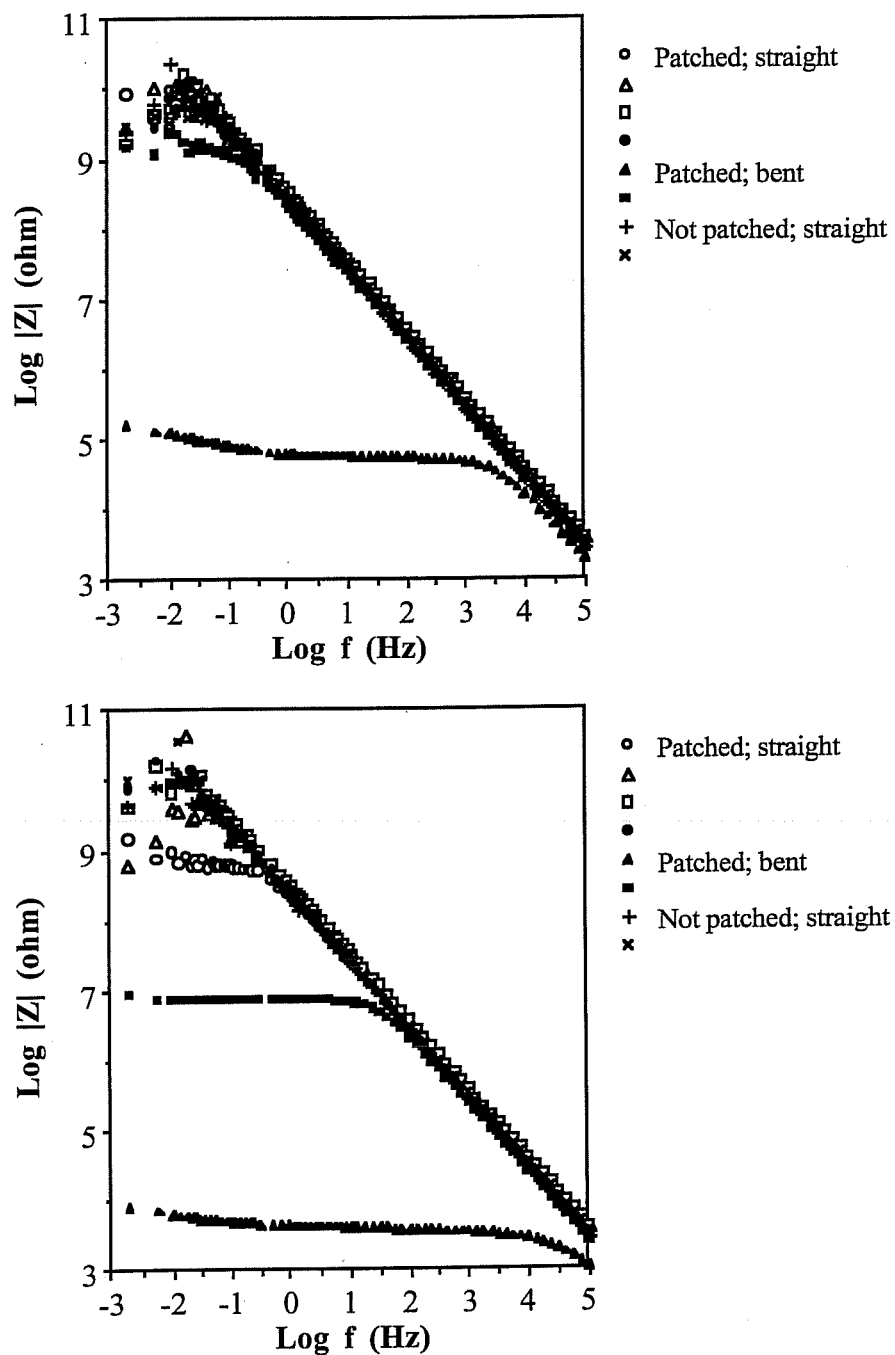
Fig. 5.48. Bode magnitude plots for C#d4 specimens on the 7th day (top) and the
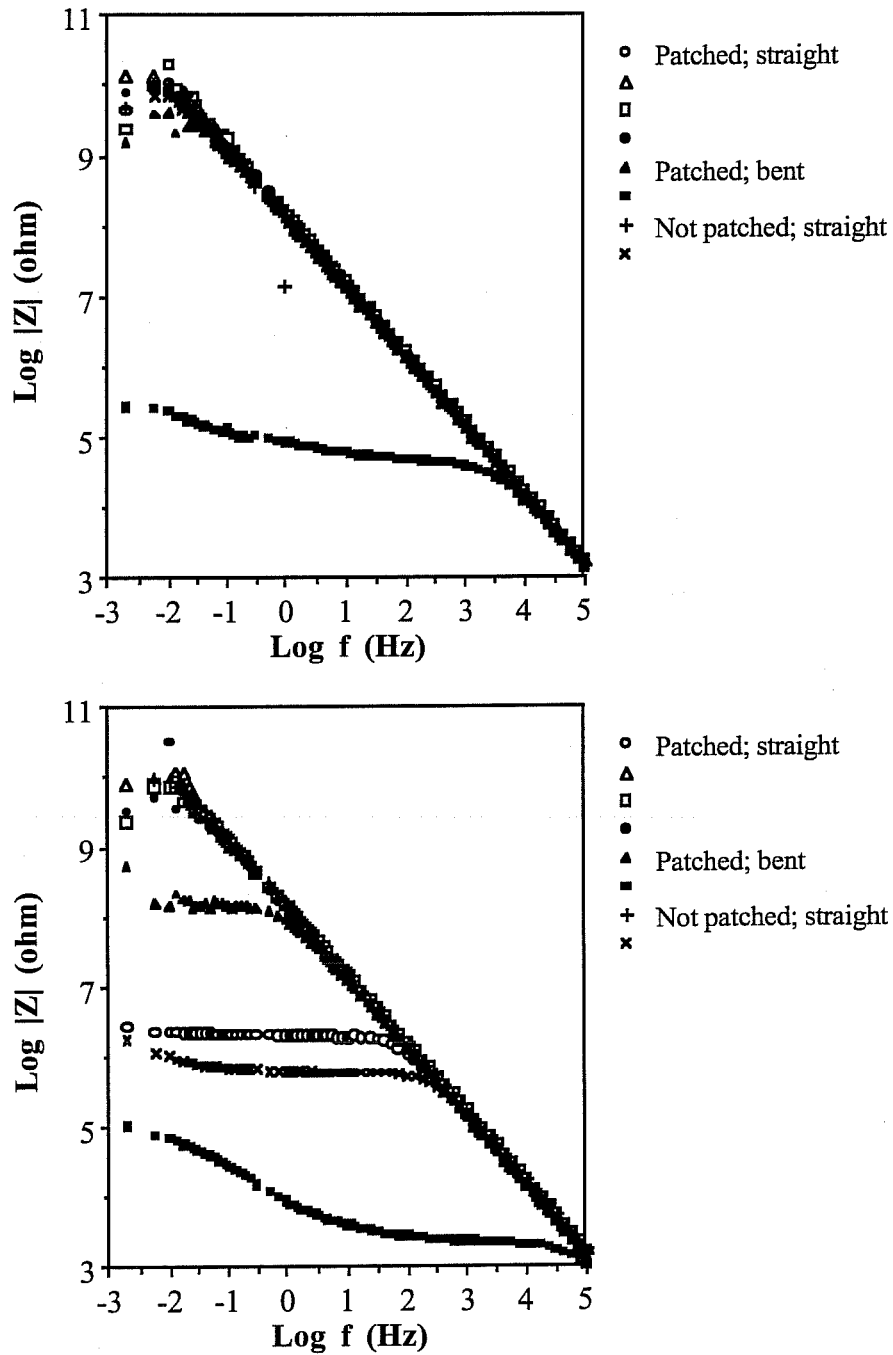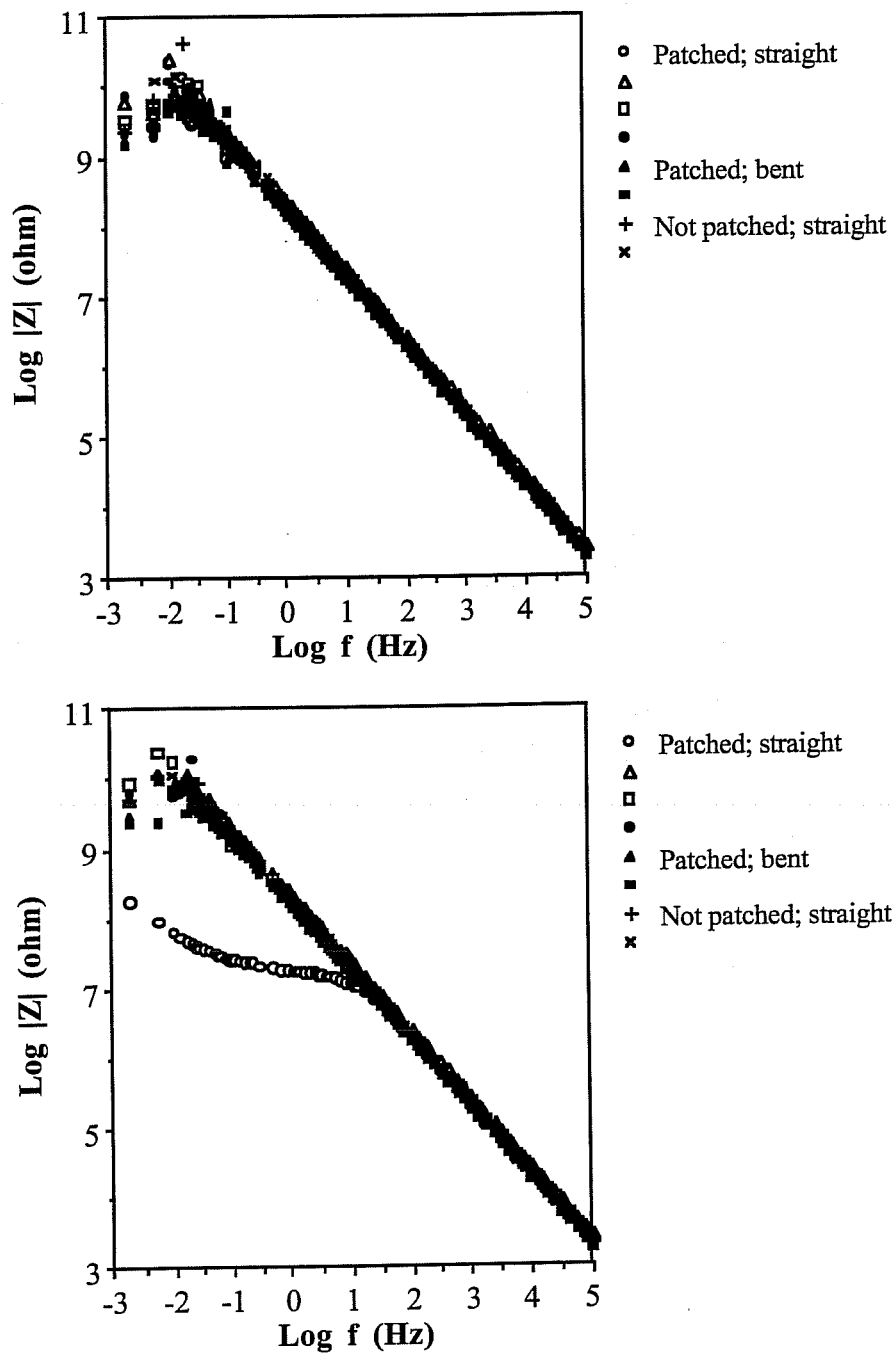200th day (bottom) after being immersed in 3.5% NaCl solution.

ECR code	Patched, straight specimen			Patched, bent specimen			Not patched, straight specimen		
	Good	Medium	Poor	Good	Medium	Poor	Good	Medium	Poor
A#a10	0	0	4/4				0	0	2/2
A#a4	0	1/4	3/4	0	0	2/2	0	0	2/2
A#b10	0	0	2/2	0	0	2/2	0	0	2/2
A#b4	3/4	1/4	0	1/2	0	2/2	1/2	1/2	0
B*c9	4/4	0	0	2/2	0	1/2	2/2	0	0
B*c5	4/4	0	0	2/2	0	0	2/2	0	0
B*c4	3/4	0	1/4	1/2	1/2	0	2/2	0	0
C#d10	4/4	0	0	0	1/2	1/2	1/2	1/2	0
C#d4	4/4	0	0	0	1/2	1/2	2/2	0	0

Table 5.4. Summary of ECR performance on the 7th day after immersion based upon impedance spectroscopy.

200th day ECR code	Patched, straight specimen			Patched, bent specimen			Not patched, straight specimen		
	Good	Medium	Poor	Good	Medium	Poor	Good	Medium	Poor
A#a10	0	0	4/4				0	0	2/2
A#a4	0	0	4/4	0	0	2/2	0	0	2/2
A#b10	0	0	2/2	0	0	2/2	0	0	2/2
A#b4	3/4	1/4	0	0	1/2	1/2	1/2	1/2	0
B*c9	3/4	1/4	0	0	1/2	1/2	1/2	1/2	0
B*c5	3/4	1/4	0	2/2	0	0	2/2	0	0
B*c4	3/4	0	1/4	0	1/2	1/2	0	2/2	0
C#d10	2/4	2/4	0	0	0	2/2	0	1/2	1/2
C#d4	3/4	1/4	0	0	1/2	1/2	2/2	0	0

Table 5.5. Summary of ECR performance on the 200th day after immersion based upon impedance spectroscopy.

inherently good coating quality and require no patching. The effect of patching becomes apparent in the case of ECRs with poor performance. In those cases, it is generally observed that patching does provide some improvement in performance, even though its effect becomes less apparent after exposure for longer periods. This observation is shown in Fig. 5.40 and Fig. 5.41. However, in Fig. 5.42, for the A#b10 specimens which also have poor performance, there seems to be no effect of patching on the performance. This may be due the existence of many tiny, pin-hole type defects, which may easily be overlooked by the naked eye during the patching practice, on this particular type of ECR. Pictures of this phenomenon will be shown later.

The ECR specimens were examined for their change in appearance after the immersion test. For the straight specimens, it is observed that all the A#a10, A#a4, and A#b10 specimens show signs of severe corrosion, especially those unpatched ones; while the specimens of the other combinations of ECR generally still look very good, with a total of two locally corroded spots visible on two different specimens only. Photo 5.38 shows the appearance of some representative specimens indicating the various extent of ECR deterioration discussed above. For the bent specimens, the situation is basically the same as that for the straight ones except that there are more corroded spots in this case for those ECRs showing slight deterioration. A correlation between this visual examination and the ECR performance evaluated by EIS is noted here that the ECR deterioration can be observed by the naked eye only on those specimens that are rated as having poor performance.
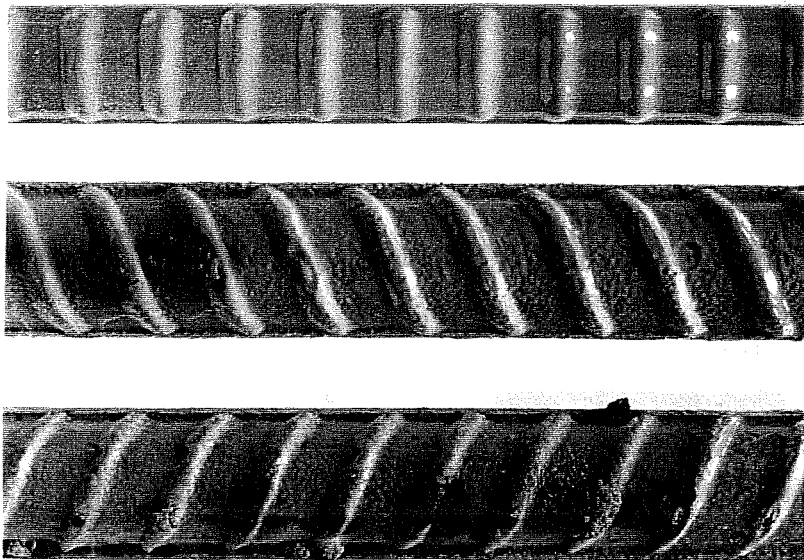
Photo 5.38. Photograph of the representative ECR specimens showing different extent of ECR deterioration after immersion in 3.5% NaCl solution for 200 days.

Photo 5.39. Close-up picture showing pin-hole corrosion on the ECR with abnormally rough surface after immersion in 3.5% NaCl solution for 200 days.

Those signs of deterioration observable by the naked eye are further examined and classified into several major types. Pictures of the representative types are shown in Photo 5.39 through Photo 5.50, and are described as follows. Photo 5.39 and Photo 5.40 show us the pin-hole corrosion on the surface of A#b10 specimens. As mentioned earlier in this section, patching does not seem to provide improvement on performance for this type of ECR. It becomes apparent here that the extremely rough surface and those masked tiny pin-holes will be the causes for that phenomenon. The pin-holes become apparent after immersion due to the color of rust. Photo 5.41 and Photo 5.42, again, show the pin-hole corrosion. Those pin-holes on the base of ribs of A#a10 specimens were observed but not patched before immersion. After immersion, very different extents of corrosion were observed. In Photo 5.41, the corrosion is seen to be mild; while in Photo 5.42, evidence of severe corrosion is still apparent even though the corrosion products were removed. Photo 5.43 and Photo 5.44 show the coating cracks on A#a4 specimens. The formation of these cracks is the consequence of corrosion activity, since both the specimens shown were thoroughly patched on every possible defect before immersion. It is believed that the corrosion reaction is caused by the diffusion of corrosive ions and water into the iron substrate. As the corrosion activity proceeds, the accumulation of corrosion products begin to lift the coating, and finally breaks it. In the upper left portion of Photo 5.43, a small piece of coating is even observed to fall off due to the oxide lifting. One hypothesis to make here is that the degradation of the epoxy may also facilitate this deterioration process, since the coating seems to become fragile after immersion. Photo 5.45 and Photo 5.46 show the blisters formed on A#a10
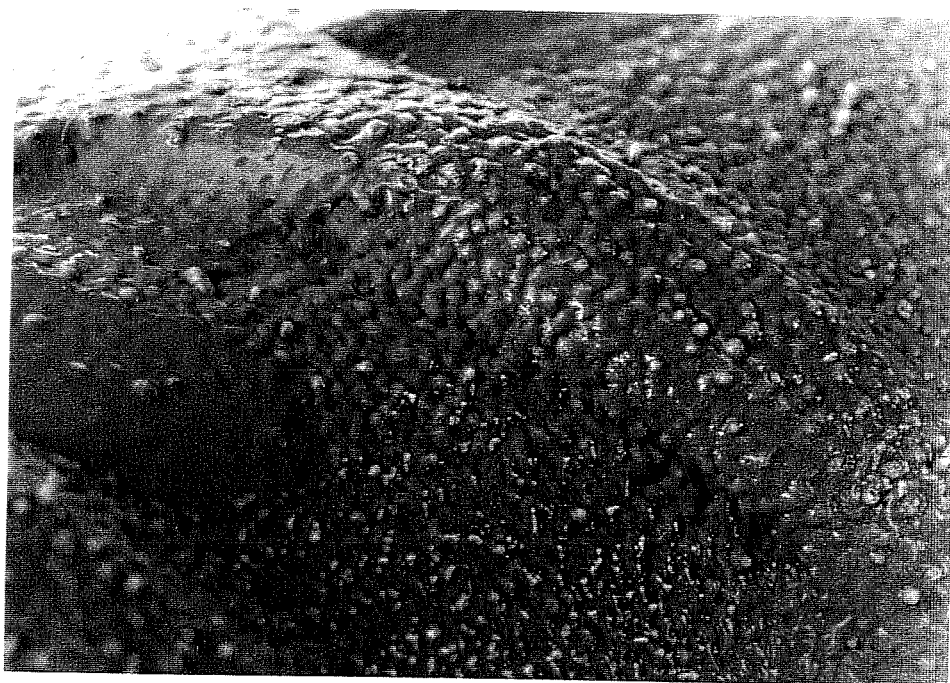
Photo 5.40. Close-up picture of pin-hole corrosion on a patched ECR indicating these tiny pin-holes might easily be neglected during patching practice.
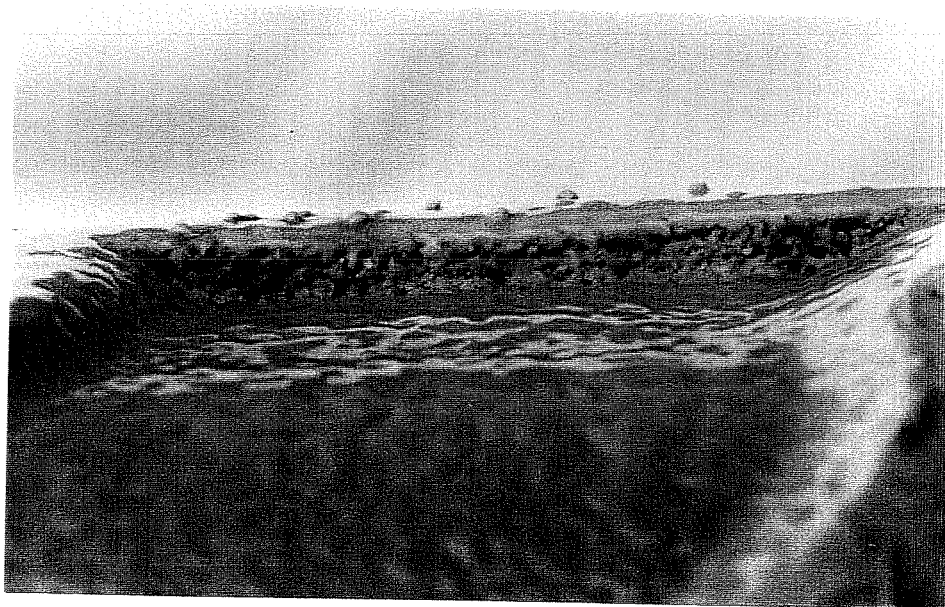
Photo 5.41. Close-up picture showing mild pin-hole corrosion on the base of a rib after immersion in 3.5% NaCl solution for 200 days.
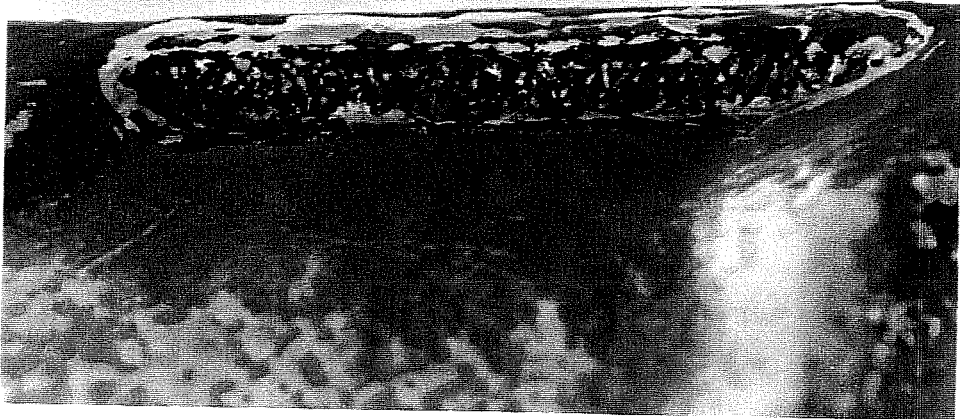
Photo 5.42. Close-up picture showing severe pin-hole corrosion on the base of a rib after immersion in 3.5% NaCl solution for 200 days.

Photo 5.43. Close-up picture showing cracks formed on a patched ECR specimen after immersion in 3.5% NaCl solution for 200 days.

Photo 5.44. Another close-up picture also showing cracks formed on ECR after immersion in NaCl solution.

Photo 5.45. Close-up picture showing blisters formed on the patched ribbed area of an ECR specimen after immersion in 3.5% NaCl solution for 200 days.

specimens. It is observed that all the blisters develop on the patched areas. The deterioration mechanism for blistering is similar to that in the case of cracking, while the formation of blisters may be because the patching material has better ductility than the original coating does. However, the blister is actually also very fragile. Photo 5.47 shows a broken blister and the corrosion products within it. Photo 5.48 shows the unpatched bare areas on an A#a4 specimen after immersion. It is apparent that severe corrosion has taken place here; while the red brown and the black colors are the evidence of $Fe_2O_3 \cdot H_2O$ and Fe_3O_4, respectively, as discussed previously. Finally, Photo 5.49 and Photo 5.50 show signs of slight corrosion around the unpatched scratches on A#b10 and C#d10 specimens. Actually, many other scratched areas do not show signs of corrosion because the coating is thick enough to withstand this minor damage. The specimen shown in Photo 5.50 is one of the two exceptional cases among those ECR combinations which are generally observed to be good, as mentioned earlier in this section.

Furthermore, those ECR specimens that are rated as having intermediate performance and do not show signs of deterioration visible to the naked eye are more carefully examined with the aid of an optical microscope. It is observed that the very, very tiny stains scattered on the surface of those specimens are actually some micro defects in the coating. Micrographs of the representative defects are shown in Photo 5.51 through Photo 5.58. Photo 5.51 and Photo 5.52 show us two micro pin-holes on B*c4 specimens with corroded and uncorroded exposed iron substrate, respectively. The approximate diameter of these two pin-holes is about 125 μm. Photo 5.53 and Photo 5.54 show the coating cracks on C#d10 and B*c9

Photo 5.46. Close-up picture showing another blister formed on the patched ribbed area of ECR after immersion in NaCl solution.

Photo 5.47. Close-up picture of a broken blister showing the corrosion products accumulated within it.
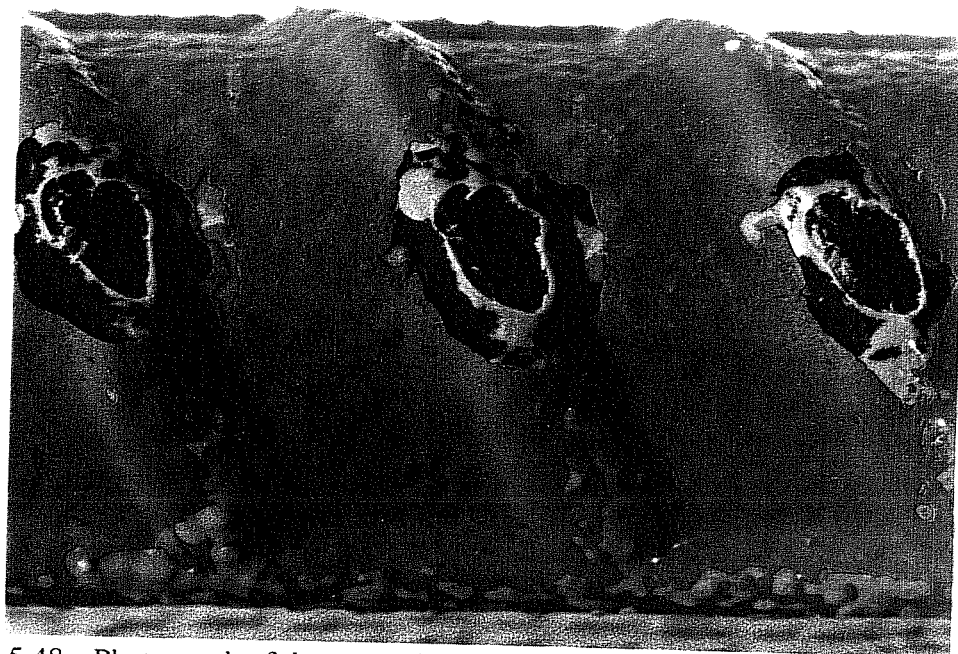
Photo 5.48. Photograph of the unpatched bare areas on an ECR specimen after immersion in 3.5% NaCl solution for 200 days showing evidence of severe corrosion.
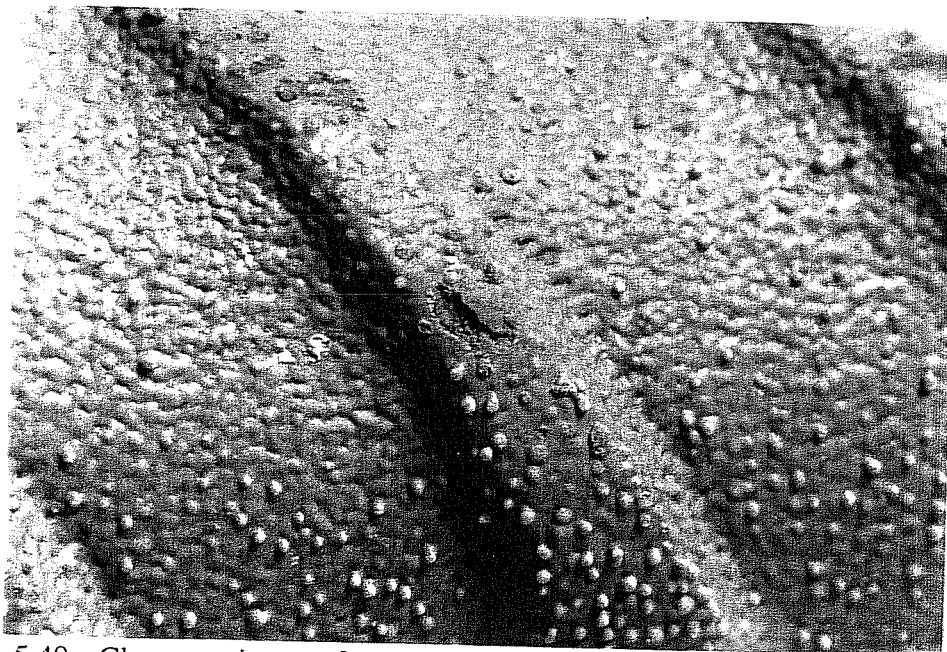
Photo 5.49. Close-up picture of an unpatched scratch showing evidence of slight corrosion after immersion in 3.5% NaCl solution for 200 days.
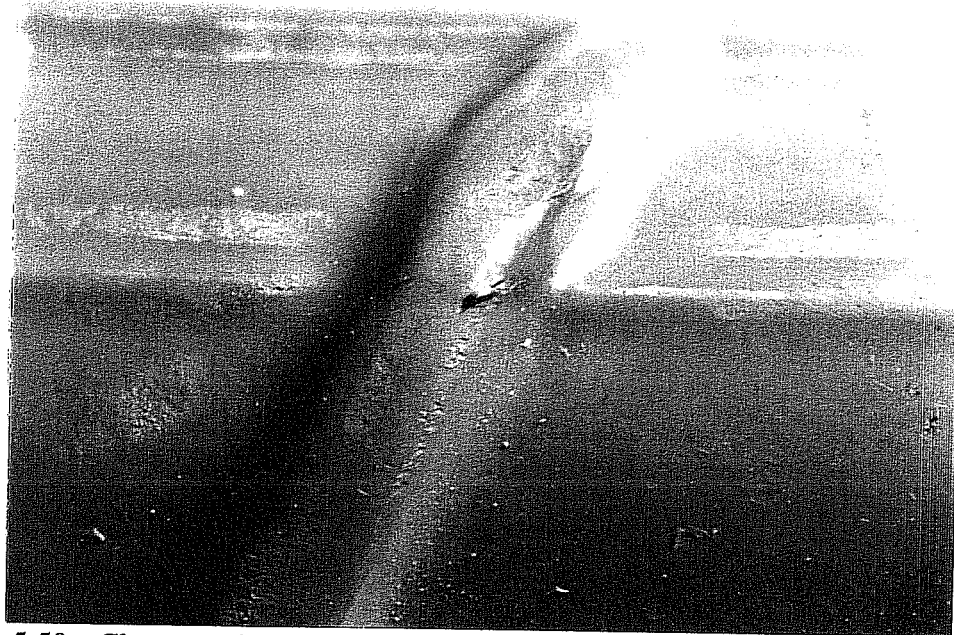
Photo 5.50. Close-up picture of another unpatched scratch also showing
evidence of slight corrosion after immersion in NaCl solution.

Photo 5.51. Optical micrograph showing a micro pin-hole on epoxy coating with
the exposed iron substrate corroded. (x200)
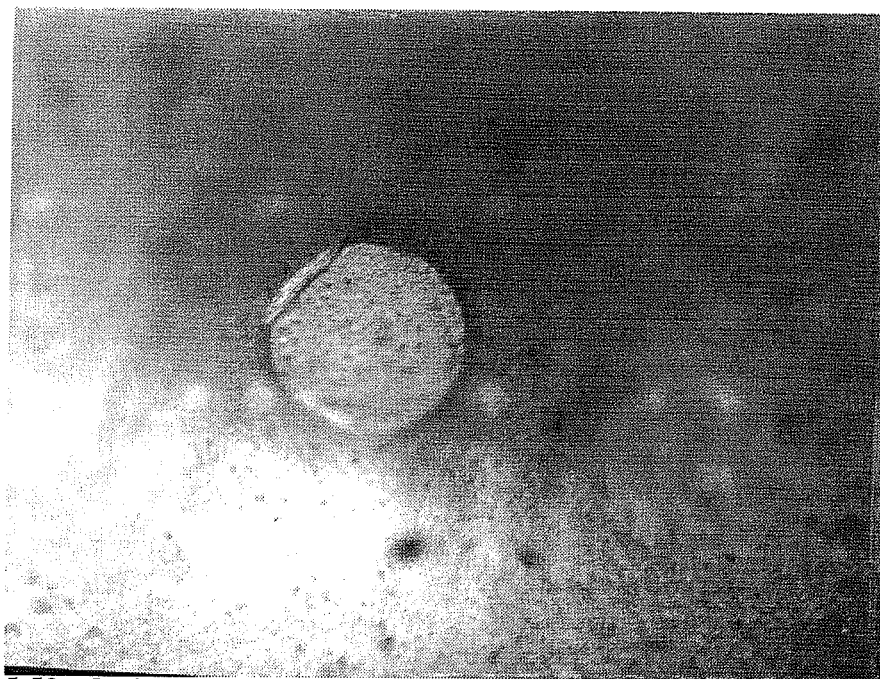
Photo 5.52. Optical micrograph showing another micro pin-hole on epoxy coating with the exposed iron substrate uncorroded. (x200)
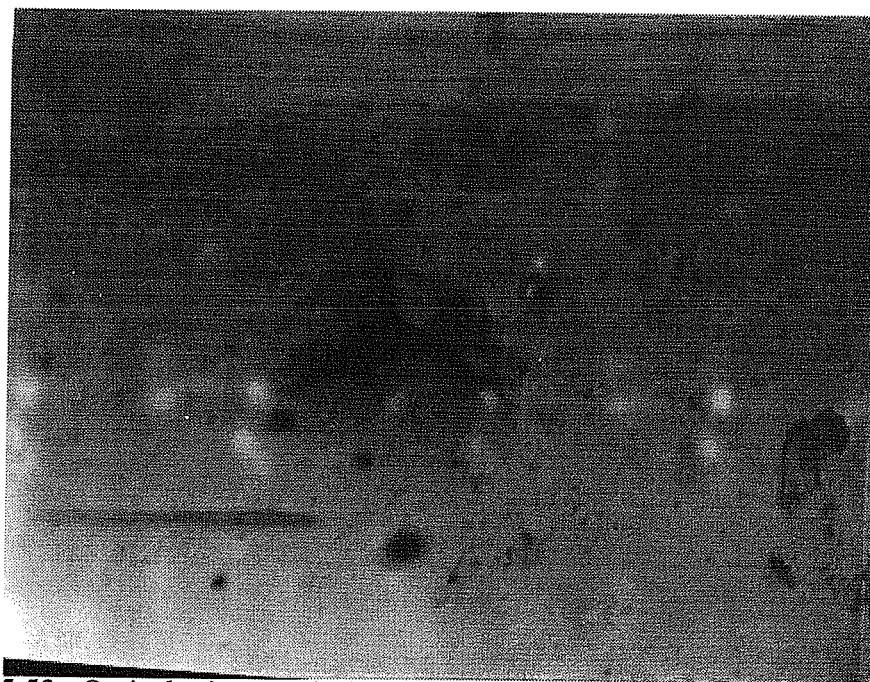
Photo 5.53. Optical micrograph showing a micro crack on epoxy coating. (x200)

specimens. The circle shown in Photo 5.54 is actually an orange-colored stain around the coating break, which is evidence of corrosion. Photo 5.55 shows a small region on a B*c5 specimen where the epoxy was apparently not well cured. Slight corrosion is observed on the exposed iron substrate. Photo 5.56 further shows a region of uncorroded exposed substrate on a B*c5 specimen; while Photo 5.57 and Photo 5.58 show two corroded exposed areas on B*c4 specimens. It is noted that the appearance of these defects is random and there is no preference on a particular type of ECR. Also, the subsequent deterioration from these defects is generally very slow, which is due to their very small size and the surrounding good quality coating.

5.2.5 Correlation between Coating Characteristics and ECR Performance

The effectiveness of ECR has given rise to much controversy recently. However, it is often found that ECR has inadequate quality before being used in construction. That is, the coating generally contains defects from the original manufacture and/or from the subsequent handling. It may be informative to find out the correlation between the above results in attempts to identify the causes of unsatisfactory ECR performance, and to provide suggestions on improving the current practice and specifications for this technology. Some of these recommendations have already been made [10].

It is first observed from Table 5.5 that the epoxy powder used and the size of ECR seem to be less relevant to the overall ECR performance; while the coater and the mill may possibly be the decisive factors. Furthermore, from Table 5.1
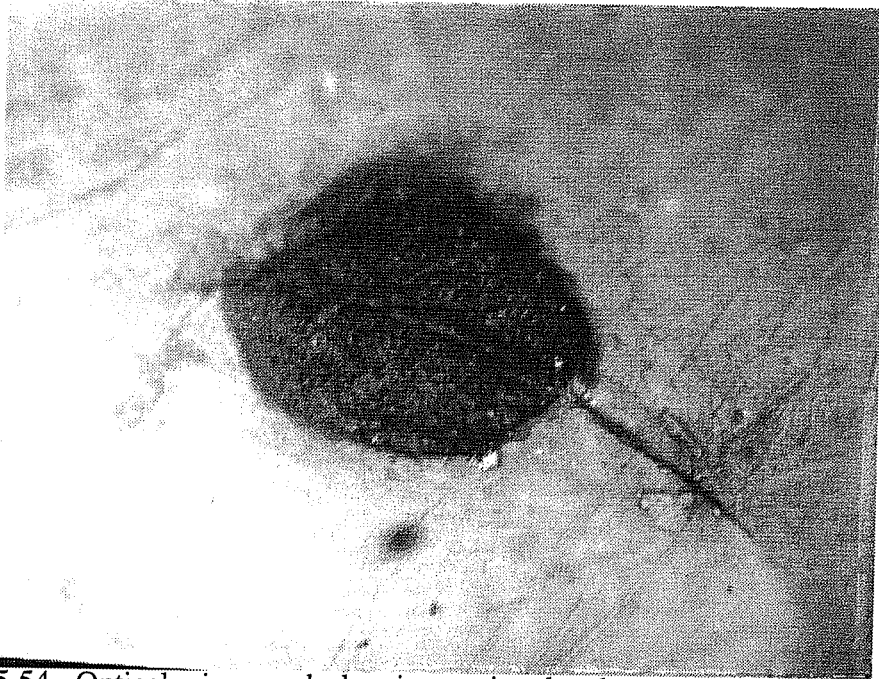
Photo 5.54. Optical micrograph showing a micro break on epoxy coating. (x200) The circle shown is actually an orange-colored stain around the break, which is evidence of corrosion.
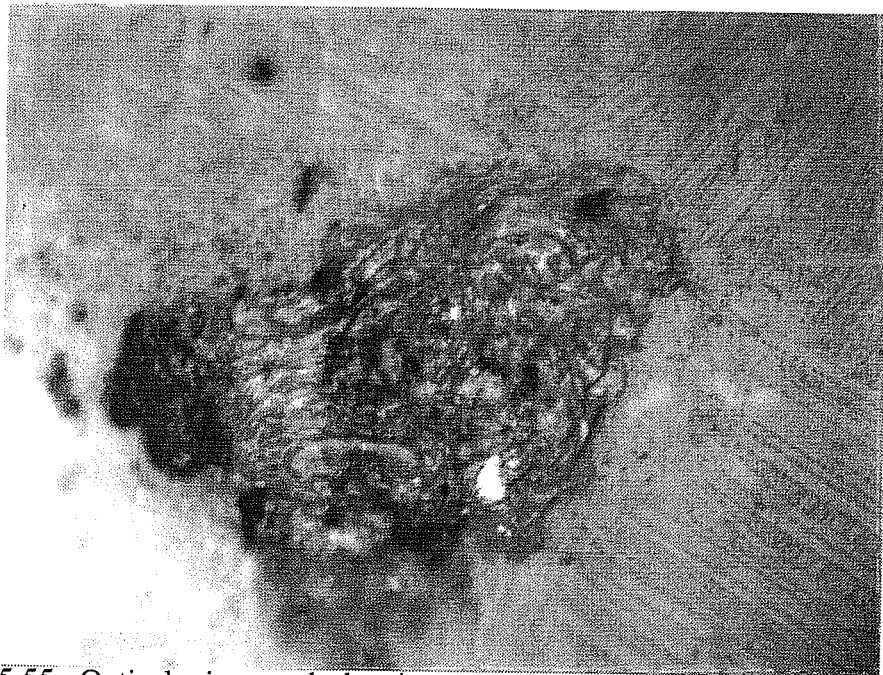
Photo 5.55. Optical micrograph showing a small region on coating where the epoxy was apparently not well cured. (x200)
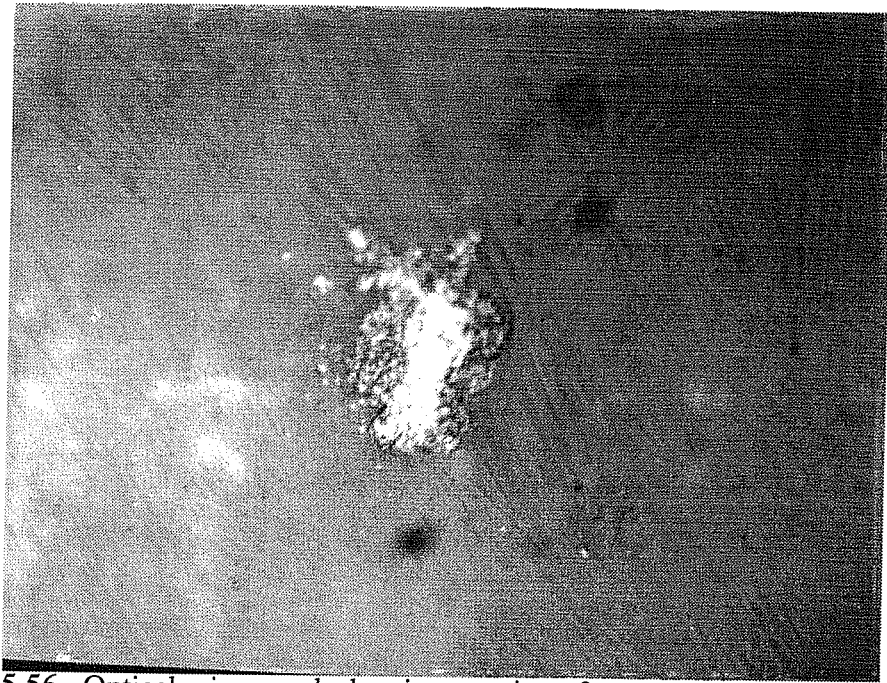
Photo 5.56. Optical micrograph showing a region of uncorroded exposed iron substrate. (x200)
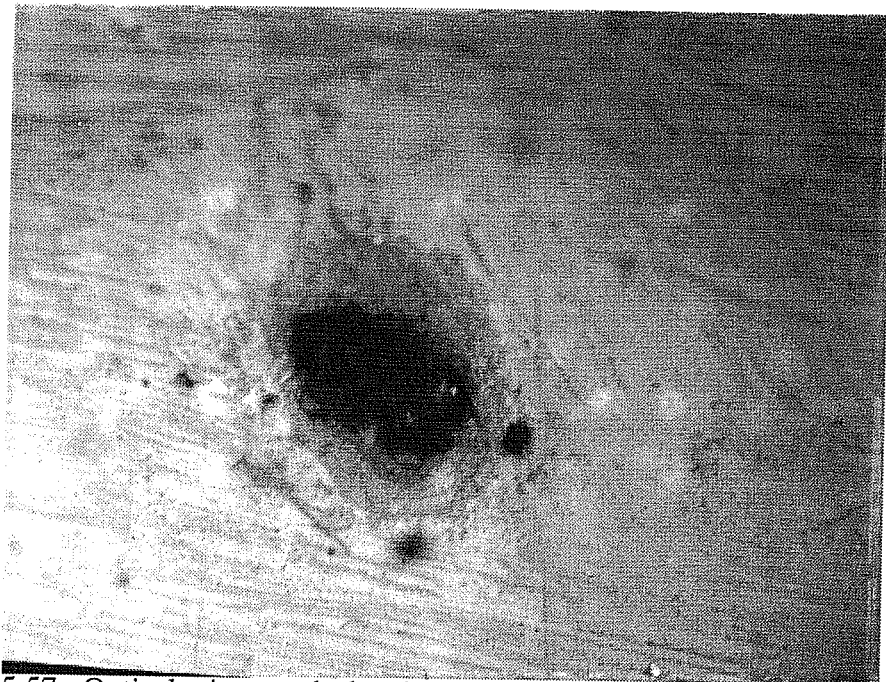
Photo 5.57. Optical micrograph showing a region of corroded exposed iron substrate. (x200)

and Table 5.2, it is then strongly believed that the coater and the influences from subsequent handling have the most effect on ECR performance. In the following, the correlation between coating thickness, coating integrity, coating adhesion, and ECR performance will be discussed in detail.

For ECR specimens showing poor performance in both the EIS response and the visual examination, they are always observed to have a thin coating and/or poor coating integrity. Also, complete coating adhesion loss occurs in these specimens even though they were not bent before immersion. These phenomena are very reasonable since the possibility for ECRs with thinner coating to have defects is relatively higher. This is true not only for the pre-existing defects, such as pin-holes, but also for the physical damage, such as scratches. Both conditions may result in penetration through the coating. Even though such defects are patched, the corrosive ions, oxygen, and water can diffuse into the iron substrate much easier to initiate corrosion activity. Afterwards, corrosion may cause the adhesion loss between the coating and the iron substrate. The above inference is further supported by the SEM micrographs of the cross-section of some representative specimens, as shown in Photo 5.59 through Photo 5.68. Photo 5.59 shows a coating break on an unpatched A#a4 specimen and the severe corroded region beneath it. Photo 5.60, which is taken at a distance from that break, indicates that the corrosion activity may further progress underneath and along the coating. Photo 5.61 shows the iron/coating interface of a patched A#a4 specimen. It is apparent that there is a complete disbondment between the coating and the iron substrate due to corrosion. A higher magnification view of Photo 5.61 is shown in Photo 5.62, in which the vertical lines observed right
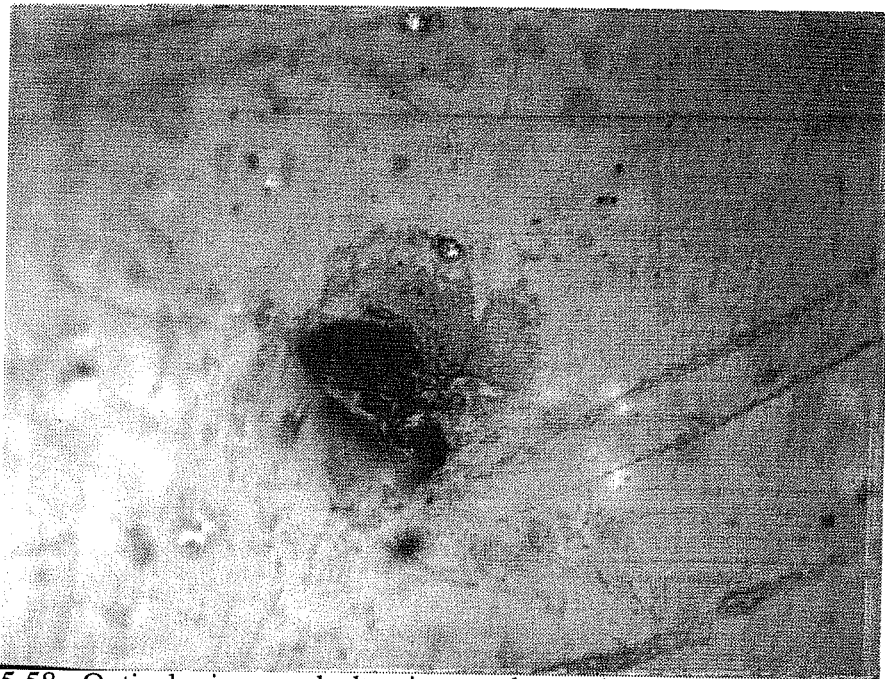
Photo 5.58. Optical micrograph showing another region of corroded exposed iron substrate. (x200)
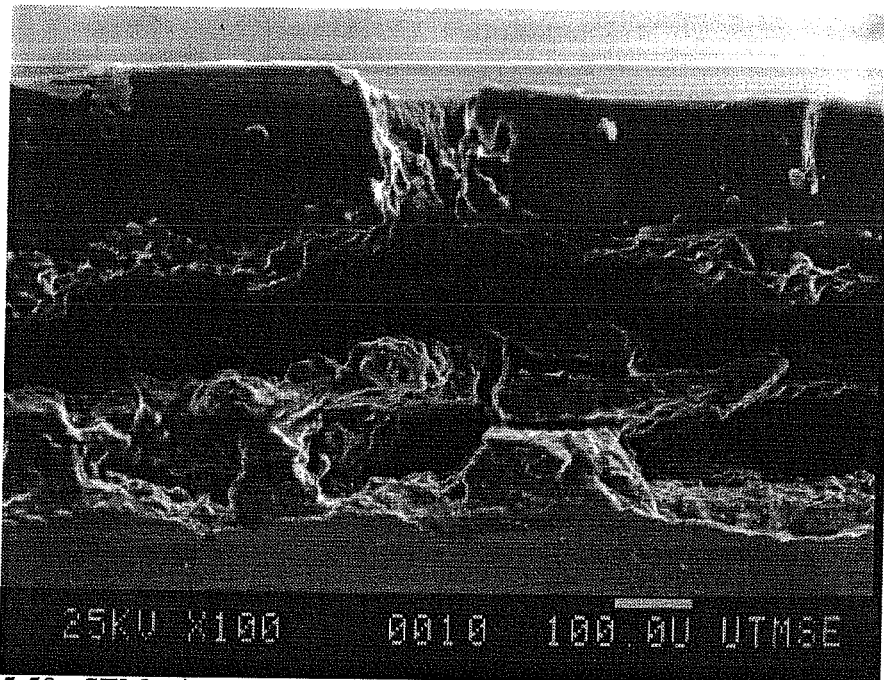
Photo 5.59. SEM micrograph showing a coating break on an unpatched ECR specimen and the severe corroded region beneath it.
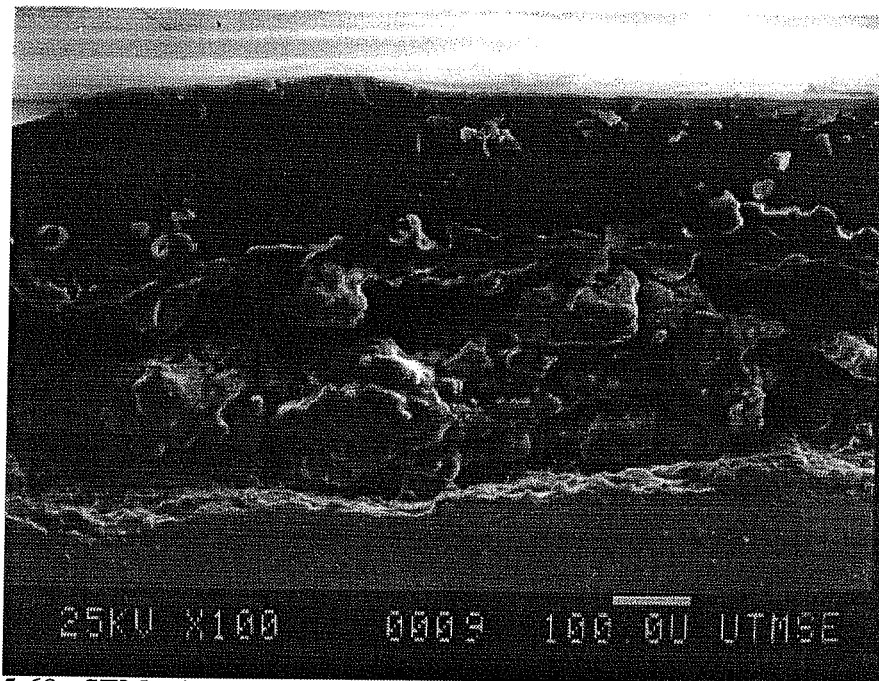
Photo 5.60. SEM micrograph which was taken at a distance from the break in Photo 5.59 showing corrosion developed underneath and along the coating.
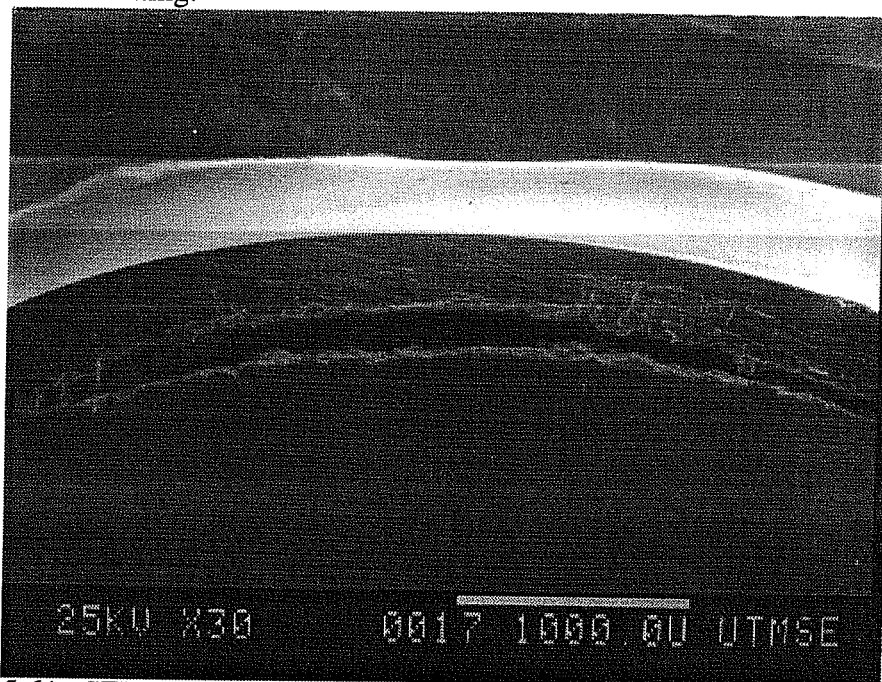
Photo 5.61. SEM micrograph showing a complete disbondment between the coating and the iron substrate due to corrosion.

above the corroded region are the coating cracks. The uppermost layer in this photo is epoxy cold mount applied to fix the specimen. Photo 5.63 shows the ribbed area of an unpatched A#a10 specimen. On the right hand side of the rib, it is observed that coating thickness is abnormally thin at the place where there is an abrupt change of surface shape. However, this area still shows no evidence of corrosion, and no pin-holes are observed. On the left hand side of the rib, corrosion is observed along with coating breaks due to corrosion. The corrosion in this side is certainly due to the pin-holes observed on the base of the ribs, as described in the preceding section. This observation may indicate that even very thin coatings can provide protection as long as there are no defects on them. Photo 5.64 shows a blister formed on the patched area of an A#a10 specimen. It is observed that the film of patching material is lifted by the accumulated corrosion products which were washed away during cutting. Photo 5.65 shows another blister on an A#a4 specimen with some epoxy cold mount cured inside. A discontinuity is observed to form on the coating, which is actually a crack on the outer appearance. It has also been observed in a newly formed, small blister on another A#a4 specimen that the coating is debonded even though there is no sign of corrosion observed inside the blister, as shown in Photo 5.66. A piece of iron clamped inside the blister is a result of the debris formed during cutting. This indicates the possibility of cathodic disbondment at the early stages of blister formation, while the chloride ions are still not present. The micrograph for an A#a4 specimen prior to exposure to solution is shown in Photo 5.67 for comparison with the above photos. The coating adhesion for this specimen is recorded as rank 2.
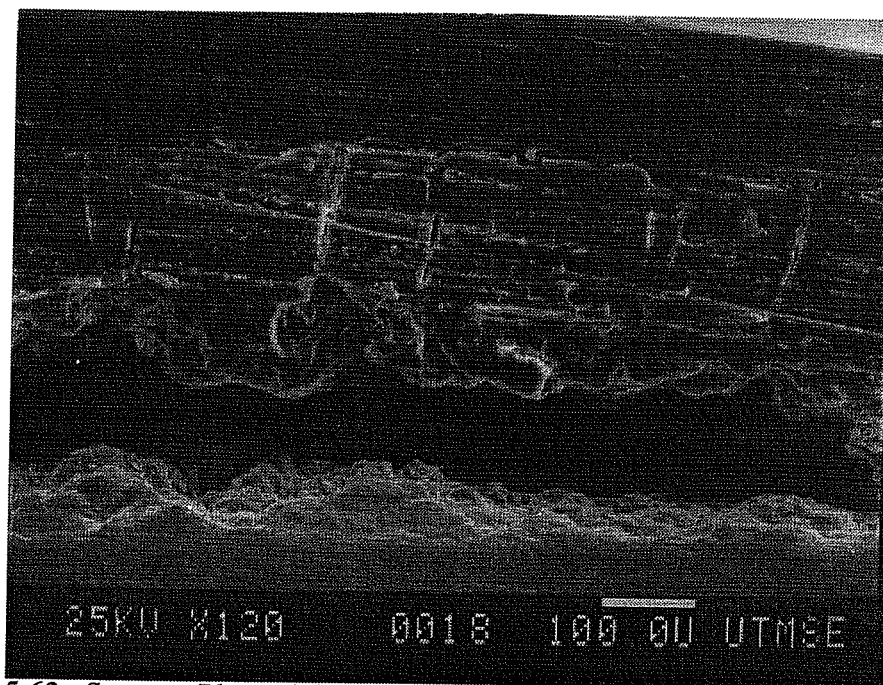
Photo 5.62. Same as Photo 5.61, at a higher magnification, showing coating cracks (observed as vertical lines) right above the corroded region.

Photo 5.63. SEM micrograph of the ribbed area of a unpatched ECR specimen showing abnormally thin coating on the right hand side of the rib, and corrosion along with coating break due to pin-holes on the left hand side of the rib.
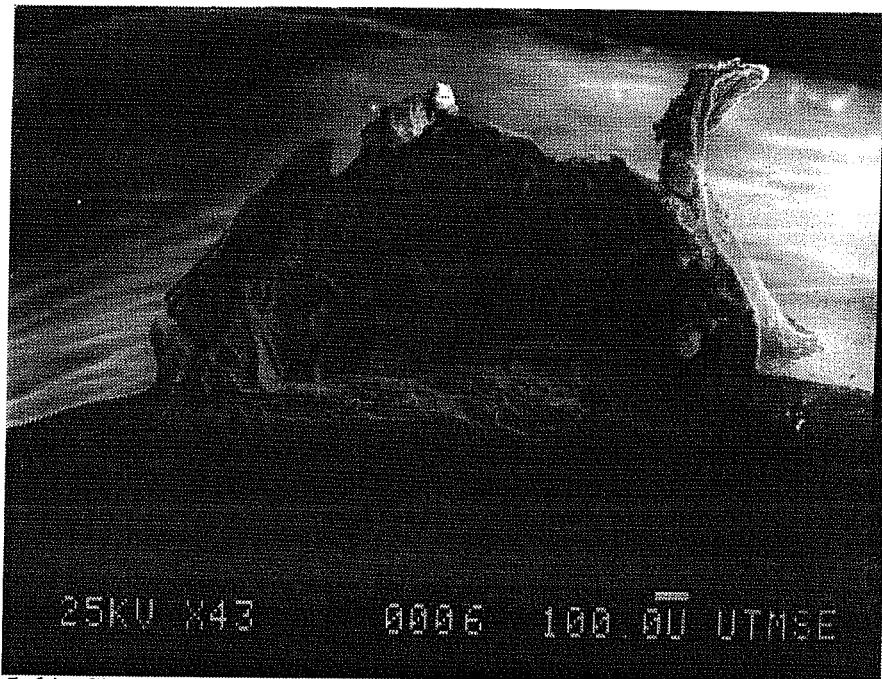
Photo 5.64. SEM micrograph of a blister formed on a patched area. The corrosion products within the blister were washed away during cutting.
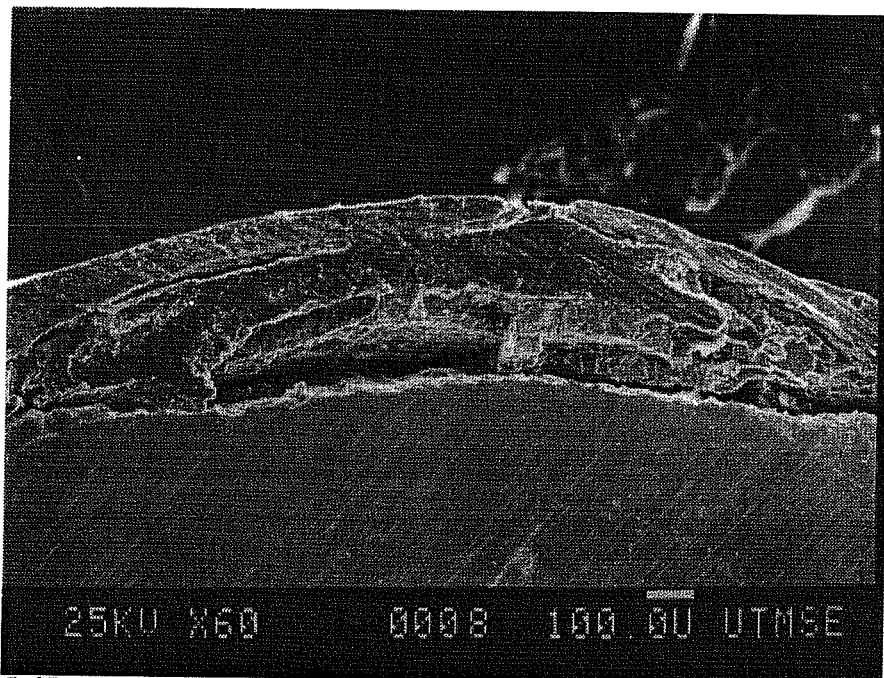
Photo 5.65. SEM micrograph of another blister with some epoxy cold mount cured within it. (Epoxy cold mount was applied to fix the corrosion products.)
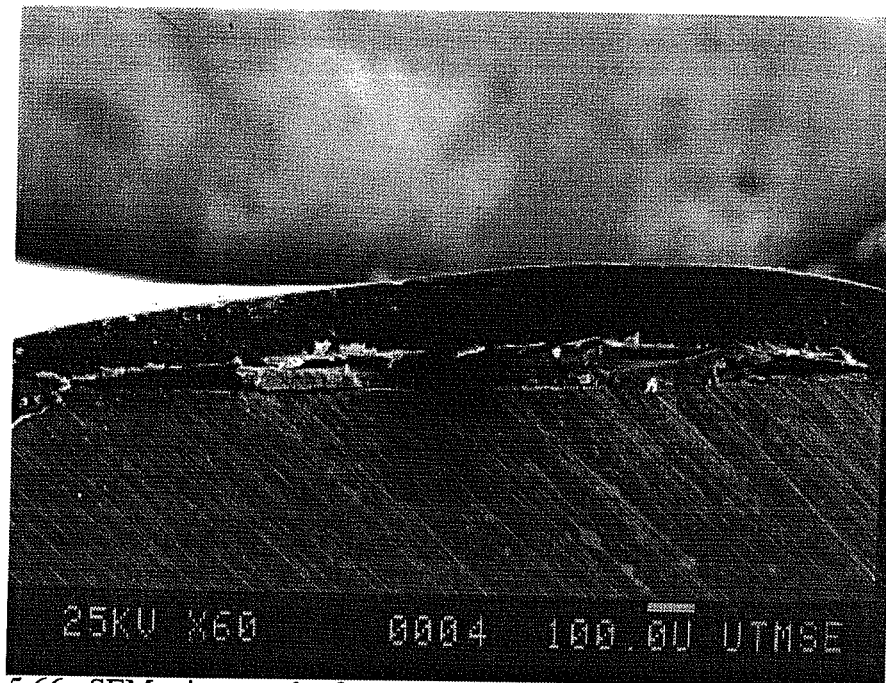
Photo 5.66. SEM micrograph of a newly formed, small blister with no sign of corrosion within it, indicating the possibility of cathodic disbondment at the early stages of blister formation.
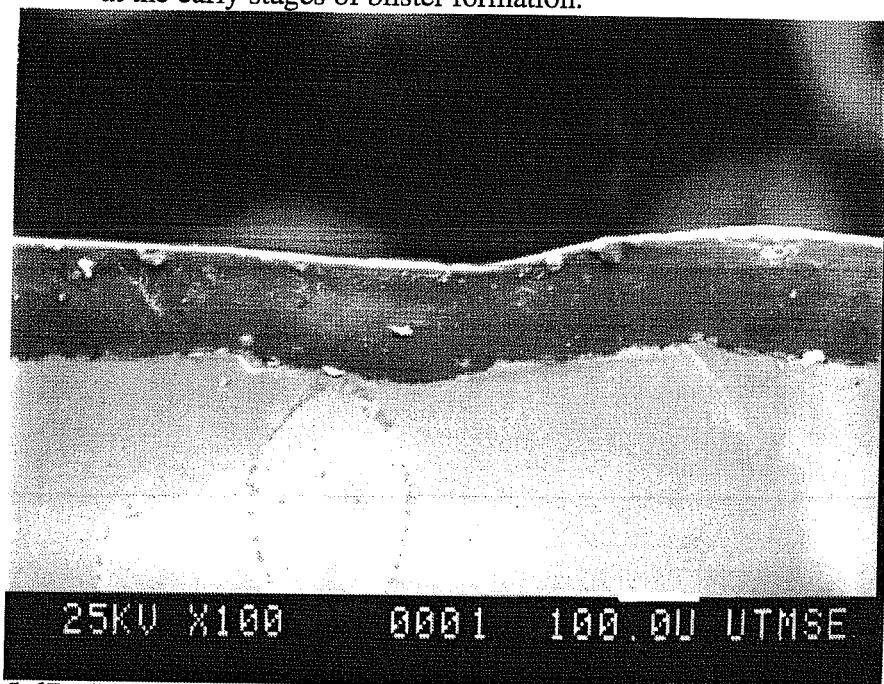
Photo 5.67. SEM micrograph of the iron/coating interface for an ECR with thin coating before exposure to solution. (Adhesion was of rank 2.)

Finally, representative micrographs for specimens with good performance are shown in Photo 5.68 and Photo 5.69 for straight and bent B*c4 specimens, respectively. It is apparent that there is no sign of deterioration observed at the coating/iron interface for the straight specimen whose coating adhesion is recorded as rank 1 after the immersion test. However, for the bent specimen with its coating adhesion recorded as rank 4, the interface also looks very good. This observation further indicates that both immersion and bending can cause adhesion loss, and also shows that bent specimens can still perform well with the debonded coating as long as there is no damage to the coating.
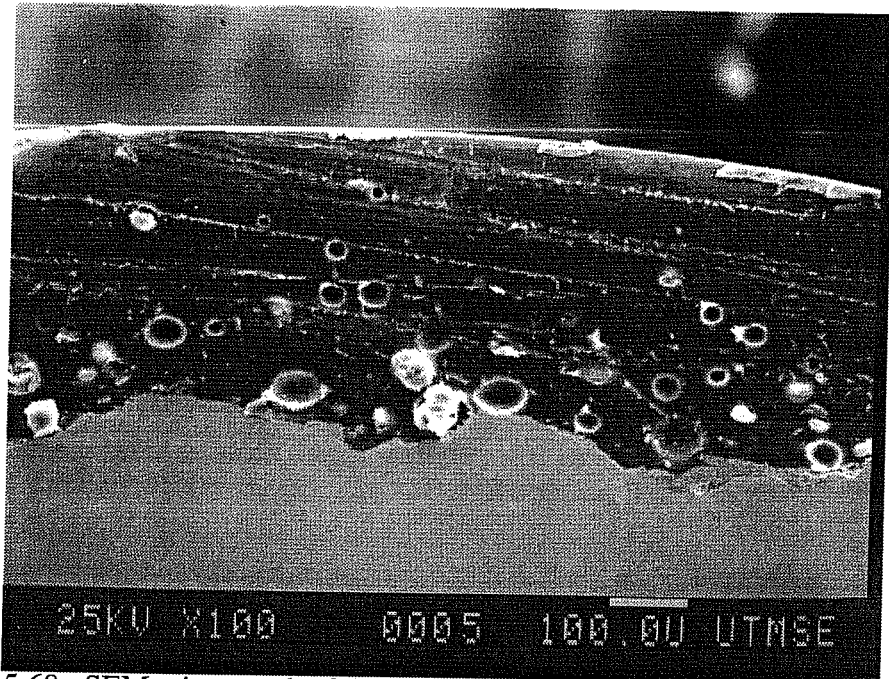
Photo 5.68. SEM micrograph of the iron/coating interface for a straight ECR
specimen exhibiting good performance. (Adhesion was of rank 1.)
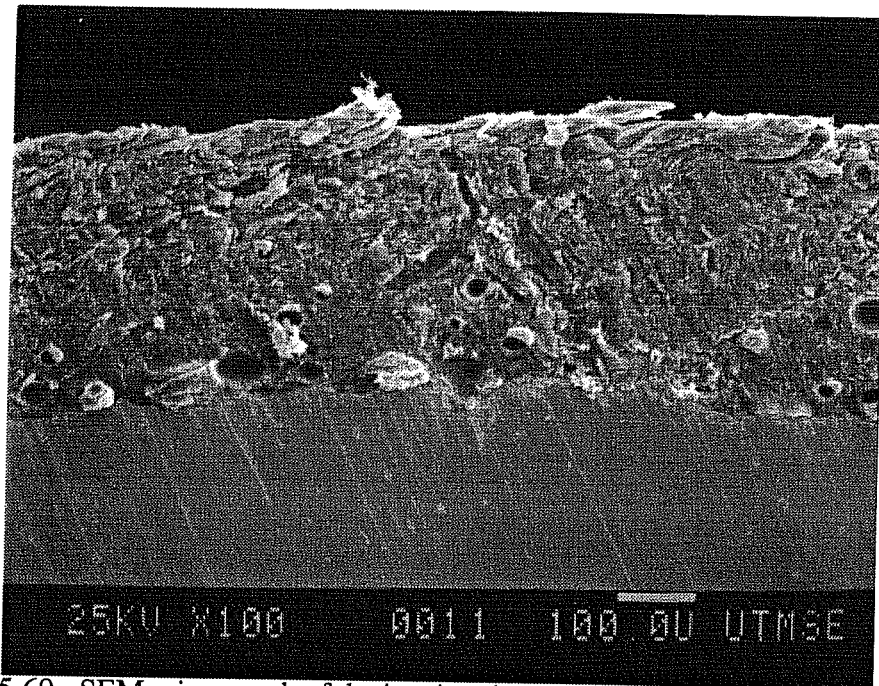
Photo 5.69. SEM micrograph of the iron/coating interface for a bent ECR
specimen exhibiting good performance. (Adhesion was of rank 4.)

Chapter 6

Conclusions and Recommendations

6.1 Conclusions

In this research, ECRs with nine kinds of coater/powder/steel/size combinations were studied through immersion tests to determine their performance in resisting corrosion. Evaluation was accomplished by the measurements of $E_{corr.}$, R_p, and EIS together with the coating characterization which included an examination of surface discontinuities, thickness measurement, and adhesion testing; and microscopic observations. All of this was done to determine the crucial factors affecting the ECR performance. In addition, polished reinforcing steel disks, uncoated reinforcing steel bars, and concrete block macrocells were also investigated to obtain a more comprehensive understanding of the corrosion behavior of reinforcing steel. Based on the approach and time frame of this work, the following preliminary conclusions may be reached.

6.1.1 Corrosion Behavior Study

The controlling mechanisms of corrosion rate for various types of reinforcing steel specimens were investigated with the aid of EIS. It was observed that for the case of polished disks the corrosion rate was completely controlled by the charge transfer reaction. For the uncoated reinforcing steel, an additional

resistance also contributed to controlling the corrosion rate, even though its effect was relatively minor and the charge transfer reaction was still the dominant mechanism. That additional resistance was believed to be contributed by the oxide films, especially the intermediate layer of Fe_3O_4, according to SEM observation.

Three different situations were observed for the ECR specimens. First, for those specimens exhibiting good coating performance, the steel substrate was well insulated by the epoxy coating and a pure capacitive behavior representing the coating property dominated the EIS response. Second, for specimens exhibiting intermediate coating performance, the coating pore resistance and a diffusion impedance dominated the EIS response. The charge transfer reaction was not observed due to its relatively small scale. Finally, for specimens exhibiting poor coating performance, the corrosion rate was generally dominated by the combined effects of coating pore resistance, charge transfer resistance, and diffusion impedance. The weight of each factor changed with time due to the complicated conditions in the real corroding system, and their relative importance could be roughly reflected in the Nyquist plot.

In the cases of concrete block macrocells, the controlling mechanisms were basically similar to those described above except that the diffusion impedance became the most dominant rate controlling mechanism for the uncoated reinforcing steel.

6.1.2 Significance of Various Coating Characteristics

The most crucial factor affecting ECR performance was the coating integrity. ECR specimens with good coating integrity generally performed very well. All ECR specimens with initial defects, even if patched, exhibited a relatively large decrease in corrosion resistance right after immersion.

Coating thickness was also important since thicker coatings generally had better coating integrity. Moreover, thicker coatings can provide more resistance to some minor damage, such as scratches, and to the diffusion of corrosive elements.

ECR specimens without immersion and bending generally had intermediate to good coating adhesion. Adhesion loss was observed to be caused by immersion and bending. The effect of immersion was much more prominent on those ECRs with thin coating and poor coating integrity, and the adhesion loss was due to underfilm corrosion and cathodic disbondment in those cases. The effect of bending was generally remarkable on every type of ECR, and adhesion loss was due to external forces that broke the bonds between the coating and the steel substrate. Surprisingly, cases in which ECR specimens with poor coating adhesion still performed well in resisting corrosion were observed. These findings indicated that: (1) adhesion loss can be the result and not necessarily the cause of ECR degradation, and (2) bent ECRs are more susceptible to corrosion because of the higher probability of damage introduced during bending.

6.1.3 Effectiveness of Epoxy Coating

The results of immersion tests indicated that ECR free of defects should provide adequate protection against corrosion. However, it is difficult to keep

ECR intact in real construction practices, and doubts are generally raised about its effectiveness as the probability of defects increases. It was also observed that even the poor ECR specimens generally still had corrosion resistance values approximately two orders of magnitude larger than those of the uncoated ones. Patching practice could only reduce the corrosion severity to a limited extent, it could not prevent corrosion.

In the concrete block macrocells, the results were more complicated. Some uncoated reinforcing steel bars even had larger corrosion resistance values than some ECR bars did. The consolidation of concrete around bars is believed to play an important role in controlling corrosion rate in these cases.

6.1.4 Comparison of Various Evaluation Methods

Among the methods applied in this work, EIS was especially useful since it could detect coating deterioration in the very beginning stages when a conductive pathway just developed, even before the corrosion process was initiated. Later on, it provided both quantitative and mechanistic information about the ECR deterioration. However, extreme care is necessary in analyzing the impedance plots to avoid misinterpretation. Both Bode and Nyquist plots should be referred to for the best assurance.

Polarization resistance measurement is a very straightforward electrochemical method to obtain quantitative results on corrosion resistance. However, resistance values could be measured only when they were below 10^6 ohms. Also, the measured resistance values should be composed of contributions from coating pore resistance, charge transfer resistance, and diffusion impedance

for the cases of coated metal systems. The results of this method were consistent (in terms of trends) with those of EIS, even though there were some differences in their quantities.

Corrosion potential monitoring is probably the easiest way to get a general idea regarding the extent of corrosion activity. However, it could not provide quantitative results and, sometimes, direct interpretation from this value might lead to erroneous inferences. It is not reliable to use this method alone.

Macrocell current measurement was found to provide generally consistent results compared to the polarization resistance measurement. This method should be a feasible and reliable means to determine the galvanic corrosion associated with reinforcing steel embedded in concrete under well controlled environments.

6.2 Recommendations

6.2.1 Specifications

It is apparent that current coating technology is able to produce high quality ECR since many test specimens exhibited satisfactory performance in much more corrosive media than would typically be encountered in real applications. Additional specifications should focus on developing a procedure to protect the coating integrity during the handling, shipping, storage, and fabrication processes. For example, protective materials, such as high density plastic sleeves, might be used to protect ECR prior to placement. Also, better patching materials and adequate repair procedures should be specified to minimize unavoidable damage.

6.2.2 Methods for Quality Control and Performance Evaluation

Since EIS can detect coating degradation during the beginning stages, and since most poor ECR exhibit a relatively large impedance decrease during the first day, a one day immersion test in 3.5% NaCl solution (with qualification based upon the EIS response) might be a reliable means for quality control. However, due to the sophisticated equipment and long time required for one complete measurement, the proposed idea of using the absolute impedance at a certain single frequency, e.g. 1 mHz, might be a good alternative.

Corrosion potential monitoring is a feasible means to qualitatively determine the corrosion activity for reinforcement in concrete but it should always be accompanied by other methods. Macrocell current measurement was proved to be useful for the laboratory specimens which were subjected to well controlled exposure. However, its feasibility in field applications might be questionable if reinforcing steel bars which would normally act as the cathode experience corrosion due to the random exposure conditions in the field. Measuring the absolute impedance at a certain single frequency or the polarization resistance should both be reliable methods for field performance evaluation.

6.2.3 Further Study

In the concrete block specimens, it was observed that some uncoated reinforcing steel bars even had larger corrosion resistance values than some ECR bars did. This is an interesting finding even though it was suspected that those ECR bars had poor integrity before placement. Further research is needed to

investigate the effect of concrete consolidation around the reinforcing bars in terms of the conductive paths for corrosive elements.

Also, a complete research program combining both laboratory tests and a real scale construction with outdoor exposure should be performed to develop a model to estimate the service life based upon the laboratory test results.

Bibliography

[1] C. L. Page and K. W. J. Treadway, "Aspects of the Electrochemistry of Steel in Concrete," Nature, **297**, May 1982, pp. 109-114.

[2] H. C. Midgley, J. W. Figg, and M. J. McLean, Concrete, **7**, 1973, pp. 24-26.

[3] "Environmental Impact of Highway Deicing," Water Pollution Control Research Series 11040 GKK 06/71, Environmental Protection Agency, Jun. 1971.

[4] "Application of Fusion Bonded Epoxy-Coated Rebar," Concrete, **23**, May 1989, pp. 16.

[5] "Durability of Concrete Bridge Decks," Final Report, Portland Cement Association and U.S. Bureau of Public Roads in Cooperation with Ten State Highway Agencies, 1970.

[6] J. L. Beaton, D. L. Spellman, and R. F. Stratfull, "Corrosion of Steel in Continuously Submerged Reinforced Concrete Piling," Highway Research Record No. 204, Highway Research Board, 1967, pp. 11-21.

[7] R. W. Poston, "Improving Durability of Bridge Decks by Transverse Prestressing," Ph.D. Dissertation, Department of Civil Engineering, The University of Texas at Austin, Austin, Texas, Dec. 1984.

[8] "Rebar Protective Coating," Highways, **57**, Sep. 1989, pp. 16.

[9] L. D. Sandvig, Highway Builder, **42**, Nov. 1974, pp. 16-17.

[10] K. Z. Kahhaleh, "Structural Integrity of Epoxy-Coated Reinforcement," Ph.D. Dissertation, Department of Civil Engineering, The University of Texas at Austin, Austin, Texas, May 1994.

[11] M. G. Fontana, Corrosion Engineering, 3rd. ed., McGraw-Hill, New York, 1986.

[12] J. R. Clifton, H. F. Baeghly, and R. G. Mathey, "Protecting Reinforcing Bars from Corrosion with Epoxy Coatings," Corrosion of Metals in Concrete, SP 49, Detroit, American Concrete Institute, 1975, pp. 115-133.

[13] K. C. Clear and Y. P. Virmani, "Corrosion of Non-Specification Epoxy-Coated Rebars in Salty Concrete," Public Roads, 47, Jun. 1983, 10 p.

[14] A. S. Safier, "Development and Use of Electrostatic Epoxy-Powder Coated Reinforcement," The Structural Engineer, 67, Mar. 1989, pp. 95-98.

[15] D. Gustafson, "Epoxy Update," Civil Engineering, 58, Oct. 1988, pp. 38.

[16] R. Powers and R. Kessler, "Corrosion Evaluation of Substructure, Long Key Bridge," Corrosion Report No. 87-9A, FL Department of Transportation, Gainesville, Florida, Sep. 1987.

[17] K. C. Clear, "Effectiveness of Epoxy Coated Reinforcing Steel," Concrete International, May 1992, pp. 58-62.

[18] L. Wolf, "Use of Epoxy-Coated Reinforcing Steel in Texas: The Tx DOT Perspective," ASTM Epoxy-Coated Reinforcement Workshop, Denver, Jun. 21-21, 1995.

[19] F. M. Lea, The Chemistry of Cement and Concrete, 3rd. ed., Chemical Publishing Co., New York, 1971.

[20] P. Peguin, M. Rubaud, P. Longuet, and A. Zelwer, Cah. Cent. scient. tech. Batim., No. 130, Cahier 1109, 1972.

[21] R. S. Barneyback, Jr. and S. Diamond, Society of Cement Concrete Research, **11**, 1981, pp. 279-285.

[22] M. Pourbaix, Atlas of Electrochemical Equilibria in Aqueous Solutions, NACE, 1974.

[23] D. A. Hausmann, Materials Protection, **6**, 1967, pp. 19-23.

[24] H. H. Uhlig and R. W. Revie, Corrosion and Corrosion Control, 3rd ed., John Wiley & Sons, New York, 1985.

[25] M. Nagayama and M. Cohen, Journal of Electrochemical Society, **109**, 1962, pp. 781-790.

[26] C. L. Page and Khalaf, Cement and Concrete Research, 1979, pp. 197.

[27] C. L. Page, "Mechanism of Corrosion Protection in Reinforced Concrete Marine Structure," Nature, **258**, Dec. 1975, pp. 514-515.

[28] D. S. Leek and A. B. Poole, "The Breakdown of the Passive Film on High Yield Mild Steel by Chloride Ions," Third International Symposium on Corrosion of Reinforcement in Concrete, UK, May 21-24, 1990, pp. 67-73.

[29] W. Hime and B. Erlin, "Some Chemical and Physical Aspects of Phenomena Associated with Chloride-Induced Corrosion," ACI SP 102, 1987, pp. 1.

[30] R. T. Foley, "Role of the Chloride Ion in Iron Corrosion," Corrosion, **26**, 1970, pp. 58-70.

[31] N. Sato, Electrochimica Acta, **16**, 1971, pp. 1683-1692.

[32] K. R. Trethewey and J. Chamberlain, Corrosion, John Wiley & Sons, New York, 1988.

[33] P. D. Cady, "Corrosion of Reinforcing Steel in Concrete - A General Overview of the Problem," ASTM STP 629, American Society for Testing and Materials, 1977, pp. 3-11.

[34] H. Lee and K. Neville, Handbook of Epoxy Resins, 2nd. ed., McGraw-Hill, New York, 1982.

[35] F. W. Billmeyer, Jr. Textbook of Polymer Science, 3rd. ed., John Wiley & Sons, New York, 1984.

[36] K. C. Clear, "Effectiveness of Epoxy-Coated Reinforcing Steel - Intrim Report," Canadian Strategic Highway Research Program, Ottawa, Ontario, Nov. 1992, 94 P.

[37] A. M. Zayed and A. A. Sagues, "Corrosion at Surface Damage on an Epoxy-Coated Reinforcing Steel," Corrosion Science, 30, 1990, pp. 1025-1044.

[38] "Standard Specification for Epoxy Coated Reinforcing Steel Bars," ASTM A775/A775M-94d, American Society for Testing and Materials, Philadelphia, 1994.

[39] A. G. Robert, "Organic Coatings: Properties, Selection, and Use," NBS, Building Science Series 7, National Bureau of Standards, Washington, D.C., 1968.

[40] G. Pourkhosrow, "Epoxy-Coated Reinforcing Steel in Bridge Decks," Report No. FHWA/OK-81(3), Oklahoma Department of Transportation, Federal Highway Administration, Oklahoma City, Oklahoma, Nov. 1981, 55 P.

[41] B. J. McFadden, "Application and Fabrication of Epoxy-Coated Reinforcing Steel," Paper No. 8, Seminar Reprints on Solving Rebar Corrosion Problem in Concrete, Chicago, Illinois, Sep. 27-29, 1982; NACE, Houston, Texas, 1983, 6 p.

[42] Y. P. Virmani, K. C. Clear, and T. J. Pasko, Jr., "Time-to-Corrosion of Reinforcing Steel in Concrete Slabs, V.5: Calcium Nitrite Admixture or Epoxy-Coated Reinforcing Bars as Corrosion Protection System," Report No. FHWA/RD-83/012, Federal Highway Administration, Washington, D.C., Sep. 1983, 71 p.

[43] J. R. Clifton, "Protection of Reinforcing Bars with Organic Coatings," Materials Performance, 15, May 1976, pp. 14-17.

[44] R. E. Weyers and P. D. Cady, "Deterioration of Concrete Bridge Decks from Corrosion of Reinforcing Steel," Concrete International, 9, Jan. 1987, pp. 15-20.

[45] G. J. Malasheskie, D. A. Maurer, D. B. Mellott, and J. L. Avellano, "Bridge Deck Protective Systems - Final Report," Report No. FHWA-PA-88-001+85-17, Federal Highway Administration, Washington, D.C., Jul. 1988, 61 p.

[46] A. M. Zayed, A. A. Sagues, and R. G. Powers, "Corrosion of Epoxy-Coated Reinforcing Steel in Concrete," Paper No. 379, Corrosion 89, NACE, New Orleans, Apr. 17-21, 1989, 20 p.

[47] A. A. Sagues and R. G. Powers, "Effect of Concrete Environment on the Corrosion Performance of Epoxy-Coated Reinforcing Steel," Paper No. 311, Corrosion 90, NACE, Las Vegas, Apr. 23-27, 1990, 15 p.

[48] A. A. Sagues, R. G. Powers, and A. M. Zayed, "Marine Environment Corrosion of Epoxy-Coated Reinforcing Steel," Corrosion of Reinforcement in Concrete, C. Page, K. Treadaway, and P. Bamforth, Eds., Elsevier Applied Science, London-New York, 1990, pp. 539-549.

[49] A. A. Sagues, "Mechanism of Corrosion of Epoxy-Coated Reinforcing Steel in Concrete - Final Report," Report No. FL/DOT/RMC/0543-3296, University of South Florida, Tampa, Florida, Apr. 1991, 75 p.

[50] A. A. Sagues, "Corrosion of Epoxy-Coated Rebar in Florida Bridges," Interim Summary Report, State Job No. 99700-7556-010, University of South Florida, Tampa, Florida, Apr. 1992, 42 p.

[51] A. A. Sagues, "Corrosion Processes and Field Performance of Epoxy-Coated Reinforcing Steel in Marine Substructures," Paper No. 299, Corrosion 94, NACE, 1994, 15 p.

[52] S. K. Lee, J. F. McIntyre, and W. H. Hartt, "New Developments in Laboratory Testing of Epoxy Coated Reinforcing Steel," Paper No. 290, Corrosion 94, NACE, 1994, 37 p.

[53] S. K. Lee, J. F. McIntyre, and W. H. Hartt, "Accelerated Testing of Epoxy Coated Reinforcing Steel, Part 1: Hot Water Exposure/Electrochemical Impedance Spectroscopy," Paper No. 11, Corrosion 95, NACE, 1995, 36 p.

[54] R. J. Stratfull, "Half-Cell Potentials and the Corrosion of Steel in Concrete," Highway Research Record, 433, 1973, pp. 12.

[55] J. R. VanDeveer, Journal of American Concrete Institute, 12, 1975, pp. 597.

[56] M. N. Haque and M. Kawamura, "Carbonation and Chloride-Induced Corrosion of Reinforcement in Fly Ash Concrete," ACI Materials Journal, 89, 1992, pp. 41.

[57] N. S. Rengaswamy and S. Srinivasan, "Some Studies on Concrete Resistivity and Rebar Potential," Transactions of the SAEST, 23, 1988, pp. 225.

[58] E. J. Simmons, Corrosion, **11**, 1955, pp. 255.

[59] R. V. Skold and T. E. Larsen, Corrosion, **13**, 1957, pp. 139.

[60] M. Stern and A. L. Geary, Journal of Electrochemical Society, **104**, 1957, pp. 56.

[61] M. Stern and E. D. Weisert, ASTM Proceeding, **32**, 1959, pp. 1280.

[62] D. A. Jones, Principles and Prevention of Corrosion, Macmillan, New York, 1992.

[63] "Basics of AC Impedance Measurements," Application Note AC-1, Electrochemical Instruments Group, EG&G Princeton Applied Research, Princeton, NJ., 1985, 12 p.

[64] A. J. Bard and L. R. Faulkner, Electrochemical Methods, Wiley, New York, 1980.

[65] "Standard Test Method for Determining the Effects of Chemical Admixtures on the Corrosion of Embedded Steel Reinforcement in Concrete Exposed to Chloride Environments," ASTM G109-92, American Society for Testing and Materials, Philadelphia, 1992.

[66] J. Holm, "Comparison of the Corrosion Potential of Calcium Chloride and a Calcium Based Non-Chloride Accelerator - A Macro-Cell Corrosion Approach," Corrosion, Concrete and Chlorides, ACI SP 102, F. W. Gibson, Ed., American Concrete Institute, Detroit, 1987, pp. 35-48.

[67] N. S. Berke, D. F. Shen, and K. M. Sandberg, "Comparison of the Polarization Resistance Technique to the Macrocell Corrosion Technique,"

Corrosion Rate of Steel in Concrete, ASTM STP 1065, N. S. Berke, V. Chaker, and D. Whiting, Eds., American Society for Testing and Materials, Philadelphia, 1990, pp. 38-51.

[68] G. W. Walter, "A Review of Impedance Plot Methods Used for Corrosion Performance Analysis of Painted Metals," Corrosion Science, **26**, 1986, pp. 681-703.

[69] L. Beaunier, I. Epelboin, J. C. Lestrade, and H. Takenouti, Surface & Coating Technology, **4**, 1976, pp. 237-254.

[70] G. W. Walter, "Application of Impedance Measurements to Study Performance of Painted Metals in Aggressive Solutions," Journal of Electroanalytical Chemistry, **118**, 1981, pp. 259-273.

[71] M. W. Kendig, E. M. Meyer, G. Lindberg, and F. Mansfeld, "A Computer Analysis of Electrochemical Impedance Data," Corrosion Science, **23**, 1983, pp. 1007-1015.

[72] F. Mansfeld, M. W. Kendig, and S. Tsai, "Recording and Analysis of AC Impedance Data for Corrosion Studies, Part Two: Experimental Approach and Results," Corrosion, **38**, 1982, pp. 570-580.

[73] F. Mansfeld, "Recording and Analysis of AC Impedance Data for Corrosion Studies, Part One: Background and Methods of Analysis," Corrosion, **37**, 1981, pp. 301-307.

[74] D. C. Silverman and J. E. Carrico, "Electrochenical Impedance Technique - A Practical Tool for Corrosion Prediction," Corrosion, **44**, 1988, pp.280-287.

[75] W. J. Lorenz and F. Mansfeld, "Determination of Corrosion Rates by Electrochemical DC and AC Methods," Corrosion Science, **21**, 1981, pp. 647-672.

[76] S. A. McCluney, S. N. Popova, B. N. Popov, R. E. White, and R. B. Griffin, "Comparing Electrochemical Impedance Spectroscopy Methods for Estimating the Degree of Delamination of Organic Coatings on Steel," Journal of Electrochemical Society, **139**, 1992, pp. 1556-1560.

[77] K. K. Sagoe-Crentsil, F. P. Glasser, and J. T. S. Irvine, "Electrochemical Characteristics of Reinforced Concrete Corrosion as Determined by Impedance Spectroscopy," British Corrosion Journal, **27**, 1992, pp. 113-118.

[78] S. S. Azim and S. Guruviah, "Evaluation of Organic Coating by Impedance Studies," Proceeding of the 10th. International Congress on Metallic Corrosion, 1987, pp. 1393-1397.

[79] E. Frechette, C. Compere, and E. Chali, "Evaluation of the Corrosion Resistance of Painted Steels by Impedance Measurements," Corrosion Science, **33**, 1992, pp. 1067-1081.

[80] M. Kendig, F. Mansfeld, and S. Tsai, "Determination of the Long Term Corrosion Behavior of Coated Steel with A.C. Impedance Measurements," Corrosion Science, **23**, 1983, pp. 317-329.

[81] J. Hubrecht and J. Vereecken, "Corrosion Monitoring of Iron, Protected by an Organic Coating, with the Aid of Impedance Measurements," Journal of Electrochemical Society, **131**, 1984, pp. 2010-2015.

[82] S. Feliu, J. C. Galvan, and M. Morcillo, "Limitations and Possibilities of the Typical Electrochemical Impedance Measurements for Studying Anti-Corrosive

Paint Coatings," Proceeding of the 10th. International Congress on Metallic Corrosion, 1987, pp. 1235-1242.

[83] F. Mansfeld, M. W. Kendig, and S. Tsai, "Evaluation of Corrosion Behavior of Coated Metals with AC Impedance Measurements," Corrosion, **38**, 1982, pp. 478-485.

[84] F. Qiu, "Measuring the Corrosion of Steel in Concrete by Employing AC Impedance Technique," Proceeding on 'Corrosion and Corrosion Control for Offshore and Marine Construction', Xiaman, China, Sep. 6-9, 1988, pp.616.

[85] J. Kasthurirangan, "An Electrochemical Study of the Corrosion of Reinforcing Steel in Saline Aqueous Media," Master Thesis, Department of Mechanical Engineering, The University of Texas at Austin, Austin, Texas, Aug. 1992.

[86] U. Schwertmann and R. M. Cornell, Iron Oxides in the Laboratory, VCH, New York, 1991.

VITA

Hengching Chen was born in Taiwan, The Republic of China, on December 26, 1962, the son of Shih-Hung Chen and Yung-Hsueh Chao. In September 1982, he entered Chung-Yuan Christian University in Chungli, Taiwan. After receiving the degree of Bachelor of Science in Mechanical Engineering in May 1986, he served as a second lieutenant in Chinese Army Artillery for two years. In September 1989, he attended The Graduate School of The University of Texas at Austin. He received the degree of Master of Science in Mechanical Engineering in August 1991, and continued his study to seek the doctoral degree in Materials Science and Engineering.

Permanent address: No. 307 Mintsu Rd.

Changhua, Taiwan

R.O.C.

This dissertation was typed by the author.